Investigation of C9orf72-SMCR8 complex stability and turnover

Lily Alokowa Koryang
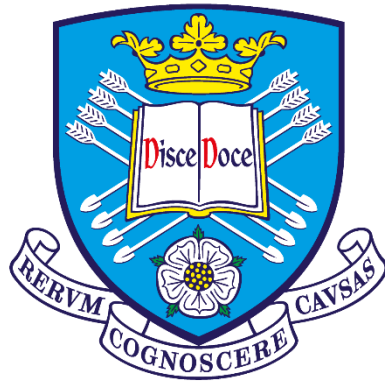
Submitted for the degree of Doctor of Philosophy (PhD)

Sheffield Institute for Translational Neuroscience

University of Sheffield

September 2021

Abstract

Amyotrophic lateral sclerosis (ALS) and frontotemporal dementia (FTD) are neurodegenerative diseases characterised by the loss of upper and lower motor neurons and atrophy of the frontal and temporal regions of the brain respectively. There is a substantial overlap in pathology, clinical presentation, and genetics of ALS and FTD.

A GGGGCC hexanucleotide repeat expansion in the first intron of the C9orf72 gene is the most common cause of familial ALS and FTD. Haploinsufficiency, RNA toxicity and dipeptide protein toxicity are all thought to contribute mechanistically towards C9orf72-related ALS/FTD. Evidence points towards haploinsufficiency as a modifier of disease which led us to hypothesise that restoring C9orf72 levels will be beneficial for C9ALS/FTD patients by restoring autophagy and promoting the clearance of DPRs.

We provide evidence that C9orf72 is degraded via the ubiquitin proteasome system. We also demonstrate that formation of a complex between C9orf72 and SMCR8 stabilises the levels of both proteins. C9orf72 and SMCR8 was identified as potential substrates of the Kelch-like protein KLHL13, whereby siRNA-mediated knockdown of KLHL13 increases C9orf72 and SMCR8 levels and slows their turnover. A yeast two hybrid identified the deubiquitinating enzyme USP8 as a potential interactor of C9orf72 and we confirmed this interaction by co-immunoprecipitation. We found USP8 does not regulate C9orf72 protein levels, suggesting another function for this interaction. Finally, we provide evidence that the SUMO interacting motif (SIM) and lysine 90 residue in C9orf72 is involved in the stabilisation of the C9orf72-SMCR8 complex which points towards the potential involvement of SUMOylation in complex stability.

In summary, we identified C9orf72 as a substrate of the proteasome and highlighted KLHL13 as a novel modifier of C9orf72 and SMCR8 levels, which may have important therapeutic considerations. We provide support for the involvement of the C9orf72 SIM and K90 residue in C9orf72-SMCR8 complex stability.

Acknowledgements

Firstly, I would like to thank my supervisor Professor Kurt De Vos for the opportunity to work in his laboratory group and for all his help and encouragement throughout my PhD. His expertise and input into the project have been invaluable. Secondly, I would like to thank my secondary supervisor Dr Andrew Grierson for his input into my project. The advice I received from my supervisors and Dr Alison Twelvetrees in laboratory meetings positively impacted the direction and outcome of my project and for that I am thankful.

I would also like to thank the rest of the De Vos group, both past and present for all their help during the completion of my PhD. I am grateful for the funding that allowed me to carry out this work as without it this work would not have been possible, so thanks are given to the Alzheimer's Society. Next, to the people in SITraN, thank you for all the laughter, joy and entertainment that you have provided over the past four years. Thank you to my friends that have been there throughout the highs and lows of my PhD and for always being there to listen.

I am eternally grateful to my family for their support and encouragement for the duration of my PhD. A special thanks is extended to my mom for always only being one phone call away with words of encouragement through the harder times. Finally, I would like to thank my partner, Will for all his support during this PhD and for always being there with a listening ear and comforting hug. I could not have done this PhD without all the support and love those above have provided. Thank you.

This thesis is dedicated to my dad – it is because of you I am where I am today.

Table of contents

1. Contents

List of tables

List of figures

Abbreviations

Adenosine monophosphate	AMP
Adenosine triphosphate	ATP
Amino acid	AA
Amyotrophic lateral sclerosis	ALS
Antisense oligonucleotide	ASO
Autophagy related	Atg
Behavioural variant FTD	BVFTD
C9orf72 related ALS/FTD	C9LS/FTD
Cation-independent M6PR	ci-M6PR
Central DENN	cDENN
Central nervous system	CNS
Chromosome 9 open reading frame 72	C9orf72
Clustered Regularly Interspaced Short Palindromic Repeats	CRISPR
CRISPR-associated Protein 9	CAS9
Cullin ring ligase	CRL
Deoxyribonucleic Acid	DNA
Deubiquitinating enzymes	DUBs
Differentially Expressed in Normal and Neoplastic cells	DENN
Dipeptide Repeat Protein	DPR
Downstream DENN	dDENN
Empty vector	EV
Endoplasmic reticulum	ER
Excitatory amino acid transporter 2	EAAT2
FAK Family Kinase-Interacting Protein of 200 kDa	FIP200
Familial ALS	FALS
Folliculin	FLCN
Folliculin Interacting Protein 2	FNIP2
Frontotemporal dementia	FTD
Fused in Sarcoma	FUS
Gain of function	GOF
Glycine-Alanine	GA
Glycine-Arginine	GR
Glycine-Proline	GP
GTPase activating protein	GAP
Guanine nucleotide dissociation factor	GDI
Guanine nucleotide exchange factor	GEF
Homologous to E6AP C-terminus	HECT
Induced pluripotent stem cells	iPSC
Kelch-like	KLHL

Kelch-like 13	KLHL13
Kelch-like 9	KLHL9
Kilodalton	kDa
Knockout	KO
L-Azidohomoalanine	L-AHA
Loss of function	LOF
Lysosome-associated membrane protein	LAMP
Mammalian Target of Rapamycin Complex 1	MTORC1
Mannose-6-Phosphate Receptor,	M6PR
Messenger RNA	mRNA
Microgram	μg
Microlitre	μl
Microtubule Associated Protein Tau	MAPT
milligram	mg
Millimolar	mM
Minutes	Mins
Motor neuron disease	MND
Mouse embryonic fibroblast	MEF
Nanogram	ng
Nanomolar	nM
NEDD8-activating enzyme	NAE
N-Ethylmaleimide	NEM
Neural-precursor-cell-expressed developmentally down-regulated 8	NEDD8
Non-targeting control	NTC
Nuclear factor kappa-light-chain-enhancer of activated B cells	NFκB
Optineurin	OPTN
Phosphate buffered saline	PBS
Polyethylenimine	PEI
Polymerase chain reaction	PCR
Post-translational modification	PTM
Primary progressive aphasia	PPA
Progranulin	PGRN
Proline-Arginine	PA
Proline-Arginine	PR
Radioimmunoprecipitation assay	RIPA
Reactive oxygen species	ROS
Real Time Quantitative PCR	RT-qPCR
Really interesting new gene	RING
Repeate-associated non-ATG	RAN
Ribonucleic acid	RNA

Room temperature		RT
Second	s	s
Sentrin specific proteases		SENP
Sequestosome 1		SQSTM1
Small ubiquitin-like modifier		SUMO
Smith-Magenis Syndrome Chromosome Region, Candidate 8		SMCR8
Sodium Dodecyl Sulphate Poly-Acrylamide Gel Electrophoresis		SDS-PAGE
Sporadic ALS		sALS
Superoxide Dismutase 1		SOD1
Synaptic vesicle		SV
TANK binding kinase 1		TBK1
TAR DNA binding protein 43 kDa		TDP-43
Tris Buffered Saline Buffer with Tween 20		TBST
Ubiquitin proteasome system		UPS
Ubiquitin specific protease		USP
Unc51-Like Autophagy Activating Kinase 1		ULK1
Upsteam DENN		uDENN
WD Repeat Domain 41		WDR41
Yeast two hybrid		Y2H

Declaration

I, Lily Koryang, confirm that except for the co-immunoprecipitation assays in Figure 5.2*C and* Figure 5.4 *and the stabilisation assay in* Figure 5.2*A, B the Thesis is my own work. The co-immunoprecipitation and stabilisation assays in the named figures were performed in collaboration with Amber Morgan, an MSc student working in our laboratory group. I am aware of the University's Guidance on the Use of Unfair Means (www.sheffield.ac.uk/ssid/unfair-means). This work has not previously been presented for an award at this, or any other, university.*

1. Introduction

1.1. Amyotrophic lateral sclerosis (ALS) and Frontotemporal Dementia (FTD)

Motor neuron disease (MND) is an umbrella term for diseases in which motor neurons are selectively affected. The most common MND is amyotrophic lateral sclerosis (ALS). In ALS the upper motor neurons located in the motor cortex and the lower motor neurons located in the anterior horn of the spinal cord and brain stem are affected. Presentation of the disease can vary from spinal-onset in which patients present with muscle weakness to bulbar-onset in which patients have difficulties with dysarthria and dysphagia (speech and swallowing difficulties respectively) (Hardiman et al., 2017).

The hallmark of ALS is progressive degeneration of these motor neurons that result in symptoms ranging from muscle weakness, muscle twitching and spasticity due to upper motor neuron degeneration to eventual muscle atrophy from degeneration of lower motor neurons (Chiò et al., 2011; Riva et al., 2016). The incidence of ALS is around 2 - 3 per year per 100,000 of the population and death typically occurs within 3 – 5 years from the onset of disease as a consequence of breathing difficulties and eventual respiratory failure. (Hardiman et al., 2017; Huisman et al., 2011; Logroscino et al., 2010). The progression of ALS varies with multiple factors influencing rate of progression. Such factors include an older age of onset, presence of cognitive impairment and mixed upper and lower motor neuron involvement (Al-Chalabi and Hardiman, 2013; Byrne et al., 2012; Wijesekera et al., 2009). 10% of ALS cases are familial (fALS) and are normally inherited in an autosomal dominant manner. However, autosomal recessive and X-linked inheritance patterns of fALS have also been reported (Boylan, 2015). Currently there is no cure for ALS and the only FDA-approved treatments are the glutamate antagonist Riluzole and the antioxidant Edaravone (Jaiswal, 2019).

Whilst ALS is the most common MND, frontotemporal dementia (FTD) represents the second most common cause of dementia, after Alzheimer's disease. FTD is a progressive neurological disorder that arises due to neuronal atrophy of the frontal and temporal regions of the brain (Lillo and Hodges, 2009). The two main presentations of FTD affect behaviour and language and are clinically classified into three different variants depending on the predominant features (Belzil et al., 2016; Woollacott and

Rohrer, 2016). The first of these, the behavioural variant (bvFTD) represents the most common FTD phenotype and is characterised by a gradual decline in both behavioural and social interaction owing to atrophy of the frontal regions of the brain (Sivasathiaseelan et al., 2019; Woollacott and Rohrer, 2016). Such behavioural changes are often mistaken for psychiatric illness which increases the risk of bvFTD misdiagnosis (Woolley et al., 2011). The second presentation - primary progressive aphasia (PPA) - is an umbrella term that is used to describe dementias in which language is impaired (Graff-Radford and Woodruff, 2007). In contrast to bvFTD, PPA is associated with temporal lobe degeneration which leads to language deficits. PPA can be divided into semantic variant PPA and non-fluent primary progressive aphasia (nfPPA) and disease progression is often slower for patients with semantic variant PPA (Flanagan et al., 2015). Clinically, semantic variant PPA patients present with a loss of semantic memory whereas nfPPA manifests as phonological and grammatical errors, possibly alongside a loss of expressive language (Ferrari et al., 2011; Graff-Radford and Woodruff, 2007). The average age of onset of FTD usually occurs between 50 – 65 years and like ALS, most cases of FTD are sporadic. However, FTD has a stronger genetic component when compared to ALS with approximately one third of FTD cases being familial (Moore et al., 2020; Woollacott and Rohrer, 2016). Clinically, FTD can exist alone or alongside other diseases. Such diseases include Corticobasal degeneration, Parkinsonism and Progressive Supranuclear Palsy (Hodges et al., 2003; Olney et al., 2017; Woolley et al., 2011). The most notable however is an overlap clinically and neuropathologically with ALS (detailed further below).

1.2.   The ALS/FTD spectrum

Increasing evidence for the overlap in clinical symptoms between patients with ALS and FTD have led to the suggestion that ALS and FTD do not represent distinct diseases but instead lie on a continuum and represent extremities of the same disease. Evidence for an overlap in clinical symptoms spans over 40 years with reports of ALS patients having FTD-like symptoms (Mitsuyama, 1979). Since then, reports differ between the exact proportion of ALS patients with FTD symptoms or a definitive FTD diagnosis and studies have varied between 14% to up to 50% of ALS patients having problems with cognitive impairment (Lomen-Hoerth et al., 2003; Ringholz et al., 2005). Interestingly, reports have

shown that in patients presenting with MND that go on to develop FTD-like symptoms, progression of dementia is remarkably quick and the mean survival is shorter for ALS-FTD patients when compared to patients with ALS alone (Caselli et al., 1993; Lillo and Hodges, 2009; Olney et al., 2005).

As with the case of ALS patients, of the patients that have been diagnosed with FTD, there is subset that later present with motor neuron dysfunction. Numerous studies have sought to quantify the percentage of FTD patients that go on to have such problems with results ranging from between 14 – 40% of FTD patients having definite ALS or features of ALS to as high as 75% (Burrell et al., 2011; Frank et al., 1997; Lipton et al., 2004; Lomen-Hoerth et al., 2002). As is the case for ALS-FTD, the median survival for patients with FTD-MND is shorter than for those with FTD alone (Hodges et al., 2003). A summary of key genes involved in the ALS/FTD overlap is shown in Figure 1.1.
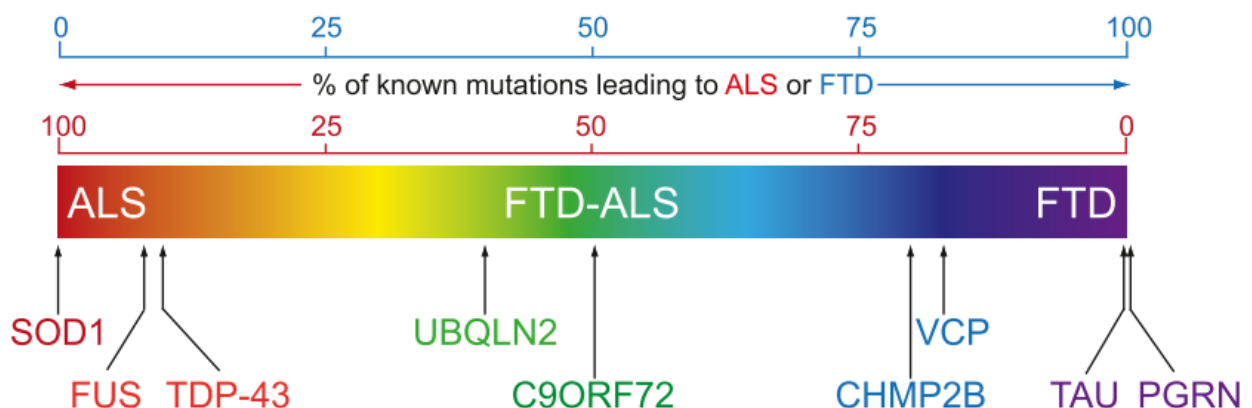
Figure 1.1: Genetic overlap of ALS and FTD

ALS and FTD represent a continuum of a broad neurodegenerative disorder with each presenting as extremes of a spectrum of overlapping clinical symptoms (ALS in red and FTD in purple). Major known genetic causes for ALS and FTD are plotted according to the ratio of known mutations that give rise to ALS or FTD. Figure obtained and used with permission (Ling et al., 2013)

1.3.   Pathological features of ALS/FTD

Abnormal accumulation of proteinaceous inclusions are a central hallmark of both sporadic ALS and familial ALS (Corbo and Hays, 1992). Such inclusions are typically found in degenerating motor neurons and glia in the brainstem, spinal cord,

hippocampus, cerebellum and frontal and temporal regions of the brain (Al-Chalabi et al., 2012). The predominant features of these inclusions are ubiquitinated aggregates that are classified according to their morphology. Aggregates can take the form of Lewy body-like inclusions or skein-like inclusions that are granular and filamentous in structure (Kawashima et al., 1998; Leigh et al., 1991; Lin and Dickson, 2008; Robinson et al., 2013). It was not until 2006 that the identity of the major component of the ubiquitinated protein inclusions was determined to be transactive response DNA binding protein 43 (TDP-43) (Arai et al., 2006; Neumann et al., 2006). Nuclear and cytoplasmic TDP-43 positive inclusions have been identified in motor neurons (upper and lower) and the frontal and temporal regions of the brain (Van Deerlin et al., 2008; Sreedharan et al., 2008). These inclusions are prevalent in over 90% of ALS cases (Figure 1.2, Ling et al., 2013). The presence of ubiquitinated protein inclusions is indicative of impairment of the proteasome system. The TDP-43 positive inclusions are commonly immunoreactive for p62. p62 is an autophagosome cargo protein encoded for by *SQSTM1* and has an important role in targeting proteins for autophagic degradation (Lamar Seibenhener et al., 2004). The presence of p62 in ubiquitinated, TDP-43 positive inclusions is further evidence of impaired protein degradation. TDP-43, ubiquitin positive inclusions are not limited to ALS. Indeed, both FTD and ALS/FTD feature TDP-43 and ubiquitin positive neuronal cytoplasmic inclusions, neuronal dystrophic neurites and neuronal intranuclear inclusions (Cairns et al., 2007; Davidson et al., 2007; Neumann et al., 2006). Bunina bodies are another type of inclusion that is found in ALS. Bunina bodies are small, eosinophilic inclusions that are immunonegative for TDP-43 and are found in the lower motor neurons (Tan et al., 2007). Transferrin has been found to localise in Bunina bodies and they have been found to be positive for cystatin C (Mizuno et al., 2006; Okamoto et al., 1993). Round hyaline inclusions are the final type of inclusions in ALS. These inclusions are filamentous in structure, can be either phosphorylated or non-phosphorylated and are thought to be ubiquitinated and lack surrounding membranes (Hirano et al., 1967; Mizusawa, 1993; Trojanowski et al., 1989).

Pathological TDP-43 can be used to distinguish between fALS and Cu/Zn superoxide dismutase (SOD1)-related fALS, with the latter being characterised by TDP-43 negative inclusions (Mackenzie et al., 2007). A feature of SOD1-related ALS are Lewy body-like inclusions in the anterior horn in lower motor neurons. These inclusions are positive for proteins including heat shock protein, SOD1, ubiquitin and phosphorylated filaments but

are TDP-43 and fused in sarcoma (FUS) negative (Mackenzie et al., 2007; Nakamura et al., 2014; Tan et al., 2007). The neuropathology of patients with mutations in *FUS* represent another exception in sALS, non-SOD1 fALS and FTD. Such inclusions can either be coarse or fine granules or filamentous in structure. In addition to being TDP-43 negative, mutant FUS inclusions are ubiquitin and p62 positive and are typically neuronal cytoplasmic inclusions found in the neurons and glia of affected regions of the spinal cord and brain, although neuronal intranuclear inclusions are also occasionally found (Blair et al., 2010; Deng et al., 2010; Verbeeck et al., 2012).

All FTD pathologies involve the aggregation of proteins. Depending on which proteins are aggregated, FTD pathologies are then subdivided into categories. FTD/TDP-43 and FTD/FUS pathologies are the same as the above and account for approximately 50% and 10% of cases respectively (Figure 1.2, Ling et al., 2013). FTD/FUS pathologies are a subsection the FTD/FET (FUS, Ewing's sarcoma protein (EWS) and TATA-binding protein associated factor 15 (TAF15)) family pathology. The remaining two pathologies are FTD/ubiquitin proteasome system (UPS) which account for less than 1% of pathologies and involves only the aggregation of proteins associated with the UPS. The remaining 40% of pathologies - FTD/tau – are associated with aggregated, hyperphosphorylated tau inclusions. The discovery of both TDP-43 and FUS as major components of inclusions in both ALS and FTD is further evidence for a disease spectrum in which pure ALS and pure FTD are the extremities of the same disease.
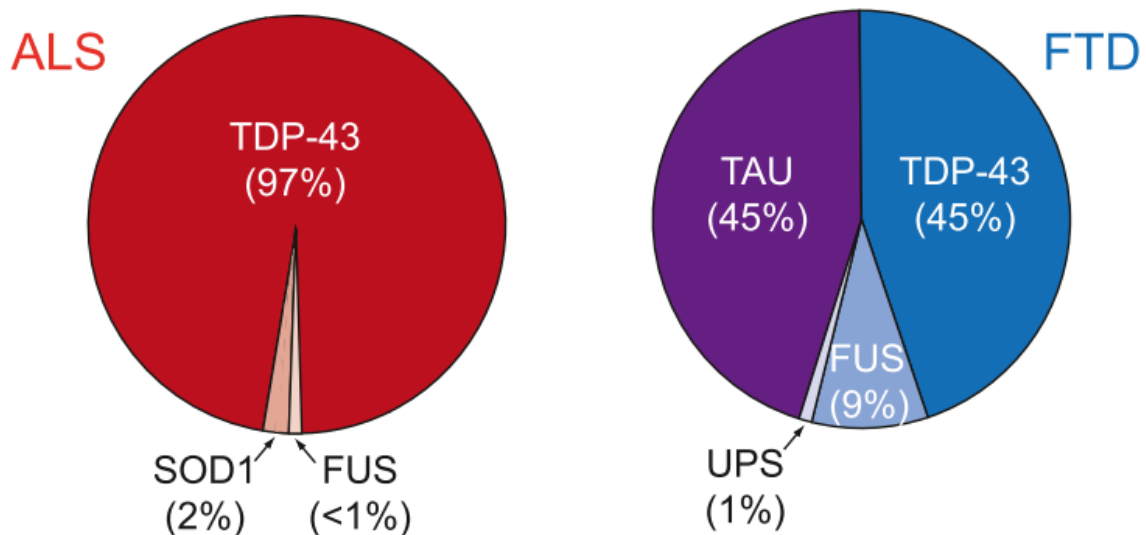
Figure 1.2: Pathological inclusions in ALS and FTD.

Pathological protein inclusions in ALS and FTD, according to the major protein misaccumulated. Inclusions of TDP-43 and FUS/TLS in ALS and FTD reflect the pathological overlap of ALS and FTD. (Ling et al., 2013) Figure obtained with permission.

1.4.   Genetics of ALS/FTD

Only 10% of ALS cases are thought to have a familial inheritance, with the remaining 90% of ALS cases being sporadic. The first mutation identified as causative of fALS was *SOD1*. Mutations in *SOD1* account for approximately 20 - 25% of fALS and up to 4% of sporadic ALS (Pasinelli and Brown, 2006; Rosen et al., 1993a). Since then, mutations in *TARDBP*, *FUS* and *C9orf72* have been identified to cause ALS. *TARDBP* and *FUS* mutations each account for around 4% of fALS cases and fewer still for sALS (Kabashi et al., 2008; Kwiatkowski Jr. et al., 2009; Sreedharan et al., 2008; Vance et al., 2009) whereas mutations in *C9orf72* are responsible for approximately 40% of fALS and 11% of overall ALS cases (DeJesus-Hernandez et al., 2011; Renton et al., 2011). This makes mutations in *C9orf72* the most common cause of ALS. Collectively, mutations in *SOD1*, *TARDBP*, *FUS* and *C9orf72* are responsible for approximately 68% and 11% of fALS and sALS respectively (Renton et al., 2014).

FTD has a larger familial component in comparison to ALS with up to 40% of cases having a hereditary basis and 10% inherited in an autosomal dominant manner

(Abramzon et al., 2020; Rohrer et al., 2009). Similarly to ALS, mutations in *C9orf72* represent the most common cause of familial FTD, being responsible for 25% of cases (Renton et al., 2014). Collectively mutations in microtubule associated protein tau (*MAPT*), progranulin (*PGRN*) and *C9orf72* are responsible for 60% of familial FTD cases (Olszewska et al., 2016). Although infrequent, mutations in *TARDBP*, the gene encoding TDP-43 have been identified as causative of familial FTD in less than 1% of cases (Tan et al., 2017). In bv-FTD patients, mutations in *FUS* have been identified both with and without ALS, although the prevalence of this is much lower than for ALS patients (Huey et al., 2012; Van Langenhove et al., 2010). The identification of *TARDBP* and *FUS* mutations in ALS and FTD cases in addition to the pathological evidence further substantiates the idea that ALS and FTD lie on a neurodegenerative continuum. A summary of the major genes that have been identified as causative of ALS/FTD is given in Table 1.1. Aside from mutations that have been identified as causative of ALS, FTD or ALS/FTD, in recent years several risk variants for ALS and FTD have been identified thanks to advances in next generation sequencing in addition to global collaborations. These include but are not limited to mutations in TANK-binding kinase 1 (*TBK1*), Coiled-Coil-Helix-Coiled-Coil-Helix Domain Containing 10 (*CHCHD10*), tubulin-alpha 4a (*TUB4A*) and NIMA-related kinase 1 (*NEK1*) (Nguyen et al., 2018a).

Numerous studies have demonstrated that the rate of occurrence of ALS patients or families having two or more mutations in genes associated with ALS is higher than the incidences that would occur by chance (Van Blitterswijk et al., 2012; Nguyen et al., 2018b; Veldink, 2017). Indeed, some *SOD1* carriers never develop ALS and it has been observed that additional ALS-associated mutations in *C9orf72* mutation patients may acts as genetic modifiers of disease presentation, leading to the suggestion that ALS is an oligogenic disease in which multiple disease variants conspire to determine disease presentation (Felbecker et al., 2010; Lattante et al., 2015). In fact, some of the genes that have been identified as causative of ALS in a minor number of cases are also implicated in other non-FTD neurodegenerative diseases. For example, mutations in *SPG11* are the third most common cause of autosomal recessive hereditary spastic paraplegia (Stevanin et al., 2007).

Despite the genetic diversity of ALS, FTD and ALS/FTD patients, many of the causative genes encode for proteins of similar function or that are involved in similar pathways,

ranging from RNA metabolism and protein turnover to axonal transport and neuroinflammation. It is therefore unsurprising that dysfunction of many of these pathways are involved in the pathogenesis of disease. By understanding the role of these proteins in their biological pathways, possible modifiers may be identified which has important implications for drug development.

Table 1.1: Genes associated with ALS and FTD

Gene	Gene name	Onset	Inheritance	Reference
ALS genes				
ALS2	Alsin	Juvenile	AR	(Hadano et al., 2001)
ALS3	-	Juvenile	AD	(Hand et al., 2002)
ALS7	-			(Sapp et al., 2003)
ANG	Angiogenin	Adult	AD	(Greenway et al., 2006)
ANXA11	Annexin A11	Adult	AD	(Smith et al., 2017)
ERBB4	Ethylene-responsive element-binding protein 4	Adult	AD	(Takahashi et al., 2013)
FIG4	Factor induced gene 4	Adult	AD	(Chow et al., 2009)
GLT8D1	Glycosyltransferase 8 Domain Containing 1	Adult	AD	(Cooper-Knock et al., 2019)
HNRNPA1	Heterogeneous Nuclear Ribonucleoprotein A1	Adult	AD	(Kim et al., 2013)

KIF5A	Kinesin Family Member 5A	Adult	AD	(Nicolas et al., 2018)
MATR3	Matrin 3	Adult	AD	(Johnson et al., 2014a)
NEK1	Never in mitosis gene a (NIMA)-related kinase 1	Adult	AD	(Brenner et al., 2016)
PFN1	Profilin 1	Adult	AD	(Wu et al., 2012)
SETX	Senataxin	Juvenile	AD	(Chen et al., 2004)
SIGMAR1	sigma non-opioid intracellular receptor 1	Juvenile	AR	(Luty et al., 2010)
SOD1	Cu/Zn superoxide dismutase 1	Adult	AD, AR	(Rosen et al., 1993b)
SPG11	Spatacsin	Juvenile	AR	(Orlacchio et al., 2010)
VAPB	Vesicle-associated membrane protein-associated protein B	Adult	AD	(Nishimura et al., 2004)
FTD genes				
MAPT	Microtubule Associated Protein Tau	Adult	AD	(Hutton et al., 1998)
GRN	Granulin Precursor	Adult	AD	(Baker et al., 2006; Cruts et al., 2006)
TBP	TATA-box binding protein gene	Adult	AD	(Olszewska et al., 2019)
ALS/FTD genes				

AXTN2*	Ataxin 2		AD	(Elden et al., 2010)
C9orf72	Chromosome 9 open reading frame 72	Adult	AD	(DeJesus-Hernandez et al., 2011; Renton et al., 2011)
CCNF	Cyclin F	Adult	AD	(Williams et al., 2016)
CHCHD10	Coiled-coil-helix-coiled domain 10	Adult	AD	(Johnson et al., 2014b)
CHMP2B**	charged multivesicular body protein 2B	Adult	AD	(Parkinson et al., 2006)
FUS*	Fused in sarcoma	Adult	AD	(Kwiatkowski Jr. et al., 2009; Vance et al., 2009)
OPTN*	Optineurin	Adult	AD	(Maruyama et al., 2010)
SQSTM1	Sequestosome 1	Adult	AD	(Fecto et al., 2011)
TARDBP*	Transactive response DNA binding protein 43	Adult	AD	(Sreedharan et al., 2008)
TBK1	TANK-binding kinase 1	Adult	AD	(Cirulli et al., 2015; Freischmidt et al., 2015)
TUB4A*	Tubulin alpha 4A	Adult	AD	(Smith et al., 2014)
UBQLN2*	Ubiquilin 2	Adult	X-linked	(Deng et al., 2011)

10

VCP**	Valosin-containing protein	Adult	AD	(Johnson et al., 2010)

* denotes predominantly ALS genes, ** denotes predominantly FTD genes

1.5.   Mechanisms of disease

1.5.1. Oxidative stress

Oxidative stress occurs from the imbalance of reactive oxygen species (ROS) and antioxidants in addition to the inability to repair ROS-mediated toxicity (Betteridge, 2000; Kandlur et al., 2020) and has been implicated in the pathogenesis of ALS. The majority of ROS are produced as by-product of the mitochondrial respiratory chain although other enzymes such as CYP450 and xanthine oxidase have been identified as sources of ROS (Hrycay and Bandiera, 2015). The ROS causes oxidative damage to the cellular targets (proteins, phospholipids, mitochondria and DNA) of these species (Barber et al., 2006). One of the defence mechanisms cells use to prevent oxidative stress is the catalytic removal of ROS. Superoxide dismutases (SODs) are amongst the enzymes that are involved in the catalytic removal of ROS (Fridovich, 1975). Thus, the identification of *SOD1* mutations in ALS patients highlighted oxidative stress as a potential mechanism of disease. Indeed, numerous studies have demonstrated evidence of oxidative damage in the post-mortem neuronal tissue, spinal cord and urine of sALS and SOD1 ALS patients (Ferrante et al., 1997; Mitsumoto et al., 2008; Shaw et al., 1995a; Shibata et al., 2001). However, whether oxidative stress is the cause or the effect of the disease still remains unclear (Agar and Durham, 2003). The observation that approximately half of *SOD1* mutations do not cause a loss in SOD1 activity (Crosby et al., 2018) in addition to a lack of overt neurodegeneration in SOD1 knockout mice (Reaume et al., 1996) suggests that reduced SOD1 activity (and therefore an increase in ROS) is not the primary cause of ALS.

1.5.2. Impairment of mitochondrial function

The roles of mitochondria are numerous. Mitochondria are involved in ATP production, apoptosis, phospholipid biogenesis and calcium homeostasis and are fundamentally important for cell survival and metabolism. Many genes that have been associated with ALS such as *FUS*, *TARDBP*, *C9orf72* and *VAPB* play a role in mitochondrial related functions. Furthermore, several lines of evidence from both *in vivo* and *in vivo* models have linked mitochondrial dysfunction in the pathogenesis of ALS (reviewed Smith et al.,

2019). Mutations in a number of ALS genes from *CHCHD10, SOD1, TDP-43* to *C9orf72* and *FUS* result in the aberrant morphology of mitochondria and the mitochondrial network (Deng et al., 2015; Higgins et al., 2003; Magrané et al., 2013; Onesto et al., 2016; De Vos et al., 2007). In addition to disruption of the mitochondrial network and morphology, a number of ALS-associated proteins have been identified as interacting with mitochondria. These include SOD1, C9orf72, the glycine-arginine dipeptide repeat protein (DPR) from the C9orf72 hexanucelotide repeat expansion and the RNA-binding proteins TDP-43 and FUS (Blokhuis et al., 2016; Higgins et al., 2002; Lopez-Gonzalez et al., 2016; Wang et al., 2016). As described above, oxidative stress has been implicated in mitochondrial damage and so it is unsurprising that mitochondrial dysfunction has been implicated in the aetiology of ALS. Aside from oxidative stress, defective mitochondrial respiration and ATP production, impaired calcium homeostasis and increased pro-apoptotic signalling have all been linked to the pathogenesis of ALS. Furthermore, impaired mitochondrial dynamics resulting in impaired axonal transport of mitochondria, dysfunctional mitophagy (the degradation of mitochondria) and a defective mitochondrial network due to aberrant mitochondrial fusion and fission have also been linked to ALS (Smith et al., 2019). Moreover, the close contacts formed between mitochondria and the endoplasmic reticulum (ER) that are involved in calcium signalling, mitochondrial and phospholipid biogenesis and trafficking (amongst others functions) have been shown to be disrupted in ALS (Sakai et al., 2021; Stoica et al., 2014, 2016). It is evident that mitochondria dysfunction play an important role in the pathophysiology of ALS.

1.5.3. Excitotoxicity

Glutamate is an abundant neurotransmitter in the central nervous system (CNS). Excitotoxicity has been implicated in a number of neurodegenerative diseases including ALS (Rothstein et al., 1990; Shaw et al., 1995b). Excitotoxicity results from the overactivation of glutamate receptors which causes an abnormal influx of Ca^{2+} in the post-synaptic neuron. In ordinary circumstances, levels of glutamate are regulated by glutamate uptake and transport mechanisms and therefore defects in this pathway result in an excess of glutamate and the overstimulation of neurons by Ca^{2+}. This influx of Ca^{2+} perturbs Ca^{2+} homeostasis. As described above, mitochondria are involved in Ca^{2+} homeostasis and dysfunction of this due to glutamate excitotoxicity leads to downstream

mitochondrial dysfunction and an increase in ROS (Bosch et al., 2000; Harteneck et al., 2000). Motor neurons are vulnerable to defective Ca^{2+} regulation which can result in motor neuron degeneration. Dysregulation of the AMPA (α-amino-3-hydroxy-5-methyl-4-isoxazolepropionic acid) receptor, a receptor abundant in humans is evident in post-mortem tissue from ALS patients and the overstimulation of AMPA results in motor neuron death in rats (Bosch et al., 2000; Corona and Tapia, 2004; Gregory et al., 2020). Furthermore, ALS TDP-43 pathology is observed in motor neurons of sALS patients that lack an AMPA receptor subunit (Aizawa et al., 2010). This is evidence of a relationship between glutamate excitotoxicity and ALS pathology. Excitatory amino acid transporter 2 (EAAT2) is an important transporter involved in the clearance of extracellular glutamate following its cleavage at the synaptic cleft (Rosenblum and Trotti, 2017). EAAT2 primarily resides on astrocytes and knockout of EAAT2 has been demonstrated to increase extracellular glutamate and cause motor neuron degeneration whereas stimulation of EAAT2 has been shown to be neuroprotective (Kong et al., 2014; Rothstein et al., 1996). Collectively, these several lines of evidence highlight excitotoxicity as an important mechanism in ALS aetiology so much so that Riluzole - the first FDA approved drug for ALS – functions as an anti-excitotoxic drug (Doble, 1996).

1.5.4. Synaptic dysfunction

Synapses represent the junction in between neurons that allow for the passage of electrical information from one neuron to the next. Given this, it is unsurprising that excitotoxicity (as described above) contributes to synaptic dysfunction. In addition to excitotoxicity, there is evidence of defective synaptic transmission and plasticity in ALS/FTD. TDP-43 forms RNA granules in synapses and neuronal process (Liu-Yesucevitz et al., 2014). These granules are trafficked along dendrites and regulate local protein synthesis, regulating synaptic function and plasticity (Liu-Yesucevitz et al., 2011). Two ALS-associated mutations, *TDP-43*^{Q343R} and *TDP-43*^{A315T}, have been shown to increase RNA granules size and decrease the trafficking of granules which results in aberrant synaptic function and plasticity (Liu-Yesucevitz et al., 2014). Loss of the *Drosophila* TDP-43 homologue has also been shown to result in morphological synaptic defects and impair motor neuron locomotion (Diaper et al., 2013; Feiguin et al., 2009). Both human and animal models have demonstrated dendritic spine degradation in

corticospinal neurons (Fogarty et al., 2017; Genç et al., 2017; Jara et al., 2012). Along with TDP-43 related ALS/FTD synaptic dysfunction, FUS-linked synaptic defects have also been shown. Cytoplasmic mislocalisation of FUS is a key hallmark of FUS-linked ALS. This cytoplasmic FUS has been shown to lead to synaptic defects that were more pronounced in inhibitory synapses (Scekic-Zahirovic et al., 2021). Moreover, accumulation of FUS in the synapse at early stages of disease leads to impaired synapses and exogenous expression of mutant FUS altered synaptic numbers (Sahadevan et al., 2021; Salam et al., 2021). C9orf72-related synaptic dysfunction has also been demonstrated and is discussed in 1.6.5.

1.5.5. Defective axonal transport

Axonal transport is an important mechanism for maintaining the structure and function of neurons. As neurons can reach over 1 metre in length, ensuring the proper movement and distribution of intracellular cargo is vital. Aberrant axonal transport has been linked to several neurodegenerative diseases including ALS (Mejzini et al., 2019; De Vos and Hafezparast, 2017). Axonal transport is classified as fast or slow depending on the speed cargo is distributed, however, both fast and slow axonal transport use the same molecular machinery. Evidence implicating axonal transport in ALS/FTD pathogenesis includes defects in motor proteins and the cytoskeleton that under basal conditions aid in the anterograde and retrograde transport of cargo.

Kinesins are a family of motor proteins that are involved in the anterograde transport of cargo. Mutations in kinesin 5A (*KIF5A*) strongly implicate kinesins in ALS aetiology (Brenner et al., 2018; Nicolas et al., 2018; Zhang et al., 2019). KIF5A contains a cargo binding domain at its C-terminus and mutations in this domain have been linked to ALS and are predicted to cause loss of function phenotypes (Brenner et al., 2018; Nicolas et al., 2018). Indeed, loss of KIF5A in mice leads to neurodegeneration and paralysis, supporting this hypothesis (Xia et al., 2003). In addition to evidence supporting a direct involvement of kinesin in ALS pathogenesis, the observation that inclusions of FUS (a commonality in ALS patients) recruit kinesin mRNA and protein suggest that kinesins may be indirectly affected in ALS (Yasuda et al., 2017).

The motor protein dynein 1 is involved in retrograde transport (Hirokawa et al., 2010). *DCTN1* encodes for p150[Glued], a component of the dynactin complex that regulates the function of dynein 1 (King, 2012). Mutations in *DCTN1* lead to dysfunctional dynein-mediated cargo transport by prohibiting the binding of p150[Glued] to microtubules and mutations in this gene have been identified in both sporadic and familial ALS patients (Ikenaka et al., 2013; Levy et al., 2006; Münch et al., 2007). Furthermore, dynein-mediated retrograde transport is defective in motor neurons from SOD1 ALS-mutant mice (Bilsland et al., 2010; Kieran et al., 2005). Moreover, in SOD1 mutant mice, anterograde transport of mitochondria is affected (Moller et al., 2017) demonstrating that both antero- and retrograde trafficking is defective in SOD1-related ALS.

In addition to motor proteins, cytoskeletal components such as microtubules and neurofilaments are vital for axonal transport and the accumulation of neurofilaments is a pathological hallmark of sporadic and familial ALS (Mizusawa et al., 1989). In line with this, deletion of NF-L, the major neurofilament subunit required for neurofilament assembly delayed onset and disease and slowed progression in SOD1[G85R] mice (Williamson et al., 1998). Mutations in neurofilament heavy chain (*NFH*) and peripherin (*PRPH*) have been proposed to disrupt axonal transport by the accumulation of phosphorylated neurofilaments and the disruption of the neurofilament network assembly respectively and mutations in both *NFH* and *PRPH* have been identified in ALS patients (Figlewicz et al., 1994; Gros-Louis et al., 2004; Mizusawa et al., 1989). In addition, ALS-associated *TUB4A* mutations destabilise the microtubule network and mutant SOD1 interacts with tubulin, both of which affect microtubule dynamics which may possibly impair the transport of cargo (Kabuta et al., 2009; Smith et al., 2014). Axonal transport defects have been found in SOD1, TDP-43, FUS and C9orf72 related ALS in addition to the mentioned genetic forms that directly affect the machinery (De Vos and Hafezparast, 2017). Taken together, evidence of involvement of motor proteins and cytoskeletal components in ALS implicate axonal transport as a key component in ALS.

1.5.6. Astrocyte toxicity

Astrocytes are a type of glial cell and function as support cells that help to maintain an optimum environment which allows neurons to function correctly. The roles of astrocytes include removal of neurotransmitters from the synapse, removal of metabolic waste,

regulating the formation of synapses and local ion concentrations and supplying metabolites to neurons. Astrogliosis (changes in astrocyte gene expression, structure and function) occurs as a response to CNS damage or injury in a number of neurodegenerative diseases, including ALS. Given their crucial role in maintaining homeostasis in the CNS, it is unsurprising that defects in astrocyte function can result in neuronal toxicity.

Astrogliosis has been shown to occur in the degenerating upper and lower motor neurons of both sALS and fALS patients (Nagy et al., 1994; Schiffer et al., 1996; Stephenson et al., 1991). In addition, astrogliosis has been demonstrated in animal models expressing *TDP-43* ALS-linked mutations as evidenced by an increase in GFAP-positive astrocytes (a marker of reactive astrocytes). It has also been suggested that motor neuron degeneration may be driven by loss of TDP-43 in astrocytes (Yang et al., 2014). Furthermore, the observation that motor neuron degeneration is concomitant with astrogliosis in C9orf72 and FUS ALS mouse models, implicates astrogliosis as an important factor in ALS (Liu et al., 2016b; Sharma et al., 2015). Despite this, astrogliosis presents with certain complexities. For example, in the SOD1^{G37R} and SOD^{G85R} mouse models, astrogliosis occurs before neurodegeneration and progresses alongside disease progression (Bruijn et al., 1997; Wong et al., 1995). However, in the SOD1^{G93A} mouse model (the most widely used model for SOD1), reactive astrocytes develop after motor neuron degeneration (Hall et al., 1998; Levine et al., 1999; Pehar et al., 2018; Vargas and Johnson, 2010). Interestingly, it has been shown that coculture of ALS-associated mutant astrocytes with healthy motor neurons can induce motor neuron degeneration (Haidet-Phillips et al., 2011; Marchetto et al., 2008; Nagai et al., 2007; Qian et al., 2017). Astrocyte activation is also seen in FTD. Translocator protein is an 18 kDa protein that is expressed in activated astrocytes. Studies have shown increased levels of translocator protein in affected brain regions of FTD patients including frontal, prefrontal and hippocampus regions of the brain (Cagnin et al., 2004). Collectively, these studies demonstrate that biological astrocyte changes are associated with motor neuron degeneration and implicate a role for astrocytes in non-cell autonomous motor neuron degeneration.

1.5.7. Neuroinflammation

Neuroinflammation can be triggered in response to injury, degeneration or infection whereby local glia cells (astrocytes and microglia) and circulating immune cells (monocytes, neutrophils and lymphocytes) enter the CNS (McCauley and Baloh, 2019). In ALS, neuroinflammation is characterised by an innate immune response and although the most pronounced feature is activation of astrocytes and microglia (described above), ALS patient post-mortem tissue show T-cell, dendritic cell, macrophages and mast cells (Engelhardt et al., 1993; Graves et al., 2004; Henkel et al., 2013; Holtmaat and Caroni, 2016; Kawamata et al., 1992; Zhang et al., 2011). Despite neuroinflammation being ubiquitous in ALS, it is not fully understood whether neuroinflammation is a secondary consequence of the disease or whether it is contributory or even causative of the disease.

T-cells aid in regulating acquired immune responses to a range of antigens and specific T-cell subpopulations have been shown to contribute to the neuroinflammatory response in ALS by penetrating the CNS during disease progression (Beers et al., 2008; Chiu et al., 2008; McGeer and McGeer, 2002). Indeed, in early stages of disease, CD4+ T-cells have been observed in the spinal cord of SOD1^{G93A} mice and have also been observed at end stage of disease together with CD8+ T-cells (Beers et al., 2008; Chiu et al., 2008; Engelhardt et al., 1993). Furthermore, levels of inflammatory markers such as CD4 and CD8 lymphocytes, neutrophils and CD16 monocytes have been shown to be altered in blood samples from ALS patients (Goldknopf et al., 2006; Murdock et al., 2017; Zhang et al., 2005; Zondler et al., 2016). Concordant with this, fewer Tregs (regulatory T lymphocytes that regulate effector T-cell proliferation and cytokine production), have been found in both ALS patient and animal models (Beers et al., 2017, 2018; Mantovani et al., 2009; Sheean et al., 2018). In ALS mutant mice, the level of Tregs negatively correlated with disease progression and passive transfer of Tregs was able to extend survival (Zhao et al., 2012a). Furthermore, fewer Treg levels were observed in patients in which disease rapidly progressed (Henkel et al., 2013).

Some ALS/FTD-associated genes (*C9orf72*, *PGRN*) are expressed less in neuronal cells when compared to non-neuronal cells such as microglia, whilst other ALS/FTD-linked genes have been thoroughly researched regarding their role in regulation of immune cells function (McCauley and Baloh, 2019). The question of whether mutations in these genes could affect immune cell function and consequently contribute to disease therefore arises. Indeed, mutant SOD1 microglia produce more superoxide, nitric oxide and tumour

necrosis factor alpha (TNFα) that when cocultured with motor neurons cause more damage than functional microglia (Weydt et al., 2004; Xiao et al., 2007; Zhao et al., 2004, 2010). Furthermore, in a coculture of motor neurons and mutant SO1 microglia, NFκB (nuclear factor kappa-light-chain-enhancer of activated B cells) inhibition in SOD1[G93A] mice attenuates the disease by quelling the toxicity of mutant SOD1 microglia (Frakes et al., 2014).

In addition, loss of TBK1 in dendritic cells has been shown to result in an increased inflammatory state as evidenced by activation of CD4 and CD8 T-cells (Xiao et al., 2017). Mutations in *OPTN*, a binding partner of TBK1 have also been implicated in the neuroinflammation pathway. In sALS and fALS patients with *OPTN* mutations, NFκB reactivity is increased (Sako et al., 2012). Furthermore, loss of OPTN has been shown to increase NFκB activity, leading to neuronal degeneration whilst induced cell death can be rescued by OPTN WT (but not mutant) overexpression (Akizuki et al., 2013). Taken together, these lines of evidence implicate a neuroinflammatory mechanism in ALS/FTD.

1.5.8. Defective RNA metabolism

The identification of mutations in the *TARDBP* being causative of ALS highlighted aberrant RNA metabolism as a potential key player in ALS aetiology. *TARDBP* encodes for the RNA binding protein TDP-43. RNA binding proteins have many roles in RNA metabolism including splicing, nucleocytoplasmic transport and storage in stress granules (Mejzini et al., 2019). Since the identification of *TARDBP*, mutations in several genes for RNA binding proteins have been found. These include *FUS*, *EWS*, *TAF15*, *hnRNPA1* and *MATR3* (Johnson et al., 2014c; Kim et al., 2013; Neumann et al., 2011). Details of how defective RNA metabolism may lead to ALS/FTD are outlined below.

1.5.8.1. Splicing

Splicing is performed by the spliceosome and is an important cellular mechanism for the regulated production of splice variants (Chabot and Shkreta, 2016). TDP-43 has an important regulatory splicing role and decreases in TDP-43 has been shown to result in the abnormal inclusion of cryptic exons which results in nonsense mediated decay (Ling et al., 2015). Additionally, loss of TDP-43 in mice leads to defects in neuronal function

and morphology (Yang et al., 2014). Given the similarity in function between TDP-43 and FUS, it is unsurprising that loss of FUS has also been associated with changes in alternative splicing of numerous mRNAs (Lagier-Tourenne et al., 2012). TDP-43 and FUS mislocalise to the cytoplasmic and form aggregates in ALS patients. These cytoplasmic aggregates can sequester other splicing factors (Reber et al., 2016; Wang et al., 2015; Yu et al., 2015). ALS-linked mutations in *hnRNAP2* also causes cytoplasmic aggregation and loss of hnRNAP2 results in alternative splicing and increases nuclear-insolubility (Kim et al., 2013; Martinez et al., 2016)

1.5.8.2. Nucleocytoplasmic transport

Nucleocytoplasmic transport is a process regulated by the GTPase Ras-related nuclear protein (Ran). In this process, Ran facilitates the transport of proteins and RNAs through the nuclear pore complex by regulating the ability of nuclear transport receptors to export or import their cargo (Cautain et al., 2015; Kim and Taylor, 2017). Several lines of evidence now point to nucleocytoplasmic transport as a key pathway in ALS. Firstly, the aggregation of TDP-43 and FUS, a hallmark of ALS. Under basal conditions, both TDP-43 and FUS localise to the nucleus, however, in ALS these proteins are mislocalised to the cytoplasm. In addition, ALS-linked mutations in the nuclear localisation signals of both *FUS* and *hnRNPA1* have been identified (Dormann et al., 2010a; Gal et al., 2011; Liu et al., 2016a). Interestingly, disease severity in these FUS patients have been linked to the degree in which mutations in the FUS nuclear localisation signal affects nucleocytoplasmic transport (Bosco et al., 2010; Dormann et al., 2010a). Furthermore, a rare mutation in the RNA export mediator *GLE1* has been identified in a subset of ALS patients and GLE1 has been found to be a modifier of disease in *Drosophila* models of C9orf72-related ALS (Freibaum et al., 2015; Kaneb et al., 2015). The role of nucleocytoplasmic transport defects in the pathogenesis of C9orf72-related ALS/FTD is described in more detail in Chapter 1.6.

1.5.8.3. Stress granule formation

Stress granules are cytoplasmic, transient ribonucleoproteins that are able to sequester specific mRNAs, preventing their translation. Mutations in RNA binding proteins that have been linked to ALS and FTD often contain prion-like domains which are involved in stress

granule dynamics and formation (Mejzini et al., 2019). It follows that mutations in these genes perturb homeostasis by affecting stress granules formation and transience. Indeed, a toxic gain-of-function may stem from the increased longevity of stress granules as a result of mutations in *TDP-43* and *FUS* (Vance et al., 2013). Furthermore, inclusions of ALS and FTD-linked *FUS* mutations have been shown to be immunoreactive for stress granule markers (Dormann et al., 2010b; Gal et al., 2011). In addition, mutations in the prion-like domain of the RNA-binding proteins *hnRNAP1* and *hnRNAP2* have been shown to drive cytoplasmic inclusions and the formation of stress granules (Kim et al., 2013; Zhang et al., 2018a). The degradation of stress granules relies on autophagy and consequently the lysosome. VCP is an ATPase that has an essential role in autophagy and mutations in *VCP* have been linked to ALS (Ju et al., 2009; Koppers et al., 2012; Tiloca et al., 2012). Unsurprisingly, loss of VCP inhibits the degradation of stress granules and ALS-associated mutations in *VCP* show an increase in stress granules in cell models (Buchan et al., 2013; Uversky, 2017). Collectively, these findings strongly implicate a role of stress granules in ALS.

1.5.9. DNA damage

The DNA damage response involves recognition of DNA damage and subsequent signalling for repair (Walker and El-Khamisy, 2018). This enables neurons to function normally as it prevents the accumulation of genomic instability and consequent neuronal loss (Jackson and Bartek, 2009; Madabhushi et al., 2014). Accumulation of genetic instability can arise from impaired ability to remove reactive oxygen species which can overwhelm the DNA damage response and from the inability to recognise or remove damaged DNA (Mitra et al., 2019; Wang et al., 2013). Single stranded breaks in the DNA duplex due to DNA damage are more common than double stranded breaks. To combat this, cells have rigorous repair mechanisms that involve homologous recombination. Neurons are post-mitotic cells and are therefore inherently homologous recombination-deficient so must rely on non-homologous end joining repair mechanisms which are often susceptible to errors (Walker and El-Khamisy, 2018).

Several ALS-associated proteins have been shown to be involved in double strand break repair. VCP has been shown to interact with proteins involved in non-homologous end joining to regulate the DNA repair pathway and reduction of VCP leads to an increase in

double strand breaks (Acs et al., 2011; van den Boom et al., 2016; Meerang et al., 2011; Singh et al., 2019). Furthermore, DNA damage repair factors are unable to be recruited to sites of DNA damage when levels of VCP are reduced (Acs et al., 2011; Meerang et al., 2011). *FUS*, another ALS-associated gene has been linked to the DNA damage response. Similarly to VCP, depletion of FUS increases DNA damage (Wang et al., 2013). In addition, FUS has been shown to regulate recruitment of histone deacetylases 1 (HDAC1), leading to activation of non-homologous end joining and ALS-linked mutations in *FUS* disturbs double strand break repair (Wang et al., 2013). Finally, mutations in *NEK1* and *C21orf2* (an interactor of NEK1) have been identified as risk factors for ALS (Kenna et al., 2016; Van Rheenen et al., 2016). NEK1 and C21orf2 has a role in repair of double strand breaks and depletion of either NEK1 or C21orf2 results in defects in this repair (Fang et al., 2015; Higelin et al., 2018; Pelegrini et al., 2010). This points toward DNA damage being a mechanism for disease in the ALS/FTD pathway.

To summarise, several intertwining mechanisms are involved in ALS, ALS/FTD and FTD pathogenesis (Figure 1.3 Van Damme et al., 2017). Dysfunction of protein homeostasis is another key mechanism which is described later (see Chapter 1.7.3.3). Many of these mechanisms influence and impact one another, making it difficult to unravel the aetiology of disease and distinguish between primary causes and secondary consequences. The large heterogeneity between patients stemming from the vast number of genetic variants and risk factors also contributes to the difficulty. Mutations in *C9orf72* represent the most common cause of familial ALS/FTD and is involved in many of the mechanisms discussed above. The following section outlines the involvement of C9orf72 in ALS/FTD.
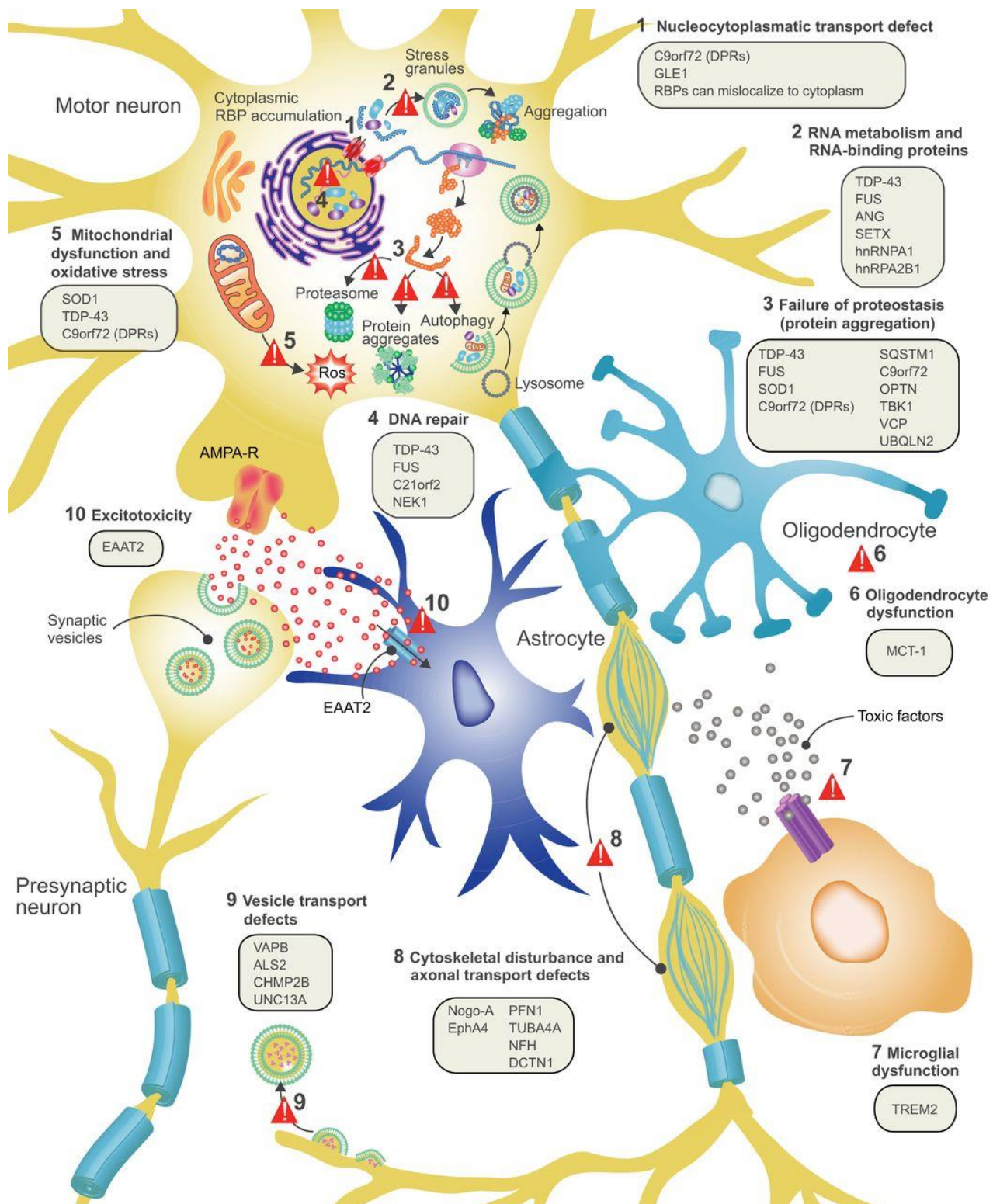
Figure 1.3: Proposed disease mechanisms for ALS/FTD

Proposed disease mechanisms contributing to ALS and FTD aetiology are: (1) Nucleocytoplasmic transport defects. (2) Altered RNA metabolism. (3) Impaired proteostasis with accumulation of aggregating proteins (4) Impaired DNA repair (5) Mitochondrial dysfunction and oxidative (6) Oligodendrocyte dysfunction and degeneration (7) Neuroinflammation. (8) Defective axonal transport (9) Defective vesicular transport. (10) Excitotoxicity receptors. Figure obtained with permission under the Creative Commons Attribution License (Van Damme et al., 2017)

1.6. C9orf72 ALS/FTD

A link between ALS/FTD and chromosome 9 open reading frame 72 (*C9orf72*) was identified in 2006, as a locus on chromosome 9p13.2 – p21.3 by two independent studies (Morita et al., 2006; Vance et al., 2006). Following this, genome-wide association studies isolated the locus as chromosome 9p21 (Laaksovirta et al., 2010; Pearson et al., 2011; Shatunov et al., 2010). Subsequently, in 2011 two independent groups identified a GGGGCC hexanucleotide repeat expansion within intron 1 in of *C9orf72* as causative of ALS/FTD. It is now understood the repeat expansion in *C9orf72* represents the most common cause of familial ALS/FTD (C9orf72-related ALS/FTD termed C9ALS/FTD). Between the two studies, repeat size was characterised as 2 – 23 and 250 – 1600 for unaffected and affected individuals respectively. Difficulties in ascertaining accurate size of the expansion arise due to its size and GC content, somatic instability and repetitive flanking sequences and the threshold for pathogenic repeat size resulting in disease is still unclear (DeJesus-Hernandez et al., 2011; Gijselinck et al., 2016). Further complexities exist surrounding whether age of disease onset correlates with repeat expansion size. Studies have reported positive, negative and no corelation between the two factors (Dols-Icardo et al., 2014; Fournier et al., 2019; Gijselinck et al., 2016). Notably, the positive correlation became insignificant when results were adjusted for age of sample collection. As age of sample collection may influence repeat size, it would be interesting to observe whether the absence and negative correlation remains when adjusted for this factor.

1.6.1. C9orf72 protein

Alternative splicing of *C9orf72* gives rise to three transcript variants, V1, V2 and V3. These variants encode two alternative isoforms; V1 and V3 give rise to a 481 amino acid (aa) isoform termed C9orf72 long (C9orf72L) whereby V2 generates a shorter isoform of 221aa termed C9orf72 short (C9orf72S) (Figure 1.4, Belzil et al., 2013; DeJesus-Hernandez et al., 2011). V2 and V3 have non-coding exon 1A is the 5'-untranslated region (UTR) whereas V1 has non-coding exon 1B as the 5'UTR. Therefore, the repeat expansion is in either the promoter region (V1) or intron 1 (V2 and V3).

1.6.2. C9orf72 is a DENN domain containing protein

Bioinformatic analysis revealed C9orf72 is structurally homologous to Differentially Expressed in Normal and Neoplasia cells (DENN) family (Figure 1.4, Levine et al., 2013). As such C9orf72 was proposed to function as a ras-related protein in brain (Rab) GTPase (referred to as Rab GTPases or Rabs hereon in). The eight families of DENN domains proteins in humans all share the same general tripartite structure; a central DENN domain flanked by upstream and downstream modules (uDENN and dDENN respectively, Figure 1.4) (Levivier et al., 2001; Marat et al., 2011). Several DENN domain containing proteins have been identified that regulate activation of Rab GTPases by functioning as Rab guanine nucleotide exchange factors (Rab GEFs).

Approximately 70 Rab GTPases have been identified in humans; Rab GTPases are a large, conserved family of small GTPases that regulate intracellular trafficking. By interacting with effectors such as motor proteins, tethering factors and phosphatases, Rabs trigger downstream trafficking events (Jean and Kiger, 2012; Kjos et al., 2018; Lürick et al., 2017). The post-translational modification of Rabs with geranylgeranyl makes them functionally active and via the geranylgeranyl group, Rabs reversibly associate with membranes (Anant et al., 1998; Stenmark, 2009). Akin to other small GTPases, Rabs are nucleotide-dependent molecular switches – they cycle between active GTP-bound states and inactive GDP-bound states. Through interaction with guanine nucleotide exchange factors (GEFs), GTPase activating proteins (GAPs) or GDP dissociation inhibitor (GDI), Rab activity is tightly regulated (Guadagno and Progida, 2019; Müller and Goody, 2018). GEFs preferentially interact with GDP Rabs, activating Rabs by catalysing GDP to GTP exchange; in this active state, Rabs are membrane localised and interact with effectors. Interaction of Rabs with GAPs inactivates Rabs by hydrolysing GTP to GDP. GDI facilitates the return of Rabs to the cytosol by solubilising Rabs thereby removing them from the membrane.

As mentioned, since C9orf72 is a DENN domain protein, it was postulated to function as a Rab GEF. Indeed, two independent studies identified C9orf72 as a GEF for Rab GTPases (Sellier et al., 2016; Yang et al., 2016). When in complex with Smith-Magenis syndrome chromosome region, candidate 8 (SMCR8) and WD repeat domain 41 (WDR41), C9orf72 was found to function as a GEF for Rab8a and Rab39b (Sellier et al.,

2016; Yang et al., 2016) and as an effector for Rab1a (Webster et al., 2016). The Rab GEF activity of the C9orf72-SMCR8-WDR41 complex has recently been contested. Cryo-EM of the C9orf72-SMCR8 complex and the Folliculin-Folliculin Interacting Protein 2 (FLCN-FNIP2, a GAP of RagC/D) shows the complexes have structural similarities (Norpel et al., 2021; Shen et al., 2019; Su et al., 2020; Tang et al., 2020; Tsun et al., 2013). A fluorescence GEF activity assay was used to investigate the GEF activity of the C9orf72 complex and found that the C9orf72-SMCR8-WDR41 and the C9orf72-SMCR8 complex did not catalyse the release of N-methylanthraniloyl-GDP from Rab8a or Rab11a, suggesting they do not function as Rab GEFs (Tang et al., 2020). The GAP activity of FLCN is dependent on the R164 residue and sequence alignment demonstrated this corresponds to the R147 residue of SMCR8. Consistent with GAP activity function, the C9orf72-SMCR8 complex but not the C9orf72-SMCR8[R147A] complex displayed GAP activity for Rab8a and Rab11a *in vitro* (Tang et al., 2020). Moreover, the C9orf72-SMCR8-WDR41 and C9orf72-SMCR8 complex has been shown to be a GAP for ARF1 (Su et al., 2020).

A
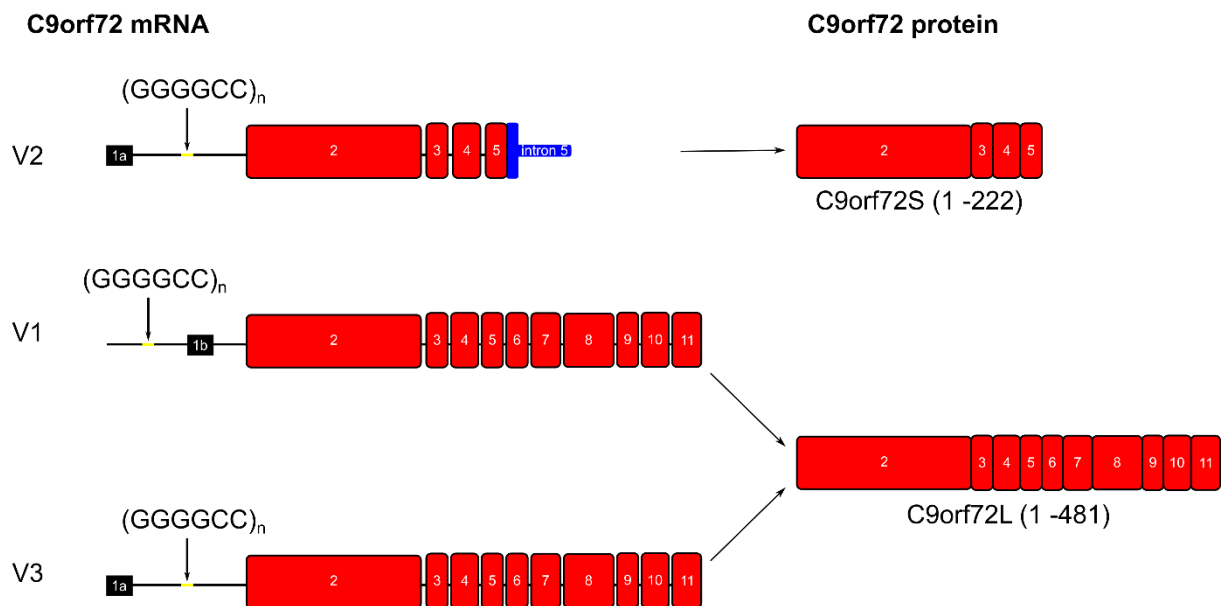
B
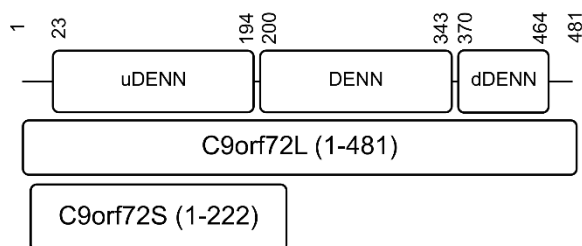
Figure 1.4:C9orf72 is a DENN domain protein that has three transcript variants.

(A) Alternative splicing of the *C9orf72* gene leads to three transcript variants. The location of the $(G_4C_2)_n$ hexanucleotide repeat expansion is shown in yellow. V2 is the shorter transcript, with the 5'-untranslated region (UTR, black) as non-coding exon 1a, exons 2 – 5 (red) and intron 5 partially retained (blue). V1 and V3 have non-coding exon 1b and exon 1a as the 5'-UTR, respectively. Exons 2 -11 are contained in V1, with the repeat expansion located upstream of the 5'-UTR. V3 also contains exons 2-11. The three transcript variants give rise to two putative isoforms of C9orf72, C9orf72S and C9orf72L. The shorter V2 transcript encodes for C9orf72S, a 222 amino acid (aa) protein, whereas V1 and V3 encode for the longer, 481 aa protein C9orf72L. (B) C9orf72 is a DENN domain protein that is predicted to contain three DENN domains. The uDENN (also referred to as longin) domain is N-terminal, the DENN domain is central and the dDenn domain is C-terminal. C9orf72L, the 481 aa protein is predicted to include all three DENN domains, whilst the 222 aa C9orf72S predominantly contains the uDENN domain.

1.6.3. Role in autophagy

Macroautophagy (referred to hereafter as autophagy) is a degradative process in which target proteins are sequestered by an autophagosome (a double membraned vesicle) and subsequently fused with a lysosome to form an autolysosome where degradation takes place (described in detail in 1.7.3.2). The role of C9orf72 in autophagy is as follows – it has been shown to regulate the initiation of autophagy and act as an effector of Rab1a, an autophagy related Rab-GTPase (Webster et al., 2016). During autophagy, LC3-I is lipidated forming LC3-II which is recruited to the autophagosome membrane where it remains until it is degraded in the autolysosome. In cell models where autophagy is both induced and inhibited, control cells exhibit an increase in autophagosomes that is not apparent in C9orf72 depleted cells, suggesting a role for C9orf72 in the initiation of autophagy (Webster et al., 2016). ULK1, FAK family kinase-interacting protein 200 kDa (FIP200) and autophagy-related protein 13 (Atg13) form a complex that regulates autophagy initiation. Phosphorylation of FIP200 and Atg13 by ULK1 activates the complex, allowing translocation to the phagophore assembly site (Ganley et al., 2009; Jung et al., 2009; Kim et al., 2011). The C9orf72-SMCR8-WDR41 complex interacts with the ULK1 initiation complex (Sellier et al., 2016; Webster et al., 2016). Supporting a role of C9orf72 in autophagy initiation, loss of C9orf72 prevented translocation of the activated ULK1 complex to the phagophore thereby impairing autophagy (Webster et al., 2016). SMCR8 is also a DENN domain containing protein and it was found that GEF activity of Rab8a and Rab39b occurs through SMCR8 rather than C9orf72 (Sellier et al., 2016).

The recruitment and activation of Rab-GTPases occurs in a sequential manner, allowing accurate directionality of membrane traffic. Opposing GEF and GAP cascade mechanisms aid in the correct spatial and temporal recruitment of Rabs. In this cascade mechanism, an activated upstream Rab along with its effector recruits the GEF for a downstream Rab. Once activated, the downstream Rab recruits the GAP for the upstream Rab thereby inactivating it (Mizuno-Yamasaki et al., 2012). C9orf72 was found to be an effector of Rab1a and the role of C9orf72 in autophagy initiation is Rab1a-dependent (Webster et al., 2016). A proposed mechanism arises in which Rab1a recruits C9orf72 which forms a complex with its interacting partners WDR41 and SMCR8 and

acts as a GEF through SMCR8 to facilitate translocation of the ULK1 initiation complex to the phagophore and initiate autophagy.

In addition to this, it has been found that phosphorylation of SMCR8 by TBK1 is important for autophagy. Reduced SMCR8 levels lead to impaired autophagy as evidenced by an increased in p62 aggregates (Sellier et al., 2016). This autophagy defect can be rescued by expression of either wild type SMCR8 or a phosphomimetic SMCR8 (Sellier et al., 2016). Furthermore, phosphomimetic SMCR8 was able to rescue the autophagy defect observed upon TBK1 depletion. Finally, it was also observed that the interaction between the C9orf72-SMCR8-WDR41 complex and Rab8a and Rab39b was mediated by p62 and OPTN, two autophagy receptors that together with Rabs, their effectors and kinase regulators initiate autophagy directly at the protein aggregation site. TBK1 has been shown to phosphorylate both p62 and OPTN, supporting this model (Matsumoto et al., 2015; Richter et al., 2016; Wild et al., 2011).

1.6.3.1.   Lysosome defects

Loss of C9orf72 in mouse models results in accumulation of enlarged lysosomes in C9orf72-deficient microglia and macrophages (O 'Rourke et al., 2016; Sullivan et al., 2016). Furthermore, increased levels of autophagy markers p62 and LC3-II have been observed in C9orf72 knockout (KO) mice, suggesting defects in lysosomal clearance (O 'Rourke et al., 2016; Ugolino et al., 2016). Moreover, genes involved in lysosome function were revealed to be enriched when pathway analysis of genes co-expressed with C9orf72 was performed. Evidence from cell models corroborates defective lysosome morphology, revealing swollen lysosomes and perinuclear lysosomal clustering in C9orf72 KO lines generated by CRISPR-Cas9 (Amick et al., 2016). Furthermore, in C9orf72 KO cells, mammalian target of rapamycin complex 1 (mTOR1) signalling due to changes in amino acid availability is compromised (Amick et al., 2016; Ugolino et al., 2016). Through phosphorylation of members of the ULK1 initiation complex, mTOR1 acts as a negative regulator of autophagy (Ganley et al., 2009; Hosokawa et al., 2009; Jung et al., 2009; Kim et al., 2011).

Under basal conditions mTOR translocates to the lysosome surface where it is activated, a process induced by amino acid starvation and is impaired in C9orf72 KO cells. (Amick

et al., 2016; Sancak et al., 2008, 2010). Consistent with this, in both human cell lines and mouse embryonic fibroblasts (MEFs), C9orf72 KO led to decreased phosphorylation of S6 kinase B1, a downstream target of mTOR (Ugolino et al., 2016). Additionally, transcription factor EB (TFEB) levels increased. TFEB is a substrate of mTOR that regulates lysosomal biogenesis and autophagy related genes and its phosphorylation by mTOR inhibits translocation to the nucleus and its subsequent downregulation (Sardiello et al., 2009; Settembre et al., 2011). C9orf72 KO *in vivo* and *in vitro* increased TFEB levels and LAMP1 and LAMP2 (lysosomal-associated membrane protein 1 and 2 respectively), downstream targets of TFEB. Collectively, this suggests loss of C9orf72 leads to defective lysosome morphology and function, impairment of mTOR activation with possible consequences on lysosome biogenesis.

Interestingly, reduced SMCR8 levels have also been implicated in altered mTOR1 signalling (Amick et al., 2016; Lan et al., 2019). SMCR8 KO cells exhibit increased basal mTOR activity and cell size compared to C9orf72 KO or C9orf72 and SMCR8 double KO cells and akin to C9orf72 KO, SMCR8 KO cells display defective mTOR1 signalling response to changes in amino acids (Amick et al., 2016). In contrast, no perinuclear clustering is observed in SMCR8 KO cells. Despite both C9orf72 and SMCR8 KO resulting in defective mTOR1 signalling, KO of both C9orf72 and SMCR8 did not result in defective mTOR1 signalling. Moreover, in C9orf72 and SMCR8 mutant macrophages, mTOR1 signalling was increased as a result of impaired lysosomal degradation (Shao et al., 2019a).

Insertion of an epitope tag on endogenous C9orf72 via CRISPR-Cas9 revealed highly selective localisation of C9orf72 to the lysosome under starvation induced by amino acid depletion. (Amick et al., 2016). In support of a role of C9orf72 at the lysosome, proteomic analysis revealed C9orf72 interacting partners SMCR8 and WDR41 localise to lysosomal membranes (Schröder et al., 2007). Indeed, WDR41 has been shown to be necessary for the recruitment of the C9orf72-SMCR8-WDR41 complex to lysosomes as C9orf72 localisation to lysosomes is abolished in WDR41 knockout cells (Amick et al., 2018). Amick et. al, showed localisation of C9orf72 to lysosomes is restored by expression of WDR41, demonstrating the specificity of the phenotype. Further investigations revealed WDR41 interacts with the cationic lysosomal amino acid transporter PQLC2 through a flexible loop extending from the β-propeller of WDR41 that inserts into a PQLC2 internal

cavity and this interaction mediates the recruitment of the C9orf72-SMCR8-WDR41 complex to lysosomes (Amick et al., 2020; Talaia et al., 2021). Collectively, these findings suggest a role for C9orf72 at the lysosome.

1.6.4. Role in immune system

Knockout animal models have been utilised to study the role of C9orf72. Whilst KO mice do not develop motor neuron defects, several studies have reported impaired immune system related pathology including increased proinflammatory cytokine production, enlarged lymph nodes and splenomegaly, autoinflammation and altered immune cell populations (Atanasio et al., 2016; Burberry et al., 2016; O 'Rourke et al., 2016; Sudria-Lopez et al., 2016). Moreover, heterozygous mice display partial immune-related phenotypes, suggesting C9orf72 haploinsufficiency is sufficient to generate an immune response (Burberry et al., 2016; O 'Rourke et al., 2016). The identification of the peripheral immune cells contributing to the immune phenotype is yet to be determined; however, expression of C9orf72 was determined to be highest in myeloid cells (O 'Rourke et al., 2016). Moreover, loss of C9orf72 in brain microglia resulted in defects in immune response, with the immunological phenotype corroborated by transcriptomics. C9orf72 and SMCR8 double KO mice have increased immune defects compared to the single KO mice (Shao et al., 2019a).

1.6.5. Role at the synapse

Evidence of synaptic defects in models of C9ALS/FTD has begun to carve out a role for C9orf72 at the synapse. Mouse brain subcellular fractionation revealed an enrichment of C9orf72 in the synaptosome (Frick et al., 2018). In accordance, immunohistochemistry for C9orf72 showed pronounced staining in the hippocampal mossy fibre reminiscent of staining patterns for classical presynaptic markers. The presynaptic localisation of C9orf72 is also recapitulated in human iPSC-derived motor neurons whereby C9orf72 colocalises with a small subset of synaptic vesicles, suggesting a transient interaction of C9orf72 with synaptic vesicles (Frick et al., 2018). Furthermore, C9orf72 interacts with all members of the Rab3 family, a family of Rabs abundant in synaptic vesicles and in C9orf72 KO mice, levels of Rab3a are increased in the synaptosome (Frick et al., 2018; Xiao et al., 2019). As C9orf72 is a DENN domain containing protein, further work

exploring the possible role of C9orf72 as a GEF for Rab3 is needed. Other studies have corroborated C9orf72 presynaptic localisation; however, have also shown C9orf72 to localise postsynaptically (Xiao et al., 2019). Postsynaptic loss of C9orf72 resulted in reduced Rab39b and increased GluR1 (glutamate receptor 1) levels, indicating post synaptic C9orf72 and Rab39b may regulate GluR1 levels. Induced motor neurons (iMNs) from C9ALS/FTD patient-derived iPSCs displayed reduced SV2 (synaptic vesicle-associated protein 2) levels, expression of synaptic genes and density of excitatory synaptic contacts (Catanese et al., 2021; Jensen et al., 2020). SV2 forms a complex with other synaptic vesicle proteins whereby it plays a vital role in active zones and synaptic release machinery (Custer et al., 2006). Furthermore, patient-derived cortical neurons also display reduced SV2 levels, pre-synaptic dysfunction and impaired synaptic potentiation (Jensen et al., 2020; Perkins et al., 2021). Moreover, a C9orf72 loss of function zebrafish model that recapitulates the motor defects of ALS/FTD shows reduced synaptic vesicle cycling (Butti et al., 2021). In addition, C9orf72 deficient mice show enhanced synaptic pruning as a result from of loss of C9orf72 in microglia (Lall et al., 2021).

1.6.6. Mechanisms of disease

How the hexanucleotide repeat expansion causes C9ALS/FTD is proposed to occur in three ways (Figure 1.5). Firstly, haploinsufficiency due to loss of function (LOF) of C9orf72 has been proposed, resulting from reduced mRNA transcript levels leading to reduced protein levels (Waite et al., 2014). The two remaining mechanisms constitute a gain of function (GOF). Sequestration of RNA binding proteins by the repeat RNA into RNA foci represents the first mechanism, whilst repeat associated non-ATG (RAN) translation of the repeat expansion into aggregate-prone, toxic DPR represents the second. How these mechanisms conspire to give rise to C9ALS/FTD remains unclear; however, it is thought the mechanisms are not mutually exclusive.

1.6.6.1. RNA toxicity

The rich GC content of the sense $(GGGGCC)_n$ and antisense $(CCCCGG)_n$ transcripts results in highly stable DNA and RNA which has been shown to form atypical secondary structures including R-loops and G-quadruplexes, termed RNA foci (Fratta et al., 2012;

Kovanda et al., 2015; Reddy et al., 2013). Indeed, C9ALS/FTD patient fibroblasts and astrocytes display more abundant G-quadruplex RNA foci compared to controls (Conlon et al., 2016). Through interaction of these RNA foci with RNA binding proteins, impairment of RNA translation, splicing and other events occur (Kumar et al., 2017; McEachin et al., 2020). RNA foci have been detected in several C9ALS/FTD cases, including the brain and spinal cord in patient or animal tissue, peripheral blood and human and patient-derived cell models (Chew et al., 2015; Cooper-Knock et al., 2014a; DeJesus-Hernandez et al., 2011; Lagier-Tourenne et al., 2013; Zu et al., 2013). Whilst foci are predominantly neuronal and nuclear, cytoplasmic foci have been observed in addition to foci in astrocytes, oligodendrocytes and microglia (Cooper-Knock et al., 2015a; Lagier-Tourenne et al., 2013; Mizielinska et al., 2013). Whether a correlation between RNA foci and clinical phenotypes exist remains to be resolved with conflicting studies demonstrating either an inverse or absent correlation between RNA foci and disease onset (DeJesus-Hernandez et al., 2017; Mizielinska et al., 2013). Similarly, it is unclear whether neuropathology correlates with sense or antisense RNA foci, with reports suggesting ALS TDP-43 pathology (nuclear depletion and cytoplasmic mislocalisation) is more evident with antisense foci, as is a correlation between perinucleolar RNA foci and cytoplasmic TDP-43 aggregation (Aladesuyi Arogundade et al., 2019; Cooper-Knock et al., 2015b).

Studies have tried to model RNA toxicity to establish its contribution to ALS aetiology. Injection of either sense or antisense RNA of pathogenic length led to the formation of cytoplasmic RNA foci and motor axon defects in zebrafish (Swinnen et al., 2018). Crucially, DPR proteins were unable to be detected in the sense or antisense RNA injected fish but were detected in fish injected with DPR RNA suggesting toxicity was RNA-mediated and not as a consequence of RNA translation and DPR proteins production. Motor impairments were also observed in mice expressing expanded repeat RNA compared to controls (Chew et al., 2015). However, as DPRs were RAN translated from the repeat, it is unclear whether motor defects occurred from RNA or DPR toxicity. Similar locomotor deficits were observed in *Drosophila* models expressing expanded sense repeat RNA compared to non-expanded sense repeats and controls (Xu et al., 2013). Given DPR generation was not assessed, it remains unclear whether defects were due to RNA or DPR toxicity. Nevertheless, Pur α was identified as an RNA binding protein of repeat RNA. Using an array of techniques, RNA binding proteins ADABR2,

ALYREF, SRSF1, Zfp106, nuceolin and multiple hnRNPs have also been identified as interactors of RNA foci (Conlon et al., 2016; Cooper-Knock et al., 2014b; Donnelly et al., 2013; Haeusler et al., 2014; Hautbergue et al., 2017; Mori et al., 2013a). It is thought sequestration of these RNA binding proteins by repeat RNA foci induce RNA toxicity by decreasing the number of functional RNA binding proteins available.

Pur α has been identified by several groups as an RNA binding protein sequestered by repeat RNAs, particularly CGG repeats and has been implicated in RNA transport (Jin et al., 2007). Whilst the consequences of sequestration of Pur α is unknown, it is possible depletion of functional Pur α arises from the accumulation of repeats that sequester Pur α. Given its role in transport, it is possible this depletion leads to mRNA transport defects and eventual neuronal death. In support of this, overexpression of Pur α reduced RNA foci and attenuated RNA repeat-induced toxicity (Swinnen et al., 2018). SRSF1, a splicing factor that interacts with nuclear export receptor NXF1 to facilitate nuclear export has been shown to be sequestered by RNA repeats. Interestingly, sequestration triggers nuclear export of the repeats through interaction of SRSF1 and NXF1 resulting in RAN translation and DPR toxicity (Hautbergue et al., 2017). Similarly, it has been proposed that binding of ALYREF, an mRNA export adaptor could facilitate the export of repeat transcripts and subsequent RAN translation into DPRs (Cooper-Knock et al., 2014b). Finally, multiple members of the hnRNP family, a family of splicing factors have been identified as sequestered by repeat RNAs (Conlon et al., 2016; Martinez et al., 2016; Mori et al., 2013a). Loss of hnRNPA2 and hnRNP H results in alternative splicing of its targets in C9orf72 patient-derived fibroblasts and motor neurons and patient brains respectively (Conlon et al., 2016; Martinez et al., 2016). Notably, mutations in *hnRNP* have been identified as causative of ALS (Liu et al., 2016a).

1.6.6.2. DPRs

Bidirectional RAN translation of the hexanucleotide repeat expansion in all three reading frames generates five DPRs – glycine/alanine (GA), glycine/proline (GP), glycine/arginine (GR), proline/alanine (PA) and proline/arginine (PR) (see Figure 1.5). DPRs form inclusions in the cytoplasm or the nucleus and are also found in dystrophic neurites (Ash et al., 2013; Mackenzie et al., 2013, 2015; Mann et al., 2013; Mori et al., 2013b; Schludi et al., 2015; Zhang et al., 2014c; Zu et al., 2013). Such DPR inclusions

are p62, ubiquitin positive and TDP-43 negative and are found throughout the CNS in the hippocampus, basal ganglia, frontal cortex, cerebellum and motor cortex and less so in the spinal cord (Ash et al., 2013; Mackenzie et al., 2013, 2015; Mann et al., 2013; Mori et al., 2013b; Schludi et al., 2015). It has suggested that DPR accumulation and the resultant pathology may predate TDP-43 pathology, providing a possible explanation for a lack of TDP-43 positive inclusions (Baborie et al., 2015; Vatsavayai et al., 2016).

DPR inclusions translated from the sense strand (poly-GA, poly-GP and poly-GR) occur more frequently in the hippocampus, cerebellum and neocortical regions whereas DPRs translated from the antisense strand (poly-PR and poly-PA) are more infrequent (Ash et al., 2013; Gendron et al., 2013; Mackenzie et al., 2013, 2015; Mori et al., 2013b, 2013c). Multiple animal models have shown expression of DPRs translated from the hexanucleotide repeat expansion results in neuromuscular junction defects (Freibaum et al., 2015; Perry et al., 2017; Zhang et al., 2015). Mouse models exhibit variability, with one BAC mouse model showing neuromuscular junction denervation whilst intact neuromuscular junctions are observed in other BAC mouse models and mouse models with inducible C9orf72 KO in neuronal and glia cells (Koppers et al., 2015; Liu et al., 2016b; O'Rourke et al., 2015; Peters et al., 2015). In *Drosophila* models, expression of the pathogenic repeat resulted in a reduction in the number of active zones and bouton counts (Freibaum et al., 2015; Perry et al., 2017; Zhang et al., 2015). In accordance, compromised synaptic vesicle release and reduced SV2 levels are observed in cortical neurons expressing GA DPRs (Jensen et al., 2020). Exogenous expression of SV2 rescues the abrogation of synaptic release and GA-induced toxicity. Arginine-containing DPRs have been shown to interact with ribosomal proteins and reduce translation in iPSC-derived motor neurons and *in vivo* (Moens et al., 2019). Expression of eukaryotic translation initiation factor 1A, an essential protein for translation initiation rescues translation defects in poly-GR expressing cells, however this is also accompanied by a reduction in poly-GR (Moens et al., 2019). Others have also demonstrated that arginine-rich DPRs inhibit global translation in addition to binding nucleoli, disrupting nuclear function and phase separation and reducing actin cytoskeleton assembly (Kanekura et al., 2016; Kwon et al., 2014; Radwan et al., 2020; White et al., 2019). Other DPR proteins have been shown to impair nucleocytoplasmic transport and proteasome function has been shown to be impaired by cell-to-cell transmission of poly-GA (Khosravi et al., 2020; Zhang et al., 2016).

1.6.6.3. Haploinsufficiency

C9orf72 LOF arises from the hexanucleotide repeat expansion causing a downregulation of *C9orf72* gene expression. Exploration into possible mechanisms responsible for the reduction in C9orf72 mRNA have primarily focused on epigenetics. One study demonstrated that trimethylated histones bind strongly to the *C9orf72* repeat expansion, but not the non-pathogenic repeats (Belzil et al., 2013). Given trimethylation of histones is known to repress gene expression, this represents a possible explanation for the reduction in *C9orf72* gene expression. Additionally, *C9orf72* gene expression was restored in C9ALS/FTD patient-derived fibroblasts, by treatment with a demethylating agent which resulted in a reduction of C9orf72 binding to trimethylated histones. Furthermore, hypermethylation of both the *C9orf72* repeat expansion and the 5' CpG island located in the C9orf72 promoter region has been reported in several studies (Belzil et al., 2014; Gijselinck et al., 2016; Jackson et al., 2020; Xi et al., 2013, 2015). Methylation of the *C9orf72* promoter has been shown to be neuroprotective and associated with longer survival and *C9orf72* methylation levels positively and negatively correlated with repeat size and age of onset respectively (Gijselinck et al., 2016; McMillan et al., 2015; Russ et al., 2015).

Of the three transcript variants arising from alternative splicing of the *C9orf72* gene, the V1 transcript (that along with V3 gives rise to a 481 aa protein) has been found to express at higher levels in CNS tissue from non-mutation carriers (van Blitterswijk et al., 2015; Rizzu et al., 2016). Post-mortem analysis of C9ALS/FTD patients revealed a decrease in C9orf72 mRNA transcripts in the frontal cortex, cerebellum, motor cortex and spinal cord (Belzil et al., 2013; van Blitterswijk et al., 2015; DeJesus-Hernandez et al., 2011; Fratta et al., 2013; Gijselinck et al., 2012; Rizzu et al., 2016; Waite et al., 2014). Furthermore, a similar reduction in C9orf72 mRNA levels was observed in patient blood samples (Ciura et al., 2013; DeJesus-Hernandez et al., 2011). Comparison of individual transcript levels revealed the V1 transcript to be significantly reduced, whilst V2 is reduced to a lesser extent and V3 appears unaffected (van Blitterswijk et al., 2015; DeJesus-Hernandez et al., 2011; Waite et al., 2014). The repeat expansion is in the promoter region in V1 whereas it is in the first intron in V2 and V3. Therefore,

transcriptional defects may arise in V1 that would not be present in V2 or V3 (Braems et al., 2020).

The questionable specificity of C9orf72 antibodies has complicated the determination of whether C9orf72 protein levels are reduced. Post-mortem analysis revealed a decrease in C9orf72L protein levels in the frontal cortex of *C9orf72* repeat expansion patients, however, no decrease in the cerebellum was detected (Saberi et al., 2018; Waite et al., 2014; Xiao et al., 2015). Furthermore, sensitive, robust mass spectrometry-based quantification of C9orf72 revealed in the frontal cortex of *C9orf72* mutation carriers, C9orf72S was below the detection threshold but C9orf72L was significantly reduced (Viodé et al., 2018). More recent, knockout mouse-validated antibodies revealed a small (20%) decrease in C9orf72L protein levels in the cerebellum of *C9orf72* mutation carriers (Frick et al., 2018). The antibodies in this study did not detect C9orf72S in the cerebellum despite being able to detect both C9orf72L and C9orf72S in HEK293 cells.

Evidence for the contribution of C9orf72 haploinsufficiency to disease comes from a variety of methods including animal models, cell models and human patient samples. *C. elegans* deficient of the C9orf72 orthologue exhibit locomotor defects that are age-dependent and eventually lead to paralysis and degeneration of motor neurons (Therrien et al., 2013). Furthermore, such defects were additive for mutant TDP-43, highlighting both LOF and GOF mechanisms are involved (Therrien et al., 2013). Similar locomotive defects have been observed in zebrafish models whereby the C9orf72 orthologue was knocked down, mediated by morpholinos and resulted in motility defects and axonal deficits (Ciura et al., 2013; Yeh et al., 2018). The wealth of evidence from C9orf72 mouse models largely points to a lack of overt neurodegeneration or motor phenotypes and instead implicates an inflammatory phenotype (Atanasio et al., 2016; Burberry et al., 2016; Koppers et al., 2015; O 'Rourke et al., 2016; Sudria-Lopez et al., 2016; Sullivan et al., 2016). Given complete, but not partial loss of C9orf72 results in an immunological phenotype in mice, it follows that if LOF could be a stand-alone mechanism for disease, C9orf72 patients should be expected to present with an immune phenotype. Whilst an increased prevalence of autoimmune disease has been identified in a single study of a cohort of C9ALS/FTD patients (Miller et al., 2016), as C9orf72 patients tend to exhibit a reduction, but not complete loss of C9orf72, this suggests LOF may not be the sole contributor to disease. Further evidence against a primary LOF mechanism stem from a homozygous C9orf72 patient. A different clinical presentation or an increase in disease

severity compared to heterozygous patients would be expected from a pure homozygous patient. However, no difference in clinical phenotype was observed for a homozygous C9orf72 patient compared to heterozygous (Fratta et al., 2013).

In C9ALS/FTD patient-derived iMNs, the repeat expansion reduced C9orf72 expression and triggered neurodegeneration (Shi et al., 2018). In addition, the iMNs exhibited glutamate excitotoxicity. Given motor neuron survival was rescued by restoring C9orf72, this demonstrates the contribution of C9orf72 haploinsufficiency to disease. However, it must be noted that DPR accumulation also reduced upon expression of C9orf72, which may also contribute to the increase in survival. Furthermore, axonal trafficking defects present in iMNs with the repeat expansion are exacerbated by knocking out C9orf72 (Abo-Rady et al., 2020). Such defects were not present in iMNs from healthy controls in which C9orf72 was knocked out which is suggestive of a synergistic GOF and LOF mechanism.

Whilst the evidence is clear a LOF mechanism alone is not responsible for disease, evidence also exist against a GOF alone mechanism. BAC transgenic mice with a human *C9orf72* repeat expansion do not exhibit neurodegeneration, or only mild symptoms (Jiang et al., 2016; O'Rourke et al., 2015; Peters et al., 2015). Given the presence of RNA foci and DPRs in the CNS of these mice, this suggests that a GOF mechanism alone is insufficient to cause disease. C9orf72 haploinsufficiency has been shown to exacerbate gain of toxicity in C9orf72 mice whereby a reduction or loss of C9orf72 in these mice leads to DPR protein accumulation, motor deficits and hippocampal neuronal loss (Zhu et al., 2020). Another mouse model also showed similar results, with C9orf72 haploinsufficiency exacerbating motor deficits in a dose-dependent manner in C9orf72 BAC and heterozygous crossed mice (Shao et al., 2019b). Additionally, a C9orf72 knock-in rat model consisting of eighty repeats flanked by exons 1a and 1b resulted in a decrease in C9orf72 protein, motor deficits and a loss of spinal motor neurons (Dong et al., 2020).

Overall, evidence points towards a multiple-hit mechanism in which LOF and GOF conspire to cause disease. RNA foci and toxic, aggregate prone DPRs accumulate in neurons as a result of GOF mechanisms. C9orf72 haploinsufficiency then exacerbates disease by impairing clearance of accumulated DPRs. Given the role of C9orf72 in the initiation of autophagy, this is likely due to defective autophagy.
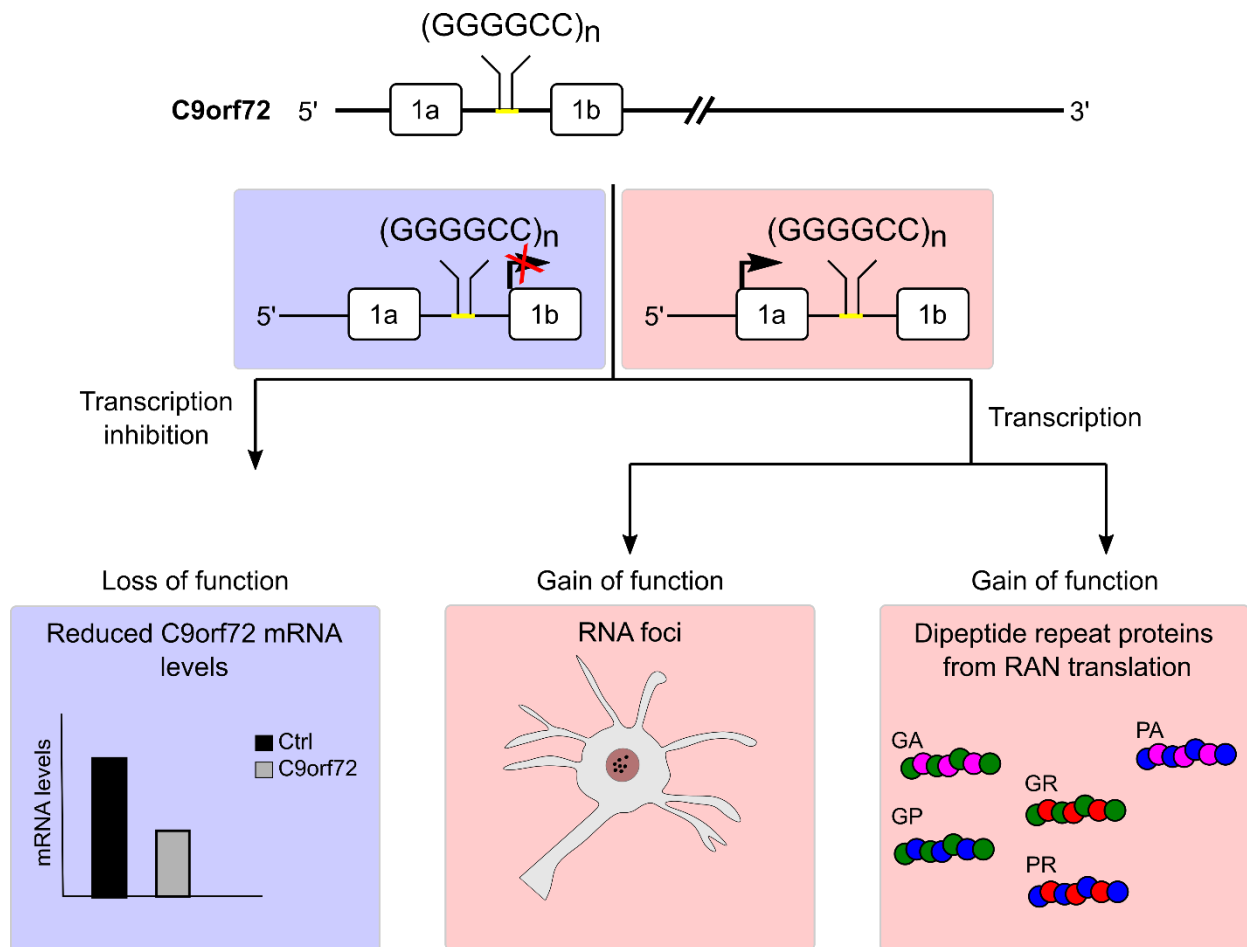
Figure 1.5: Mechanisms of disease for C9orf72.

The GGGGCC hexanucleotide repeat expansion is thought to cause disease through 3 proposed mechanisms. Bottom left: Downregulation of C9orf72 gene expression, leads to reduced mRNA levels. Bottom, middle: Due to the high GC content of the repeat expansion, RNA foci can form that can sequester RNA binding proteins. Bottom right: Bidirectional transcription of the repeat expansion, followed by non-ATG RAN translation gives rise to 5 dipeptide repeat proteins – glycine-alanine (GA, green/purple), glycine-proline (GP, green/blue), glycine-arginine (GR, green/red), proline-alanine (PA, blue/purple) and proline-arginine (PR, blue/red).

1.7. Potential post-translational modification of C9orf72 and SMCR8 that regulate C9orf72 and SMCR8 function

The modification of target amino acids following their translation into proteins by a variety of different functional groups is termed post-translational modifications (PTMs). These functional groups are covalently attached to the protein and in doing so, regulates the functionality of these proteins. Examples of such PTMs include phosphorylation, ubiquitination, SUMOylation and acetylation. Several PTMs can occur at a given time to influence, amongst other things, a proteins structure, localisation and turnover (Didonna and Benetti, 2016; Sambataro et al., 2017). Aberrations in PTM of proteins have been associated with a variety of diseases including Huntington's, Alzheimer's, Parkinson's, cancer and ALS.

1.7.1. Phosphorylation of C9orf72 and SMCR8

Protein phosphorylation in eukaryotic organisms occurs almost entirely on serine, threonine, or tyrosine residues and can act as a modulator of protein-protein interactions, protein localisation and enzyme activity, amongst other things(Sharma et al., 2014). The C9orf72 sequence contains a predicted phosphorylation site at S9 which is flanked by proline residues (PPPSP); the PPPSP motif has been shown to be important for the phosphorylation of the endocytic receptor megalin (Mertins et al., 2016; Sharma et al., 2014; Yuseff et al., 2007). This may suggest that C9orf72 could be phosphorylated at this residue, although the importance of this is unknown. SMCR8 has been shown to be phosphorylated by ULK1 or TBK1 and an SMCR8 phosphomimetic is able to rescue the autophagy defect caused by C9orf72 depletion, suggesting phosphorylated SMCR8 is important for autophagy (Sellier et al., 2016).

1.7.2. Ubiquitination, NEDDylation and protein turnover of C9orf72 and SMCR8

Ubiquitin (Ub) is a small, 8 kDa protein that is highly conserved amongst eukaryotes (de la Vega et al., 2011) The covalent attachment of a ubiquitin molecule onto a target protein is termed ubiquitination. This three-step process involves E1-activating, E2-conjugating and E3-ligating enzymes (Figure 1.6). In the first of the three steps, the C-terminus of ubiquitin is activated in an ATP-dependent manner. This involves firstly the formation of

a Ub-adenylate intermediate that reacts with the catalytic cysteine residue of the E1 enzyme, forming a E1-Ub thiol ester (Kumar et al., 2020; Pickart and Eddins, 2004). The activated ubiquitin is transferred to the active site cysteine residue of the E2 enzyme, forming a thioester bond. In the final step, ubiquitin is covalently attached to the lysine residue of the target protein. Due to the nature of the E2-E3 interaction, substrate specificity is highly controlled as E3 ligases link Ub-loaded E2 and substrate proteins.

The fate of a protein following ubiquitination is dependent on the ubiquitin linkages formed. A single ubiquitin moiety can be added onto a protein; this is known as monoubiquitination. Monoubiquitination has been shown to regulate the stability of proteasomal and ribosomal subunits, subcellular localisation, intracellular trafficking and even the proteasomal degradation of some substrates (Braten et al., 2016; Fukuda et al., 2012; Gupta-Rossi et al., 2004; Jung et al., 2017b; Su et al., 2013). Multi-monoubiquitination or multi-polyubiquitination refers to the addition of single or multiple ubiquitin molecules onto several lysine residues of a substrate protein and has also been shown to target proteins for degradation (Chen et al., 2014a; Rodriguez et al., 2000). Ubiquitin contains seven lysine residues; therefore, a single ubiquitin molecule can be further ubiquitinated through one of its lysine linkages in the same process outlined above. The resultant protein is said to be polyubiquitinated. Polyubiquitinated proteins have been shown to result in a number of different fates including DNA repair, endocytosis, immune response, autophagy and most notably proteasomal degradation and autophagy (see 1.7.3.1 and 1.7.3.2) (Liu et al., 2018; Mukhopadhyay and Riezman, 2007; Tan et al., 2008; Urushitani et al., 2004; Wu et al., 2019).
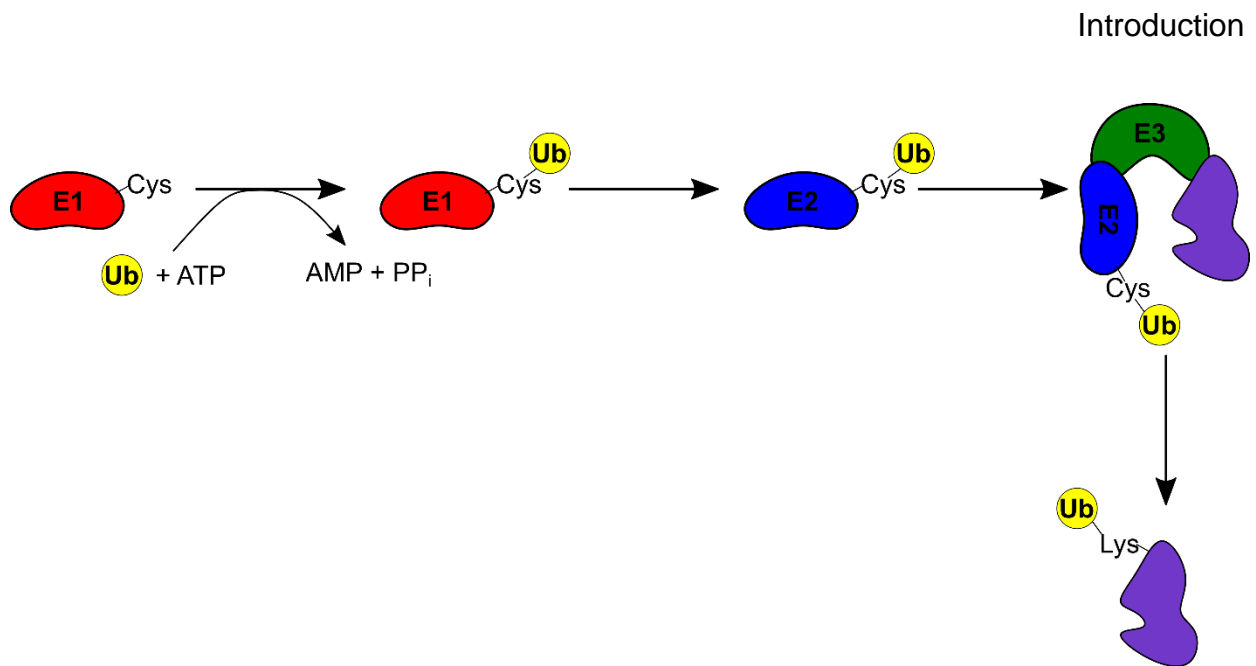
Figure 1.6: Three step ubiquitination process.

Ubiquitin (yellow) is attached to the catalytic cysteine residue (Cys) of the E1-conjugating enzyme (red) in an ATP-dependent manner. Following this, ubiquitin is transferred to the catalytic cysteine of the E2-activating enzyme (blue) and subsequently transferred to the target lysine residue (Lys) of the substrate protein (purple), facilitated by the E3-conjugating enzyme (green).

1.7.2.1.   E3 ligases

There are three classes of E3 ligase: homologous to E6-associated protein C- terminus (HECT), really interesting new gene (RING), and RING-in-between-RING (RBR) E3s (Figure 1.7). The RBR family represent the smallest family of E3 ligases with around 14 members. The general structure of a RBR E3 ligase consists of an in between ring (IBR) domain flanked either side by RING1 or RING2 (Wang et al., 2017a). The E3-ligating mechanism of RBRs has been shown to follow a hybrid between HECT and RING mechanisms (Lazarou et al., 2013; Smit et al., 2012; Wenzel et al., 2011). The recruitment of E2-Ub is performed by RING1; the ubiquitin is then transferred to the catalytic cysteine in RING2. Following this, RING2 conjugates the ubiquitin to the lysine residue of the target protein (Wenzel et al., 2011). Probably the most notable RBR E3 ligase is Parkin, mutations in which can cause familial Parkinson's disease (Kitada et al., 1998; Lazarou et al., 2013). There are approximately 30 members of the HECTs E3 family, making it the second largest family of E3 ligases. The HECT domain is C-terminal and consists of two different lobes – an N-lobe and a C-lobe. The N-lobe is the site for binding the E2-Ub loaded enzyme whilst the C-lobe contains an active site cysteine

residue that receives and passes the ubiquitin from the E2 enzyme (Goto et al., 2021; Wang et al., 2017a). A flexible tether exists between the two lobes which is crucial to allow rotation of the two lobes during the enzymatic reaction. The interaction of the HECT domain with the E2 followed by transfer of the ubiquitin to the C-lobe and the lysine of the target protein attacking the ubiquitin on the C-lobe represent two distinct steps. The RING family of E3 ligases represent the largest family of E3s, with over 600 members in humans. In contrast to HECT E3 ligases, RING E3 ligases do not contain a catalytic cysteine residue and as such catalyses ubiquitination by bringing E2-Ub and the target protein in close proximity, allowing the direct transfer of ubiquitin from the E2-Ub to the substrate protein (Bulatov and Ciulli, 2015; Wang et al., 2017a).

A proportion of the RING E3s are composed of multiple subunits for example the Cullin RING ligases (CRLs). CRLs are modular and are composed of a Cullin backbone (Cul1, 2, 3 4A, 4B or 5), RING finger protein and a substrate recognition protein that is often tethered to the cullin scaffold via an adaptor protein (Figure 1.7). In contrast to Cul1, Cul2, Cul4 and Cul5 which utilise adaptor proteins to recruit specific substrate receptors, Cul3 recruits a Bric-a-brack,Tram-track, Broad complex (BTB) domain-containing proteins that combine the adaptor and substrate receptor functions (Geyer et al., 2003). Members of the Kelch-like (KLHL) family have been identified as substrate binding subunits of the Cul3 (Dhanoa et al., 2013; Shi et al., 2019). KLHLs comprise of a Kelch domain which is important for substrate binding, a linker BACK domain and a BTB domain which binds to Cul3 (Canning et al., 2013; Furukawa et al., 2003; Shi et al., 2019). In addition, as the BTB domain can dimerise, it is able to recruit two Cul3 subunits to the complex. The functional roles of KLHLs are diverse, and KLHLs have been shown to act in complex with Cul3 to targeting proteins for proteasomal degradation (see 1.7.3.1) (Furukawa and Xiong, 2005; Furukawa et al., 2003). The most notable of these is KLHL19 (also referred to as KEAP1) that targets the antioxidant factor Nrf2 for ubiquitination and proteasomal degradation (Furukawa and Xiong, 2005).

CRLs are activated by a process called NEDDylation. Similar to ubiquitination, NEDDylation is a multistep process comprising of three distinct steps and results in the addition of neural precursor cell-expressed developmentally downregulated 8 (NEDD8) to target proteins. NEDDylation involves E1 NEDD8-activating enzyme (NAE), E2 NEDD8-conjugating enzymes and E3 NEDD8-ligating enzymes. NEDD8 is attached to the lysine residue of target proteins through its C-terminal di-glycine (Walden et al.,

2003). In the first step of the process, NAE activates NEDD8 in an ATP-dependent manner and results in the formation of NAE-NEDD8 through the catalytic cysteine residue of NAE (Gong and Yeh, 1999). Following this, NEDD8 is transferred to the catalytic cysteine residue of the E2 NEDD8-conjugating enzyme and subsequently transferred to the lysine of the target protein (Huang et al., 2007). The final step is catalysed by the E3 NEDD8-ligating enzyme. The activation of cullins stimulates the ubiquitination and subsequent degradation of CRL targets (Duda et al., 2008).
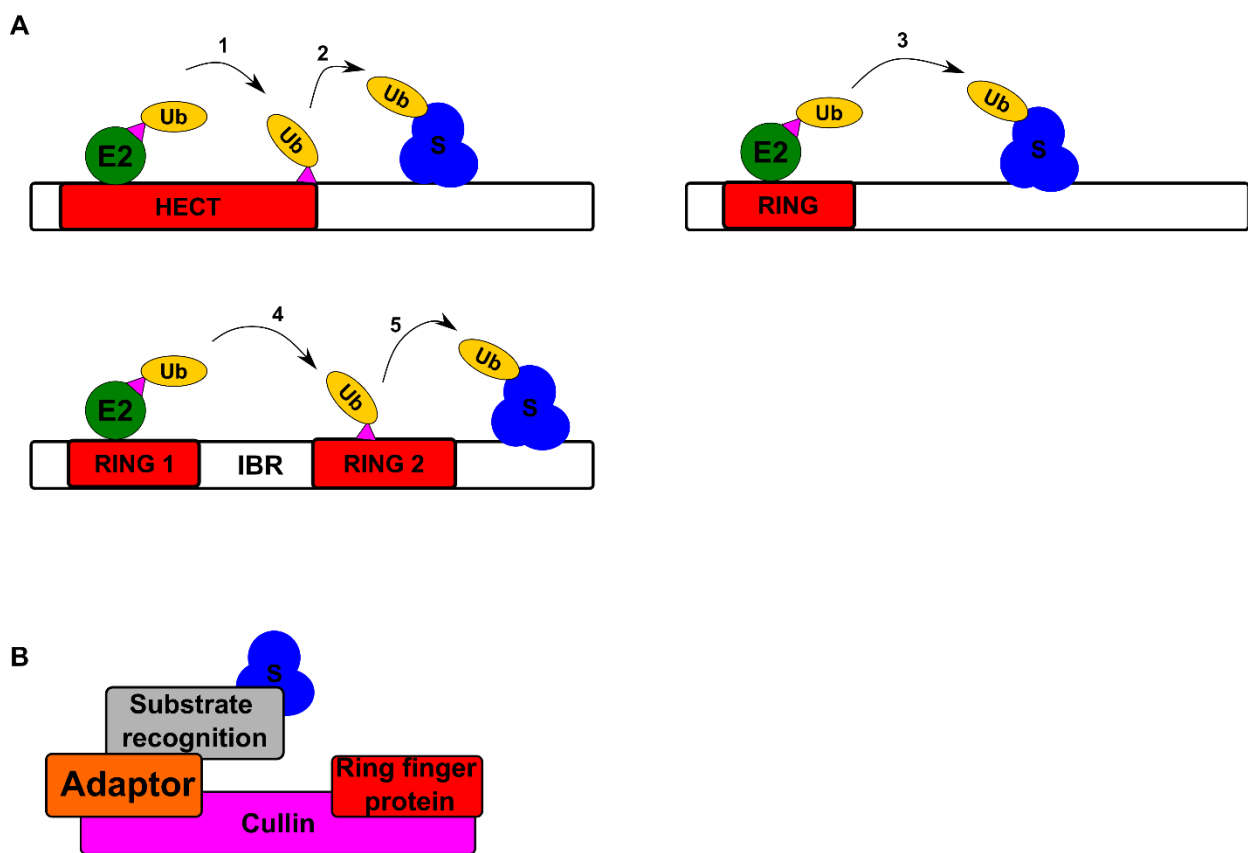
Figure 1.7: General mechanism of action for E3 ligase ubiquitination and the general structure of Cullin ligases.

(A) Top left: HECT E3 ligases contain a HECT domain (red rectangle) that can bind the E2-Ub thioester (green circle and yellow oval, respectively). Ubiquitin is bound to the E2-conjugating enzyme through the enzymes catalytic cysteine residue (purple triangle). The substrate (blue) is also bound to the HECT ligase. Ubiquitin is transferred to the active cysteine residue in the HECT ligase (1) before being transferred to the lysine residue of the target protein (2). Top right: RING E3 ligases contain a RING domain (red rectangle) and binds both the E2-Ub thioester and the substrate. The ubiquitin is transferred directly to the substrate (3). Bottom left: RBR E3 ligase follow a HECT/RING hybrid mechanism. RBR ligases contain two RING domains and an in between ring (IBR) linker. The E2-Ub binds to the RING 1 domain and the ubiquitin is transferred to RING 2 (4). The ubiquitin is then transferred to the substrate (5). (B) The general structure of Cullin ligases (members of the RING E3 ligase family). Cullin ligases contain a cullin scaffold

(purple), to which a ring finger protein (red) and adaptor protein (orange) is bound. A substrate recognition protein (grey) is bound to the adaptor and binds the substrate (blue).

1.7.2.1. Deubiquitinating enzymes

Ubiquitination is a reversible process and the removal of ubiquitin from a substrate is performed by deubiquitinating enzymes (DUBs). There are approximately 100 DUBs in humans, that are categorised in seven distinct families: the largest subfamily are ubiquitin specific proteases (USPs) followed by JAB1/MPN/Mov34 metalloenzymes (JAMMs), ovarian tumour proteases (OTUs), MIU-containing novel DUB (MINDY), ubiquitin C-terminal hydrolases (UCHs), Machado-Josephin domain containing proteases (MJDs) and zinc finger-containing ubiquitin peptidase 1 (ZUP1). These DUBs have several roles ranging from removing ubiquitin from polyubiquitinated proteins and antagonising E3 ligase-mediated ubiquitination to generating free ubiquitin by ubiquitin recycling and processing polyubiquitin precursors into single ubiquitin moieties (Das et al., 2020; Eletr et al., 2014). By cleaving ubiquitin molecules from substrate proteins by hydrolysing the isopeptide bond between ubiquitin and the substrate protein DUBS are important regulators of degradation. The specific lysine residues targeted by DUBs are DUB-dependent, with some DUBs displaying no preference between lysine linkages and others showing preferences for K48 or K63 polyubiquitin chains (Reyes-Turcu et al., 2009). Furthermore, the specificity of DUBs arises from their modular nature, as they contain additional non-catalytic domains to mediate binding with specific linkages, to specific substrates (Eletr et al., 2014).

The PTM of DUBs can regulate their catalytic activity, subcellular location, stability and interaction with partner proteins. USP14 is a regulator of the proteasome whereby association with the proteasome directly increases its activity (Leggett et al., 2002). Moreover, USP14 preferentially deubiquitinates substrates destined for proteasomal degradation that are ubiquitinated at multiple sites and S432 phosphorylation of USP14 increases DUB activity in the proteasome and is required for regulating proteasome activity (Lee et al., 2016; Xu et al., 2015). Interestingly, USP14 also regulates autophagy by regulating Beclin 1 ubiquitination (Xu et al., 2016). The USP8 enzyme contains a microtubule interacting domain that is required for localisation to endosomes and stabilisation of its interacting partner STAM (Row et al., 2007). S680 phosphorylation of USP8 is necessary for its localisation as a S680A mutant is restricted to nuclear localisation whereby it cannot interact with 14-3-3 protein (Row et al., 2006). The ubiquitination of ATXN3 at K117 and SUMOylation at K166 enhances its catalytic activity

and stability respectively (Todi et al., 2010; Zhou et al., 2013b). DUBs have a range of substrates and as such, it is unsurprising that many DUBs have been implicated in disease (Lim et al., 2020).

1.7.3. Functional roles of ubiquitination

Ubiquitination of target proteins has many functional consequences, with one of them being degradation. The two main degradative pathways in eukaryotes are the ubiquitin proteasome system and autophagy (summarised in Figure 1.8).

1.7.3.1.   The ubiquitin proteasome system

The ubiquitin proteasome system (UPS) is the primary pathway for the degradation and clearance of proteins. The pathway consists of two steps – ubiquitination (outlined in 1.7.1 above) and proteolytic degradation, which is carried out by the 26S proteasome. The 26S proteasome is a macromolecular complex comprised of the 20S core particle and the 19S regulatory particle (Voges et al., 1999). The barrel structure of the core particle is composed of four rings stacked together – two inner β-subunit rings and two outer α-subunit rings. Proteolytic sites reside in the core particle with caspase-like, trypsin-like and chymotrypsin-like activity (Bard et al., 2018; Davis et al., 2021). Proteasomal substrates are recognised by the 19S regulatory particle, which assists in unfolding the protein and delivering it to the 20S core particle for degradation. Through forming a narrow channel that can only be opened by the 19S regulatory particle, the N-terminal α-subunits of the 20S core particle act as barriers, making access to the internal degradation chamber highly controlled. Substrate proteins ubiquitinated through K48 linkages are often targeted to the proteasome, making K48 the canonical proteasomal degradation signal (Jacobson et al., 2009).

1.7.3.2.   Autophagy

The second pathway that exists for protein degradation in eukaryotic cells is autophagy. Autophagy stems from Greek, literally means "self-eating" (auto = self, -phagy = eating)

and broadly consists of three main types – microautophagy, chaperone-mediated autophagy (CMA) and macroautophagy. Mitophagy (the selective degradation of mitochondria) is also a type of autophagy but will not be discussed here. Briefly, microautophagy involves non-selective lysosomal degradation in which cytoplasmic cargo is directly engulfed by autophagic tubes (see Li et al., 2012 for review). The main functions of microautophagy include membrane homeostasis and cellular survival under nitrogen starvation. CMA involves heat shock cognate protein of 70 kDa (hsc70), a cytosolic chaperone protein which recognises a specific motif in substrate proteins and targets them for lysosomal degradation by binding to LAMP2A (Dice, 1990; Nedelsky et al., 2008). Following translocation of the substrate into the lysosome, the substrate protein is degraded. Macroautophagy (hereafter referred to simply as autophagy), is a highly conserved process among eukaroytes and maintains cellular and protein homeostasis routinely in cells or as a response to cellular stresses such as starvation (Ramesh and Pandey, 2017). The main targets for autophagic degradation are soluble proteins, insoluble protein aggregates, and organelles and ubiquitinated proteins. Three distinct steps – initiation, elongation and maturation/degradation make up the process of autophagy. ULK1, ATG13, and FIP200 form the autophagy initiation complex and under nutrient-rich conditions, mTOR regulates autophagy by inactivation of this complex (Kim et al., 2011). Together with the PI3K complex (Vps34, Beclin-1 (BECN1) and p150), the autophagy initiation complex regulates the formation of the phagaphore, the precursor to the autophagosome. Lipidation of cytoplasmic light chain 3 (LC3) by phosphatidylethanolamine (LC3-I → LC3-II) result in recruitment of LC3-II to the phagaphore. Elongation of the phagophore engulfs cytoplasmic substrates and forms a double membraned vesicle termed an autophagosome to which LC3-II is membrane bound, allowing detection of LC3-II as a marker of autophagosome formation (Rubinsztein et al., 2012; Tanida et al., 2008). Finally, fusion of the autophagosomes with lysosomes to form an autolysosome releases the lysosomal degradative enzymes which degrade the sequestered target proteins. Given the critical role of the UPS and autophagy in the clearance of proteins, protein aggregates, and misfolded protein it is unsurprising that dysfunction of either pathway is associated with many diseases, including ALS and FTD (see 1.7.3.3).
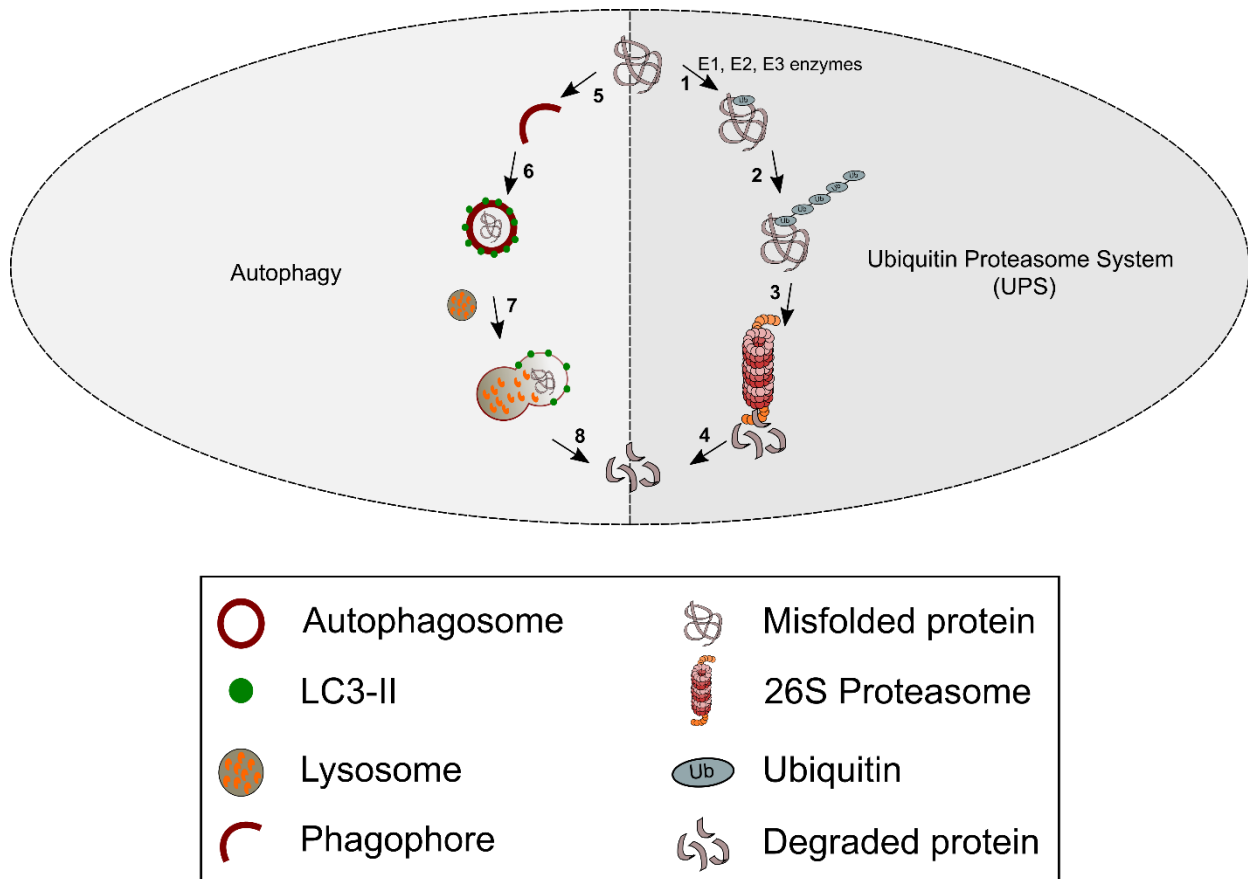
Figure 1.8:Summary of the ubiquitin proteasome system (UPS) and autophagy

Key steps in the ubiquitin proteasome system pathway (1 – 4). Through a cascade reaction involving E1-activating, E2-conjugating and E3-ligating enzymes, a ubiquitin protein is added onto the substrate (1). The ubiquitin can be further ubiquitinated, forming a polyubiquitinated chain (2). The polyubiquitin chains acts as a signal for proteasome-mediate degradation and the substrate is translocated to the 26S proteasome (3), where it is degraded (4). In autophagy, following initiation the phagophore elongates (5) and engulfs the target protein (6) forming an autophagosome. Fusion of the autophagosome with the lysosome (7) releases the lysosomal degradative enzymes which degrade the protein (8).

1.7.3.3. Dysfunction in protein homeostasis

Protein homeostasis is vital for ensuring cell survival and maintenance. It involves the correct balance between protein synthesis and protein degradation. Ubiquitinated, cytoplasmic protein inclusions are a key hallmark of ALS/FTD pathology (see Chapter 1.3) and suggests impaired protein homeostasis. The two main pathways for protein degradation in eukaryotic cells are the UPS and autophagy.

A wealth of evidence implicates several familial and sporadic ALS/FTD genes and proteins in proteasome dysfunction and disease pathogenesis. Firstly, mutations in *UBLQN2* which encodes for ubiquilin 2, a protein with a fundamental role in the UPS pathway are associated with ALS/FTD and X-linked ALS (Deng et al., 2011; Teyssou et al., 2017; Zhang et al., 2014b). Ubiquilin 2 facilitates the degradation of proteins via the UPS by binding polyubiquitinated proteins and delivering them to the proteasome. Accordingly, ALS-linked mutants of ubiquilin 2 impair this function and result in accumulated polyubiquitinated proteins due to proteasome binding and substrate delivery deficiencies (Chang and Monteiro, 2015). Moreover, ubiquilin 2 has been found to transport heat shock protein 70 (HSP70)-bound cargo for proteasomal degradation and mutations in *UBQLN2* impede binding to HSP70 and subsequent proteasomal degradation (Hjerpe et al., 2016). Similarly to ubiquilin 2, VCP has been shown to facilitate proteasomal degradation by delivering substrates to the proteasome (Dai and Li, 2001; Wójcik et al., 2004). Mutations in *VCP* that are linked to ALS have been shown to impair proteasome complex binding and cause TDP-43 pathology (Barthelme et al., 2015).

ALS-associated mutant SOD1 is an additional protein that has been shown to impact proteasomal degradation. Mutant SOD1 directly interacts with a component of the proteasome complex, possibly hindering proteasomal degradation in various ALS models (Cheroni et al., 2009; Kabashi et al., 2004; Urushitani et al., 2002). Additionally, SOD1^{G93A} mice exhibit a downregulation in proteasome subunit expression (Marino et al., 2015). Like SOD1, mutant VAPB has been shown to interact with a component of the proteasome together with stimulating ubiquitinated aggregate formation and accumulation of proteasomal substrates (Moumen et al., 2011). In addition to the fALS cases described above, dysfunctional proteasome homeostasis has also been observed

in sALS. Indeed, motor neurons from sporadic patients exhibit reduced proteasome function and activity (Kabashi et al., 2012).

Aside from the UPS, autophagy represents the other main degradative pathway and is essential for neuronal health. Indeed, neuronal specific ablation of vital autophagy genes leads to neurodegeneration in mice and the accumulation of cytoplasmic aggregates (Hara et al., 2006; Komatsu et al., 2006). Furthermore, inducing autophagy in ALS-associated SOD1 mice prolongs survival (Hetz et al., 2009). Several other genes involved in regulation of autophagy have been implicated in ALS/FTD including *C9orf72* (see 1.6.3). Optineurin is an autophagy receptor containing a ubiquitin binding domain. ALS-linked mutations of *OPTN* have been identified in this domain, alluding to a defect in substrate delivery to the autophagosome due to inability to bind to the substrate (Maruyama et al., 2010). *SQSTM1* encodes for p62, another autophagy receptor. p62 contains a LC3 interacting region (LIR) that facilitates delivery of substrates to the autophagosome by binding to the developing phagophore via LC3 (Pankiv et al., 2007). The ALS-mutated LIR (SQSTM1^{L341V}) is defective in LC3 recognition, implicating autophagy in ALS/FTD pathogenesis. Defective retrograde transport may lead to the accumulation of autophagosomes. The dynein-dynactin complex (which facilitates retrograde transport) regulates neuronal autophagosome transport and ALS-linked mutations in *DCTN1* cause aggregation of dynactin (Levy et al., 2006; Maday et al., 2012). Furthermore, disruption of the dynein-dynactin complex leads to impaired autophagic clearance with loss of DCNT1 resulting in the impaired transport and accumulation of autophagosomes (Ikenaka et al., 2013; Ravikumar et al., 2005).

Finally, in addition to the ALS and ALS/FTD genes, FTD genes and proteins have been implicated in dysfunctional protein homeostasis. For example, PGRN (for which mutations represent the most common cause of familial FTD) regulates the lysosomal pathway and its deficiency leads to abnormal lysosome morphology (Elia et al., 2019; Tanaka et al., 2017). Furthermore, TMEM106B, a risk factor for FTD is involved in lysosomal trafficking (Schwenk et al., 2014; Stagi et al., 2014). Reduced TMEM106B expression disrupts lysosomal trafficking and causes impaired degradation of autophagic cargo (Lüningschrör et al., 2020). Moreover, *CHMP2B* mutations are causative of FTD and rare cases of ALS and mutant CHMP2B impairs autophagy and leads to autophagosome accumulation (Filimonenko et al., 2007; Lee et al., 2009). Collectively

this wealth of evidence implicates proteosome dysfunction as a key player in ALS aetiology.

1.7.4. SUMOylation of C9orf72 and SMCR8

Bioinformatics suggests that C9orf72 may be SUMOylated. Insertion of the C9orf72 protein sequence into SUMOylation prediction software gives rise to three potential lysine residues as SUMO sites (see Table 5.1). As the name suggests, small ubiquitin-like modifier (SUMO) is a ubiquitin-like protein that is highly conserved across eukaryotes. There are three different paralogs - SUMO1, SUMO2 and SUMO3 and as SUMO2 and SUMO3 share 97% sequence similarity, they are often referred to as SUMO2/3 (Mahajan et al., 1997; Matunis et al., 1998). Similarly to ubiquitination, SUMOylation of proteins has a variety of different functions and have been implicated in transcription regulation, DNA repair and protein degradation, amongst others (Lee et al., 2015b; Rott et al., 2017; Sun et al., 2020a; Widago et al., 2012). The SUMOylation pathway is a multiple-step pathway that involves E1-activating, E2-conjugating and E3-ligating enzymes. Post-translation, SUMO is non-functional and must first be modified by SUMO proteases that remove a C-terminal residue to expose a di-glycine (GG) motif. The GG motif of mature SUMO is attacked by the conserved cysteine residue of the heterodimeric E1-activating enzyme (SAE1/UBA2) in an ATP-dependent reaction, forming a thioester (Desterro et al., 1997, 1999). Following this, activated SUMO is transferred to the catalytic cysteine in Ubc9, the sole SUMO E2-conjugating enzyme, forming another thioester. Interestingly, Ubc9 can directly transfer SUMO to the lysine of target proteins, in an E3 ligase-independent manner (Gareau and Lima, 2010). Nevertheless, E3-ligating enzymes facilitate the formation of an isopeptide bond between the lysine of that target substrate and SUMO. Similar to ubiquitination, this is achieved via 2 main strategies. Recruitment of the substrate and the E2-SUMO by E3-ligases to form a complex represents the first method and enhancing the conjugation of the E2 enzyme by coordinating an optimal conformation for SUMOylation is the second (Reindle et al., 2006; Reverter and Lima, 2005; Yunus and Lima, 2009). In the former, substrate specificity is due to E3-substrate interactions whilst the latter it is imparted by the E2 ligase. Like ubiquitination, SUMOylation is a reversible process, and the removal of SUMO is performed by SUMO proteases. In contrast to ubiquitination, these proteases have dual roles, firstly in the maturation of the SUMO precursor and secondly in the deconjugation of SUMO. There are around 6 sentrin SUMO-specific proteases (SENPs) in humans. A summary of the different enzymes involved in ubiquitination and SUMOylation is presented in Table 1.2.

Functionally, SUMOylation of substrate proteins has been shown to result in a variety of functions and SUMOylation itself is necessary for development. Knockout of the SUMO E2-conjugating enzyme Ubc9 in mice has been shown to be lethal, with mice dying at the early post implantation stage (Nacerddine et al., 2005). In addition, PML nuclear bodies and nucleoli are disrupted in cells in which Ubc9 has been depleted (Nacerddine et al., 2005). SUMOylated proteins have been implicated in numerous processes including nucleocytoplasmic localisation, proteasome-mediated degradation, mitotic chromosome assembly and disease (Lee et al., 2015b; Pelisch et al., 2014; Waltersa et al., 2021) . SUMOylation of TDP-43 regulates its splicing activity, localisation and recruitment to stress granules (Maraschi et al., 2021). Senataxin (mutations in which have been linked to juvenile ALS) has been shown to be SUMOylated and when SUMOylated is involved in genome stability, SG disassembly and degradation of RNA (Bennett and La Spada, 2021; Hecker et al., 2006). Furthermore, both mutant and wild type SOD1 is SUMOylated which increases its aggregation and stability (Fei et al., 2006). Mutant SOD1 aggregation can be inhibited by inhibiting K75 SUMOylation (Dangoumau et al., 2016).

The motif Ψ-K-x-D/E (Ψ is a hydrophobic residue, K the SUMO acceptor lysine, x is any amino acid and D/E is aspartic/glutamic acid) has been identified as a SUMO consensus motif, whereby proteins containing the motif are likely to be SUMOylated (Sampson et al., 2001). Proteins with this motif can directly interact with the Ubc9-SUMO complex and as such may regulate the interaction between the substrate and SUMO by influencing its stability (Sampson et al., 2001). In addition, extended SUMO consensus motifs have been identified (Ψ-K-x-D/E-x-x-S-P) in which phosphorylation of nearby serine residues are a prerequisite to SUMOylation or enhances SUMO conjugation (Hietakangas et al., 2003, 2006; Mohideen et al., 2009). Similarly, a negatively charged SUMOylation motif has been identified that enhances SUMO conjugation (Yang et al., 2006). However, numerous SUMOylated proteins have been identified in which the SUMOylated residue is a non-consensus lysine (Hendriks et al., 2018).

Table 1.2: Summary of the different enzymes involved in ubiquitination and SUMOylation in humans

	Ubiquitin	SUMO
E1-activating enzyme	UBE1 and UBE1L2	Single E1-activating enzyme (SAE1/UBA2)

E2-conjugating enzyme	~30	Single E2-conjugating enzyme (Ubc9)
E3-ligating enzyme	Over 600	~7
Deubiquitinating/DeSUMOylating enzyme	Ubiquitin specific proteases and ubiquitin C-terminal hydrolyases	SENP1, SENP2, SENP3, SENP5, SENP6, SENP7

In addition to the covalent interaction between SUMO and its substrates, SUMO can interact non-covalently with proteins bearing a stretch of hydrophobic residues with the general sequence V-I/V-I/V/-V (Minty et al., 2000; Song et al., 2004). This sequence is termed a SUMO interacting motif (SIM). The interaction between SUMO and proteins containing a SIM can be regulated by other PTMs such as phosphorylation and acetylation and it is possible for the SIM-SUMO interaction to be paralog specific (Stehmeier and Muller, 2009; Ullmann et al., 2012). For example, the SIM of the transcriptional coregulator Daxx binds to SUMO1 and phosphorylation promotes affinity towards this SUMO paralog (Chang et al., 2011; Lin et al., 2006). Furthermore, the SUMO-SIM interaction can mediate protein-protein interactions, the distribution of proteins and enhanced SUMOylation of proteins by Ubc9-SUMO has been found for proteins containing a SIM (Kim et al., 2009; Mahajan et al., 1997; Matunis et al., 1998). RanGAP1 can be nuclear pore complex-associated where its SUMOylated form binds to RanBP2 or cytosolic (Mahajan et al., 1997). Mutations that inhibit RanGAP1 SUMOylation result in inhibiting targeting to the nuclear pore complex (Matunis et al., 1998). The SIM of the Srs2 DNA helicase of *Saccharomyces cerevisiae* has two different functions - firstly, it mediates its SUMOylation by binding to SUMO through its SIM and secondly it bind to SUMOylated PCNA (Kolesar et al., 2012). The two different functions have antagonistic effects as SUMOylation of Srs2 reduces the Srs2 SIM-PCNA SUMO interaction and the Srs2 SIM-PCNA SUMO interaction disfavours SUMOylation (Kolesar et al., 2012).

1.8.   Hypothesis and aims

The most common genetic cause of familial ALS and FTD is a GGGGCC hexanucleotide repeat expansion in the C9orf72 gene. The C9orf72 protein is a DENN-domaining containing protein that has been shown to have roles at the synapse and in the immune system. Additionally, C9orf72 has been shown to be involved in the initiation of autophagy and regulating the trafficking of Rab GTPases. Reduced C9orf72 mRNA levels resulting in haploinsufficiency (a LOF mechanism) alongside two GOF mechanisms – RNA toxicity and toxic, aggregate-prone DPRs have been proposed as the disease-causing mechanisms of C9ALS/FTD. Several lines of evidence now point towards haploinsufficiency as a disease modifier, exacerbating toxic GOF mechanisms. Such evidence includes the observation that a reduction in C9orf72 exacerbates DPR accumulation in mice expressing a pathogenic repeat (Zhu et al., 2020). Moreover, reduced C9orf72 levels impairs autophagy and subsequently the clearance of DPRs, which leads to the toxic accumulation of DPRs (Boivin et al., 2020).

Given the possible role of haploinsufficiency in disease, we therefore hypothesised that restoring C9orf72 levels may be of benefit for C9ALS/FTD patients by restoring autophagy and consequently aiding in the clearance of DPRs. Therefore, the overarching aim of my PhD was to characterise the molecular pathways involved in C9orf72 turnover.

My objectives were:

- To identify the pathway(s) involved in turnover of C9orf72
- To identify key enzymes involved the turnover of C9orf72
- To investigate whether C9orf72 levels can be altered by manipulating levels of key enzymes involved in C9orf72 degradation
- To investigate how complex formation with SMCR8 affects C9orf72 stability

2. Materials and methods

2.1. Cell culture

2.1.1. Cell lines

HEK293, HEK293 C9orf72 knockout (KO), Hela and Hela C9orf72 KO cells were cultured in a 37°C, 5% CO_2 atmosphere. All cells were cultured in Dulbecco's Modified Eagle's Medium (DMEM, Sigma-Aldrich) supplemented with 10% fetal bovine serum (FBS, Labtech) and 1 mM sodium pyruvate (Sigma-Aldrich).

The HEK293 C9orf72 KO and HeLa C9orf72 KO cell lines were produced and characterised in-house by Dr Christopher Webster using CRISPR-Cas9 guide RNA transfection and subsequent selection by puromycin. The HEK293 KO and HeLa KO cell lines were sequenced by Dr Yolanda Gibson and Dr Chris Webster respectively.

2.1.2. PEI DNA transfection

Cells were seed such that they were 70-80% confluent on the day of transfection. All plasmid DNA used for transfection (Table 2.3) was purified as per 2.2.4. A pCI-neo vector was used as an empty vector (EV) control in all transfection experiments. Transfection mix was prepared in OptiMEM (Gibco, Life Technologies) using a 1:3 (w/v) ratio of plasmid DNA to polyethylenimine (PEI) (1 mg/ml, pH 6.8; PolySciences). The total amount of DNA was equal to 1% of the total volume of transfection mix (Table 2.1). All cells were transiently transfected according to the manufacturer's protocol. The PEI/OptiMEM mix was vortexed and incubated at room temperature (RT) for 5 minutes to give mix B. Mix A consisted of the DNA/OptiMEM mix. Following the addition of mix B to mix A, the transfection mix was vortexed, incubated at RT for 20 minutes and then added to cells dropwise. The transfection media was removed and replaced with fresh DMEM 6 hours post transfection. Cells were maintained at 37 °C in a 5% CO_2 incubator for 24 hrs post-transfection before being used for experimentation.

Table 2.1: PEI transfection reagents

Dimension of plate	DNA per well (µg)	PEI per well (µl)	OptiMEM/DNA volume (µl)	OptiMEM/PEI volume (µl)
10 cm² plate	10	30	500	500
6 well plate	2	6	100	100
12 well plate	1	3	50	50
24 well plate	0.5	1.5	25	25

2.1.3. Lipofectamine2000 DNA transfection

Cells were seeded such that they were 70-80% confluent on the day of transfection. All plasmid DNA used for transfection (Table 2.3) was purified as per 2.2.4. Transfection mix was prepared in OptiMEM (Gibco, Life Technologies) using a 1:2 (w/v) ratio of plasmid DNA to Lipofectamine2000 (Invitrogen). The total amount of DNA was equal to 1% of the total volume of transfection mix (Table 2.2). All cells were transiently transfected according to the manufacturer's protocol. The Lipofectamine2000/OptiMEM mix was vortexed and incubated at room temperature (RT) for 5 minutes to give mix B. Mix A consisted of the DNA/OptiMEM mix. Following the addition of mix B to mix A, the transfection mix was vortexed, incubated at RT for 20 minutes and then added to cells dropwise. The transfection media was removed and replaced with fresh DMEM 6 hours post transfection. Cells were maintained at 37 °C in a 5% CO_2 incubator for 48 hrs post-transfection before being used for experimentation.

Table 2.2: Lipofectamine2000 transfection reagents

Dimension of plate	DNA per well (µg)	Lipofectamine 2000 per well (µl)	OptiMEM /DNA volume (µl)	OptiMEM/Lipofectamine2000 volume (µl)
10 cm² plate	10	20	500	500
6 well plate	2	4	100	100
12 well plate	1	2	50	50

| 24 well plate | 0.5 | 1 | 25 | 25 |

Table 2.3: List of plasmid DNA for PEI/Lipofectamine2000 transfection

Name	Backbone	Host	Resistance	Source
EGFP	PEGFPc2	DH5α	Kan	Clontech
EGFP-USP8	pEGFPc1	DH5α	Kan	Donated by Prof Sylvie Urbé
EGFP-USP8 C786A	pEGFPc1	XL10 Gold	Kan	In house mutagenesis (Dr Emma Smith)
Empty vector (EV)	pCIneo	DH5α	Amp	Promega
HA-Ubiquitin	pRK5-HA	DH5α	Amp	Addgene 17608
Myc-C9orf72L	pRK5	DH5α	Amp	In house (Prof Kurt De Vos)
Myc-C9orf72L	pCIneo	XL10 Gold	Amp	In house (Prof Kurt De Vos)
Myc-C9orf72L K14R	pCIneo	XL10 Gold	Amp	In house mutagenesis (Dr Chris Webster)
Myc-C9orf72L K388R	pRK5	XL10 Gold	Amp	In house mutagenesis (see 2.2.1)
Myc-C9orf72L K83R	pRK5	XL10 Gold	Amp	In house mutagenesis (Amber Morgan)
Myc-C9orf72L K90R	pRK5	XL10 Gold	Amp	In house mutagenesis (Amber Morgan)
Myc-C9orf72L SIM	pRK5	XL10 Gold	Amp	In house mutagenesis (Dr Chris Webster)
SMCR8-Myc/DDK	pCMV6entry-myc/DDK	DH5α	Kan	Origene
Ubc9	pcDNA3	DH5α	Amp	Donated by Dr Chun Guo

YFP	pcDNA3	DH5α	Amp	Donated by Dr Chun Guo
YFP-SUMO1	PEYFPc1	DH5α	Kan	Donated by Dr Chun Guo
YFP-SUMO1 ΔGG	PEYFPc1	DH5α	Kan	Donated by Dr Chun Guo
YFP-SUMO2/3	PEYFPc1	DH5α	Kan	Donated by Dr Chun Guo
YFP-SUMO2/3 ΔGG	PEYFPc1	DH5α	Kan	Donated by Dr Chun Guo

2.1.4. siRNA transfection

Cells were seeded such that they were 70-80% confluent 4 days post transfection. Small interfering RNA (siRNA) (10 µM, Table 2.4) was obtained from Sigma Aldrich and prepared in nuclease free water (Qiagen) from a 100 µM stock. Transfection mix was prepared using a 1:1 (v/v) ratio of siRNA to Lipofectamine RNA iMax (Invitrogen). The total amount of siRNA was equal to 1.2% of the total volume of transfection mix (Table 2.5). All cells were transiently transfected according to the manufacturer's protocol. The RNA iMax/OptiMEM mix was vortexed and incubated at RT for 5 minutes to give mix B. Mix A consisted of the siRNA/OptiMEM mix. Following the addition of mix B to mix A, the transfection mix was incubated at RT for 20 minutes and then added to cells dropwise. The transfection media was removed and replaced with fresh DMEM 6 hours post transfection. Cells were maintained at 37 °C in a 5% CO_2 incubator for 4 days post-transfection before being used for experimentation.

Table 2.4: List of siRNA sequences

Oligo	Targeted sequence 5' → 3'
Non targeting control	Mission universal negative control #1
USP8 RNAi-1	TGAAATACGTGACTGTTTA
USP8 RNAi-2	GGACAGGACAGTAGATATT
KLHL9 RNAi-1	GGGCACAAGAATGGAGATCTT

KLHL9 RNAi-2	ATGGATGCAGGTTGCATCATT
KLHL13 RNAi-1	GCTGCCAGTTTCCTACAGATT
KLHL13 RNAi-2	AACGGCAGTTGATACAGTCTT
SMCR8 RNAi-1	GCCATTAATGAAGAAGAATT
SMCR8 RNAi-2	CCCAATTCCTAAAGTGTTATT

Table 2.5: siRNA transfection reagents and volumes

Dimension of plate	siRNA volume per well (µl)	OptiMEM/siRNA volume (µl)	OptiMEM/RNA iMAX volume per well (µl)
6 well plate	2.4	100	100
12 well plate	1.2	50	50
24 well plate	0.6	25	25

2.2.   Cloning

2.2.1. Site-directed mutagenesis

Mutagenesis primers designed using the QuikChange primer design program (Agilent) were purchased from Integrated DNA Technologies (Table 2.6). Mutagenesis was performed according to the manufacturers' protocol. In brief, 75 ng plasmid DNA template and 125 ng of forward and reverse primer was amplified using a thermocycler. The following parameters were used: 1 cycle (95 °C, 2 mins), 18 cycles (95 °C, 20 s; 60 °C, 10 s; 68 °C, 30 s/kb plasmid length) to melt dsDNA, anneal primers and elongate respectively. Parental DNA template was digested using *Dpn* I enzyme (37 °C, 5 mins) before transformation of the resulting plasmid DNA into ultracompetent XL-10 Gold cells as per 2.2.2. All constructs were sequenced to confirm the correct insertion of the mutation (Core Genomic Facility, Sheffield) and the trace data visualised using FinchTV software.

Table 2.6: List of mutagenesis primers

Construct	Primer sequence (5' → 3')	Reverse primer sequence (5' → 3')
C9orf72L K388R	GATAAGCCAGGTCTCAGCTGAA AGACCTGATCCAGG	CCTGGATCAGGTCTTTCAGCTG AGACCTGGCTTATC

2.2.2. Transformation of DNA

Transformation was performed according to the manufacturer's protocol. Approximately 5 ng of plasmid DNA was added to 25 µl of either competent DH5α or ultracompetent XL-10 Gold cells. In the case of XL-10 Gold cells, an additional 1 µl of β-mercaptoethanol per 25 µl of cells was added. Cells were incubated for 30 mins at 4 °C followed by heat shock at 42 °C for 30 s. Cells were incubated at 4 °C for 2 mins prior to the addition of 975 µl of LB Broth (Fisher Scientific) and incubation at 37 °C with constant agitation. Cells were then plated onto pre-warmed LB selection plates (Ampicillin, 100 µg/ml, Melford; Kanamycin, 50 µg/ml, Sigma Aldrich) as appropriate and grown at 37 °C overnight.

2.2.3. Glycerol stock preparation

Transformed bacteria was grown in 5 ml LB Broth overnight at 37 °C with constant agitation. Glycerol stocks were prepared using a 1:1 ratio of bacteria broth and 50% glycerol (Sigma Aldrich). Following thorough mixing, the stocks were stored at -80 °C.

2.2.4. Bacterial culture and purification of plasmids

Onto the appropriate LB selection plates (Ampicillin, 100 µg/ml, Melford; Kanamycin, 50 µg/ml, Sigma Aldrich) a small amount of glycerol stock was streaked. Starter cultures consisting of a single colony in 1 ml LB broth with the appropriate antibiotic added was grown for 8 hrs at 37 °C with constant agitation. To 5 ml of LB broth, 100 µl of the starter culture and the appropriate antibiotic was added and grown overnight at 37 °C with constant agitation. Plasmids were purified using the Macherey-Nagel NucleoSpin

Plasmid Miniprep kit according to the manufacturer's protocol. In brief, bacteria were pelleted by centrifugation (4000 x g, 20 mins) prior to resuspension in A1 buffer. Following this, the bacteria were lysed using alkaline/SDS lysis by the addition of A2 buffer (RT, 5 mins). The lysis buffer was neutralised by the addition of A3 buffer before pelleting the bacterial debris by centrifugation (11,000 x g, 10 min). Following transfer of the supernatant to a silica membrane spin column, the DNA was washed once in AW buffer, centrifuged (11,000 x g, 1 min) and washed once in A4 buffer before centrifugation (11,000 x g, 1 min). Spin columns were dried by centrifugation (11,000 x g, 2 min) prior to the addition of AE buffer and incubation at RT for 1 min. DNA was eluted into new collection tubes by centrifugation (11,000 x g, 1 min). The concentration of DNA was determined using a Nanodrop ND-1000 spectrophotometer.

2.3.   Protein biochemistry

2.3.1. Protein harvesting

Cells were washed once in phosphate-buffered saline (PBS; NaCl, 137 mM; KCl, 2.7mM; KH_2PO_4, 1.5 mM; Na_2HPO_4, 8 mM). Cells were incubated in trypsin-EDTA at 37 °C for 5 mins prior to quenching with DMEM. Cells were pelleted (17,000 x g, 1 min) prior to washing in PBS and centrifuged (17,000 x g, 1 min). Cell pellets were lysed at 4 °C for 20 mins in either radioimmunoprecipitation assay (RIPA; Tris-HCl, pH 6.8, 50 mM; NaCl, 150 mM; EDTA, 1 mM; EGTA, 1 mM; SDS, 0.1%; Triton X-100, 1%; 1X protease inhibitors) or Britton-Robinson 80 (BRB80; PIPES, 80 mM, pH 6.8; EDTA, 1 mM; $MgCl_2$, 1 mM; IPEGAL, 1%; NaCl, 150 mM). Following this, the supernatant was pelleted at 4°C by centrifugation (17,000 x g, 1 min). The protein concentration was determined as in 2.3.2.

2.3.2. Determination of protein concentration

Protein concentrations were determined by Bradford assay. Bradford reagent (Biorad) was diluted 1:5 in distilled water. Bovine serum albumin (BSA, Sigma Aldrich) was diluted to 1 mg/ml in Bradford reagent. Serial dilutions of the BSA solution were performed to

give a range of known concentrations. The BSA serial dilutions served as the standard. Samples were diluted 1:500 in Bradford reagent. The absorbance of the BSA standards and samples were determined at 595 nm using a S1200 diode array spectrophotometer (Biochrom) with Bradford reagent serving as the blank. In the presence of protein, a change in colour from red to blue is observed in the Bradford reagent, which corresponds to a shift in maximum absorbance from 470 nm to 595 nm. As the amount of protein is proportional to the change in colour, the amount of protein in a sample can be determined by the absorbance at 595 nm. A standard curve was constructed using the BSA absorbance values and the protein concentration in the samples determined from the gradient of the standard curve using the equation below.

$$protein\ concentration = absorbance\ x\ gradient\ x\ diution\ factor$$

2.3.3. Immunoprecipitation

When transfection was required, cells were seeded such that they were approximately 70% confluent on the day of transfection. Alternatively, for endogenous proteins cells were harvested when they were 100% confluent. The following day, cells were washed once in PBS prior to addition of either RIPA or BRB80 lysis buffer at 4°C. Cells were scraped and lysed at 4°C for 1 hr, with rotation before being pelleted (17,000 x g, 1 min). Protein concentration was determined as per 2.3.2. A stock of 1 µg/µl of lysates in 1X laemmli (60 mM Tris-HCl, pH 6.8; 2% SDS; 10% glycerol; 5% β-mercaptoethanol; 0.01% bromophenol blue) was reserved for input samples. 0.5 – 1 mg of lysate was incubated in 1 – 2 µg of antibody for 16 hrs at 4°C with constant rotation. The primary antibody was captured on 20 µl of Protein G magnetic Sepharose beads (GE Helathcare) for 2 hrs at 4°C with constant rotation. Alternatively, Protein G Sepharose fast flow beads (GE Healthcare) washed with the lysis buffer was used. The beads were centrifuged (3000 x g, 30 s), the supernatant removed and the beads washed 3 times in lysis buffer. Protein was eluted from the beads in 40 µl of 2X laemmli (120 mM Tris-HCl, pH 6.8; 4% SDS; 20% glycerol; 10% β-mercaptoethanol; 0.02% bromophenol blue). In the case of FLAG-tagged constructs, immunoprecipitation was performed using anti-FLAG magnetic agarose beads (Sigma-Aldrich). Samples were then analysed via SDS-PAGE and immunoblot (see 2.3.4).

2.3.4. Sodium dodecyl sulfate polyacrylamide gel electrophoresis (SDS-PAGE) and immunoblot

Protein samples were incubated for 5 mins at 100 °C to denature proteins. Proteins were separated according to size using a polyacrylamide gel. Depending on the size of the protein of interest being studied, the resolving gel chosen was between 7.5 – 15%. Precision plus protein standards all blue ladder (Biorad) was loaded alongside the samples to determine the molecular weight of the protein samples. A mini-PROTEAN tetra cell (Biorad) filled with running buffer (192 mM glycine, 25 mM Tris, 0.1% SDS) was used to run the gels at 100 V until samples were resolved. Following separation proteins were transferred to a nitrocellulose membrane at 30 V for 16 hrs (GE Healthcare), using the mini trans-blot cell (Biorad) filled with transfer buffer (192 mM glycine, 25 mM Tris, 20% methanol). To confirm successful transfer, membranes were stained with reversible Ponceau S (0.1% Ponceau S, 5% acetic acid) and the stain removed by washing with distilled water.

Membranes were blocked in blocking buffer (TBST, 20 mM Tris-HCl, pH 7.5; 137 mM NaCl; 0.1% TWEEN-20; dried milk, 5%) for 1 hr at RT with shaking. Membranes were incubated in primary antibody (Table 2.7) in blocking buffer for 1 hr at RT with constant roation. Following 3 x 10 mins washes in TBST, membranes were incubated in secondary antibody (Table 2.8) in TBST for 1 hr at RT. Membranes were washed for a further 3 x 10 mins in TBST prior to detection. For detection, membranes probed with HRP were incubated in enhanced chemiluminescence solution (ECL, Thermo Fisher) consisting of a 1:1 dilution of luminol and peroxide solutions for 3 mins. Imaging was then performed on either Syngene G:box (Syngene) or Odyssey CLx imaging system (Licor).

2.3.5. Drug treatments

Stocks of Bafilomycin A1 (Sigma Aldrich) and MG132 (Sigma Aldrich) were prepared by solubilising the lyophilised powder in water. To assess the involvement of specific pathways, cells were treated with Bafilomycin A1 (100 nM) or MG132 (5 µM) for varying times. Stocks of cycloheximide (Sigma Aldrich) were prepared by solubilising the

lyophilised powder in ethanol. Cells were treated with cycloheximide (20 µg/ml) to inhibit protein translation. To inhibit Cullin NEDDylation, cells were treated with MLN4924 (Sigma Aldrich, 1 µM) from a prepared stock of MLN4924 in DMSO. A stock of N-Ethylmaleimide (NEM, Sigma Aldrich) was prepared in ethanol and added to lysis buffer (20 mM) to prevent deSUMOylation of proteins. Samples were harvested and analysed via SDS as per 2.3.1, 2.3.3 and 2.3.4 respectively).

Table 2.7: List of primary antibodies used for immunoblotting.

Antibody	Species	Dilution	Source
Actin	Mouse	1:5000	Millipore MAB1501
C9orf72	Rabbit	1:1000	ProteinTech, 25757
C9orf72	Rabbit	1:250	Santa Cruz sc-138763
C9orf72	Rabbit	1:250	ATLAS HPA023873
C9orf72	Mouse	1:1000	Genetex GTX632041
Cyclin D1	Rabbit	1:1000	Abcam ab134175
FLAG (M2)	Mouse	1:2000	Sigma Aldrich
GAPDH	Rabbit	1:1000	Cell signalling 14C10
GFP (JL8)	Mouse	1:5000	Clontech 632381
HA	Rabbit	1:1000	Sigma Aldrich H6908
HA7	Mouse	1:1000	Sigma Aldrich H9658
LC3	Rabbit	1:1000	Novus Biological NB100-2220

Myc (9B11)	Mouse	1:2000	Cell signalling 2276S
SMCR8	Rabbit	1:1000	Bethyl Laboratories A304-694A
Tubulin	Rabbit	1: 8000	Abcam ab4074
USP8	Rabbit	1:1000	ATLAS, HPA004869

Table 2.8: List of secondary antibodies used for immunoblotting.

Antibody	Species	Dilution	Source
Anti-mouse IgG (H+L) coupled to horseradish peroxidase	Goat	1:5000	Dako
Anti-mouse IgG (L) coupled to horseradish peroxidase	Goat	1:10 000	Dako
Anti-rabbit IgG (H+L) coupled to horseradish peroxidase	Goat	1:5000	Dako
Anti-rabbit IgG (L) coupled to horseradish peroxidase	Goat	1:10000	Dako
Anti-mouse IgG coupled to IRDye680	Donkey	1:5000	Licor
Anti-mouse IgG coupled to IRDye800	Donkey	1:5000	Licor
Anti-rabbit IgG coupled to IRDye680	Donkey	1:5000	Licor
Anti-rabbit IgG coupled to IRDye800	Donkey	1:5000	Licor

2.4.   RT-qPCR

2.4.1. RNA extraction

RNA was extracted from cells using TRIzol (Life Technologies) according to the manufacturers' protocol. Briefly, cells were incubated in TRIzol at RT for 5 mins prior to the addition of chloroform (Thermo Fischer) in a 1:5 ratio of TRIzol to chloroform with vigorous mixing. Following incubation at RT for 3 mins, cells were pelleted (17,000 x g, 15 mins) at 4°C. RNA was precipitated from the aqueous phase by the addition of isopropanol and incubation at RT for 10 mins. Following centrifugation (17,000 x g, 10 mins) at 4°C, the RNA pellet was washed in 75% ethanol before subsequent centrifugation (7500 x g, 5 mins). The pellet was air dried at RT for 10 mins before resuspension in nuclease free water. The resuspended pellet was incubated at 60°C for 10 mins and the concentration determined using a Nanodrop Spectrophotometer.

2.4.2. cDNA synthesis

1 µg of RNA was resuspended in 1 X DNase buffer (NEB) and the reaction volume made up to 9 µl using nuclease free water. Contaminating genomic DNA was removed by the addition of 1 µl of DNase 1 followed by incubation at 37°C for 10 mins. The enzyme was heat inactivated at 75°C for 10 mins by the addition of EDTA (Amnsesco; 2.5 mM). cDNA was synthesised using qScript cDNA mastermix (Quanta bio). The mastermix consists of a reaction buffer containing optimised concentrations of $MgCl_2$ and dNTPs alongside recombinant ribonuclease inhibitor protein, qScript reverse transcriptase, titrated concentrations of random hexamer and oligo(dT) protein primers and enzyme stabilisers and performance enhancing additives. 4 µl of mastermix was added to the RNA sample and made up to a total volume of 20 µl in nuclease free water. cDNA was synthesised in a thermocycler with the following parameters: 1 cycle (5 mins, 25 °C), 1 cycle (30 mins, 42°C) and 1 cycle (5 mins, 80°C).

2.4.3. RT-qPCR

Primer specific mastermixes were prepared using forward and reverse primers (Table 2.9), 1 X HOT FIREpol Eva green qPCR Mix (Solis Biodyne) and nuclease free water.

Prior to their addition in the mastermix, stock primers were reconstituted in nuclease free water to 100 µM and stored at -20 °C until needed. cDNA was diluted to 10 ng/µl in nuclease free water. To 9 µl of the primer specific mastermix, 1 µl of diluted cDNA was added. Reactions were performed in triplicate in a CFX96 touch real-time PCR thermocycler (BioRad). The following conditions were used: 1 cycle (95 °C, 5 mins), 39 cycles (95 °C, 30 s; 60 °C, 1 min); 1 cycle (95 °C, 1 min; 65 °C, 30 s), 60 cycles (starting at 65 °C with a 0.5 °C increase per cycle). The initial 95 °C step denatures the dsDNA and is followed by 39 cycles of denaturation and annealing. The final melt curve step with an incremental 0.5 °C increase ensures single products are produced. Data was analysed using BioRad CFX Manager software and mRNA levels determined using the ΔΔCt method (Livak and Schmittgen, 2001).

Table 2.9: List of primers for RT-qPCR.

Gene	Forward primer (5' → 3')	Reverse primer (5' → 3')	Conc. (nM)
KLHL9 #1	AGGAGGAGTTTTGAGGCAGC	GGTAACGGGGAGCATCCATT	125
KLHL9 #2	TGTCTGAACCTGGTGCTTCC	CTGGAGGTGGGGGATGTAGA	125
KLHL13 #1	GCAGGACCTACACGCATCTT	GGCATCAGGGTCACATCACA	125
KLHL13 #2	CGAAATGGGCCTCTCATCCC	TCCTTCAAGTCGAAGCTGGT	125
GAPDH	GGGTGGGGCTCATTTGCAGGG	TGGGGGCATCAGCAGAGGGG	300

2.5. Bioinformatics for the prediction of potential ubiquitination/SUMOylation sites

Online software was utilised to predict potential ubiquitination and SUMOylation sites in C9orf72 and SMCR8. The C9orf72 protein sequence was inserted into UbPred (http://www.ubpred.org/), a ubiquitination predictor that utilises a database consisting of 266 non-redundant, experimentally verified ubiquitination sites to predict putative lysine

residues with a high/medium/low confidence score. Following this site-directed mutagenesis was used to mutate the high and medium hits. Similarly, for SUMOylation prediction, the GPS SUMO web server (http://sumosp.biocuckoo.org/) was utilised which utilises group-based prediction alongside Particle Swarm Optimisation to predict possible SUMOylation sites (Zhao et al., 2014). The C9orf72 and SMCR8 protein sequence was inserted into GPS SUMO to give the predicted position and predicted peptide of the SUMOylation or SIM (SUMO interacting motif) site, the predicted score and its corresponding cut off value.

3. Investigating protein turnover of C9orf72

3.1.　　　Introduction

The most common genetic cause of ALS/FTD is due to a GGGGCC hexanucleotide repeat expansion in the first intron of the *C9orf72* gene. Although it is unknown how C9ALS/FTD arises, evidence points towards both loss of function and gain of function mechanisms. Several lines of evidence implicate C9orf72 haploinsufficiency in disease. Firstly, reduced C9orf72 mRNA levels have been found in patient post-mortem tissue and blood samples (Belzil et al., 2013). Further, loss of C9orf72 mimics the p62 pathology seen in C9ALS/FTD patients (Webster et al., 2016) and reduced C9orf72 levels results in reduced basal levels of autophagy (Sellier et al., 2016; Webster et al., 2016). This suggests that a reduction in autophagy due to C9orf72 haploinsuffiency may contribute towards disease. The lack of neurodegeneration seen in C9orf72 knockout models suggest that haploinsufficiency alone is not sufficient to cause disease (Koppers et al., 2015; Peters et al., 2015; Sudria-Lopez et al., 2016).

Aggregate-prone, DPRs formed from RAN translation of the repeat expansion have been detected in post-mortem tissue of C9ALS/FTD patients (Ash et al., 2013; Mori et al., 2013b) and have been shown to cause toxicity in a number of *in vitro* and *in vivo models* (Lee et al., 2017; May et al., 2014; Swinnen et al., 2018). Emerging evidence indicates that C9orf72 haploinsufficiency may exacerbate DPR toxicity, possibly due to reduced autophagy and clearance of DPRs (Boivin et al., 2020; Zhu et al., 2020). Collectively, this suggests that C9orf72 haploinsufficiency is a disease modifier that may contribute to and worsen disease by acting synergistically with the toxic gain of function DPRs. Given this, restoring C9orf72 levels may be beneficial for patients and represents a possible therapeutic avenue for C9ALS/FTD.

Protein homeostasis is fundamental in order to maintain the correct balance between protein synthesis, protein trafficking and protein degradation. In doing so, steady state levels of proteins are tightly regulated. Protein degradation is achieved via two main pathways – the UPS and autophagy. Determining the degradation pathway for a protein allows for exploration into modifiers of that pathway. Therefore, this chapter focuses on investigating the turnover of C9orf72. Antibodies for detecting endogenous C9orf72 were

optimised and the stability of the C9orf72-SMCR8 complex was investigated. The involvement of the UPS or autophagy in C9orf72 and SMCR8 degradation was explored.

3.2. Endogenous C9orf72 antibody optimisation

Until recently, the availability of commercial antibodies to detect endogenous C9orf72 were lacking due to their uncertain specificity. The first steps were therefore to optimise the commercially available antibodies for their ability to detect endogenous C9orf72. In order to do this, lysate from HEK293 and HEK293 C9orf72 KO cells (hereafter C9orf72^{KO}) were separated and probed via SDS-PAGE and immunoblot. Four different commercially available antibodies were used to detect endogenous C9orf72. The Santa Cruz, ProteinTech and Genetex antibodies were able to detect endogenous C9orf72 as evidenced by the band present at 50 kDa in the HEK293 cells that is absent in the C9orf72^{KO} cells (Figure 3.1A) demonstrating the binding was specific to C9orf72. The Genetex antibody gave more bands at higher molecular weights. These bands were aspecific to C9orf72 as they were present in both HEK293 and HEK293 C9orf72^{KO} cells. The ATLAS antibody was unable to detect endogenous C9orf72 as no bands could be seen at 50 kDa. As a control for antibody detection, the three antibodies were also used to detect overexpressed C9orf72. C9orf72 has three transcript variants that give rise to two putative isoforms - C9orf72 long (C9orf72L, 50 kDa) and C9orf72 short (C9orf72S, 25 kDa). Both transcript variants were used a positive control. All three antibodies were able to detect both C9orf72L and C9orf72S (Figure 3.1B), providing further evidence the ATLAS antibody was unable to detect endogenous C9orf72.

The ProteinTech antibody was selected to optimise further owing to the greater proportion of aspecific bands from the Genetex antibody and as the Santa Cruz antibody was no longer commercially available. The incubation temperature and the antibody concentration were optimised. To do this, lysate from HEK293 and C9orf72^{KO} cells were separated via SDS-PAGE and probed via immunoblot. Varying concentrations of the ProteinTech antibody were used for either 1 hr at RT or 16 hrs at 4 °C. Endogenous C9orf72 was detected with all three antibody concentrations (Figure 3.1C). Specificity was confirmed by the presence of a band at 50 kDa in the HEK293 cells that were not present in the C9orf72^{KO} cells. Incubation in antibody overnight gave more aspecific bands. Overall, both the Genetex and the ProteinTech antibody can reliably detect endogenous C9orf72.
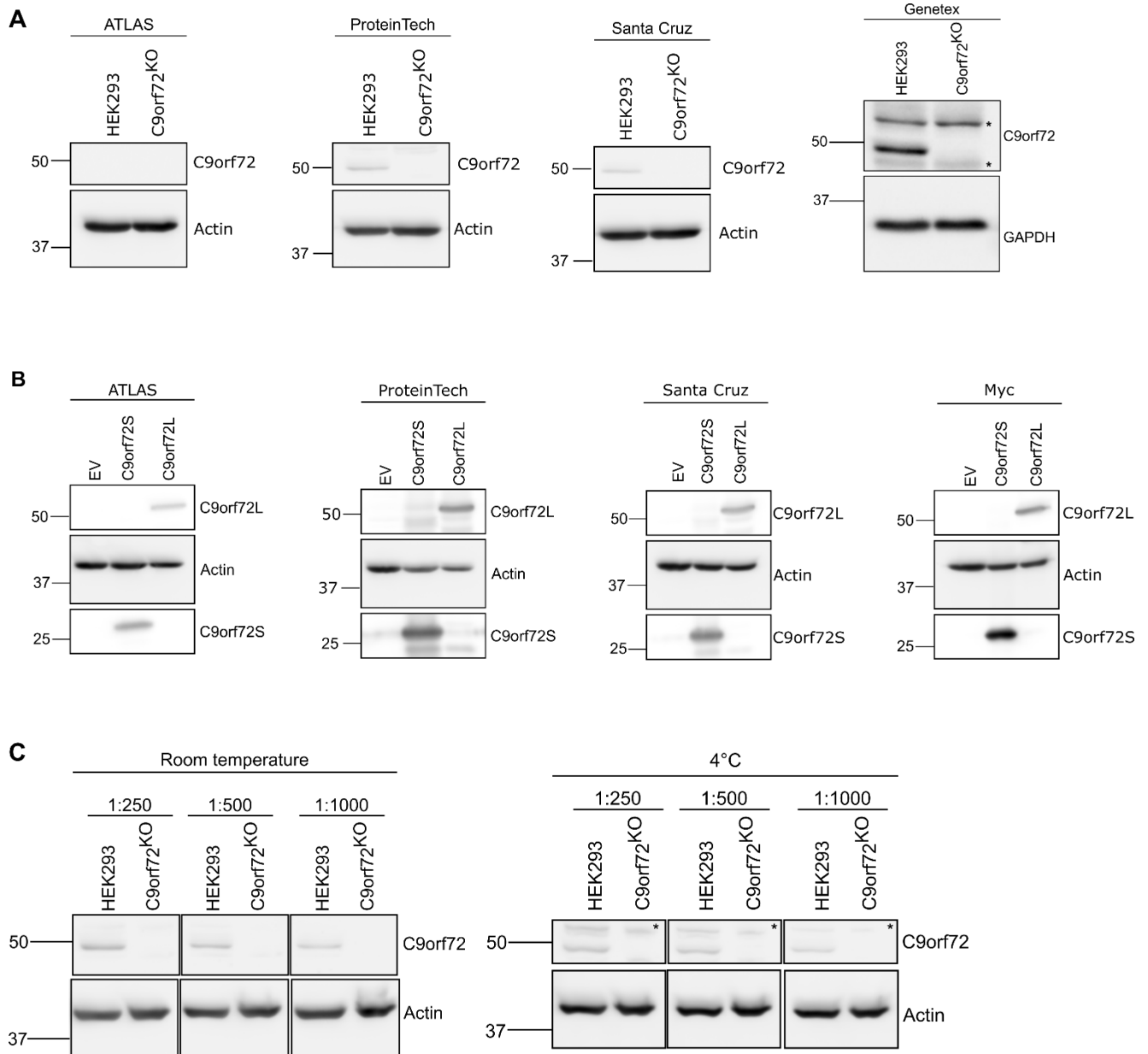
Figure 3.1: C9orf72 antibody optimisation for detection of endogenous C9orf72

(A) Lysates from HEK293 and HEK293 C9orf72^KO cells were subjected to SDS-PAGE and immunoblot for endogenous C9orf72 levels using anti-C9orf72 antibodies from ATLAS, ProteinTech, Santa Cruz and Genetex. Anti-actin or anti-GAPDH antibodies were used as a loading control. Black asterisks represent aspecific bands. (B) HEK293 cells were transfected with either an empty vector (EV), Myc-Corf72L or Myc-C9orf72S and lysates subjected to SDS-PAGE and immunoblot for C9orf72 levels using anti-C9orf72 antibodies from ATLAS, ProteinTech, and Santa Cruz or anti-Myc antibodies. Anti-actin antibodies were used as a loading control. (C) Lysates from HEK293 and HEK293 C9orf72^KO cells were subjected to SDS-PAGE and immunoblot for endogenous C9orf72 levels using anti-C9orf72 ProteinTech antibodies at varying dilutions (1:250, 1:500, 1:1000). Anti-actin antibodies were used as a loading control. Antibodies were incubated either at room temperature for 1 hr or at 4 °C for 16 hrs. Black asterisks represent aspecific bands.

3.3. C9orf72 is stabilised by SMCR8

We established that endogenous C9orf72 can be reliably detected using commercial antibodies. Given C9orf72 and SMCR8 form a complex (Amick et al., 2016; Sellier et al., 2016), we wanted to characterise the C9orf72^{KO} cell line to establish whether loss of C9orf72 had an effect on endogenous SMCR8 levels. To do this, lysate from HEK293 and HEK293 C9orf72^{KO} cells were separated by SDS-PAGE and probed via immunoblot. C9orf72 was detected in the HEK293 cells but not in the C9orf72^{KO} cells, as expected. Interestingly, the level of SMCR8 in the C9orf72^{KO} cells was significantly reduced compared to the HEK293 cells (Figure 3.2A, B). This strongly suggests that loss of C9orf72 results in lower SMCR8 levels.

To explore this further, we investigated whether levels of endogenous C9orf72 changed upon reduction of SMCR8 levels. To do this, cells were transfected with non-targeting (NTC) or SMCR8-targeting siRNA for 4 days. To determine whether the effect was specific to loss of SMCR8, rescue experiments were performed by exogenous expression of either empty vector (EV) or SMCR8-Myc/DDK. Levels of C9orf72 and SMCR8 were determined by SDS-PAGE and immunoblot. Knockdown of SMCR8 via siRNA resulted in a marked decrease in levels of SMCR8 compared to NTC (Figure 3.2C, E). In the same sample, levels of endogenous C9orf72 decreased (Figure 3.2C, D). Expression of SMCR8-Myc/DKK but not EV restored levels of C9orf72 (Figure 3.2C, D). Taken together, this suggests that C9orf72 levels can be regulated by expression of SMCR8.

We observed loss of C9orf72 reduced SMCR8 levels. Additionally, loss of SMCR8 reduced C9orf72 levels which could be restored by exogenous SMCR8 expression. This suggests that either C9orf72 or SMCR8 levels can be altered by decreasing the expression of the other protein. To investigate whether the reverse is true, that is whether C9orf72 or SMCR8 levels can be increased by expression of the other protein, HEK293 cells were co-transfected with Myc-C9orf72 or SMCR8-Myc/DDK and either EV or the complex partner. Cells were harvested and analysed via SDS-PAGE and immunoblot. Transfection of Myc-C9orf72 or SMCR8-Myc/DDK alongside EV served as a baseline. Upon co-expression of the proteins together, levels of Myc-C9orf72 increased markedly above baseline (Figure 3.2F, G). Similarly, SMCR8-Myc/DDK levels significantly

increased upon co-expression of C9orf72 and SMCR8 (Figure 3.2F, H). Collectively, this suggests that C9orf72 and SMCR8 can be stabilised by their complex partner.
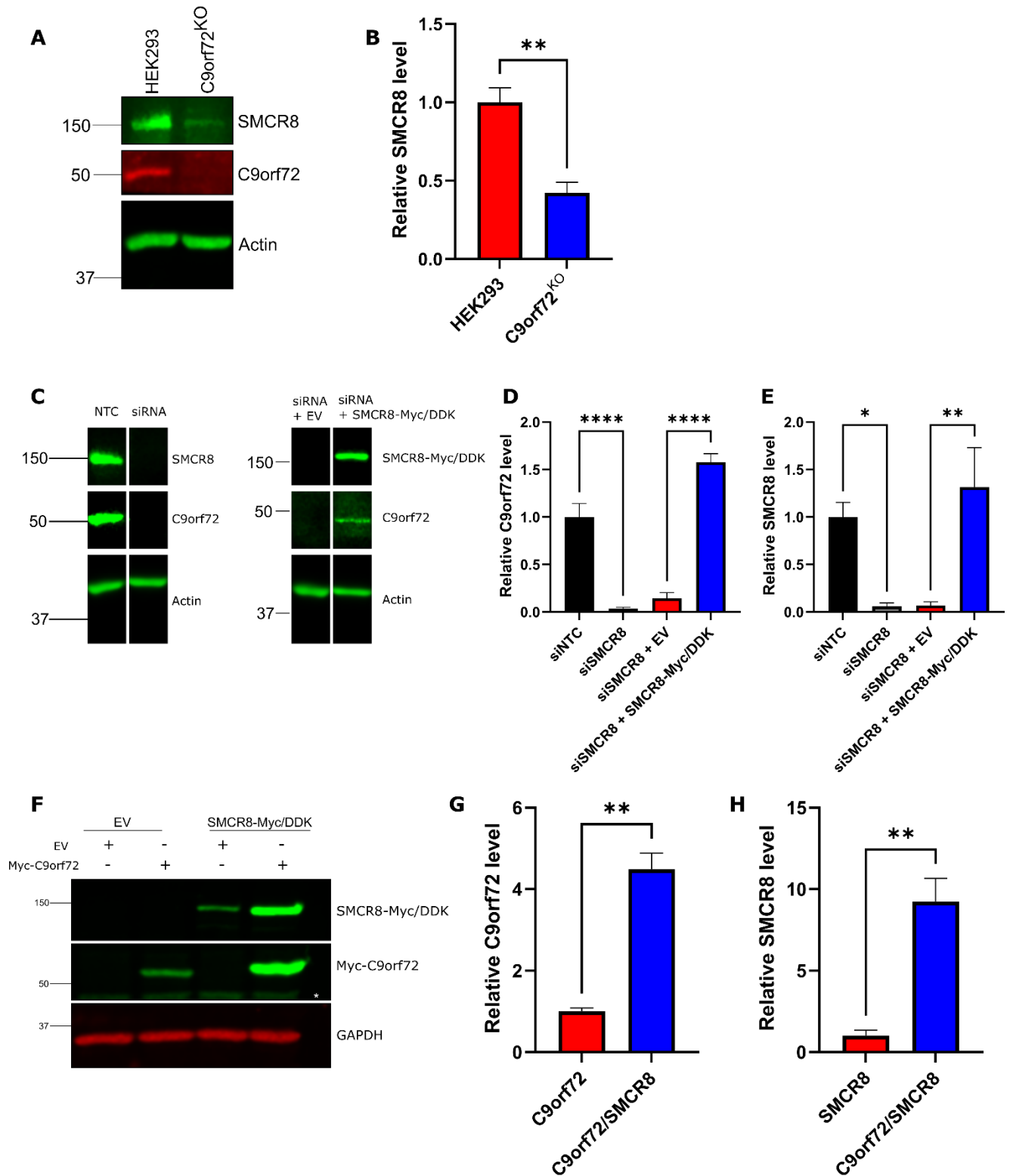
Figure 3.2: C9orf72 is stabilised by SMCR8.

(A) Lysates from HEK293 and HEK293 C9orf72^KO cells were subjected to SDS-PAGE and immunoblot for C9orf72 and SMCR8 using anti-C9orf72 and anti-SMCR8 antibodies. Anti-actin antibodies were used for a loading control. (B) Quantification of relative SMCR8 levels (Mean ± SEM; one-way ANOVA with Fisher's LSD test, ** p ≤ 0.01; N = 3 experiments). (C) HEK293 cells were transfected with non-targeting control (NTC) or SMCR8-targeting siRNA for 4 days. SMCR8-targeting siRNA samples were either left alone (siRNA) or transfected with empty vector (siRNA + EV)

or SMCR8 (siRNA + SMCR8-Myc/DDK). Lysates were prepared and subjected to SDS-PAGE and immunoblot for endogenous C9orf72 using anti-C9orf72 antibodies, SMCR8 using either endogenous anti-SMCR8 antibodies or anti-FLAG antibodies and anti-actin antibodies for the loading control. (D) Quantification of relative C9orf72 level (Mean ± SEM; one-way ANOVA with Fisher's LSD test, **** $p \leq 0.0001$; N = 3 experiments). (E) Quantification of relative SMCR8 level (Mean ± SEM; one-way ANOVA with Fisher's LSD test, * $p \leq 0.05$, ** $p \leq 0.01$; N = 3 experiments). (F) HEK293 cells were transfected with an empty vector (EV) control, or co-transfected with Myc-C9orf72/EV, SMCR8-Myc/DDK/EV or Myc-C9orf72/SMCR8-Myc/DDK. White asterisks represent aspecific bands. (G) Quantification of relative C9orf72 level (Mean ± SEM; one-way ANOVA with Fisher's LSD test, ** $p \leq 0.01$; N = 3 experiments). (H) Quantification of relative SMCR8 level (Mean ± SEM; one-way ANOVA with Fisher's LSD test, ** $p \leq 0.01$; N = 3 experiments).

3.4.　　C9orf72 is degraded via the proteasome

Determining the degradative pathway for C9orf72 allows for the exploration into possible regulators of the pathway. In doing so, this opens potential therapeutic avenues to explore in relation to C9ALS/FTD haploinsufficiency. To establish an assay for monitoring protein degradation over time, we set up a cycloheximide (CHX) chase assay. The CHX chase assay is an established method for the determination of protein half-life - the time taken for the protein level to reach half of its original level (Zhou, 2004). The assay is based on inhibiting the global translation of proteins using CHX which allows the decay of a given protein to be monitored over time.

To begin to investigate the degradation and turnover of C9orf72, HEK293 cells were transfected with Myc-C9orf72. Following this, transfected cells were either left untreated or treated with CHX and harvested 0, 2, 4, 8, 16 and 24 hrs post-treatment. Samples were analysed via SDS-PAGE and immunoblot for Myc-C9orf72 levels. In cells that were transfected with Myc-C9orf72 and untreated, levels of C9orf72 remained relatively stable over the 24 hr time period (Figure 3.3A). In contrast, in cells that were treated with cycloheximide, there was a steady decrease in Myc-C9orf72 of the 24 hrs (Figure 3.3A). A marked decrease in Myc-C9orf72 was seen after 4 hrs and its levels were almost completely gone by 16 hrs. As a positive control for CHX treatment, levels of cyclin D1 were also analysed. Cyclin D1 is a regulator of cyclin dependent kinases and is a well characterised and common marker of cycloheximide treatment as it has a short half-life between 30 and 70 mins (Chen et al., 2015; Diehl et al., 1995; Hao et al., 2011). For CHX treated cells, cyclin D1 levels steadily decreased over the 24 hr period and a marked decreased was seen after 2 hrs (Figure 3.3A) indicating that the assay worked and the treatment was effective.

Protein degradation follows an exponential decay as described by the decay equation $A_t = A_0 e^{-\lambda t}$ where A_t is the protein level at time t, A_0 is the protein level at time zero, t is the time and λ is the decay constant (Belle et al., 2006). It follows that the half-life, $t_{1/2} = \ln(A_0/A_t)/\lambda$. To determine the half-life, we calculated the relative amount of protein at each time point across three independent experiments and the resulting averages were plotted on a graph. Using the % ln of these values, a straight line graph was plotted and the half-life calculated. The half-life of Myc-C9orf72 was calculated as above and was approximately 3.2 hrs.

The two main pathways that are involved in the degradation of proteins are the UPS and autophagy. The 26S proteasome is comprised of two subunits – the 20S core and the 19S regulatory units. The 19S recognises and binds ubiquitinated proteins destined for degradation and directs them to the 20S core for degradation. MG132 is a peptide aldehyde that inhibits the proteolytic activity of the 26S proteasome by binding to the active site of the β-subunits of the 20S core (Guo and Peng, 2013). In contrast, bafilomycin is an inhibitor of autophagy. Bafilomycin acts by inhibiting the fusion between lysosomes and autophagosomes and their subsequent acidification, thereby preventing degradation of material engulfed in the autophagosome (Yamamoto et al., 1998; Yuan et al., 2015). Therefore, to test whether either pathway was involved, cells were co-treated with CHX and MG132 (CHX/MG132) or CHX and bafilomycin (CHX/bafilomycin) and harvested 0, 2, 4, 8, 16 and 24 hrs post-treatment as above. For CHX/Bafilomycin, cyclin D1 levels steadily decreased over the 24 hr time period and was barely detectable at 24 hrs (Figure 3.3C). In contrast, in CHX/MG132 cells, the levels of cyclin D1 remained steadier from 2 – 24 hrs and was still visible by 24 hrs (Figure 3.3B). As a positive control for bafilomycin treatment, levels of LC3 were determined. During the autophagic process, LC3-I is lipidated to form LC3-II, which is conjugated to the membrane of the autophagosome. As bafilomycin prevents degradation by inhibiting the fusion between autophagosome and lysosomes, increased LC3-II levels can act as a marker of autophagy inhibition. The level of LC3-II increased over time in CHX/Bafilomycin treated cells indicating that the treatment was effective, and autophagy was inhibited.

Inhibition of autophagy did not affect the degradation of Myc-C9orf72 which resulted in a half-life of approximately 3.9 hrs which is comparable to cells treated with CHX (Figure 3.3D). In contrast, CHX/MG132 treatment significantly increased Myc-C9orf72 levels compared to CHX treated cells (Figure 3.3D). This suggests C9orf72 is unable to be degraded and points towards the degradation mechanism being the proteasome.

Next, we wanted to determine whether the findings for the overexpressed C9orf72 half-life and degradation pathway were replicated endogenously. To do this, HEK293 cells were treated with CHX and harvested 0, 2, 4, 8, 16 and 24 hrs post-treatment. Samples were analysed via SDS-PAGE and immunoblot. As before, cyclin D1 was used as a positive control for cycloheximide. As a positive control for detection, C9orf72[KO] cells were run alongside treated cells. Similar to overexpressed C9orf72 (Figure 3.3A), levels of endogenous C9orf72 remained steady over the 24 hr period in untreated cells (Figure

3.3E, F). As expected, during this period levels of cyclin D1 also as remained steady. CHX treatment caused a steady decrease in cyclin D1 levels and was markedly decreased 2 hrs, confirming CHX treatment was effective. Unexpectedly, endogenous levels of C9orf72 remained steady over 24 hrs (Figure 3.3E, F). As the level of cyclin D1 was undetectable by 2 hrs in CHX treated cells, this demonstrates the CHX treatment was effective. This suggests that endogenous C9orf72 is stable over the observed 24 hr period.
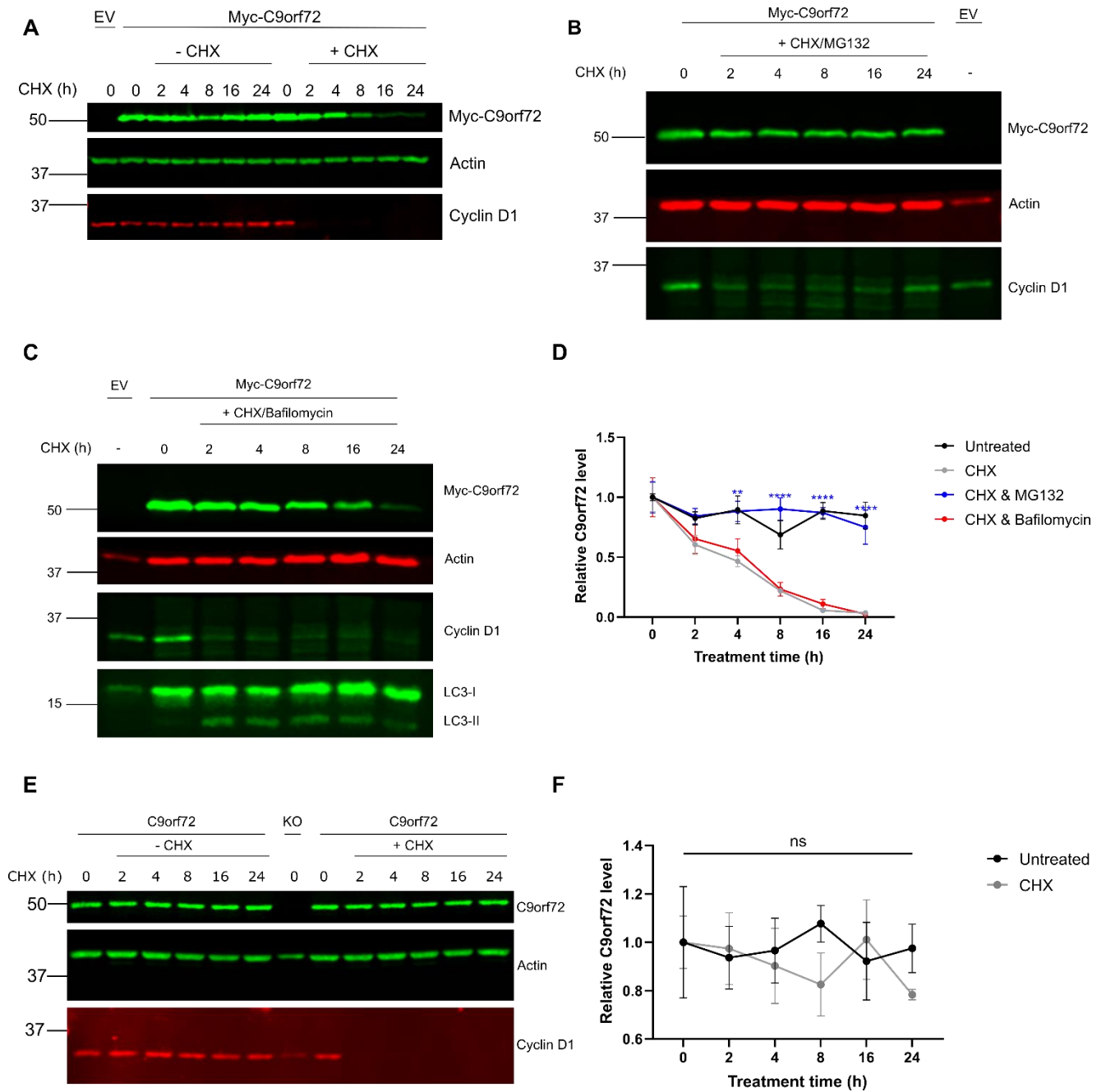
Figure 3.3: C9orf72 is degraded via the ubiquitin proteasome system

(A) HEK293 cells were transfected with Myc-C9orf72 and either untreated or treated with cycloheximide (CHX). Cells were harvested 0, 2, 4, 8, 16 or 24 hrs post-treatment and analysed via SDS-PAGE and immunoblot for levels of Myc-C9orf72 using anti Myc antibodies, actin using anti-actin antibodies or cyclin D1 using anti-cyclin D1 antibodies. (B) HEK293 cells were transfected with Myc-C9orf72 and treated with CHX and MG132 (CHX/MG132). Cells were harvested 0, 2, 4, 8, 16 or 24 hrs post-treatment and analysed via SDS-PAGE and immunoblot for levels of Myc-C9orf72 using anti Myc antibodies, actin using anti-actin antibodies or cyclin D1 using anti-cyclin D1 antibodies. (C) HEK293 cells were transfected with Myc-C9orf72 and treated with CHX and bafilomycin (CHX/Bafilomycin). Cells were harvested 0, 2, 4, 8, 16 or 24 hrs post-treatment and analysed via SDS-PAGE and immunoblot for levels of Myc-C9orf72 using anti Myc antibodies, actin using anti-actin antibodies, cyclin D1 using anti-cyclin D1 antibodies or LC3 using anti-LC3 antibodies. (D) Quantification of the relative levels of Myc-C9orf72 following treatment (Mean ± SEM; two-way ANOVA with Fisher's LSD test, ** $p \leq 0.01$, **** $p \leq 0.0001$; N = 3 experiments). (E) HEK293 cells were either

left untreated or treated with CHX and harvested 0, 2, 4, 8, 16 or 24 hrs post-treatment. Cells were analysed via SDS-PAGE and immunoblot for levels of C9orf72 using anti-C9orf72 antibodies, actin using anti-actin antibodies or cyclin D1 using anti-cyclin D1 antibodies. (D) Quantification of the relative levels of C9orf72 following treatment (Mean ± SEM; two-way ANOVA with Fisher's LSD test, ns = non-significant; N = 3 experiments).

3.5. Overexpressed SMCR8 levels increase upon proteasome inhibition and co-expression of C9orf72 and SMCR8 stabilises half-life.

We have shown that C9orf72 is degraded via the proteasome and endogenous C9orf72 is stable over a 24 hr period. The above data also indicated that endogenous C9orf72 levels can be altered by varying the expression of SMCR8. As C9orf72 and SMCR8 are known to form a complex we hypothesised that the stability of endogenous C9orf72 is due to interaction with SMCR8. Therefore, we investigated whether co-expression of C9orf72 and SMCR8 altered the half-life of the proteins.

To investigate the degradation of SMCR8, SMCR8-Myc/DDK was transfected in HEK293 cells and treated with CHX. As the half-life of Myc-C9orf72 was determined to be 3.2 hrs, cells were harvested 0, 2, 4 and 8 hrs post-treatment. Samples were then analysed via SDS-PAGE and immunoblot for the levels of SMCR8. As before, levels of cyclin D1 were analysed as a positive control for CHX treatment. The levels of cyclin D1 decreased steadily over the 8 hr period of CHX treatment, confirming the treatment was effective. In the same sample, the level of SMCR8-Myc/DDK decreased steadily over time (Figure 3.4A). Calculation of the half-life was performed as before and resulted in a half-life of approximately 5.8 hrs. To determine the degradation pathway, cells were treated with CHX/MG132 or CHX/bafilomycin and harvested 0, 2, 4 and 8 hrs post-treatment. As before, cyclin D1 and LC3 levels were analysed as a positive control for CHX treatment and autophagy inhibition respectively. In CHX/bafilomycin treated cells, the levels of cyclin D1 decreased over time with a marked reduction at 2 hrs, confirming treatment was effective. Additionally, the levels of LC3-II increased from 0 – 2 hrs and remained steady confirming autophagy was inhibited. In these cells, SMCR8 levels decreased over the 8 hr period in a similar manner to CHX treated cells and resulted in a half-life of 4.0 hrs (Figure 3.4B, D). In contrast, in CHX/MG132 treated cells, SMCR8 levels remained steady over the 8 hr period, resulting in a half-life of 14.7 hrs (Figure 3.4C, D). Despite this, quantification revealed no significant difference in SMCR8 levels between treated samples.

To determine whether co-expression of SMCR8 and C9orf72 altered half-life, Myc-C9orf72 and SMCR8-Myc/DDK were co-expressed, treated with CHX and harvested 0, 2, 4 and 8 hrs post-treatment. Samples were analysed via SDS-PAGE and immunoblot for levels of C9orf72 and SMCR8. Levels of cyclin D1 decreased steadily over the 8 hr

period, with a perceptible decrease after 2 hrs, confirming the treatment was effective (Figure 3.4A). In contrast to when expressed alone, co-expression of SMCR8-Myc/DDK and Myc-C9orf72 resulted in steady levels of both proteins over the 8 hr period. (Figure 3.4A, E). Consequently, the half-life of SMCR8 significantly increased from 5.8 hrs when expressed alone to 10.2 hrs when co-expressed. Similarly, when compared to the previously calculated half-life, the half-life of Myc-C9orf72 increased from 3.2 to 14.4 hrs when expressed alone or in a complex respectively. Taken together, this data suggests that co-expression of C9orf72 and SMCR8 increases half-life through possible stabilisation of the C9orf72-SMCR8 protein complex.
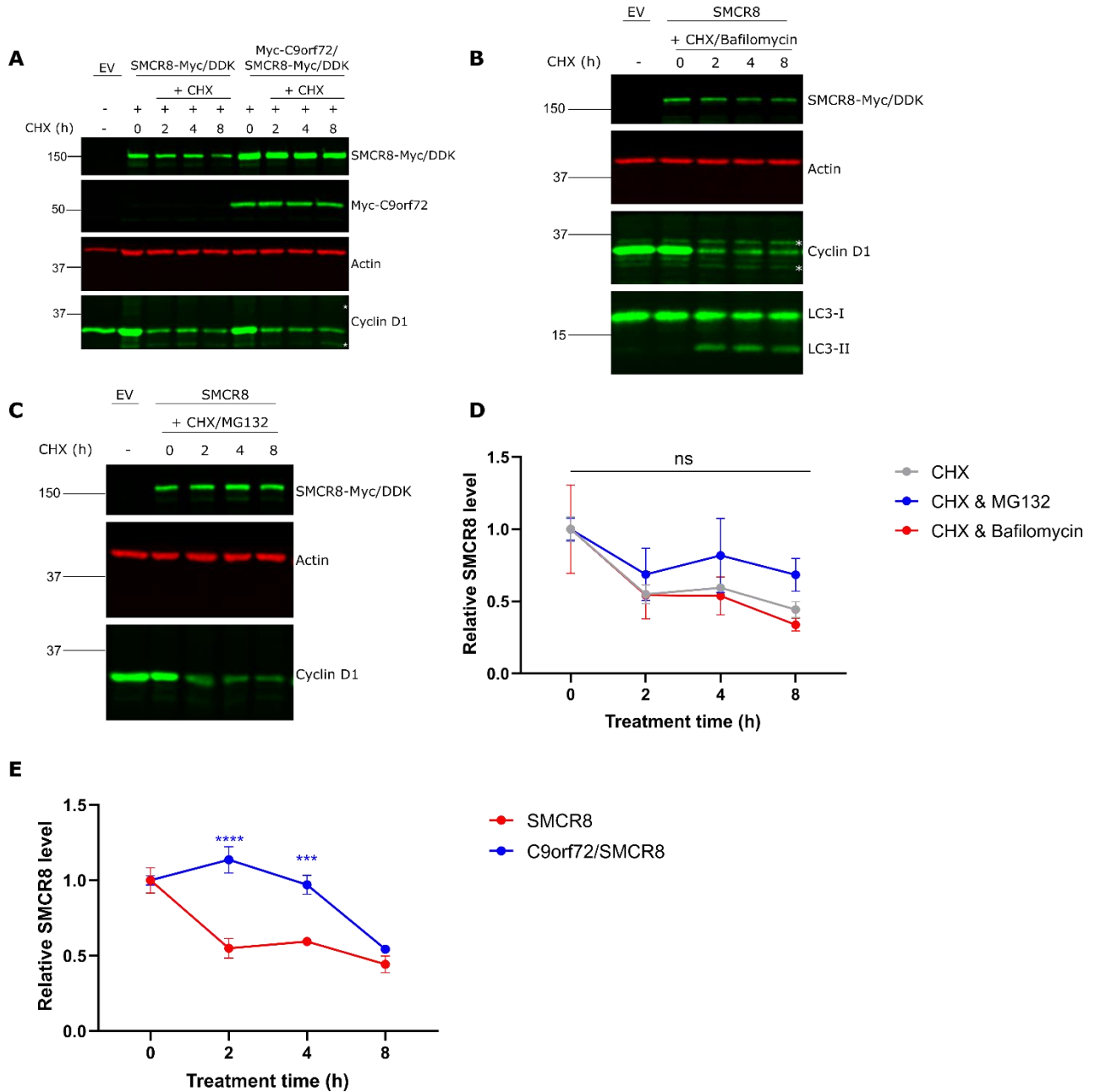
Figure 3.4: Co-expression of C9orf72 and SMCR8 stabilises C9orf72 and SMCR8

(A) HEK293 cells were transfected with SMCR8-Myc/DDK or co-transfected with Myc-C9orf72 and SMCR8-Myc/DDK. Cells were treated with cycloheximide and harvested 0, 2, 4 or 8 hrs post-treatment. Lysates were analysed via SDS-PAGE and immunoblot for levels of SMCR8-Myc/DDK using anti-FLAG antibodies, Myc-C9orf72 using anti-Myc antibodies, actin using anti-actin antibodies or cyclin D1 using anti-cyclin antibodies. White asterisks represent aspecific bands. (B) HEK293 cells were transfected with SMCR8-Myc/DDK and treated with CHX and bafilomycin (CHX/Bafilomycin). Cells were harvested 0, 2, 4 and 8 hrs post-treatment and analysed via SDS-PAGE and immunoblot for levels of SMCR8-Myc/DDK using anti-FLAG antibodies, actin using anti-actin antibodies, cyclin D1 using anti-cyclin D1 antibodies or LC3 using anti-LC3 antibodies. White asterisks represent aspecific bands. (C) HEK293 cells were transfected with SMCR8-Myc/DDK and treated with CHX and MG132 (CHX/MG132). Cells were harvested 0, 2, 4 and 8 hrs post-treatment and analysed via SDS-PAGE and immunoblot for levels of SMCR8-Myc/DDK using anti-FLAG antibodies, actin using anti-actin antibodies or cyclin D1 using anti-cyclin D1 antibodies.

(D) Quantification of the relative levels of SMCR8-MycDDK following treatment (Mean ± SEM; two-way ANOVA with Fisher's LSD test, ns = non-significant; N = 3 experiments). (E) Quantification of the relative level of SMCR8 following single expression (SMCR8) or co-expression with Myc-C9orf72 (C9orf72/SMCR8) (Mean ± SEM; two-way ANOVA with Fisher's LSD test, *** p ≤ 0.001, **** p ≤ 0.0001; N = 3 experiments).

3.6.   C9orf72 is ubiquitinated

The ubiquitination of proteins is a prerequisite to proteasomal degradation. In this process, the 8 kDa protein ubiquitin is attached to a lysine residue of the substrate protein. As ubiquitin has seven internal lysine amino acids, these lysine residues can be conjugated to another ubiquitin to form a polyubiquitin chain which acts as a signal for proteasomal degradation (Sun and Chen, 2004).. To further characterise proteasomal degradation of C9orf72, we first established an essay for detecting C9orf72 ubiquitination.

A co-immunoprecipitation assay was used to detect C9orf72 ubiquitination. To determine whether endogenous C9orf72 ubiquitination could be detected via this assay, HA-Ubiquitin was expressed in HEK293 and C9orf72^{KO} cells. Endogenous C9orf72 was immunoprecipitated and both whole cell lysate and immune pellets analysed via SDS-PAGE and immunoblot for endogenous C9orf72 and HA-Ubiquitin. Endogenous C9orf72 was enriched in HEK293 cells, and no C9orf72 was detected in C9orf72^{KO} immune pellets, as expected (Figure 3.5A). In HEK293 cells expressing HA-Ubiquitin, a smear indicative of a ubiquitin chain is present that is reduced in C9orf72^{KO} cells (Figure 3.5A). This suggest that endogenous C9orf72 is ubiquitinated. As the smear does not appear in HEK293 cells without HA-Ubiquitin, this suggests the smear is HA-Ubiquitin specific. Overall, this demonstrates endogenous C9orf72 ubiquitination can be detected via this assay.

As any C9orf72 mutants made would be a product of exogenous expression, we wanted to determine whether exogenous C9orf72 ubiquitination could also be detected via this assay. To do so, HEK293 cells were co-transfected with Myc-C9orf72 and either EV or HA-Ubiquitin. To increase ubiquitination signal, degradation via the proteasome was blocked using MG132 for some samples. Lysates were enriched for Myc-C9orf72 using an anti-Myc antibody and the resulting immune pellet subjected to SDS-PAGE and immunoblot for Myc-C9orf72 and HA-Ubiquitin. Myc-C9orf72 was enriched in all C9orf72-containing immune pellets (Figure 3.5B). Interestingly, whole cell lysate expression of Myc-C9orf72 was more pronounced in the sample containing co-expression of Myc-C9orf72 and HA-ubiquitin compared to co-expression of Myc-C9orf72 and EV (Figure 3.5B). A smear indicative of a ubiquitin chain is observed in co-expressed Myc-C9orf72 and HA-Ubiquitin samples, that intensifies upon MG132 treatment. This

indicates C9orf72 is polyubiquitinated. Conversely, in the sample co-transfected with Myc-C9orf72 and EV no smear was observed demonstrating that the smear in the Myc-C9orf72/HA-Ubiquitin sample is specific to ubiquitin. This indicates that C9orf72 ubiquitination can be detected via a co-immunoprecipitation assay.

Bioinformatic analysis was used to determine the most probable sites of ubiquitination and C9orf72 mutants were made. The amino acid sequence of C9orf72 was input into UbPred (http://www.ubpred.org), a ubiquitination predictor site. The output from this prediction is a confidence score which indicates a low, medium or high confidence and corresponds to the sensitivity and specificity indicated below.

Score	Score range	Sensitivity	Specificity
High confidence	$0.84 \leq s \leq 1.00$	0.197	0.989
Medium confidence	$0.69 \leq s \leq 0.84$	0.346	0.950
Low confidence	$0.62 \leq s \leq 0.69$	0.464	0.903

The C9orf72 proteins contains 26 lysine residues and the lysine residues at position 14 and 388 were the most probable candidates. Mutation of these lysine residues to arginine allowed assessment of whether this lysine residue is required for ubiquitination. HEK293 cells were co-transfected with Myc-C9orf72, the K14R mutant or the 388R mutant and either EV or HA-Ubiquitin. Some samples were treated with MG132 to increase the ubiquitination signal. Lysates were enriched for Myc-C9orf72 using an anti-Myc antibody and the resulting immune pellet analysed via SDS-PAGE and immunoblot for Myc-C9orf72 and HA-Ubiquitin. Similar to Myc-C9orf72, the expression levels of the K14R mutant in the whole cell lysate is greater when co-expressed with HA-Ubiquitin compared to EV (Figure 3.5B). Myc-C9orf72 and the K14R mutant was enriched in all C9orf72 containing samples. A ubiquitination smear for Myc-C9orf72 K14R is observed that intensifies upon MG132 treatment (Figure 3.5B). A higher molecular weight, ubiquitin-positive band is observed in the Myc-C9orf72 K14R and HA-Ubiquitin sample with and without MG132 that is also present in the wild type. As both Myc-C9orf72 and the K14R mutant have similar levels of ubiquitination, this strongly suggests K14 is not the sole site for C9orf72 ubiquitination.

In the case of the 388R mutant, once again expression levels of the mutant in the whole cell lysate are greater when co-expressed with HA-Ubiquitin compared to EV (Figure

3.5C). A ubiquitination smear for both Myc-C9orf72 and the 388R mutant is observed that intensifies upon MG132 treatment. Higher molecular weight, Myc-positive bands, indicative of ubiquitinated C9orf72 is observed for Myc-C9orf72 and the K388R mutant in the immune pellet samples (Figure 3.5C). Interestingly, these higher molecular weight bands do not increase upon MG132 treatment, although in both untreated and MG132 treated samples, the higher molecular weight bands are slightly decreased for the 388R mutant. As both Myc-C9orf72 and the K388R mutant have similar levels of ubiquitination, this strongly suggests K388 is also not the sole site for C9orf72 ubiquitination.
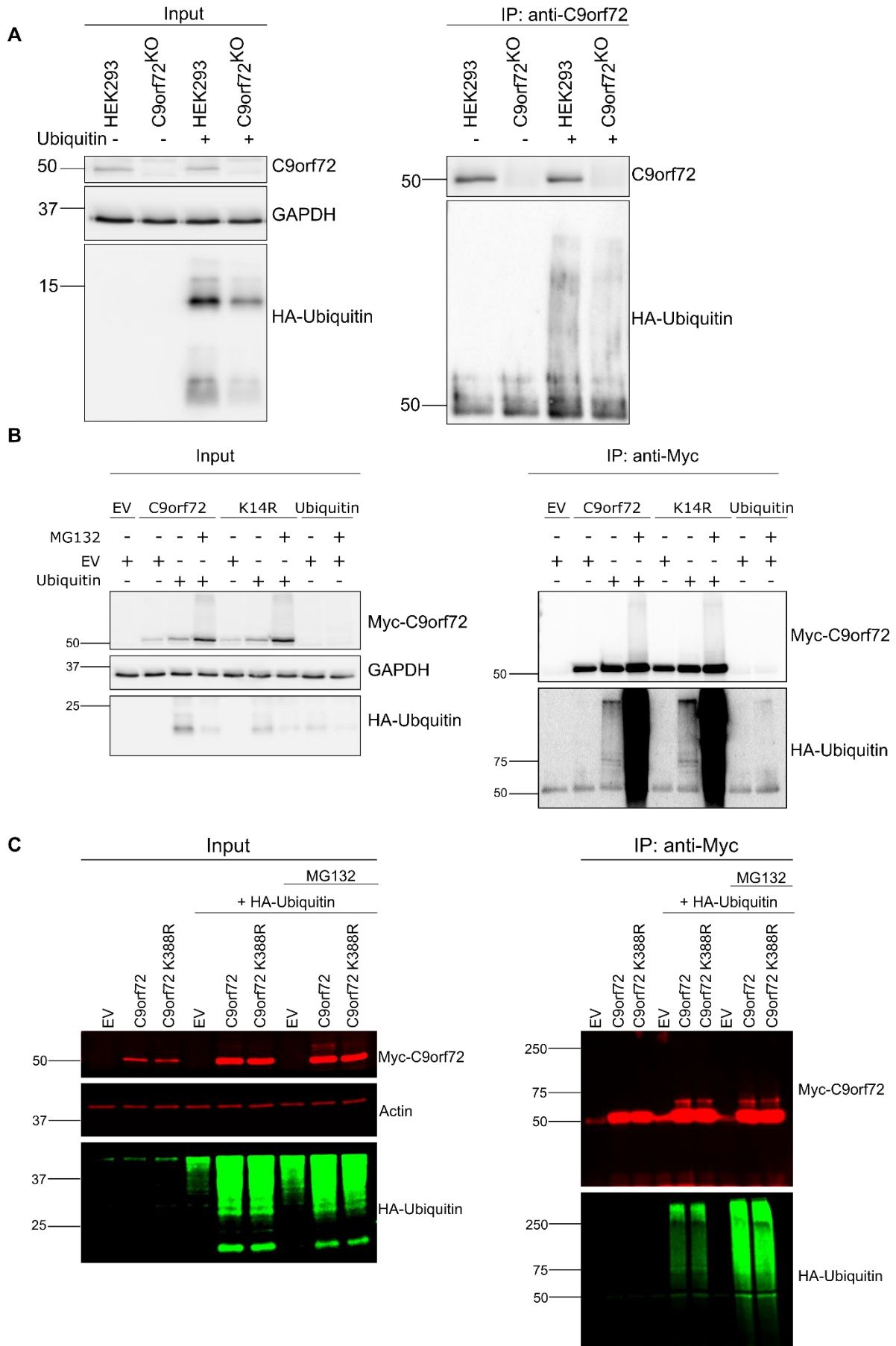
Figure 3.5:C9orf72 is ubiquitinated but K14 and K388 are not the sole ubiquitination sites

(A) HEK293 cells were either untransfected or transfected with HA-Ubiquitin. Cells were immunoprecipitated using anti-C9orf72 antibodies and whole cell lysate and immune pellets probed via SDS-PAGE and immunoblot for levels of C9orf72 using anti-C9orf72 antibodies or HA-Ubiquitin using anti-HA antibodies. Whole cell lysate was also probed for GAPDH as a loading control using anti-GAPDH antibodies. (B) HEK293 cells were transfected with Myc-C9orf72, Myc-C9orf72 K14R or co-transfected with Myc-C9orf72/HA-Ubiquitin or Myc-C9orf72 K14R/HA-Ubiquitin. Some samples were treated with MG132. Cells were immunoprecipitated using anti-Myc antibodies and whole cell lysate probed via SDS-PAGE and immunoblot for C9orf72 levels using anti-Myc antibodies or HA-Ubiquitin using anti-HA antibodies. GAPDH was used as a loading control for whole cell lysate. (C) HEK293 cells were transfected with Myc-C9orf72, Myc-C9orf72 K388R or co-transfected with Myc-C9orf72/HA-Ubiquitin or Myc-C9orf72 K388R/HA-Ubiquitin. Some samples were treated with MG132. Cells were immunoprecipitated using anti-Myc antibodies and whole cell lysate probed via SDS-PAGE and immunoblot for C9orf72 levels using anti-Myc antibodies or HA-Ubiquitin using anti-HA antibodies. Actin was used as a loading control for whole cell lysate.

3.7.   Discussion

This chapter investigated the turnover of the C9orf72 protein and in line with the hypothesis identified the degradation pathway of C9orf72. It was found that C9orf72 is degraded via the proteasome. Interestingly, under basal conditions C9orf72 is stabilised by SMCR8 as evidenced by the increase in half-life following co-expression of C9orf72 and SMCR8.

The antibodies from ATLAS, ProteinTech and Santa Cruz were able to detect overexpressed C9orf72 but only the ProteinTech and Santa Cruz antibodies could detect endogenous C9orf72. In addition, the Genetex antibody could detect endogenous C9orf72 but was not tested for overexpressed detection. This is similar to the findings by Laflamme et. al that demonstrated when analysed by immunoblot, the Santa Cruz antibody was unable to detect endogenous C9orf72 in human lysate samples (Laflamme et al., 2019). In contrast, whilst in our experiments the ProteinTech antibody appeared to give less aspecific bands compared to the Genetex, Laflamme et. al showed the reverse. This is possible due to differences in immunoblot procedure – an overnight transfer to nitrocellulose, followed by blocking for 1 hr at RT in 5% milk and 1 hr at RT antibody incubation in 5% milk in our case compared to blocking in 5% milk followed by 4 °C overnight antibody incubation in TBST in the case of Laflamme et. al. Alternatively, the differences seen between these antibodies could arise from potential differences in antibody lot numbers.

We utilized the cycloheximide chase assay to investigate the degradation of overexpressed C9orf72 and used proteasome and autophagy inhibitors (the two main degradative pathways) to confirm the degradative pathway. Myc-C9orf72 steadily degraded over a 24 hr period following CHX addition and had a calculated half-life of 3.2 hrs. Inhibition using CHX/MG132 but not CHX/bafilomycin restored Myc-C9orf72 levels to that of untreated cells, suggesting the UPS is the degradation pathway. One study suggests the degradation mechanism for exogenous C9orf72 is cell type-dependent (Manner et al., 2019). Manner et. al shows exogenous C9orf72 levels decrease upon autophagy activation in N2a cells. When autophagy activation is coupled with UPS inhibition C9orf72 levels are restored. This suggests exogenous C9orf72 is degraded via the proteasome. However, the same study shows autophagy induction combined with autophagy inhibition restores exogenous C9orf72 levels in primary neurons, but not in

N2A cells. Due to the lack of densitometry analysis in the study, visual comparison of LC3-II levels upon autophagy inhibition in N2A and primary neurons, revealed an increase in LC3-II levels as expected in N2A cells but appeared unchanged in primary neurons. Therefore, it is uncertain whether the change in exogenous C9orf72 protein levels in these conditions is due to autophagy inhibition.

The recent availability of commercial antibodies for endogenous C9orf72 allowed for exploration of turnover at the endogenous level. For disease models and potential therapeutics, endogenous results are more relevant. To our surprise, we found in contrast to exogenous C9orf72, treatment with CHX over a 24 hr period did not alter the level of endogenous C9orf72. C9orf72, SMCR8 and WDR41 are known to form a complex (Sellier et al., 2016; Yang et al., 2016). Therefore, a possible explanation for the apparent lack of degradation could emerge from investigation into whether complex formation stabilises proteins. WDR41 forms a complex with C9orf72 and SMCR8 and mediates the localisation of C9orf72-SMCR8 complex to lysosomes and recent cryo-EM structure of the C9orf72-SMCR8-WDR41 complex revealed WDR41 interacts with the C-terminal of SMCR8, with no direct contact with C9orf72 (Amick et al., 2018; Tang et al., 2020). Therefore, WRD41 was not expressed alongside SMCR8. Indeed, co-expression of SMCR8-Myc/DDK and Myc-C9orf72 significantly increased their levels compared to expression of either protein alone, suggesting that co-expression of C9orf72 and SMCR8 can increase stability. This was tested endogenously in a related approach. Reduced SMCR8 levels via siRNA knockdown resulted in significantly reduced endogenous C9orf72 levels that could be restored by exogenous SMCR8 expression. We also noted that SMCR8 levels in the CRISPR-generated HEK293 C9orf72[KO] stable cell line was reduced compared to wild type. This strengthens the idea of complex stabilisation and is in line with literature. In brain lysates and mouse embryonic fibroblasts (MEF) samples, knockdown of SMCR8 resulted in significantly reduced endogenous C9orf72 protein levels, but unchanged C9orf72 mRNA levels (Lan et al., 2019). Additionally, Lan et al. showed knockdown of endogenous C9orf72 levels markedly reduced SMCR8 levels. Interestingly, in the same study SMCR8 and C9orf72 levels were reduced to a lesser extent upon WDR41 knockdown suggesting WDR41 stabilises the C9orf72-SMCR8 heterodimer. As WDR41 has no direct contact with C9orf72 (Tang et al., 2020), this is likely through SMCR8. It must be noted that WDR41 knockdown efficiency was not assessed in these experiments. Further evidence is provided by the levels of SMCR8 in

C9orf72 KO and C9orf72 in SMCR8 KO cell lines which are reduced compared to controls and the level of SMCR8 in C9orf72 KO mice are reduced compared to wild type (Amick et al., 2016; Ugolino et al., 2016).

The turnover of SMCR8 and C9orf72-SMCR8 was investigated to determine whether stability of the complex translated to altered turnover. Treatment of SMCR8-Myc/DDK with CHX resulted in a steady decrease in exogenous SMCR8 levels that was significantly stabilised upon co-expression with Myc-C9orf72. Similarly, co-expression significantly increased the half-life of Myc-C9orf72. This is in agreement with literature, whereby co-expression of overexpressed C9orf72 and SMCR8 stabilises C9orf72 levels (Ugolino et al., 2016). In contrast to CHX/MG132 treatment of Myc-C9orf72, quantification of SMCR8 levels upon CHX/MG132 treatment of SMCR8-Myc/DDK alone revealed the increase in SMCR8-Myc/DDK levels was non-significant despite an increase in half-life from 5.8 hrs to 14.7 hrs upon CHX and CHX/MG132 treatment respectively This is likely due to the large standard error of the mean. Further investigation to reduce the error and confirm the degradation pathway of SMCR8 is warranted given SMCR8 interacts with multiple components of the ubiquitin proteasome system and is itself poly-ubiquitinated (Goodier et al., 2020). One possible explanation for the increase in half-life upon complexation arises from the possibility that degradation of the constituent proteins only occurs when the complex is broken, although this would need to be investigated. This is in line with the observation that the stability of individual subunits of a complex increases upon complexation and free subunits are often rapidly degraded (Goldberg, 2003; Yanagitani et al., 2017).

Despite the ease of use of the CHX assay, it is not without drawbacks. One such drawback stems from the mechanism of action of CHX. Under these conditions, determination of protein half-life is performed when global protein translation is arrested. Therefore, calculated half-lives may not mirror protein synthesis and degradation rates under normal conditions (Zhou, 2004). Moreover, under CHX conditions, the synthesis of enzymes such as ubiquitin ligases is prevented, and their overall stability may be affected. This could result in abnormal, longer half-lives. To overcome these issues, a pulse-chase assay may be more appropriate. In a non-radioactive approach, during *de novo* protein synthesis, L-azidohomoalanine (L-AHA) can be incorporated in place of methionine in cells grown in methionine-free medium (Chai et al., 2016; Wang et al.,

2017b; Zhang et al., 2014a). Following a reaction between a fluorescently labelled alkyne and the azide of L-AHA, fluorescently labelled proteins can be detected by immunoblot.

Immunoprecipitation of Myc-C9orf72 revealed a distinct smear of proteins immunoreactive with HA antibody that increased upon proteasome inhibition, suggesting exogenous C9orf72 is ubiquitinated. A similar protein smear was observed with the Myc antibody, which is further evidence of ubiquitination. However, because of the experimental setup, the immunoblots for Myc and HA are different. Therefore, we are assuming bands at similar molecular weights represent the same protein. Repetition of the experiment using fluorescent secondary antibodies would allow for multi-colour detection and further confirmation the bands present correspond to the same protein. Endogenous C9orf72 immunoprecipitation also resulted in a smear of protein immunoreactive for HA further suggesting that C9orf72 is ubiquitinated.

Bioinformatics analysis of the C9orf72 sequence was used to determine the most likely ubiquitination sites for C9orf72. We mutated the top hits to investigate whether these sites influenced ubiquitination of C9orf72. Due to time limitations, only K14 and K388 were investigated. Mutation of either K14 or K388 lysine residues to arginine did not alter the ubiquitination status for C9orf72, suggesting these sites alone are not the single ubiquitination site. Studies have shown that ubiquitination of certain proteins relies upon multiple ubiquitination sites (Chen et al., 2014a; Rodriguez et al., 2000). For example, p53, a protein involved in the initiation of the DNA damage response, requires ubiquitination of six lysine residues for Mdm2-mediated ubiquitination and subsequent degradation (Rodriguez et al., 2000). Mdm2 functions as a ubiquitin ligase and mutation of K370, 372, 373, 381, 382 and 386 in p53 abrogated ubiquitination. Furthermore, multiple ubiquitination sites have been identified in SMCR8 by mass spectrometry and MG132 treatment caused the accumulation of higher molecular weight SMCR8 proteins, suggesting SMCR8 may be degraded via the proteasome (Goodier et al., 2020). Therefore, it is possible C9orf72 requires ubiquitination at multiple points to act as a signal for proteasomal degradation. To test this theory, mutation of all lysine residues in C9orf72 to arginine would conclusively determine whether C9orf72 is ubiquitinated. In a more refined approach, bioinformatics analysis using multiple ubiquitination prediction software could unveil lysine residues with high probability as ubiquitination sites. Simultaneous mutation of the top hits and subsequent co-immunoprecipitation assays could reveal whether C9orf72 is ubiquitinated at multiple lysine residues. Further

refinement would allow for the exact residues to be determined. Once determined, in a related approach the turnover of the C9orf72 mutant could be assessed. Alternatively, mass spectrometry could be utilised to identify ubiquitination sites, with further validation from co-immunoprecipitation assays of the identified mutants. This multiple hit strategy would fully characterise C9orf72 ubiquitination.

4. Investigating regulation of the C9orf72-SMCR8 complex

4.1.   Introduction

One mechanism thought to contribute to C9ALS/FTD is haploinsufficiency whereby patients have reduced C9orf72 mRNA levels (DeJesus-Hernandez et al., 2011). Given C9ALS/FTD patients are haploinsufficient, identification of key regulators of C9orf72 turnover could highlight potential therapeutic targets. Targeting the turnover of the remaining C9orf72 protein to decrease its degradation rate and thereby increase remaining C9orf72 levels represents a potential method for rescuing C9orf72 haploinsufficiency and could be of benefit to C9ALS/FTD patients.

 In Chapter 3, we found that C9orf72 is degraded via the ubiquitin proteasome system. In the ubiquitin proteasome system, substrate proteins are targeted for degradation via the 26S proteasome. This is achieved by two consecutive steps – ubiquitination and proteolytic degradation and involves many key enzymes. In the first of these steps substrate proteins are covalently modified with a ubiquitin molecule. The attachment of ubiquitin to the substrate protein involves E1, E2 and E3 enzymes (Kwon and Ciechanover, 2017). E1-activating enzymes activate the ubiquitin molecule, a process requiring ATP. Following this, the activated ubiquitin is transferred to an E2-conjugating enzyme. Finally, an E3-ligating enzyme facilitates the transfer of ubiquitin to the substrate protein. As such, substrate specificity is mediated by E3 ligases. The attachment of further ubiquitin moieties through the lysine linkage in ubiquitin results in a polyubiquitin chain. This polyubiquitin chain acts as a signal for degradation and subsequently, polyubiquitinated proteins are degraded via the 26S proteasome.

Ubiquitination is a reversible process, and the removal of ubiquitin moieties is performed by deubiquitinating enzymes (DUBs). There are five main classes of DUBs; four are cysteine proteases, which include ubiquitin specific proteases (USPs), and the fifth class are metalloproteases (Farshi et al., 2015; de la Vega et al., 2011; Leznicki and Kulathu, 2017). In cleaving ubiquitin and/or disassembling polyubiquitin chains from target proteins, DUBs can regulate protein turnover by removing degradation signals (Farshi et al., 2015). Hence, DUBs represent key regulators of the UPS pathway.

Therefore, in this chapter, we attempted to identify key enzymes involved in the turnover of the C9orf72-SMCR8 complex. We explored whether changes in these enzymes influenced levels of C9orf72.

4.2.   USP8

The enzyme ubiquitin specific peptidase 8 (USP8) is a multi-domain protein containing microtubule interacting and transport (MIT), Rhodanese and ubiquitin specific protease domains. As such, USP8 is a multi-functional protein and has been shown to have roles in deubiquitination, endosomal trafficking and mitophagy (Alexopoulou et al., 2016; Durcan et al., 2014; Peng et al., 2020; Smith et al., 2016; Zhou et al., 2013a).

Previous work in the De Vos laboratory had identified USP8 as a potential interacting partner of C9orf72 via a yeast two-hybrid (Y2H). The Y2H system utilises the activation of a reporter gene as a readout of protein-protein interaction. The transcription factor Gal4 comprises of a DNA binding domain that binds to an upstream activation sequence and an activation domain that recruits transcription machinery for the transcription of the reporter gene. In the Y2H system, the binding domain is fused with the first target protein sequence – termed bait - and the activation domain is fused with the second target protein sequence – termed prey. Interaction between the bait and prey brings the binding domain and the activation domain in close enough proximity to allow the recruitment of the transcription machinery and consequently transcription of the reporter gene (Figure 4.1, Lin and Lai, 2017).The screen consisted of C9orf72L (aa 1- 481) or C9orf72S (aa 1 – 222) cloned into the pGBKT7 vector as bait and a human brain cDNA library as prey and was performed by Protein Interaction Screening of the Genomics and Proteomics Core Facilities, German Cancer Research Centre in Heidelberg, Germany. Synapsin III was isolated 37 times and Coilin was isolated 5 times when C9orf72L was used as bait and formed the basis of Dr Rebecca Cohen's and Dr Yolanda Gibson's PhD theses respectively within our laboratory. A number of mitochondrial proteins were isolated with C9orf72L and C9orf72S as bait and formed the basis of Dr Emma Smith's PhD thesis within our laboratory. USP8 was isolated 2 times when C9orf72S was used as bait.

Therefore, we hypothesised that the C9orf72 might be a substrate of USP8, whereby USP8 is able to remove polyubiquitin chains and hence regulate C9orf72 levels. This would pinpoint USP8 as a potential therapeutic target for C9ALS/FTD. Hence, we investigated a possible role for USP8 in the deubiquitination of C9orf72.
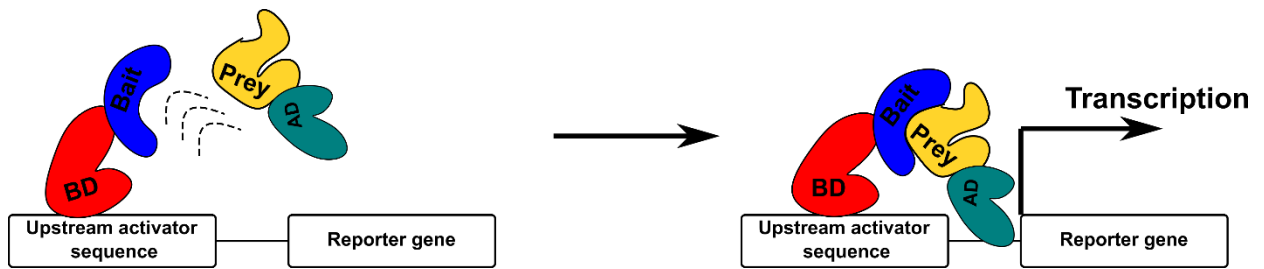
Figure 4.1: Summary of yeast-2-hybrid system.

Bait protein (blue) is fused to the binding domain (BD, red) of the Gal4 transcription factor. The prey (yellow) is fused to the activation domain (AD, green). Interaction between the bait and the prey protein results in recruitment of transcription machinery and subsequent transcription of the reporter gene.

4.2.1. C9orf72 interacts with USP8

In order to confirm the interaction between USP8 and C9orf72, a co-immunoprecipitation assay was utilised. Lysate from HEK293 cells were immunoprecipitated using an antibody against endogenous USP8. Whole cell lysate and the immune pellet were subjected to SDS-PAGE and immunoblot for C9orf72 and USP8. As a control, C9orf72[KO] cells were used. USP8 was readily detected in the input lysate and enriched in both HEK293 and C9orf72[KO] immunoprecipitated samples (Figure 4.2A). Endogenous C9orf72 co-immunoprecipitated with USP8 in the HEK293 immunoprecipitated sample, suggesting C9orf72 and USP8 interact (Figure 4.2A).

In a complementary approach, the reverse immunoprecipitation was performed. Lysate from HEK293 cells were immunoprecipitated using an antibody against endogenous C9orf72. Whole cell lysate and the immune pellet were subjected to SDS-PAGE and immunoblot for C9orf72 and USP8. C9orf72 was enriched in the HEK293 sample and USP8 co-immunoprecipitated with C9orf72 (Figure 4.2B). As no USP8 band was present in the C9orf72[KO] samples, this demonstrates the interaction is specific to C9orf72. Therefore, C9orf72 and USP8 interact by co-immunoprecipitation.
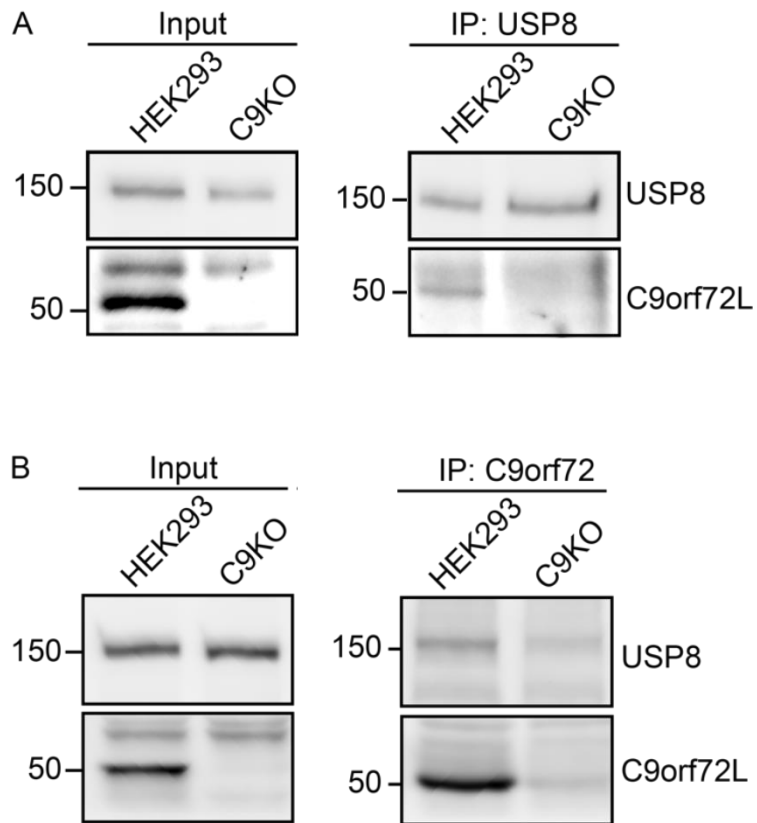
Figure 4.2: C9orf72 and USP8 interact by co-immunoprecipitation.

(A) Whole cell lysates of HEK293 or C9orf72[KO] were subjected to immunoprecipitation with anti-USP8 antibodies. Immune pellets were probed for USP8 with anti-USP8 antibodies and C9orf72 with anti-C9orf72 antibodies on immunoblot. (B) Whole cell lysates of HEK293 or C9orf72[KO] were subjected to immunoprecipitation with anti-C9orf72 antibodies. Immune pellets were probed for USP8 with anti-USP8 antibodies and C9orf72 with anti-C9orf72 antibodies.

4.2.2. USP8 does not regulate C9orf72 levels

Figure 4.2 shows that C9orf72 and USP8 interact, suggesting that C9orf72 might be a substrate and hence its levels regulated by USP8. Next, we wanted to determine whether expression of USP8 alters the levels of C9orf72. If C9orf72 is indeed a substrate of USP8, then exogenous expression of USP8 should result in an increase in deubiquitination and consequently an increase in C9orf72 level due to proteasomal degradation being prevented. HEK293 cells were co-transfected with Myc-C9orf72 and either EGFP or EGFP-USP8. Baseline levels of C9orf72 were determined by co-transfection of Myc-C9orf72 and EV. To determine whether any possible change in C9orf72 levels were due to the catalytic activity of USP8, a catalytically inactive form of USP8 was used as a control. Mutation of the catalytic cysteine to an arginine gave the catalytically inactive mutant (EGFP-USP8^{C786A}, Troilo et al., 2014). Samples were analysed via SDS-PAGE and immunoblot. Co-transfection of EGFP and Myc-C9orf72 did not increase Myc-C9orf72 levels compared to baseline (Figure 4.3A, B). In contrast, a significant increase in Myc-C9orf72 levels was observed upon EGFP-USP8 expression (Figure 4.3A, B). However, a similar increase was observed with the catalytically inactive mutant EGFP-USP8^{C786A} mutant, indicating that the observed increase was not due to deubiquitination (Figure 4.3B).

We also determined if USP8 affected endogenous C9orf72 levels. EGFP-USP8 and the catalytically inactive mutant was expressed alongside EGFP in HEK293 cells. Endogenous levels of C9orf72 in HEK293 cells were used as a baseline and C9orf72^{KO} cells were used to confirm endogenous C9orf72 detection. Whole cell lysate was analysed via SDS-PAGE and immunoblot for C9orf72 and EGFP-USP8 levels. Like Myc-C9orf72, endogenous C9orf72 levels did not increase above baseline upon expression of EGFP, but in contrast expression of both EGFP-USP8 and the C786A mutant also did not increase endogenous C9orf72 levels (Figure 4.3C, D).

In a complementary approach, we tested whether knockdown of USP8 levels affected endogenous C9orf72 levels, reasoning that if C9orf72 is a substrate of USP8, C9orf72 levels should decrease upon knockdown of USP8 compared to control. To do so, non-targeting and USP8-specific siRNA was expressed in HEK293 cells for 4 days. Whole cell lysate was analysed via SDS-PAGE and immunoblot for endogenous C9orf72 and USP8. Endogenous USP8 levels were markedly decreased in USP8 siRNA treated cells

compared to controls (Figure 4.3E, G). Knockdown of USP8 did not change endogenous C9orf72 levels (Figure 4.3E, F). Taken together these data suggest that USP8 is not a C9orf72 DUB.
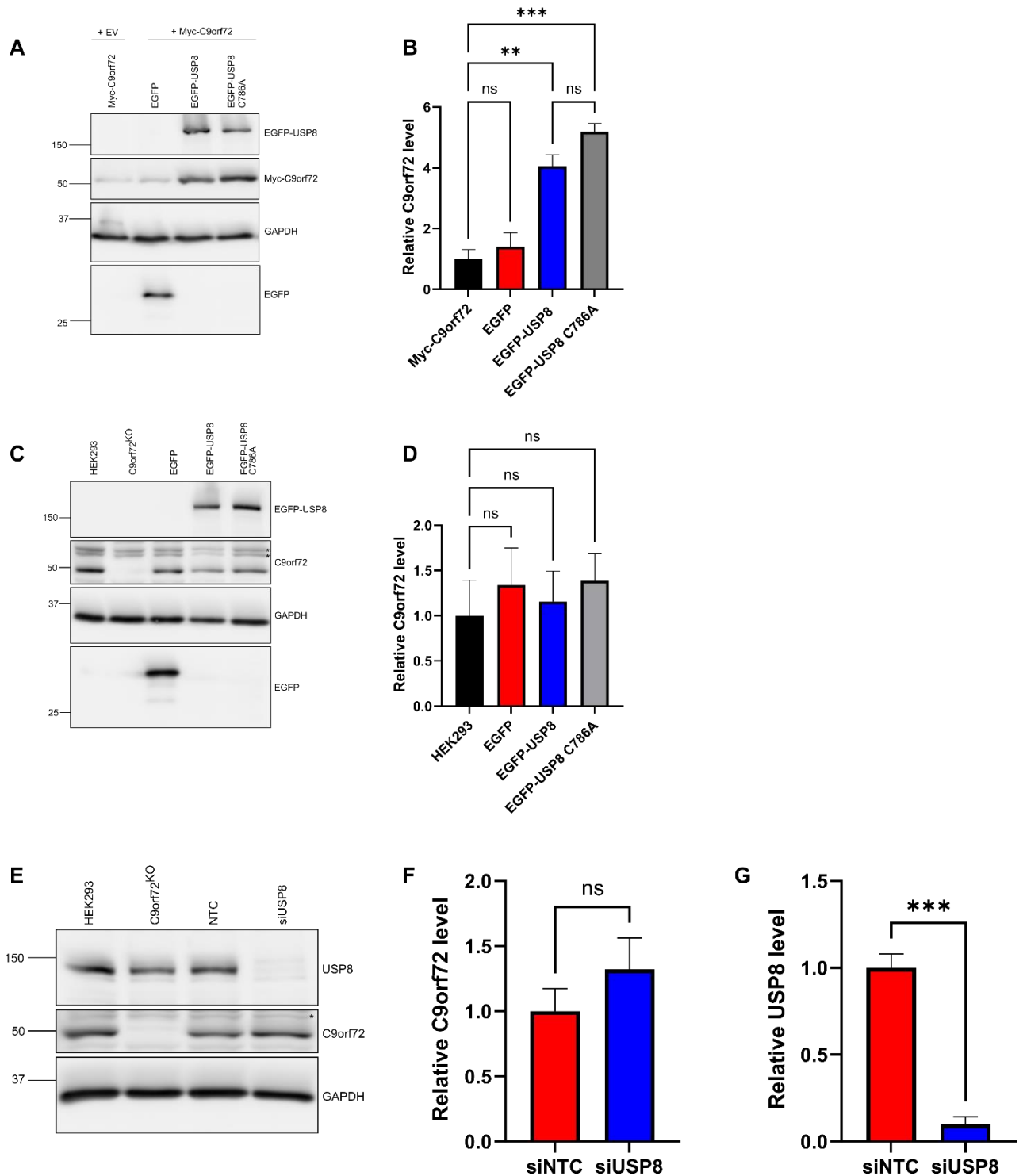
Figure 4.3: C9orf72 levels are not regulated by USP8.

(A) HEK293 cells were co-transfected with Myc-C9orf72 alongside either EGFP, EGFP-USP8 and the catalytically inactive mutant EGFP-USP8^{C786A}. Samples were subjected to SDS-PAGE and immunoblot for Myc-C9orf72 with anti-Myc antibodies, EGFP, EGFP-USP8 and EGFP-USP8^{C786A} using anti-GFP antibodies and anti-GAPDH antibodies as a loading control. (B) Quantification of the relative level of Myc-C9orf72 is shown (Mean ± SEM; one-way ANOVA with Fisher's LSD test, ** p ≤ 0.01, *** p ≤ 0.001, ns = non-significant; N = 3 experiments). (C) HEK293 cells were transfected with EGFP, EGFP-USP8 and EGFP-USP8^{C786A}. Samples were subjected to SDS-PAGE and immunoblot for C9orf72

with anti-C9orf72 antibodies, EGFP and EGFP-tagged constructs with anti-GFP antibodies and GAPDH antibodies as a loading control. Black asterisks (*) denote aspecific bands. (D) Quantification of the relative level of C9orf72 is shown (Mean ± SEM; one-way ANOVA with Fisher's LSD test, ns = non-significant; N = 3 experiments). (E) HEK293 cells were treated with non-targeting control (NTC) or USP8-specific siRNA (siUSP8). Samples were subjected to SDS-PAGE and immunoblot for USP8 with anti-USP8 antibodies, C9orf72 with anti-C9orf72 antibodies and GAPDH as a loading control. Black asterisks denote aspecific bands. (F) Quantification of the relative level of C9orf72 is shown (Mean ± SEM; unpaired two-tailed t-test, ns = non-significant; N = 3 experiments). (G) Knockdown of USP8 was confirmed using densitometry analysis (Mean ± SEM; unpaired two-tailed t-test, ** p ≤0.01; N = 3 experiments).

4.3. Investigating regulation of C9orf72-SMCR8 levels by KLHL9 and KLHL13

E3 ligases are responsible for the final step in the ubiquitination process. They catalyse the addition of ubiquitin to the lysine residue of a substrate protein and in doing so the target protein can have different functional consequences depending on the ubiquitin linkage type. For example, K48 ubiquitin chains are a well-known proteasomal degradation signal (Jacobson et al., 2009; Zheng et al., 2016). There are three classes of E3 ligases – HECT, RING and RBR. The E3 Cullin ligase complex belongs to the RING family of E3 ligases and consists of a Cullin scaffold, a KLHL substrate adaptor and RING finger protein. A mass spectrometry screen identified the Kelch-like protein KLHL13 as a potential interactor of SMCR8 (Jung et al., 2017a). KLHLs have a general structure consisting of a BTB domain, a BACK domain and a varying number of Kelch repeats. Few roles have been identified for KLHL13. One role is as a substrate-specific adaptor, forming a complex with KLHL9 and Cul3 to mediate ubiquitination and subsequent proteasomal degradation of insulin receptor substrate 1 and Aurora B (a component of the chromosomal passenger complex) (Frendo-Cumbo et al., 2019; Sumara et al., 2007). Similarly, KLHL9 has few identified roles, with most investigations focusing on the Cul3-KLHL9-KLHL13 complex and ubiquitination (Frendo-Cumbo et al., 2019; Sumara et al., 2007). KLHL9 has been identified as an inhibitor of tumour growth and Chen et. al, determined in their case this was a result of KLHL9 regulating ubiquitination for the transcription factors C/EBPβ and C/EBPδ (Chen et al., 2014b; Lee et al., 2015a). In both studies the involvement of KLHL13 has not been ruled out and so it is still undetermined whether KLHL9 acts independently in those cases. KLHL13 has also been identified as a driver of tumorigenesis in lung cancer and it was determined KLHL13's tumorigenesis function was independent of KLHL9 (Xiang et al., 2021).

We have shown that C9orf72 is a substrate of the proteasome and C9orf72 and SMCR8 complex formation stabilises their protein levels. As a substrate of the proteasome, specific E3 ligases are required for C9orf72 ubiquitination. Given KLHL13 was identified in a mass spectrometry screen with SMCR8 and KLHL13 has been shown to act as a regulator of ubiquitination when in complex with Cul3 and KLHL9, we decided to explore whether manipulation of KLHL9 and KLHL13 changes C9orf72 or SMCR8 protein levels.

4.3.1. Designing RT-qPCR primers for the detection of KLHL9 and KLHL13

To establish a KLHL knockdown model, we first needed to optimise a method for detection of the knockdown efficiency. Due to the poor specificity of commercial antibodies, we decided to quantify KLHL expression via RT-qPCR. Therefore, we needed to design RT-qPCR primers that could specifically detect KLHL9 and KLHL13. Ensembl (https://www.ensembl.org/index.html) was used to retrieve the DNA sequence of the coding exons for both KLHL9 and KLHL13. The KLHL13 transcript consisted of 7 coding exons and primers were designed to span the exon 2 – exon 3 boundary which flanks a large intron (Figure 4.4A). This reduced the risk of any false positives arising from amplification of genomic DNA as the short extension time is insufficient for the longer genomic target, but not the short cDNA sequence (Figure 4.4B). As the KLHL9 transcript consisted of only one exon, primers could not be designed to span an exon – exon junction and so were designed within the single exon (Figure 4.4A).

A

B
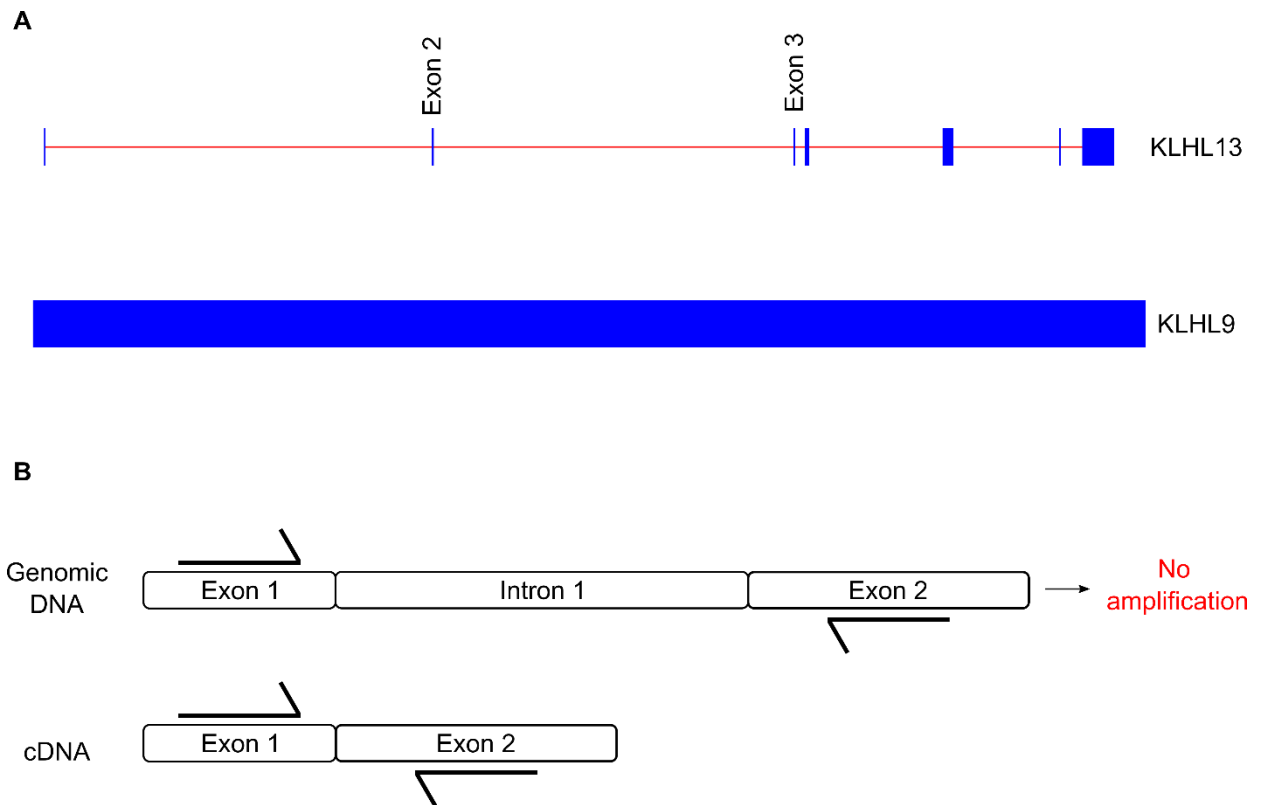
Figure 4.4:Design of RT-qPCR primers for KLHL13 and KLHL9.

(A). Top: KLHL13 transcript consists of 6 introns (red) and 7 coding exons (blue). Exons 2 and 3 are marked. RT-qPCR primers were designed to span the exon 2 – exon 3 junction. Bottom: KLHL9 transcript consists of a single coding exon. (B). RT-qPCR primers designed across an exon-exon boundary that flanks a large intron. Amplification of contaminating genomic DNA that contains the intron cannot be amplified as the short extension time is insufficient for the long genomic target. Amplification of the cDNA is possible due to the shorter length of the cDNA sequence.

4.3.2. Optimisation of siRNA-mediated knockdown of KLHL9 and KLHL13

To determine whether the designed RT-qPCR primers were able to specifically amplify their target, RNA was extracted from HeLa cells, reverse transcribed into cDNA and the cDNA subjected to RT-qPCR. HeLa cells were chosen as they contain higher basal levels of KLHL9 and KLHL13 compared to HEK293 cells (Danielsson et al., 2013; Thul et al., 2017). Primer concentration of 1 µM, 500 nM, 250 nM or 125 nM were tested. The KLHL13 primers were able to successfully amplify KLHL13 at all primer concentrations (Figure 4.5A, B). A single melt peak for each of the concentrations was produced, demonstrating the amplified cDNA belongs to a single PCR product, KLHL13. Furthermore, the range of concentrations resulted in similar Ct values as indicated by the amplification plots. Successful amplification for KLHL9 was also achieved across the range of concentrations, with no evidence of primer dimer formation (Figure 4.5C, D). This demonstrates that both the KLHL9 and KLHL13 RT-qPCR primers are able to successfully and specifically amplify endogenous KLHL9 and KLHL13. For all subsequent experiments, KLHL9 siRNA #1 and KLHL13 siRNA #1 was used at a primer concentration of 125 nM.

Next, we wanted to determine whether we could successfully knockdown KLHL9 and KLHL13. Two siRNA oligonucleotide sequences specific for KLHL9 and KLHL13 were obtained (Sumara et al., 2007). The two sequences of siRNA were expressed in HeLa cells for 4 days (individually or pooled together) alongside a non-targeting NTC siRNA. For KLHL9-specific siRNA, the levels of endogenous KLHL9 mRNA greatly reduced upon expression of the first individual sequence compared to controls (Figure 4.5E). The second KLHL9-specific siRNA reduced levels by approximately 25% compared to controls. Therefore, pooling of the sequences did not result in a further reduction of mRNA beyond that of the first sequence. Quantification revealed both the individual sequences and the pooled sequence reduced KLHL9 mRNA levels to statistically significant lower levels (Figure 4.5E). For KLHL13, a marked reduction in endogenous KLHL13 mRNA was observed for both the first and second individual sequence compared to control (Figure 4.5F). Pooling of the sequences resulted in a reduction in mRNA levels to that between the first and second sequence. Quantification revealed the decrease in mRNA for both the individual sequence and pooled sequences were

significant compared to controls (Figure 4.5F). Therefore, the KLHL9- and KLHL13-specific siRNA can reduce endogenous mRNA levels.
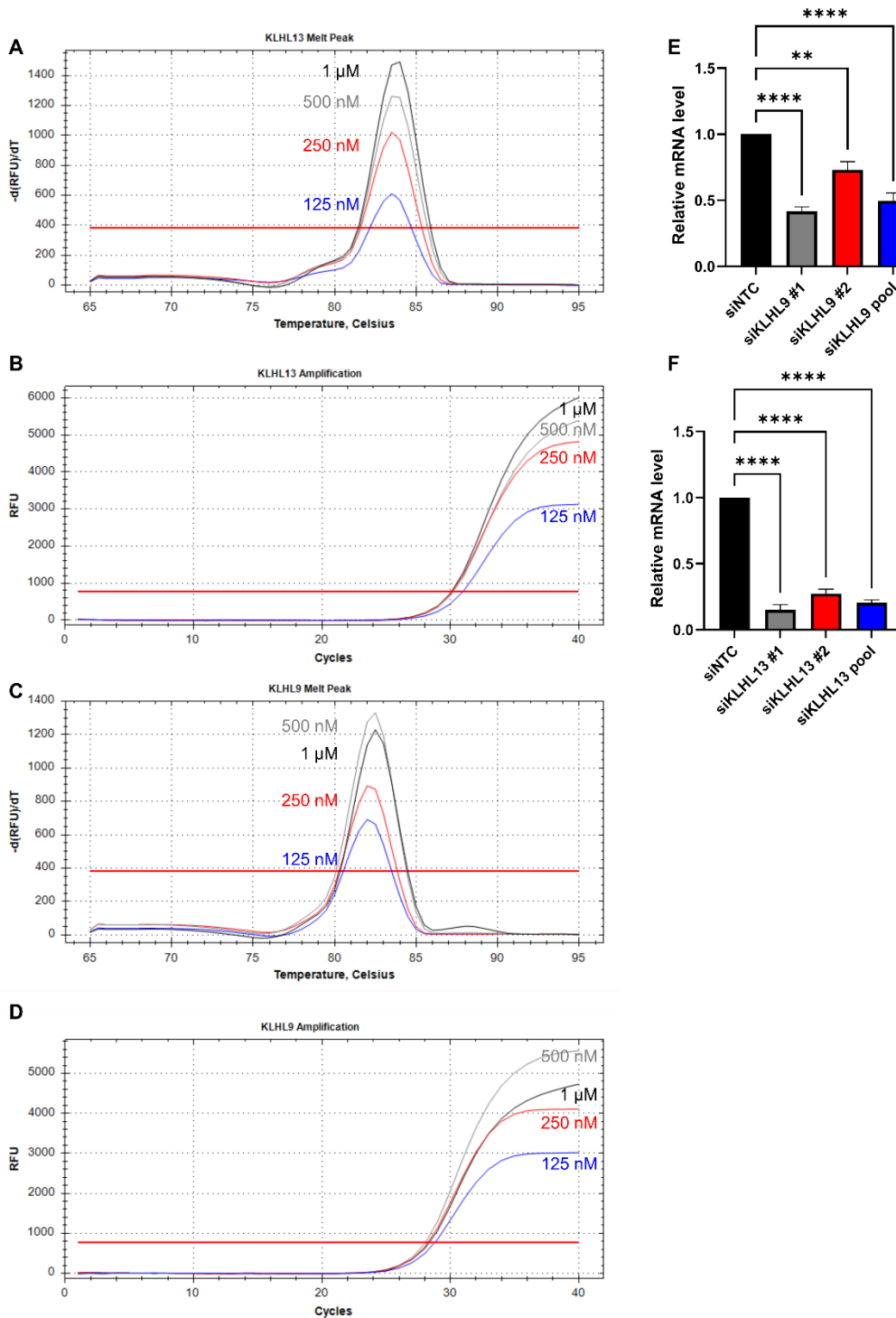
Figure 4.5 Optimisation of KLHL9 and KLHL13 siRNA.

(A-D). Optimisation of a range of concentration for RT-qPCR primers. cDNA was produced from RNA extracted from HeLa cells and subjected to RT-qPCR. (A) KLHL13 melt peak for RT-qPCR using a range of KLHL13 RT-qPCR primer concentrations. (B). KLHL13 amplification plot for RT-qPCR using a range of KLHL13 RT-qPCR primer concentrations. (C) KLHL9 melt peak for RT-qPCR using a range of KLHL9 RT-qPCR primer concentrations. (D). KLHL9 amplification plot for RT-qPCR using a range of KLHL9 RT-qPCR primer concentrations. (F) HeLa cells were transfected with non-targeting control (NTC) siRNA, and either single or pooled KLHL9-specific siRNAs. Knockdown of KLHL9 was confirmed by RT-qPCR with values normalised to GAPDH housekeeping gene (Mean ± SEM; one-way ANOVA with

Fisher's LSD test ** p ≤ 0.01 **** p ≤ 0.0001; N = 3 experiments). (G) HeLa cells were transfected with non-targeting control (NTC) siRNA, and either single or pooled KLHL13-specific siRNAs. Knockdown of KLHL13 was confirmed by RT-qPCR with values normalised to GAPDH housekeeping gene (Mean ± SEM; one-way ANOVA with Fisher's LSD test, **** p ≤ 0.0001; N = 3 experiments).

4.3.3. Knockdown of KLHL13 increases C9orf72 and SMCR8 levels

We established KLHL9 and KLHL13 siRNA can reduce endogenous mRNA levels. KLHL13 was identified as an interacting partner of SMCR8 via mass spectrometry and acts as in an E3 ligase complex with KLHL9 and Cul3, regulating ubiquitination of substrate proteins. We determined in Chapter 3, C9orf72 is a substrate of the proteasome. Therefore, we wanted to establish whether altering KLHL9 and KLHL13 levels affected C9orf72 levels.

To do so, non-targeting, KLHL9- and KLHL13-specific siRNA were expressed in HeLa cells for 4 days. 24 hrs prior to harvesting cells were transfected with either Myc-C9orf72 or SMCR8-Myc/DDK. Samples were subjected to SDS-PAGE and immunoblot for Myc-C9orf72 and SMCR8-Myc/DDK levels. Knockdown of KLHL9 and KLHL13 was confirmed using RT-qPCR. The level of KLHL9 and KLHL13 mRNA was significantly reduced across all samples (Figure 4.6C, F). For SMCR8-Myc/DDK, reduction of KLHL9 resulted in no change in SMCR8 levels (Figure 4.6A, B). Conversely, reduction of KLHL13 resulted in a significant increase in SMCR8-Myc/DDK levels. Similarly, in the case of Myc-C9orf72 a reduction in KLHL13, but not KLHL9, resulted in a significant increase in C9orf72 levels (Figure 4.6D, E).

We also tested whether a reduction in KLHL9 and KLHL13 changed endogenous levels of C9orf72 and SMCR8. Non-targeting, KLHL9- and KLHL13-specific siRNA were expressed in HeLa cells for 4 days. C9orf72 and SMCR8 levels were analysed by SDS-PAGE and immunoblot. Knockdown of KLHL9 and KLHL13 was confirmed via RT-qPCR and revealed KLHL9 and KLHL13 levels were significantly reduced (Figure 4.6J). Knockdown of KLHL9 did not alter C9orf72 levels whereas knockdown of KLHL13 resulted in an increase in C9orf72 levels (Figure 4.6G, H). SMCR8 levels appeared to increase upon knockdown of KLHL13. Nevertheless, densitometry analysis revealed the increase is not significant, possibly due to the large variation and low number of repeats (n = 2) (Figure 4.6G, I). Taken together, this demonstrates that altering KLHL13 levels can alter the levels of C9orf72 and SMCR8 and positions C9orf72 and SMCR8 as possible substrates of KLHL13.
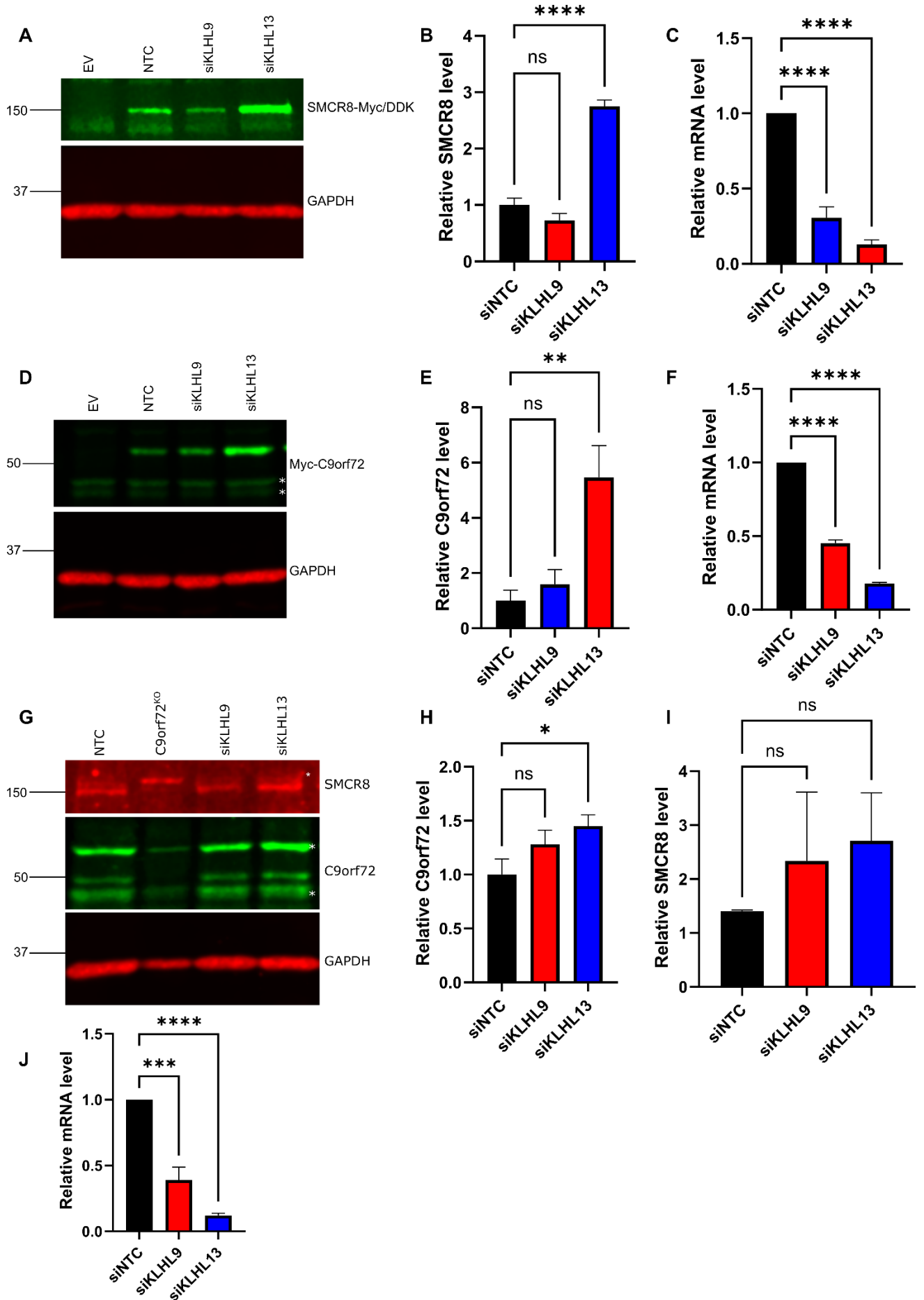
Figure 4.6: Knockdown of KLHL13 increases C9orf72 and SMCR8 levels.

(A) HeLa cells were treated with non-targeting control (NTC), KLHL9- or KLHL13-specific siRNA. Cells were transfected with SMCR8-Myc/DDK and subjected to SDS-PAGE and immunoblots for SMCR8-Myc/DDK with M2 anti-FLAG antibodies and anti-GAPDH antibodies as a loading control. (B) Quantification of relative SMCR8 levels (Mean ± SEM; one-way ANOVA with Fisher's LSD test, **** $p \leq 0.0001$, ns = non-significant; N = 3 experiments). (C) Knockdown of KLHL9 and KLHL13 was confirmed via RT-qPCR (Mean ± SEM; one-way ANOVA with Fisher's LSD test, **** $p \leq 0.0001$; N = 3 experiments). (D) HeLa cells were treated with non-targeting control (NTC), KLHL9- or KLHL13-specific siRNA. Cells were transfected with Myc-C9orf72 and subjected to SDS-PAGE and immunoblots for Myc-C9orf72 with 9B11 anti-Myc antibodies and anti-GAPDH antibodies as a loading control. White asterisks denote aspecific bands. (E) Quantification of relative C9orf72 levels (Mean ± SEM; one-way ANOVA with Fisher's LSD test, ** $p \leq 0.01$, ns = non-significant; N = 3 experiments). (F) Knockdown of KLHL9 and KLHL13 was confirmed via RT-qPCR (Mean ± SEM; one-way ANOVA with Fisher's LSD test, **** $p \leq 0.0001$; N = 3 experiments). (G) HeLa cells were treated with non-targeting control (NTC), KLHL9- or KLHL13-specific siRNA. Cells were subjected to SDS-PAGE and immunoblots for SMCR8 with anti-SMCR8 antibodies, C9orf72 with anti-C9orf72 antibodies and anti-GAPDH antibodies as a loading control. White asterisks denote aspecific bands. (H) Quantification of relative C9orf72 levels (Mean ± SEM; one-way ANOVA with Fisher's LSD test, * $p \leq 0.05$, ns = non-significant; N = 3 experiments). (I) Quantification of relative SMCR8 levels (Mean ± SEM; one-way ANOVA with Fisher's LSD test, ns = non-significant; N = 2 experiments). (J) Knockdown of KLHL9 and KLHL13 was confirmed via RT-qPCR (Mean ± SEM; one-way ANOVA with Fisher's LSD test, *** $p \leq 0.001$ **** $p \leq 0.0001$; N = 3 experiments).

4.3.4. Knockdown of KLHL13 affects C9orf72 and SMCR8 turnover

We established reducing KLHL13 levels increase C9orf72 and SMCR8 levels. The increase in C9orf72 and SMCR8 levels upon knockdown of KLHL13 suggests that C9orf72 and SMCR8 are substrates of KLHL13, consistent with C9orf72 being a substrate of the proteasome. Hence, we wanted to determine whether the increase in protein levels was due to an altered rate of turnover. To do this, we utilised the cycloheximide chase assay. Non-targeting, KLHL9- and KLHL13-specific siRNA were expressed in HeLa cells for 4 days. Myc-C9orf72 and SMCR8-Myc/DDK were expressed 24 hrs prior to harvesting. Samples were treated with CHX and harvested 0, 2, 4 and 8 hrs post treatment then subjected to SDS-PAGE and immunoblot for Myc-C9orf72 and SMCR8-Myc/DDK levels. Knockdown of KLHL9 and KLHL13 was confirmed using RT-qPCR. KLHL9 and KLHL13 levels were significantly reduced compared to controls across all samples (Figure 4.7C, F). In the case of Myc-C9orf72, reducing KLHL13 levels increased the level of Myc-C9orf72 at 0 hrs (Figure 4.6A). Moreover, the half-life of C9orf72 increased (Figure 4.7B). However, knockdown of KLHL9 did not alter the turnover rate of C9orf72 and therefore, there was no difference in the half-life for C9orf72 (Figure 4.7B). Similarly, for SMCR8-Myc/DDK, the rate of turnover and subsequently the half-life was not altered by a reduction in KLHL9 levels (Figure 4.7E). However, knockdown of KLHL13 increased the half-life of SMCR8-Myc/DDK. Taken together, this suggests that KLHL13 may be involved in the ubiquitination and subsequent degradation of C9orf72 and SMCR8.
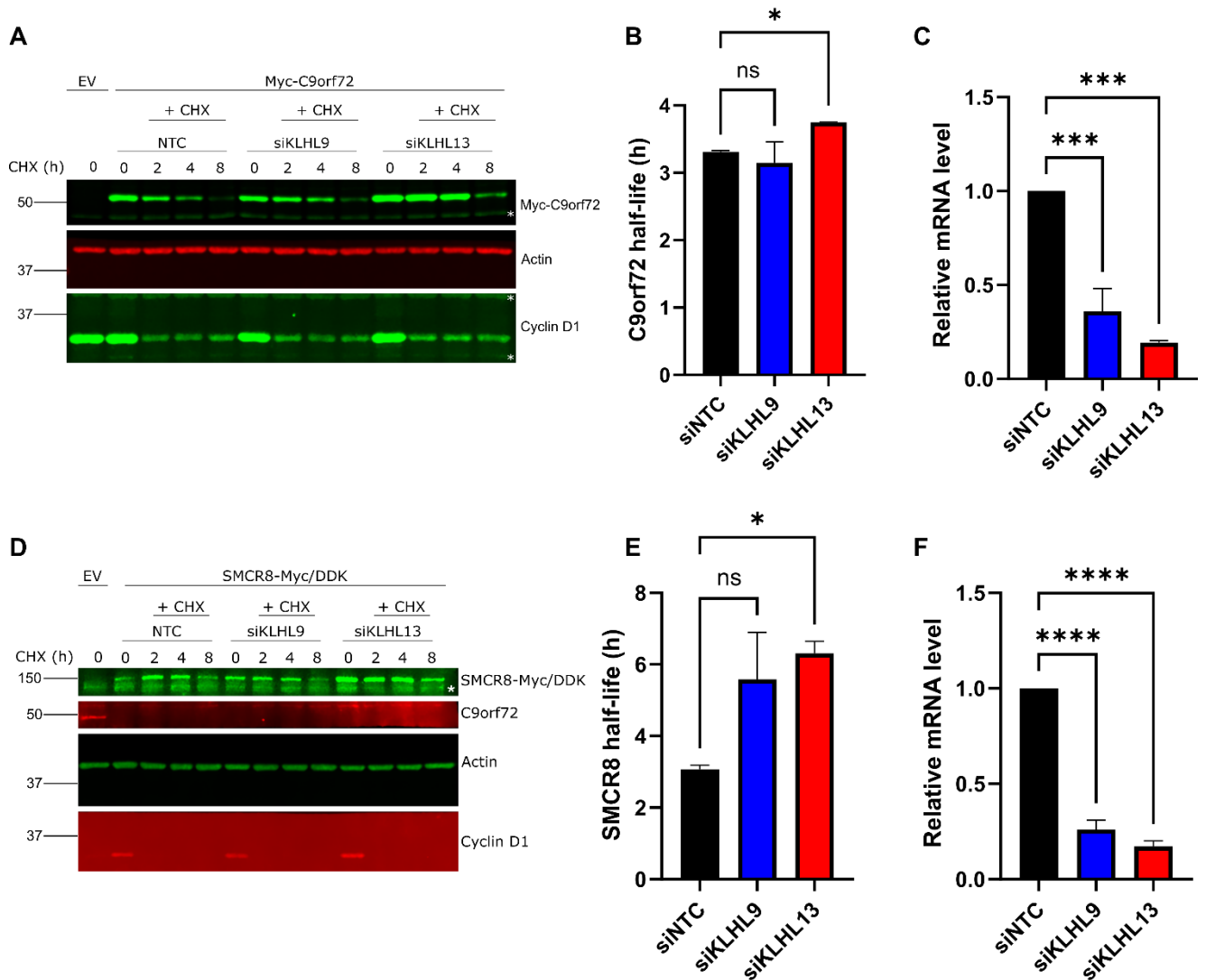
Figure 4.7: Knockdown of KLHL13 alters C9orf72 and SMCR8 turnover.

(A) HeLa cells were treated with non-targeting control (NTC), KLHL9- or KLHL13-specific siRNA and transfected with Myc-C9orf72. Cells were treated with cycloheximide (CHX) for the indicated times and subjected to SDS-PAGE and immunoblot for Myc-C9orf72 with anti-Myc antibodies, anti-Cyclin D1 antibodies and anti-actin antibodies as a loading control. White asterisks denote aspecific bands. (B) Comparison of Myc-C9orf72 half-life upon NTC, KLHL9 or KLHL13 siRNA treatment. (Mean ± SEM, RM one-way ANOVA with Fisher's LSD test, ns = non-significant; N = 2 experiments). (C) Knockdown of KLHL9 and KLHL13 was confirmed via RT-qPCR (Mean ± SEM; one-way ANOVA with Fisher's LSD test, *** p ≤ 0.001; N = 2 experiments). (D) HeLa cells were treated with non-targeting control (NTC), KLHL9- or KLHL13-specific siRNA and transfected with SMCR8-Myc/DDK. Cells were treated with cycloheximide (CHX) for the indicated times and subjected to SDS-PAGE and immunoblot for SMCR8-Myc/DDK with anti-FLAG antibodies, anti-Cyclin D1 antibodies and anti-actin antibodies as a loading control. White asterisks denote aspecific bands. (E) Comparison of SMCR8-Myc/DDK half-life upon NTC, KLHL9 or KLHL13 siRNA treatment. (Mean ± SEM, RM one-way ANOVA with Fisher's LSD test, ns = non-significant, * p ≤ 0.05; N = 2 experiments). (F) Knockdown of KLHL9 and KLHL13 was confirmed via RT-qPCR (Mean ± SEM; one-way ANOVA with Fisher's LSD test, **** p ≤ 0.0001; N = 2 experiments).

4.4.　　　Inhibition of Cullin using MLN4924 prevents SMCR8 turnover

Kelch proteins form a complex with Cul3 and mediate the ubiquitination of substrate proteins by bringing the substrate into close proximity to the RING domain of Cul3, allowing transfer of ubiquitin from the RING domain to the substrate. We determined that C9orf72 and SMCR8 are possible substrates of KLHL13 with knockdown of KLHL13 increasing C9orf72 and SMCR8 levels and half-life. Therefore, we wanted to determine whether inhibition of Cul3 altered the levels of C9orf72 and SMCR8, reasoning that if ubiquitination is prevented C9orf72 or SMCR8 protein levels may be altered. To inhibit ubiquitination a NEDD8 inhibitor, MLN4924 was utilised. MLN4924 is a AMP mimetic that inhibits activation of Cullin ligases by binding to the active site of the NEDD8 E1-activating enzyme thereby preventing NEDDylation (Brownell et al., 2010; Soucy et al., 2009).

HeLa C9orf72^{KO} cells were transfected with either Myc-C9orf72 or SMCR8-Myc/DDK. Transfected cells were then left untreated, treated with CHX alone or pre-treated with MLN4924 for 30 mins prior to the addition of CHX. Following a 4 hr incubation period, lysates were prepared and subjected to SDS-PAGE and immunoblot for C9orf72 and SMCR8 levels. Addition of CHX appeared to decrease the level of Myc-C9orf72, although this was not significant (Figure 4.8A, B). Furthermore, there was no difference in C9orf72 levels between CHX and CHX + MLN4924 treatments (Figure 4.8B). In contrast, CHX treatment significantly decreased the level of SMCR8 and this could be rescued by CHX + MLN4924 treatment (Figure 4.8C, D). There was a significant decrease in SMCR8 levels between untreated and CHX + MLN4924 treated cells. This suggests that MLN4924 treatment may partially rescue SMCR8 levels by preventing the ubiquitination and subsequent proteasomal degradation of SMCR8.
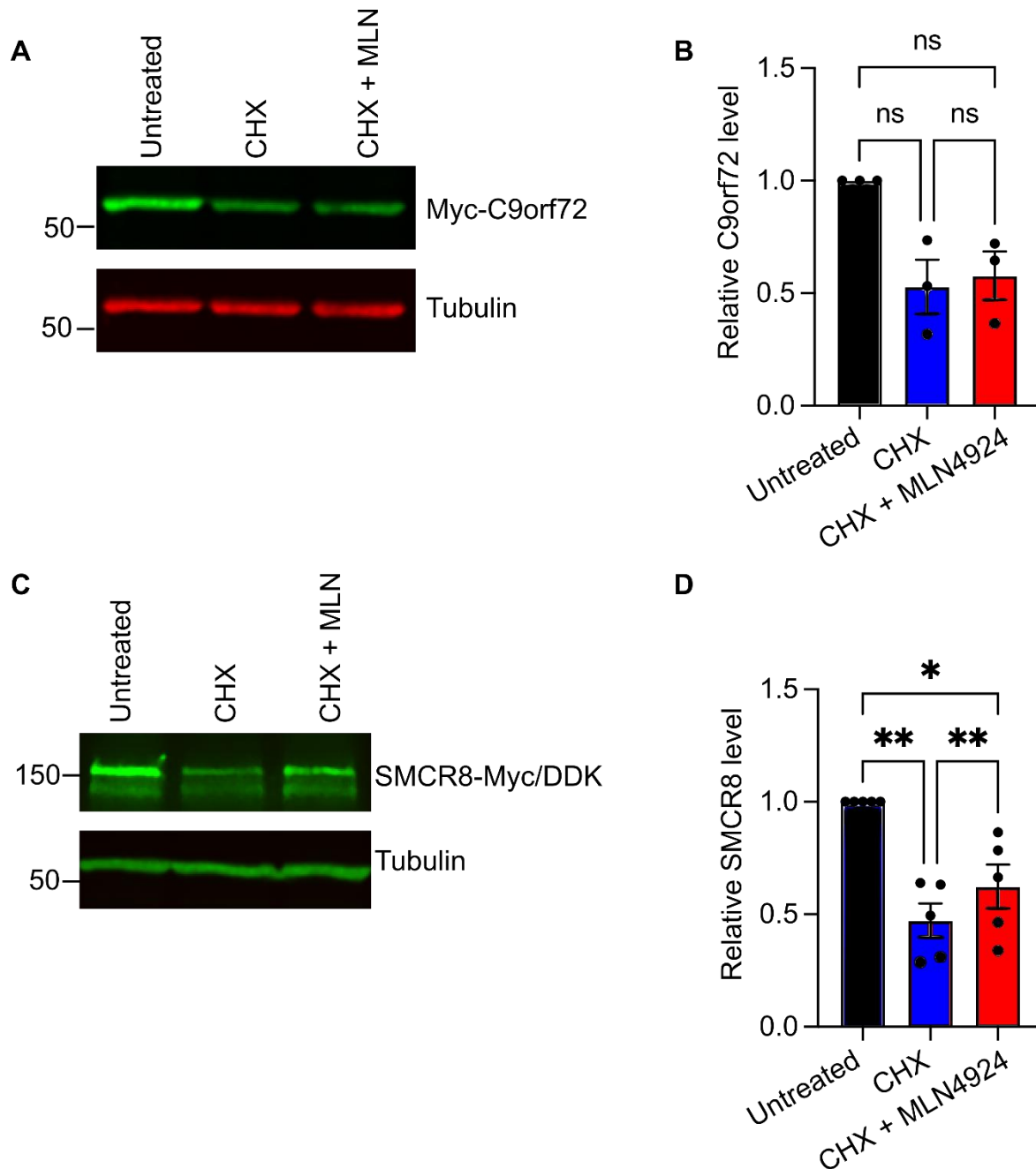
Figure 4.8: Inhibition of Cullin prevents SMCR8, but not C9orf72 turnover.

(A) HeLa C9orf72^{KO} cells were transfected with Myc-C9orf72 and left untreated or were treated with CHX alone or CHX in combination with MLN4924 (cells were pre-treated with MLN4924 30 mins prior to addition of CHX). After 4 hr incubation, cell lysates were prepared and subjected to SDS-PAGE an immunoblot for Myc-C9orf72 levels using anti-Myc antibodies. Anti-tubulin antibodies were used as a loading control (B) Quantification of relative C9orf72 levels (Mean ± SEM; One-way ANOVA with Fisher's LSD, ns = non-significant; N = 3 experiments). (C) HeLa C9orf72^{KO} cells were transfected with SMCR8-Myc/DDK and left untreated or were treated with CHX alone or CHX in combination with MLN4924 (cells were pre-treated with MLN4924 30 mins prior to addition of CHX). After 4 hr incubation, cell lysates were prepared and subjected to SDS-PAGE an immunoblot for SMCR8-Myc/DDK levels using anti-Myc antibodies. Anti-tubulin antibodies were used as a loading control (D) Quantification of relative SMCR8 levels (Mean ± SEM; One-way ANOVA with Fisher's LSD, * $p ≤ 0.05$, ** $p ≤ 0.01$; N = 5 experiments).

4.5.   Discussion

This chapter sought to identify key enzymes involved in the regulation of C9orf72 protein turnover and determine whether altering the enzymes levels influenced C9orf72 levels. In line with the hypothesis, KLHL13 was identified as a regulator of C9orf72 and SMCR8 levels.

Given USP8 was identified in a Y2H screen as a potential interactor of C9orf72, we first sough to confirm the interaction. We found that in HEK293 cells, immunoprecipitation of endogenous USP8 resulted in co-immunoprecipitation of C9orf72. Following confirmation of the C9orf72-USP8 interaction, we next sought to determine the functional relevance of this interaction. Of most interest to us was the DUB capabilities of USP8. We therefore set out to determine whether altering expression of USP8 influenced C9orf72 levels. We found that expression of USP8 increased both exogenous and endogenous C9orf72 protein levels. However, the catalytically inactive mutant also increased C9orf72 levels. This suggests the increase in C9orf72 levels is not due to the DUB activity of USP8. USP8 is a multi-domain protein that is known to have multiple functions. For example, it has been shown to regulate mitophagy, is involved in endosomal trafficking and the stabilisation of a multitude of proteins (Alexopoulou et al., 2016; Durcan et al., 2014; Macdonald et al., 2014; Peng et al., 2020; Wu et al., 2004; Zhou et al., 2013a). Given this, it is likely that the C9orf72-USP8 interaction is due USP8 functioning in one of its other capacities. A possible role for C9orf72 in regulating USP8 trafficking is discussed in Chapter 6.5. Interestingly, co-expression of C9orf72 and EGFP-USP8 (or EGFP-USP8[C786A]) increased the level of Myc-C9orf72 compared to expression of Myc-C9orf72 alone. This is similar to the increase in C9orf72 levels observed when HA-Ubiquitin is co-expressed with C9orf72 (Figure 3.5) or SMCR8 is co-expressed with C9orf72 (Figure 3.2) and hints at possible stabilisation of C9orf72 by USP8. However, unlike SMCR8 knockdown reducing C9orf72 levels, no decrease in C9orf72 levels is observed upon USP8 knockdown.

Additionally, we found that a reduction in USP8 did not alter C9orf72 levels. Indeed, if USP8 was functioning as a DUB, we would expect a reduction in USP8 levels to result in a reduction in C9orf72 levels due to the inability to remove the polyubiquitin chain from

C9orf72 that targets it for proteasomal degradation. Therefore, our findings from transient knockdown of USP8 further the idea of USP8 having a different function in this instance. As we have established an assay for identifying C9orf72 ubiquitination (Chapter 3.6), it would be interesting to explore whether reduction of USP8 using siRNA influences the ubiquitination status of C9orf72 as this would provide further evidence of whether USP8 deubiquitinated C9orf72.

Within this chapter, we explored a role for the Kelch-like proteins KLHL9 and KLHL13 in the regulation of C9orf72 and SMCR8 levels. Using HeLa cells due to their higher basal levels of KLHL9 and KLHL13, we tested siRNA against the two ligases. Due to a lack of specific antibodies, we verified knockdown using RT-qPCR. We found that the siRNA against both KLHL9 and KLHL13 successfully reduced mRNA levels. Pooling together of the individual mRNA sequences did not result in a greater reduction. Thus, the single sequences were sufficient to reduce KLHL9 and KLHL13 levels. Following this we sought to determine whether C9orf72 and SMCR8 levels could be influenced by KLHL9 or KLHL13. We determined knockdown of KLHL9 did not change SMCR8-Myc/DDK levels. However, a marked increase in SMCR8-Myc/DDK was observed upon knockdown of KLHL13. Similarly, knockdown of KLHL9 had no effect on Myc-C9orf72 levels. In contrast, knockdown of KLHL13 greatly increased the level of Myc-C9orf72. Results for endogenous C9orf72 mimicked that of overexpressed in that knockdown of KLHL13, but not KLHL9 resulted in an increase in C9orf72 levels. In the case of endogenous SMCR8, overall no change was observed from knockdown of either ligase. However, it must be noted that there is only an n = 2 for these experiments and the general trend is an increase in SMCR8 upon KLHL13 knockdown samples compared to controls. Figure 4.9 depicts the individual experimental points and demonstrates the large variation. Therefore, although the data suggests an increase in SMCR8 no solid conclusions can be drawn about the effect of KLHL13 knockdown on endogenous SMCR8 without repetition of the experiments to reduce the variation. The results from these experiments suggest that C9orf72 and SMCR8 may be a substrate of KLHL13 whereby KLHL13 may be involved in the turnover of the C9orf72-SMCR8 complex. This is consistent with the identification of KLHL13 in a mass spectrometry screen with SMCR8 and the functional role of KLHL13.
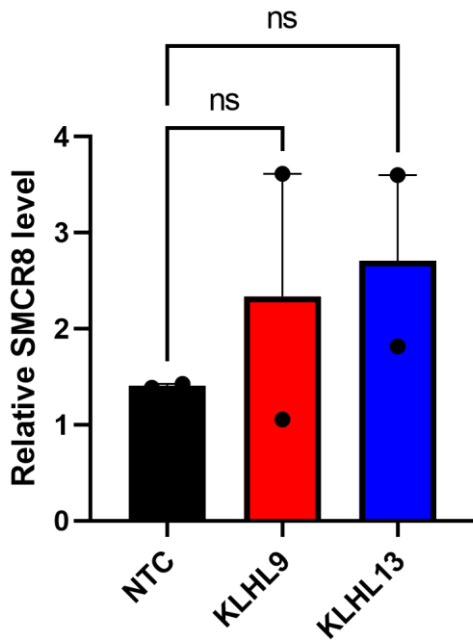
Figure 4.9: Large variation in SMCR8 levels upon knockdown of KLHL13.

Quantification of relative SMCR8 levels (Mean ± SEM with individual experimental points shown (black dots); one-way ANOVA with Fisher's LSD test, ns = non-significant; N = 2 experiments).

Following this, we went on to determine the effect of KLHL9 and KLHL13 knockdown on Myc-C9orf72 and SMCR8-Myc/DDK turnover and established that knockdown of KLHL9 did not significantly alter the rate of Myc-C9orf72 or SMCR8-Myc/DDK degradation over an 8 hr period. In contrast, loss of KLHL13 altered the rate of degradation for both C9orf72 and SMCR8 over an 8 hr period. This further suggests that KLHL13 can act as a substrate specific adaptor for C9orf72 and SMCR8 and possibly mediate ubiquitination of the proteins. Interestingly, the degradation of both C9orf72 and SMCR8 appeared to be slowed but not completely abolished by knockdown of KLHL13, suggesting that C9orf72 and SMCR8 is still able to be degraded. One possible explanation for this may be that other substrate adaptors that form a complex with Cul3 are able to ubiquitinate C9orf72 and SMCR8. Cul3 ligases associate with BTB domain containing proteins, with the best known protein being BTB-BACK Kelch domain proteins, of which the KLHL subfamily contain (Canning et al., 2013). Members of the Cullin family do not directly interact with substrate proteins but instead interact through the substrate specific BTB adaptors. Cul3 has been shown to interact with multiple KLHL proteins (Dhanoa et al., 2013; Furukawa et al., 2003). Therefore, it is possible that KLHL13 may be the primary

substrate adaptor of C9orf72 and SMCR8, and upon knockdown of KLHL13 other KLHL proteins assume responsibility. Similarly, it is possible that multiple ubiquitin ligases are responsible for ubiquitination of either C9orf72 or SMCR8. This may in part explain the increase in C9orf72 and SMCR8 levels upon knockdown of KLHL13 and why C9orf72 and SMCR8 levels start higher, and their turnover is slowed but not completely prevented. There are many cases in literature of substrates being ubiquitinated by multiple E3 ligases. For example, the ubiquitination and subsequent degradation of the tumour suppressor p53 is performed primarily by Mdm2 but also by Pirh2, MDMX and COP1 (Wang et al., 2011). The identification by mass spectrometry of other E3 ligases that interact with the C9orf72 or SMCR8 proteome in human and mouse gives credence to this idea (Goodier et al., 2020; Zhang et al., 2018b). C degrons are destabilising sequences at the C-terminus of proteins that can be recognised by receptors of Cullin ligases for proteasomal degradation (Koren et al., 2018; Lin et al., 2018) The Cul2 E3 ligase forms a complex with the substrate recognition subunit FEM1B which recognises specific, exposed C degrons and bioinformatics revealed a C degron of SMCR8 (aa 1 – 787) is recognised by Cul2-FEM1B (Chen et al., 2021; Zhao et al., 2021). Although the functional consequences of this isoform of SMCR8 remains to be determined, this suggests that Cul2-FEM1B may potentially be involved in the proteasomal degradation of this isoform of SMCR8.

Our findings that inhibition of Cullin ligases using MLN4924 partially rescues SMCR8 levels following CHX treatment potentially gives more credibility to this idea and suggests that perhaps other E3 ligases are involved. MLN4924 is an inhibitor of NAE and as such inhibits activation of all Cullin ligases. This would suggest that if other Kelch proteins were able to ubiquitinate SMCR8, their inhibition by MLN4924 would prevent ubiquitination of C9orf72 or SMCR8 if they were substrates of other Kelch proteins. As stated previously, the identification of other non-Cullin E3 ligases by mass spectrometry hints at a possible role for other ligases in the ubiquitination of C9orf72 and SMCR8. MLN4924 treatment has been shown to induce autophagy in cancer cell lines (Lv et al., 2018; Zhao et al., 2012b). It will need to be determined whether this is specific to cancer cell lines, but it may be possible that the lack of difference in C9orf72 levels between CHX and CHX/MLN4924 treated cells is due to C9orf72 being shunted to autophagy. Treatment of cells with CHX/MLN4924/bafilomycin could shed some light on this. If

C9orf72 was being degraded via autophagy, inhibition of autophagy using bafilomycin should result in an increase in C9orf72 levels.

To determine whether KLHL13 influences the ubiquitination status of C9orf72 and SMCR8, a ubiquitination assay could be employed. If KLHL13 was a *bona fide* substrate adaptor for C9orf72 and SMCR8, there should be a reduction in C9orf72 and SMCR8 ubiquitination upon knockdown of KLHL13. Furthermore, microarray or nanostring analysis could be employed to detect any regulation changes in E3 ligase or Kelch genes upon knockdown of KLHL13 which may give an indication as to whether other Kelch ligases are upregulated to ubiquitinate C9orf72 or SMCR8 in response to KLHL13 knockdown. As this approach would not determine whether any identified upregulated enzymes ubiquitinate C9orf72 or SMCR8 under basal conditions, this would have to be confirmed.

The interaction between KLHL13 and C9orf72 or SMCR8 has not been studied here. Therefore, it remains to be determined whether C9orf72, SMCR8 or both proteins interact directly with KLHL13. Results from mass spectrometry analysis of SMCR8 would suggests KLHL13 interacts directly with SMCR8, however, it is still possible C9orf72 interacts. As a substrate adaptor for the Cul3 ligase, it is generally assumed that any effect on protein levels from KLHL13 is due to KLHL13 acting directly on the substrate itself. However, as we and others have shown, C9orf72 and SMCR8 levels are highly co-dependent and a protein level decrease in one decreases the protein level of the other. Therefore, a C9orf72/KLHL13 and SMCR8/KLHL13 co-immunoprecipitation assay may elucidate which of these proteins has a direct interaction with KLHL13 and whether the increase in C9orf72 is because of a direct or indirect effect of KLHL13.

5. Investigating SUMOylation of the C9orf72-SMCR8 complex

5.1.   Introduction

In this chapter, SUMOylation of the C9orf72-SMCR8 complex was investigated. SUMOylation is a post-translational modification involving the protein small ubiquitin-related modifier (SUMO). In this process, SUMO is covalently attached to a substrate protein through lysine linkages and involves three consecutive steps requiring E1-activating, E2-conjugating and E3-ligating enzymes. Much like ubiquitination, SUMOylation is a reversible process which requires deSUMOylating enzymes.

SUMOylation has been shown to be involved in many biological processes including nuclear transport, regulation of cell cycle, DNA repair, protein localisation, stability and protein/protein interactions (Kerscher et al., 2006; Maraschi et al., 2021; Moreno-Oñate et al., 2020; Pelisch et al., 2014; Waltersa et al., 2021). A SUMOylated protein can interact with another protein in a non-covalent manner through SUMO interacting motifs (SIMs) in the interacting protein (Hecker et al., 2006; Kerscher et al., 2006). Bioinformatics revealed C9orf72 and SMCR8 contain both SIMs and SUMOylation consensus sites, suggesting the possibility of either protein being SUMOylated or possibly interacting with SUMOylated proteins through their SIMs. Therefore, we wanted to investigate a possible role for SUMOylation in the interaction between C9orf72 and SMCR8.

5.2.   Bioinformatics reveals C9orf72 has a SUMO-interacting motif and possible SUMOylation sites

As previously stated (see 1.7.3.3), the interaction between SUMO and SIM is non-covalent and SUMOylated proteins can interact with SIM-containing proteins. SIMs consist of a hydrophobic amino acid sequence with the general consensus sequence V-I/V-I/V/-V and are often flanked by negatively charged amino acids (Gareau and Lima, 2010; Song et al., 2004).

The covalent attachment of SUMO to residues in the substrate protein is through an acceptor lysine in the substrate. This acceptor lysine often falls within a SUMOylation consensus motif, with the general sequence Ψ-K-x-D/E (where Ψ is a hydrophobic residue, K the SUMO acceptor lysine, x is any amino acid and D/E is aspartic/glutamic acid). The E2-conjugating enzyme Ubc9 can recognise and bind to this motif, thereby stabilising the Ubc9-substrate interaction .(Sampson et al., 2001; Yang et al., 2006)

GPS-SUMO is a SUMOylation prediction software that utilises group-based prediction alongside Particle Swarm Optimisation to predict possible SIMs and SUMOylation sites (Zhao et al., 2014). The output from this prediction includes the position and predicted peptide of the SUMOylation or SIM site, the predicted score and its corresponding cut off value. To determine whether any putative SIMs or SUMOylation sequences were present in C9orf72, the C9orf72 protein sequence was input into GPS-SUMO and the threshold for detection set to high. A high threshold corresponds to a specificity/accuracy of 99.72%/99.36% and 98.00%/96.35% for SIM and SUMOylation consensus respectively Bioinformatics analysis revealed the C9orf72 sequence contains a SIM (Table 5.1,highlighted in red). In addition to the SIM, three lysine SUMOylation consensus sequences were identified at positions 14, 48 and 273, with K273 being the most probable SUMOylation site (Table 5.1, highlighted in blue). Therefore, it is possible C9orf72 is SUMOylated or may interact with SUMOylated proteins via its SIM, V-I-I-V.

.

Table 5.1:Bioinformatic analysis results identifying possible SUMOylation consensus sequence and SUMO interaction motifs for C9orf72

Position	Peptide	Score	Cut off	P-value	Type
14	PPSPAVAKTEIALSG	3.712	3.24	0.038	SUMOylation consensus

48	VRHIWAP**K**TEQVLLS	6.311	3.24	0.033	SUMOylation consensus
92 – 96	FVLSEKGVIIVSLIFDGNW	52.415	35.23	0.013	SUMO interaction motif
273	CEAESSF**K**YESGLFV	10.577	3.24	0.014	SUMOylation consensus

5.3. Bioinformatics revealed SMCR8 has a SUMO-interacting motif and possible SUMOylation sites

Since proteins with a SIM can interact with SUMOylated proteins, and as C9orf72 forms a complex with SMCR8, we wanted to determine whether the sequence for SMCR8 contains possible SUMOylation sites. Therefore, the sequence for SMCR8 was input into GPS-SUMO with a high threshold (specificity/accuracy of 99.72%/99.36% and 98.00%/96.35% for SIM and SUMOylation consensus respectively). Bioinformatic analysis for SMCR8 revealed a singular SUMOylation consensus sequence (Table 5.2, highlighted in blue). Interestingly, two SIMs were also identified (Table 5.2, highlighted in red). Thus, both C9orf72 and SMCR8 contain possible SIMs and SUMOylation consensus sequences.

Table 5.2: Bioinformatic analysis results identifying possible SUMOylation consensus sequence and SUMO interacting motifs for SMCR8

Position	Peptide	Score	Cut off	P-value	Type
428	SVESVLIKMEQELGD	22.829	3.24	0.002	SUMOylation consensus
472 – 476	SISSGESIEVLGTEKSTSV	48.293	35.23	0.026	SUMO interaction motif
809 - 813	RYSRYTSILDLDNKTLRCP	36.54	35.23	0.16	SUMO interaction motif

5.4.   Investigating the role of the C9orf72 SUMO-interacting motif in its interaction with SMCR8

5.4.1. C9orf72 SIM mutant expresses in HEK293 cells

Bioinformatics identified amino acids 92 – 96 of C9orf72 as a possible SIM. To begin to determine whether the SIM plays a role in the C9orf72-SMCR8 interaction, a mutant was generated by site-directed mutagenesis in which the VIIV SIM sequence was mutated to AAAA (Figure 5.1A). To determine whether mutation of the SIM motif affected the expression of C9orf72, HEK293 cells were transfected with Myc-C9orf72 or the Myc-C9orf72 SIM mutant. The lysate was separated and probed via SDS-PAGE and immunoblot. Both Myc-C9orf72 and the SIM mutant expressed to similar levels in cells, demonstrating that mutation of the SIM did not affect the expression of the C9orf72 mutant (Figure 5.1B, C).

A

60-TTT CTT GCC AAC CAC ACT CTA AAT GGA GAA ATC CTT CGA AAT GCA GAG AGT GGT GCT ATA
    F   L   A   N   H   T   L   N   G   E   I   L   R   N   A   E   G   G   A   I

GAT GTA AAG TTT TTT GTC TTG TCT GAA AAG GGA GTG AAT AAT GTT TCA TTA ATC TTT GAT
  D   V   K   F   F   V   L   S   E   K   G   V   I   I   V   S   L   I   F   D
                                        A   **A**   **A**   **A**

GGA AAC TGG AAT GGG GAT CGC AGC ACA TAT GGA CTA TCA ATT ATA CTT CCA CAG ACA GAA -121
  G   N   W   N   G   D   R   S   T   Y   G   L   S   I   I   L   P   Q   T   E

B

C
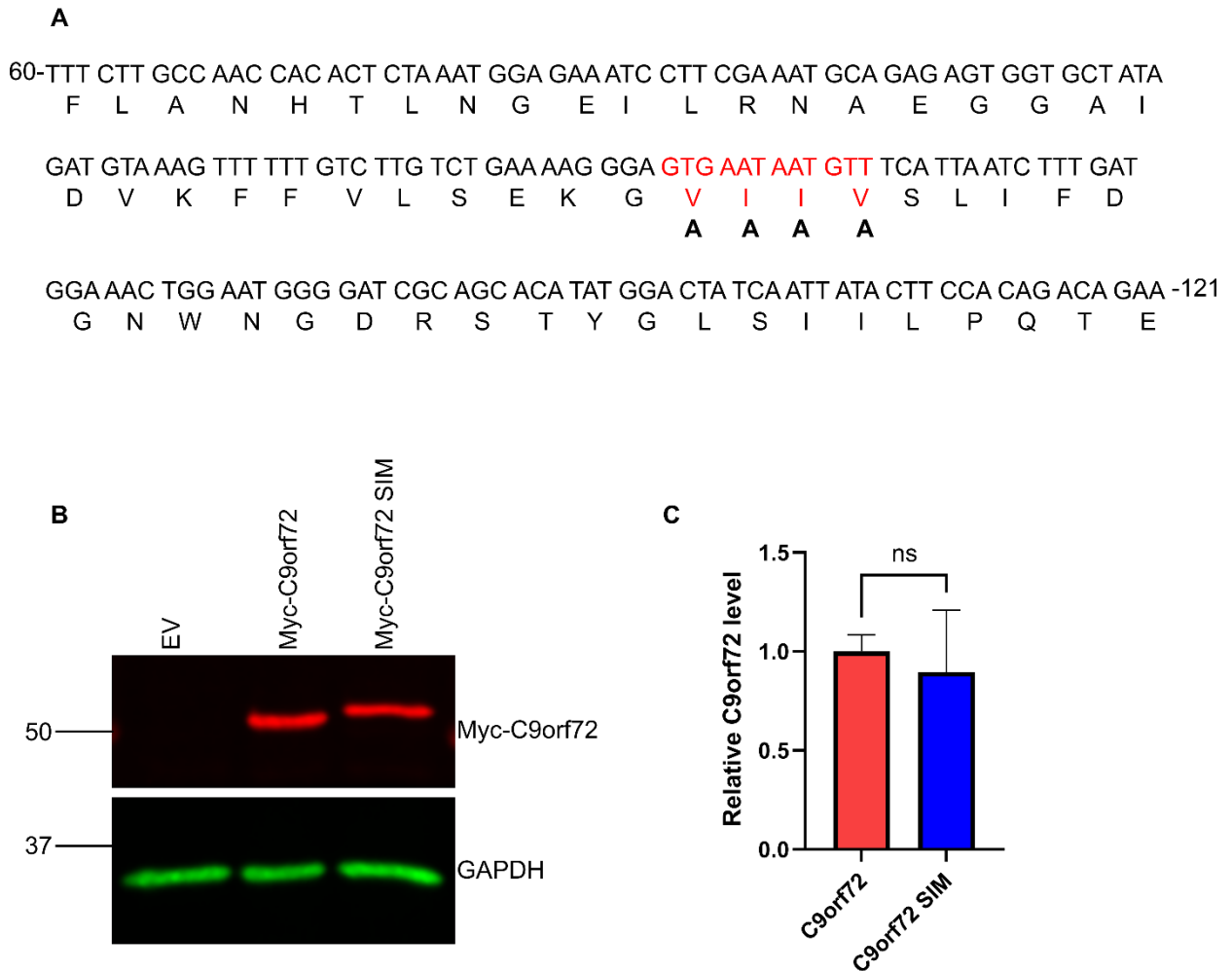
Figure 5.1: Location of SUMO interacting motif in C9orf72 and expression of C9orf72 and C9orf72 SIM mutant in HEK293 cells

(A) Partial DNA/amino acid sequence for C9orf72 with location of SUMO interacting motif (SIM, red). Site-directed mutagenesis to produce SIM mutant with the change of amino acids shown (bold). The number represent the amino acid number before and after sequence (B) Cell lysates of HEK293 cells transfected with an empty vector (EV), Myc-C9orf72 or Myc-C9orf72 SIM mutant were subjected to SDS-PAGE and immunoblot for Myc-C9orf72 using 9B11 antibodies and anti-GAPDH for a loading control. (C) Relative C9orf72 levels (Mean ± SEM, one-way ANOVA with Fisher's LSD test, ns = non-significant; N = 3 experiments).

5.4.2. Mutation of the C9orf72 SIM does not affect binding to SMCR8

As described in the introduction, SUMO/SIM interactions have been shown to regulate complex formation (Liu et al., 2011; Matmati et al., 2018; Widagdo et al., 2012). It is possible for two proteins to interact non-covalently if one protein is SUMOylated and the other protein contains a SIM (Zheng et al., 2019). C9orf72 and SMCR8 form a complex and we determined SMCR8 and C9orf72 stabilise each other. Therefore, we hypothesised the C9orf72 SIM may play a role in C9orf72-SMCR8 complex formation and stability. If this was true, we would expect the C9orf72 SIM mutant to possibly affect the binding of C9orf72 to SMCR8 or the stability of the C9orf72-SMCR8 complex.

To determine whether the SIM in C9orf72 affects its binding to SMCR8 or stability of the C9orf72-SMCR8 complex, HEK293 cells were transfected with Myc-C9orf72, Myc-C9orf72 SIM mutant, or co-transfected with Myc-C9orf72/SMCR8-Myc/DDK or Myc-C9orf72 SIM/SMCR8-Myc/DDK. Samples were subjected to SDS-PAGE and immunoblot for Myc-C9orf72 and SMCR8-Myc/DDK levels. Myc-C9orf72 and Myc-C9orf72 SIM expressed to a similar level. Co-expression of Myc-C9orf72 and SMCR8-Myc/DDK greatly increased the levels of both C9orf72 and SMCR8 (Figure 5.2A, B), consistent with stabilisation of the proteins and mimics what we had seen previously (see Figure 3.2). Co-expression of Myc-C9orf72 SIM and SMCR8-Myc/DDK also increased the levels of Myc-C9orf72 and SMCR8-Myc/DDK but to a lesser extent (Figure 5.2A, B). This suggests that the C9orf72 SIM mutant is still able to bind to SMCR8, but the stability of the complex may be affected.

To determine if the binding of C9orf72 to SMCR8 was affected we performed a co-immunoprecipitation assay. HEK293 cells were transfected with Myc-C9orf72, Myc-C9orf72 SIM, SMCR8-Myc/DDK or co transfected with SMCR8-Myc/DDK and either wild type Myc-C9orf72 or the SIM mutant. Cells were immunoprecipitated using anti-FLAG agarose beads and whole cell lysate SMCR8 -Myc/DDK levels were enriched in all SMCR8-Myc/DDK containing samples (Figure 5.2C). The ratio between C9orf72 and SMCR8 was not affected suggesting that the SIM is not involved in binding but does play a role in the stabilisation of the complex

We established co-expression of C9orf72 and SMCR8 resulted in an increase in the half-life of C9orf72 compared to when expressed alone (Figure 3.4). Therefore, in a

complementary approach, the turnover of Myc-C9orf72 SIM-SMCR8 complex was investigated, reasoning if the C9orf72 SIM is involved in stabilisation of the complex, the mutant may be unable to stabilise and hence the half-life may be altered. HEK293 cells transfected with SMCR8-Myc/DDK and either Myc-C9orf72 and Myc-C9orf72 SIM mutant were treated with cycloheximide and harvested 0, 4 or 8 hrs post-treatment. Samples were analysed via SDS-PAGE and immunoblot for C9orf72 and SMCR8. The cycloheximide treatment was effective across all samples as evidenced by the decrease in Cyclin D1 over the 8 hrs period (Figure 5.2D). SMCR8-Myc/DDK levels decreased over the 8 hr period, with a calculated half-life of 4.4 hrs (Figure 5.2D). Co-expression of C9orf72 and SMCR8 increased the half-life increased to 16.6 hrs whereas co-expression of the SIM mutant with SMCR8 yielded a half-life of 8.5 hrs. This result is consistent with the data shown in Figure 3.4 and indicates that mutation of the SIM in C9orf72 may result in a decrease in stabilisation of the C9orf72-SMCR8 complex. Unfortunately, the experiment could only be performed once, due to COVID-19 limitations.
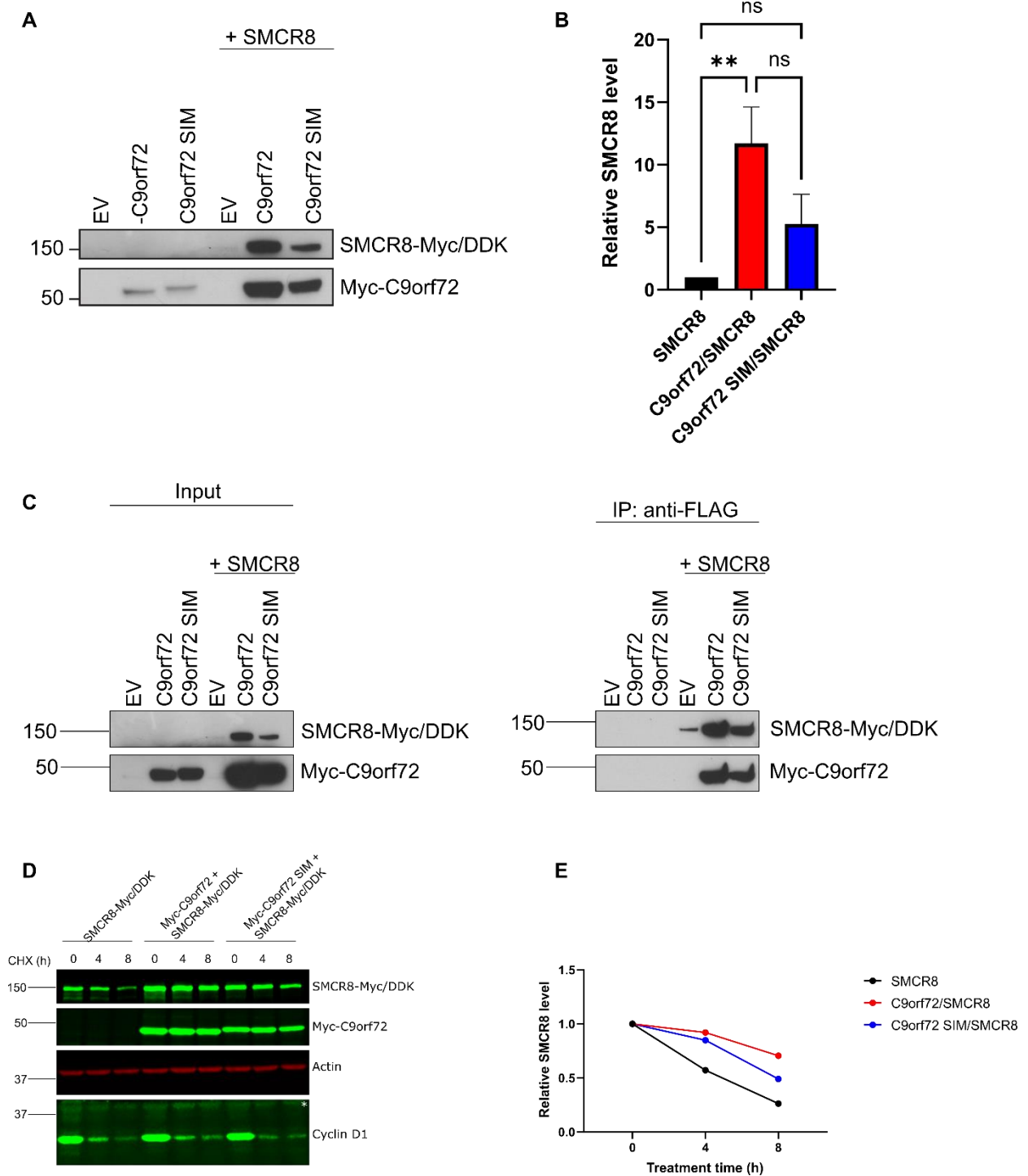
Figure 5.2: Mutation of C9orf72 SIM destabilises the C9orf72-SMCR8 complex.

(A) HEK293 cells were transfected with Myc-C9orf72, Myc-C9orf72 SIM (SUMO interacting motif) mutant, or co-transfected with SMCR8-Myc/DDK and either Myc-C9orf72 or Myc-C9orf72 SIM. Lysates were subjected to SDS-PAGE and immunoblot for Myc-C9orf72 and the SIM mutant using anti-Myc antibodies, or SMCR8-Myc/DDK using anti-FLAG antibodies. (B) Quantification of relative SMCR8 levels (Mean ± SEM, one-way ANOVA with Fisher's LSD test, ** p ≤ 0.01, ns = non-significant; N = 4 experiments). (C) HEK293 cells were transfected with Myc-C9orf72, Myc-C9orf72 SIM, SMCR8-Myc/DDK or co-transfected with SMCR8-Myc/DDK/Myc-C9orf72 or SMCR8-Myc/DDK/Myc-C9orf72 SIM. Cells were immunoprecipitated using anti-FLAG agarose beads and whole cell lysates and immune

pellets subjected to SDS-PAGE and immunoblot for Myc-C9orf72 or SMCR8-Myc/DDK levels using anti-Myc antibodies. (D). SMCR8-Myc/DDK was expressed alone or co-expressed with either Myc-C9orf72 or Myc-C9orf72 SIM in HEK293 cells. Cells were treated with cycloheximide (CHX) for 0, 4 or 8 hrs and the lysate subjected to SDS PAGE and immunoblot for Myc-C9orf72, SMCR8-Myc/DDK, Cyclin D1 and endogenous actin using anti-Myc, anti-FLAG M2, anti-Cyclin D1 and anti-actin antibodies, respectively. White asterisks denote aspecific bands (E) Relative levels of SMCR8-Myc/DDK over the 8 hr CHX treatment time. (N = 1 experiment).

5.5. Investigating the role of K90 modification in the interaction between C9orf72 and SMCR8.

The above data indicate that the C9orf72 SIM is involved in stabilisation of the C9orf72-SMCR8 complex. In addition to SUMOylation of consensus sequence sites, SUMOylation of non-consensus sites can also occur. The non-consensus SUMOylation of some proteins occurs in a SIM-dependent manner (Blomster et al., 2010; Zhu et al., 2008). It has been shown that lysine residues adjacent to SIM can be SUMOylation sites themselves (Blomster et al., 2010). K90 in C9orf72 is adjacent to the SIM so we therefore decided to investigate a possible role for K90 in stabilisation of C9orf72-SMCR8, reasoning that the SIM may influence the stability of the C9orf72-SMCR8 complex and this may involve SUMOylation of nearby residues.

5.5.1. C9orf72 K90R mutant expresses in HEK293 cells

To determine whether the SIM adjacent K90 residue is involved in the C9orf72-SMCR8 interaction, a mutant was generated in which the lysine at position 90 was mutated to an arginine by site-directed mutagenesis (K90R) to prevent possible SUMOylation. To establish whether mutation of this lysine residue affected the expression of C9orf72, HEK293 cells were transfected with Myc-C9orf72 or the Myc-C9orf72 K90R mutant. Lysates from these cells were separated and analysed via SDS-PAGE and immunoblot for levels of C9orf72. Both Myc-C9orf72 and the K90R mutant expressed to similar levels (Figure 5.3A, B) demonstrating mutation of the lysine residue had no effect on expression levels.
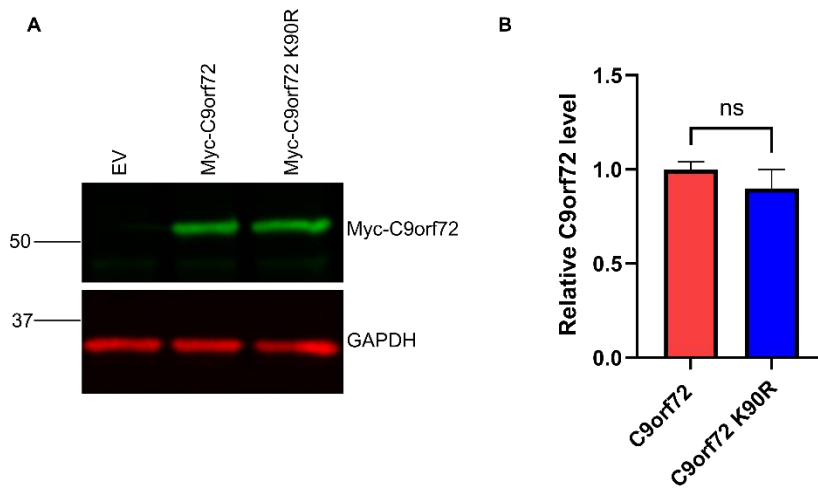
Figure 5.3: C9orf72 K90R mutant expresses in HEK293 cells.

(A) Cell lysates of HEK293 cells transfected with an empty vector (EV), Myc-C9orf72 or Myc-C9orf72 K90R (lysine to arginine mutation at position 90) mutant were subjected to SDS-PAGE and immunoblot for Myc-C9orf72 using 9B11 antibodies and anti-GAPDH for a loading control. (B) Relative levels of C9orf72 levels (Mean ± SEM, one-way ANOVA with Fisher's LSD test, ns = non-significant; N = 3 experiments).

5.5.2. C9orf72 K90 regulates C9orf72-SMCR8 stability

We showed that the C9orf72 SIM may be involved in the stabilisation of C9orf72-SMCR8 and often proteins that undergo non-consensus SUMOylation in some cases have nearby lysine residues. To begin to investigate if K90 might affect the C9orf72 SIM, we determined whether the K90 residue is important for the stabilisation of the C9orf72-SMCR8 complex, in a similar way as the SIM (see Figure 5.2A)

HEK293 cells were transfected with SMCR8-Myc/DDK, Myc-C9orf72 and Myc-C9orf72 K90R. As a control for the K90 mutation, a mutant of the nearby K83 residue was also made (Myc-C9orf72 K83R), reasoning that if the effect of the K90 residue is specific to K90, then the K83 mutant would not demonstrate this effect. Alongside the single transfection, SMCR8-Myc/DDK was co-transfected with either Myc-C9orf72, Myc-C9orf72 K90R or Myc-C9orf72 K83R. Lysates were separated by SDS-PAGE and immunoblot. Consistent with our previous results, co-expression of Myc-C9orf72 and SMCR8-Myc/DDK significantly increased the levels of both proteins compared to expression of either protein alone (Figure 5.4A, B). Similarly, co-expression of Myc-C9orf72 K83R and SMCR8-Myc/DDK resulted in a significant increase in C9orf72 and SMCR8 levels. Co-expression of Myc-C9orf72 K90R and SMCR8-Myc/DDK resulted in a significant decrease in SMCR8 levels when compared to co-expression of either C9orf72/SMCR8 or C9orf72 K83R/SMCR8 (Figure 5.4B).Taken together, the data suggests that the K90 lysine residue may be involved the stabilisation of C9orf72 and SMCR8.
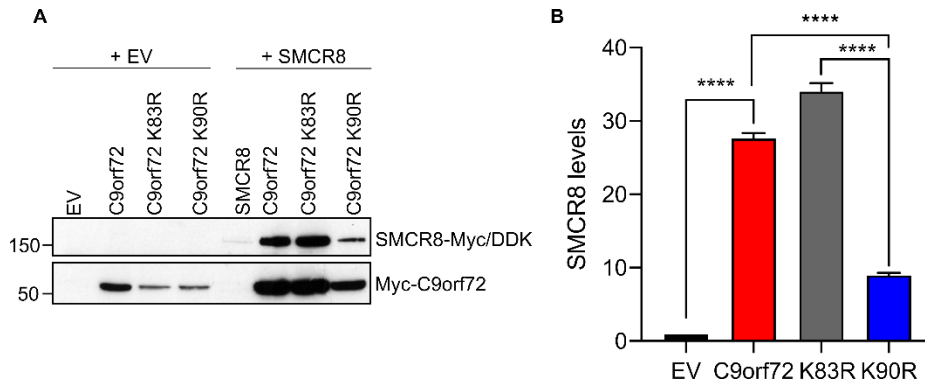
Figure 5.4: C9orf72 K90 residue regulates the stability of the C9orf72-SMCR8 complex.

(A) SMCR8-Myc/DDK, Myc-C9orf72, Myc-C9orf72 K83R, or Myc-C9orf72 K90R was transfected in HEK293 cells. SMCR8-Myc/DDK was also co-transfected with either Myc-C9orf72, Myc-C9orf72 K83R or Myc-C9orf72 K90R. Lysates were subjected to SDS-PAGE and immunoblot for levels of SMCR8-Myc/DDK or Myc-C9orf72 using anti-Myc antibody. (B) Quantification of the relative SMCR8-Myc/DDK levels (Mean ± SEM, one-way ANOVA with Fisher's LSD test, **** $p \leq 0.0001$; N = 3 experiments).

5.6. Investigating SUMOylation of C9orf72 and SMCR8

5.6.1. Expression of SUMO and SUMO ΔGG mutant in HEK293 cells

Thus far, we have shown the C9orf72 SIM and K90 lysine residue affects the stabilisation of the C9orf72-SMCR8 complex. Given both C9orf72 and SMCR8 contain SUMOylation consensus sequences, it is possible that either, or both proteins are SUMOylated. This is also consistent with the data above that suggests the mutation of the SIM and K90 lysine residue may reduce the stability of C9orf72-SMCR8, indicating the possibility of SUMOylation playing a role.

As described in the introduction there are three paralogues of SUMO in mammals – SUMO1, SUMO2 and SUMO3. As SUMO2 and SUMO3 share 96% homology they are often referred to as SUMO2/3 (Hecker et al., 2006). We obtained YFP-tagged SUMO1 and SUMO2/3 constructs from Dr Chun Guo (University of Sheffield) in addition to their respective C-terminal di-glycine truncated mutants (ΔGG). The C-terminal di-glycine needs to be exposed for SUMOylation to occur and therefore the truncated mutant without this C-terminal GG residue (ΔGG) is unable to be SUMOylated. We decided to investigate whether C9orf72 or SMCR8 is SUMOylated. To do this, we utilised an immunoprecipitation assay.

We first confirmed expression of YFP-SUMO1, YFP-SUMO1 ΔGG, YFP-SUMO2/3 and YFP-SUMO2/3 ΔGG in HEK293 cells. Wild type and ΔGG YFP-SUMO1 and YFP-SUMO2/3 were expressed in HEK293 cells. Lysates were separated and analysed via SDS-PAGE and immunoblot. YFP-SUMO1 and YFP-SUMO1 ΔGG constructs expressed in HEK293 cells (Figure 5.5A). Similarly, YFP-SUMO2/3 and YFP-SUMO2/3 ΔGG construct expressed in HEK293 cells (Figure 5.5B). This demonstrates that truncation did not prevent expression of SUMO1 or SUMO2/3.
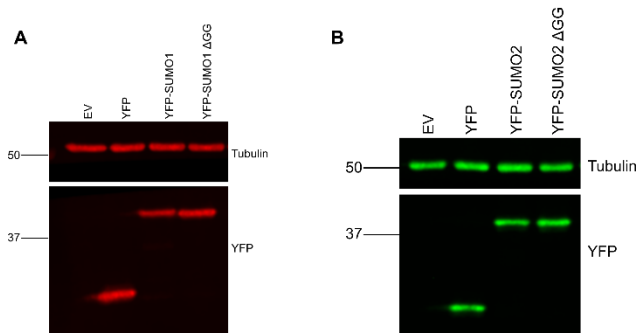
Figure 5.5: SUMO1, SUMO2/3 and their ΔGG mutants express in HEK293 cells.

(A) Cell lysates of HEK293 cells transfected with an empty vector (EV), YFP, YFP-SUMO1 and the non-SUMOylating YFP-SUMO1 ΔGG (glycine-glycine) mutant were subjected to SDS-PAGE and immunoblot for YFP-tagged constructs using anti-GFP antibody and anti-tubulin as a loading control. (B) Cell lysates of HEK293 cells transfected with an empty vector (EV), YFP, YFP-SUMO2/3 and the non-SUMOylating YFP-SUMO2/3 ΔGG mutant were subjected to SDS-PAGE and immunoblot for YFP-tagged constructs using anti-GFP antibody and anti-tubulin as a loading control.

5.6.2. C9orf72 and SMCR8 may be modified by SUMOylation

Following confirmation that YFP-SUMO1, YFP-SUMO2/3 and the respective ΔGG mutants express in HEK293 cells, we wanted to determine whether C9orf72 is SUMOylated. To do this, an immunoprecipitation assay was used. Myc-C9orf72 was co-transfected with wild type or ΔGG mutants of YFP-SUMO1 or YFP-SUMO2/3 alongside an untagged Ubc9 construct (the SUMO E2-conjugating enzyme) to enhance SUMOylation. C9orf72 was immunoprecipitated and the whole cell lysate and immune pellets probed via SDS-PAGE and immunoblot for Myc-C9orf72 and YFP to detect SUMO. Myc-C9orf72 was enriched in all Myc-C9orf72 containing samples. SUMO is an 11 kDa protein, so together with the YFP tag would be expected to yield a protein of approximately 36 kDa. Therefore, covalently bound SUMO would be expected to increase the molecular weight of the target protein by approximately 36 kDa. As SUMO is able to form polySUMO chains, increments of 36 kDa would be expected in such a case. In addition to Myc-C9orf72 at 50 kDa, a band just above 100 kDa that is immunoreactive for Myc antibody is present in the YFP-SUMO1 and YFP-SUMO2/3 expressing samples (Figure 5.6A). However, the same signal was found in the ΔGG co-transfected samples demonstrating that this band is not due to a specific SUMOylation event (Figure 5.6A). A band at approximately 250 kDa that is immunoreactive for YFP is present in YFP-SUMO1 and SUMO2/3 co-transfected with Myc-C9orf72 but not in the corresponding ΔGG samples, indicating a specific SUMOylation event. Since this band was not immunoreactive to the Myc antibody, it is likely not to be C9orf72 but may be a SUMOylated protein that interacts with C9orf72.

Next, we wanted to determine whether SMCR8 may be SUMOylated. Therefore, SMCR8-Myc/DDK was co-transfected with untagged Ubc9 alongside either YFP, YFP-SUMO1, YFP-SUMO2/3 or the ΔGG mutants. SMCR8-Myc/DDK was immunoprecipitated using anti-FLAG agarose beads and the whole cell lysate and immune pellets probed via SDS-PAGE and immunoblot for SMCR8 and YFP. SMCR8 was enriched in all SMCR8-Myc/DDK containing samples (Figure 5.6B). Aside from the band at 150 kDa representative of unmodified SMCR8-Myc/DDK, no other FLAG immunoreactive bands were present, suggesting that SMCR8 is not SUMOylated. Two bands above 250 kDa immunoreactive for YFP are present in YFP-SUMO1, YFP-SUMO2/3 but not in the ΔGG samples after immunoprecipitation of SMCR8-Myc/DDK.

Hence as was the case for C9orf72, SMCR8 may interact with SUMOylated proteins but is not itself SUMOylated.
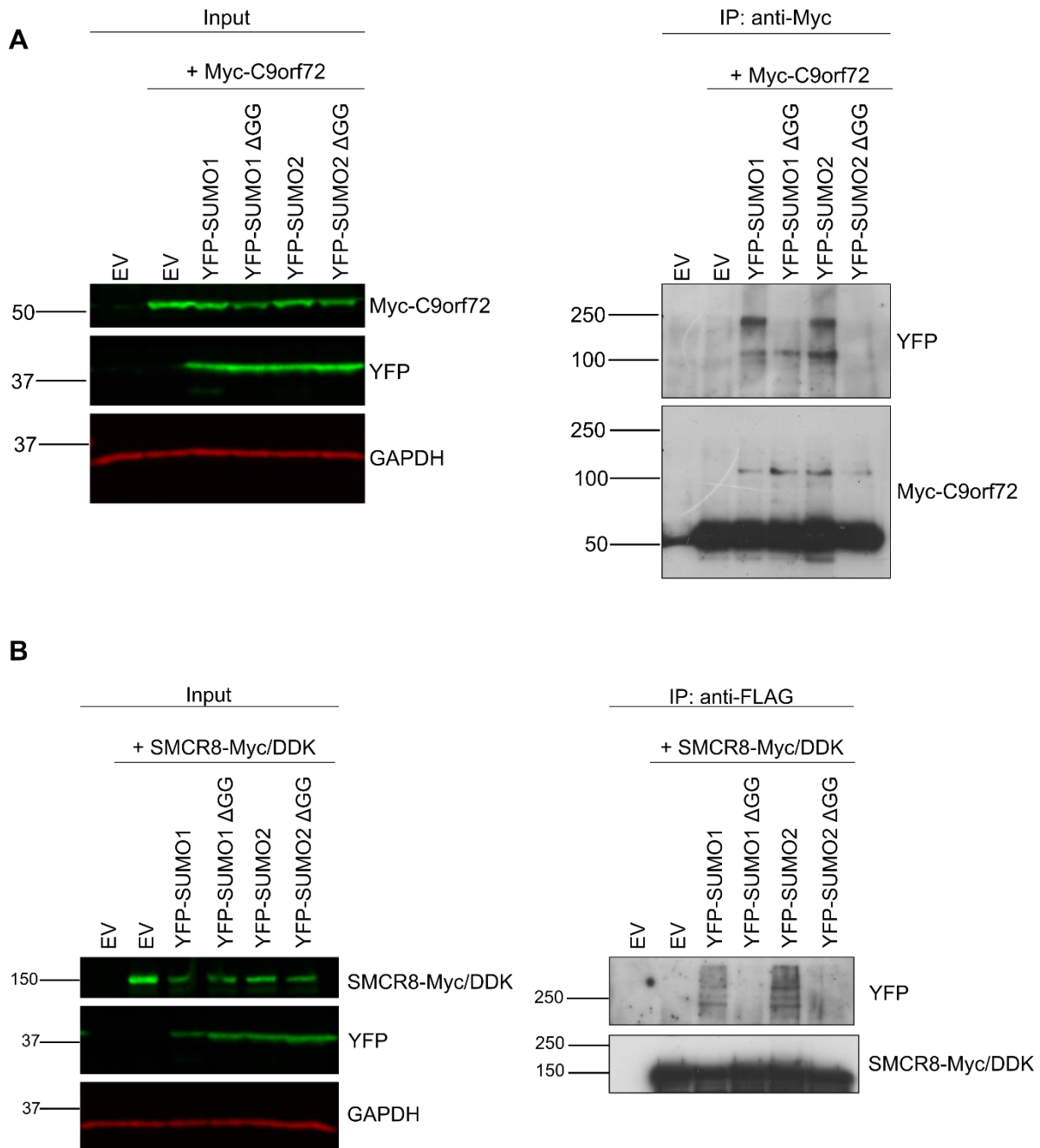
Figure 5.6:C9orf72 and SMCR8 may interact with SUMOylated proteins.

(A). HEK293 cells co-transfected with Myc-C9orf72 along with either YFP-SUMO1, YFP-SUMO2/3 or their ΔGG (glycine – glycine) non-SUMOylating mutants were immunoprecipitated using anti-Myc antibodies. Whole cell lysate and immune pellets were separated by SDS-PAGE and immunoblot for YFP-tagged constructs using anti-GFP antibody and anti-Myc antibody. (B). HEK293 cells co-transfected with SMCR8-Myc/DDK along with either YFP-SUMO1, YFP-SUMO2/3 or their ΔGG non-SUMOylating mutants were immunoprecipitated using anti-FLAG agarose beads. Whole cell lysate and immune pellets were separated by SDS-PAGE and immunoblot for YFP-tagged constructs using anti-GFP antibody and anti-FLAG antibody.

5.7.　　　Discussion

C9orf72 is known to form a complex with SMCR8 (Sellier et al., 2016; Yang et al., 2016), and this chapter focused on investigating a possible role for SUMOylation in the regulation of this complex. Initially in this chapter, bioinformatic analysis was performed on the C9orf72 and SMCR8 protein sequence to determine whether the sequence contained any potential SIMs or SUMOylation consensus sequences. We found three C9orf72 SUMOylation consensus sequences - K14, K48 and K273 (Table 5.1) and one SMCR8 SUMOylation consensus sequence - K428 (Table 5.2). These SUMOylation consensus sequences follow the general structure Ψ-K-x-D/E, where Ψ is an aliphatic amino acid and x is any amino acid. It has been shown that SUMO-Ubc9, the E2 conjugating enzyme, can recognise SUMOylation consensus sequences with this general structure and directly conjugate the lysine residue within it (Bernier-Villamor et al., 2002; Sampson et al., 2001; Zheng et al., 2019). Interestingly, K14 was also identified as the most probable site for ubiquitination and evidence exists for proteins being ubiquitinated and SUMOylated at the same site, so it is possible this is the case for C9orf72. However, we tested whether this mutation affected the ubiquitination status of C9orf72 (Figure 3.3) and found no difference in ubiquitination between the mutant and wild type C9orf72. Due to COVID-19 time restrictions we were unable to test whether the C9orf72 K14R mutant or the other lysine mutants we generated by site-directed mutagenesis are SUMOylated.

The expression of a C9orf72 SIM mutant was tested in HEK293 cells, and it was determined mutation of the C9orf72 SIM did not affect its expression. The identified SIM in C9orf72 follows the general structure V-I/V-I/V-V which has been shown to bind all SUMO paralogues (Song et al., 2004). We tested whether the SIM was necessary for binding to SMCR8 and found that mutation of the SIM to produce a non-functional SIM did not affect the binding of C9orf72 to SMCR8 but reduced the stabilisation of the C9orf72-SMCR8 complex. We mutated the potential SUMO site in SMCR8 using site-directed mutagenesis, however, due to the limitations imposed by COVID-19, we were unable to perform any experiments with this mutant.

Evidence exists for non-consensus SUMOylation – the SIM in these substrates can bind to SUMO-Ubc9, thereby promoting their own conjugation and subsequent SUMOylation (Meulmeester et al., 2008; Zhao et al., 2020; Zhu et al., 2008). Multiple proteins have

been identified that matched non-consensus SUMOylation and in a proportion of these identified proteins, the lysine SUMOylation site was SIM adjacent (Blomster et al., 2010). In C9orf72, the lysine nearest to its identified SIM is lysine 90. Therefore, a mutant was generated in which this lysine was mutated to an alanine – K90R. We tested the expression of this mutant in HEK293 cells and found no difference in expression. The effect of both the C9orf72 SIM and C9orf72 K90R mutants on the stabilisation of C9orf72-SMCR8 was investigated and it was found that while both mutants cause a less stable C9orf72-SMCR8 complex, the binding of C9orf72 to SMCR8 appeared to remain unaffected. In the case of K90, we also tested the effect of K83R mutation as a control. Upon co-expression of C9orf72 K83R with SMCR8 or C9orf72 K90R with SMCR8, the level of SMCR8 was greatly reduced for K90R whereas the level of SMCR8 for K83 co-expression was similar to that of wild type C9orf72. This suggests that the destabilising effect is specific to the K90R residue. Additionally, the effect of C9orf72 SIM on the turnover of the C9orf72-SMCR8 complex was investigated. We found that the C9orf72 SIM-SMCR8 complex resulted in a decreased half-life compared to the C9orf72-SMCR8 complex further suggesting a decrease in stabilisation. However, given this experiment was only performed once, due to COVID-19 time limitations, the experiment would need to be repeated again before any firm conclusions can be drawn. Testing whether the C9orf72 K90R mutant altered turnover of the C9orf72-SMCR8 complex was also not possible in the time frame.

The co-immunoprecipitation of C9orf72-SMCR8 and C9orf72 SIM-SMCR8 indicated that the SIM did not affect binding of C9orf72 to SMCR8. However, interpretation of the co-immunoprecipitation is somewhat hindered by the different levels of C9orf72 and SMCR8 as a result of differences in stabilisation. We set up a GST-pulldown assay to overcome this issue as it would allow standardisation of the levels of C9orf72. However, although we were able to make to GST-C9orf72 and GST-C9orf72 SIM mutants, we were unable to perform the experiments due to time limitations imposed by COVID-19.

Finally, C9orf72 and SMCR8 SUMOylation was explored. Firstly, we decided to test whether the YFP-SUMO1, YFP-SUMO2/3 and their ΔGG mutant express in HEK293. We found both the wild type and the mutant expressed in HEK293 cells, thereby confirming truncation did not affect the expression of either SUMO1 or SUMO2/3. Following this, we wanted to determine whether C9orf72 or SMCR8 is SUMOylated. Co-expression of Myc-C9orf72 alongside YFP-SUMO1, YFP-SUMO2/3, the ΔGG mutants

followed by immunoprecipitation of C9orf72 resulted in an enrichment of C9orf72 in all Myc-C9orf72 containing samples. Additionally, large molecular weight (~250 kDa) bands appeared in YFP-SUMO1 and SUMO2/3 samples that was immunoreactive for YFP, suggesting the presence of SUMOylated bands. However, these bands were not visible when probed with Myc antibody, suggesting C9orf72 is not SUMOylated but interacts with a SUMOylated protein. Similarly, for SMCR8-Myc/DDK, co-expression followed by immunoprecipitation yielded an enrichment in all SMCR8-Myc/DDK containing samples. Bands present at approximately 250 kDa suggests the presence of SUMOylated proteins. Like with C9orf72, as these proteins were not immunoreactive with the FLAG antibody, it suggests SMCR8 is not SUMOylated by interacts with a SUMOylated protein. In contrast to our results, a mass spectrometry screen for SUMOylated proteins identified the K428 residue in SMCR8 as a SUMO site and SUMO3 was identified in a mass spectrometry screen for C9orf72 interacting proteins (Goodier et al., 2020; Hendriks et al., 2018). It is possible SUMOylated SMCR8 and C9orf72 account for a relatively low proportion of either all SMCR8 or C9orf72 in cells, and therefore was below the detection limit for the immunoblot assay we utilised. To overcome this, an *in vitro* binding assay approach could be used.

6. Discussion

6.1.　　Summary

A GGGGCC hexanucleotide repeat expansion in the first intron of the C9orf72 gene is the most common cause of familial ALS and FTD (DeJesus-Hernandez et al., 2011; Renton et al., 2011). Three major pathogenic mechanisms are thought to be the cause of C9ALS/FTD. The first of these, haploinsufficiency is caused by the repeat expansion resulting in a downregulation of gene expression and therefore is a LOF mechanism (Belzil et al., 2013; Gijselinck et al., 2016; Jackson et al., 2020). The second and third mechanisms are GOF mechanisms that give rise to RNA foci and DPRs. RNA foci are the result of the high GC content of the expansion forming abnormal, stable DNA and RNA secondary structures that accumulate and sequester RNA binding proteins whereas DPRs arise from RAN translation of the repeat expansion in all three reading frames to give toxic, aggregate prone proteins that accumulate (Ash et al., 2013; Fratta et al., 2012; Kumar et al., 2017; Mori et al., 2013c; Reddy et al., 2013; Zu et al., 2013). Many roles for C9orf72 have been identified to date, including a GEF or GAP that regulates the initiation of autophagy and Rab-mediated trafficking (when in complex with SMCR8 and WDR41) in addition to roles in immune system regulation and at the synapse (Amick et al., 2016; Atanasio et al., 2016; Burberry et al., 2016; Lall et al., 2021; Lan et al., 2019; O 'Rourke et al., 2016; Sellier et al., 2016; Starr and Sattler, 2018; Su et al., 2020; Sullivan et al., 2016; Tang et al., 2020; Yang et al., 2016). It has been postulated that haploinsufficiency is a disease modifier, aggravating the effects of RNA and DPR toxicity (Abo-Rady et al., 2020; Boivin et al., 2020; Zhu et al., 2020). Given this, it follows that restoring C9orf72 levels may be a beneficial strategy for C9ALS/FTD patients as it would relieve some of the toxic effects by rescuing autophagy and subsequently increasing clearing of DPRs. Indeed, patient-derived iMNs in which the repeat expansion reduced C9orf72 expression and induced neurodegeneration through excitotoxicity and impaired clearance of DPRs exhibited improved neuronal survival by rescuing C9orf72 levels (Shi et al., 2018). Therefore, the focus of my PhD was to investigate the stability and turnover of the C9orf72-SMCR8 complex.

The focus of the first chapter was to identify the degradation pathway for C9orf72. We first optimised antibodies for the detection of endogenous C9orf72, as the specificity of

previous commercially available antibodies were questionable. The ATLAS, ProteinTech and Genetex C9orf72 antibodies, but not the Santa Cruz were able to specifically detect endogenous C9orf72 (Figure 3.1). Characterisation of the HEK293 C9orf72[KO] cell line developed in-house, knockdown of SMCR8 expression in HEK293 cells and co-expression of C9orf72 and SMCR8 revealed C9orf72 and SMCR8 are co-stabilised whereby a reduction in protein levels of one reduced the protein levels of the other (Figure 3.2). The degradation pathway of C9orf72 was determined to be the ubiquitin protease system, with exogenous C9orf72 having a half-life of approximately 3.2 hrs and interestingly, we found that endogenous C9orf72 is stable over a 24 hr period (Figure 3.3). We found this was possibly due to the C9orf72-SMCR8 complex imparting a stabilisation effect, as the half-life of C9orf72 and SMCR8 increased when co-expressed (Figure 3.4). We determined that both exogenous and endogenous C9orf72 is ubiquitinated and the K14 and K388 ubiquitination sites identified by bioinformatics are not the sole sites of ubiquitination (Figure 3.5). Overall, this chapter demonstrated that C9orf72 is ubiquitinated and turned over by the proteasome and C9orf72-SMCR8 complex formation stabilises this turnover.

The second chapter sought to identify the ubiquitin ligase involved in UPS degradation and investigate the involvement of USP8 in C9orf72 turnover. Prior to the project starting, a Y2H identified the deubiquitinating enzyme USP8 as an interacting partner of C9orf72 which highlighted C9orf72 as a potential substrate of USP8. We found endogenous C9orf72 and USP8 interacted (Figure 4.2), however, when we tested whether USP8 or a catalytically inactive USP8 mutant altered C9orf72 levels, we found no difference in C9orf72 levels upon expression of USP8 or the catalytically inactive mutant (Figure 4.3). This demonstrated C9orf72 is not a substrate of USP8. Within this chapter, we also investigated a role for the Kelch-like protein KLHL13 (identified in a mass spectrometry screen for SMCR8 interacting proteins) as a substrate specific adaptor for C9orf72 or SMCR8. KLHL13 forms a complex with KLHL9 and the E3 ligase Cul3 to regulate the ubiquitination of proteins. We found knockdown of KLHL13, but not KLHL9 increased the levels of C9orf72 and SMCR8 (Figure 4.6) and altered their turnover (Figure 4.7). Finally, we found inhibition of Cullin ligases using MLN4924 prevents SMCR8 but not C9orf72 turnover (Figure 4.8).

The final chapter focused on exploring a possible role for SUMOylation the regulation of the C9orf72-SMCR8 complex. Using bioinformatics, we determined that both C9orf72

and SMCR8 contain SUMOylation consensus sequences and SIMs (Table 5.1and Table 5.2). Using a C9orf72 SIM mutant we determined there was a decrease in stabilisation for C9orf72 SIM-SMCR8 compared to C9orf72-SMCR8, but no difference in binding (Figure 5.2). However, the half-life of SMCR8 decreased when co-expressed with C9orf72 SIM compared to when co-expressed with C9orf72 (Figure 5.2). Given several proteins were identified in which the non-consensus SUMO lysine acceptor site had a nearby SIM, we mutated the nearby lysine residue in C9orf72 (K90) and determined that the mutant affected the stabilisation but not the binding of C9orf72-SMCR8 (Figure 5.4). Finally, we investigated whether C9orf72 and SMCR8 are SUMOylated and determined both C9orf72 and SMCR8 interact with SUMOylated proteins but are not SUMOylated themselves (Figure 5.6).

6.2.   C9orf72 and SMCR8 levels are highly co-dependent

The levels of C9orf72 and SMCR8 are highly co-dependent. We and others have shown that the stability of C9orf72 and SMCR8 are highly co-dependent and the level of one can be regulated by regulating the level of the other (Figure 3.2, Amick et al., 2016; Lan et al., 2019; Ugolino et al., 2016). The reason for this co-dependency is unknown, although it appears that formation of the C9orf72-SMCR8 complex is protective against proteasomal degradation as we determined endogenous C9orf72 is stable over a 24 hr period, presumably due to SMCR8 complex formation. This is further suggested by the observation that upon co-expression of the complex, the half-life of both C9orf72 and SMCR8 increases (Figure 3.3 and Figure 3.4). Cryo-EM structure of the C9orf72-SMCR8 complex revealed it is structurally very similar to the FNIP2-FLCN, a GAP of RAG on lysosomes (Norpel et al., 2021; Su et al., 2020; Tang et al., 2020; Tsun et al., 2013). Indeed the C9orf72-SMCR8 complex was shown to function as a GAP for Rab8a, in contrast to the previously identified role as a GEF for this Rab (Sellier et al., 2016; Tang et al., 2020). Akin to our results showing that C9orf72 and SMCR8 complex formation stabilise the proteins, complexation of FNIP2 and FLCN has been shown to mutually stabilise each other (Clausen et al., 2020). What's more, Clausen et. al, demonstrated that complex formation between FNIP2 and FLCN protects FNIP2 from proteasomal degradation. Given the structural similarities between the C9orf72-SMCR8 and FNIP2-FLCN complexes, this could suggest that C9orf72 complex formation with

SMCR8 may be protective against ubiquitination. The rapid turnover of C9orf72 and SMCR8 when they are not in a complex could therefore arise to prevent the unwanted accumulation of excess subunits of the C9orf72-SMCR8 complex. The co-translational folding of proteins serves to protect a protein from non-specific interactions and in doing so allows assembly of native partners (Natan et al., 2017). Co-translational assembly is beneficial for protein complexes where a protein is unstable unless bound to a partner and also protect proteins from non-specific interactions as the exposed interfaces of unassembled protein complex subunits increase the propensity for aggregation (Duncan and Mata, 2011; Natan et al., 2017). It is possible that the co-translational folding and/or assembly of C9orf72 and SMCR8 occurs to stabilise the protein complex and would potentially be an interesting avenue to explore.

6.3.   C9orf72 is a degraded via the ubiquitin proteasome system

The data reported in this thesis points towards C9orf72 being a substrate of the ubiquitin proteasome system. This is supported by our data showing that a reduction in the Kelch-like protein KLHL13 increases C9orf72 and SMCR8 levels and slows their turnover (Figure 4.6 and Figure 4.7). This is in contrast to other reports in literature that state that C9orf72 levels increase upon inhibition of either the proteasome or autophagy and suggests C9orf72 undergoes both proteasome-mediated degradation and autophagic degradation in a cell-dependent manner (Manner et al., 2019; Ugolino et al., 2016). Our data fails to recapitulate the findings of these reports, with the levels of C9orf72 in CHX/Bafilomycin treated cells mimicking almost exactly the levels of C9orf72 in CHX treated cells (Figure 3.3). Supplementary to the main findings in the report, Ugolino et. al, demonstrate the levels of C9orf72 increase upon proteasome inhibition and to a lesser extent upon autophagy inhibition. However, the authors do not confirm whether autophagy is inhibited through the use of classic autophagy markers e.g. p62/LC3 and it appears no repetition of the results have been performed so it is possible the increase in C9orf72 is an artefact. We tested the turnover of C9orf72 only in non-neuronal cells and so have not determined whether the turnover pathway is the same in a neuronal cell line. As C9ALS/FTD is a neurodegenerative disease, confirming the turnover pathway in a neuronal cell line would impart greater confidence in the potential of KLHL13 as a therapeutic target.

Inhibition of Cul3 prevented the turnover of SMCR8, but not C9orf72 (Figure 4.8). However, there was still a significant decrease in SMCR8 levels between CHX and CHX/MLN4924 treated cells. This could be due to the relatively short treatment time (4.5 hrs) of the Cul3 inhibitor or could possibly suggest that other ligases are still able to ubiquitinate SMCR8. As there was no difference in C9orf72 levels between CHX and CHX/MLN4924 treated cells, this also suggests that C9orf72 is still able to be ubiquitinated. The identification of multiple other E3 ligases that interact with both C9orf72 and SMCR8 suggests that other ligases may be able to ubiquitinate C9orf72 (Goodier et al., 2020; Zhang et al., 2018b). Multiple E3 ligases have been shown to ubiquitinate p53 (Wang et al., 2011). If multiple E3 ligases are responsible for C9orf72 or SMCR8 ubiquitination, targeting the primary ubiquitination ligase would potentially be the best course of action in therapeutic terms. This is because there are many targets for substrate adaptors/E3 ligases and so a multiple hit therapeutic strategy may increase the number of off-target effects compared to targeting a single substrate adaptor/E3 ligase.

We determined that C9orf72 is ubiquitinated although the K14 and K388 residues are not the sole site for ubiquitination. As ubiquitinated proteins are substrates for both autophagy and the UPS, the identification of ubiquitinated C9orf72 alone does not confirm the degradation pathway for C9orf72. Unfortunately, due to time limitations, we could not test the ubiquitination status of the other lysine mutants predicted by bioinformatics. As described in Chapter 1.7.2 there are multiple modes of ubiquitination: mono-, multi-mono-, and polyubiquitination. Multi-monoubiquitination has been shown to also produce a proteasomal degron (Kwon and Ciechanover, 2017) and therefore it is possible that C9orf72 requires multi-monoubiquitination to be degraded. The identification of C9orf72 ubiquitination sites by mass spectrometry could determine whether C9orf72 is ubiquitinated at multiple residues and may provide insight into potential DUB candidates as some DUBs deubiquitinate at specific lysine linkages (Leznicki and Kulathu, 2017).

In any case, as C9ALS/FTD patients have reduced C9orf72 levels, therapies to increase C9orf72 levels may be of benefit. As C9orf72 and SMCR8 levels are highly co-dependent, two beneficial strategies may exist – directly targeting C9orf72 turnover to increase its levels or indirectly stabilising C9orf72 levels by stabilising SMCR8 levels. The former strategy is reliant upon the identification of the specific DUB or E3 ligase for

C9orf72 and exploration of the merits of either strategy is discussed further below. The effectiveness of any proposed treatments should be tested on their ability to stabilise C9orf72 levels. Moreover, the haploinsufficient nature of C9ALS/FTD should be mimicked to determine the validity of any treatments.

6.4. Targeting proteasomal turnover as a therapeutic strategy for C9ALS/FTD

6.4.1. Targeting the E3 ligase

KLHL proteins are substrate adaptors and as such do not function as ubiquitinating E3-ligase enzymes on their own, but instead when in complex with Cul3. Therefore, there is potential to target Cul3 or the Kelch-like ligase in a therapeutic strategy. Indeed, targeting Cul3 has been explored as an attractive therapeutic target in cancer therapy (Li et al., 2021; Xiang et al., 2021). The most common strategy involves targeting NEDDylation of Cul3. As discussed previously, NEDDylation is a three-step process that results in the addition of NEDD8 onto a lysine residue in the substrate protein (Ohh et al., 2002; Wu et al., 2005). Members of the Cullin family are known substrates of NEDDylation which activates Cullin, stimulating ubiquitination and subsequent degradation of proteins. Consequently, targeting NEDDylation has been explored as an anticancer therapy. The initiation of the NEDDylation processes is performed by NAE and as such inhibitors of NAE represent therapeutic targets. Moreover, the mechanism of action for NAE inhibitors have several points to potentially target. Firstly, as the activating step is ATP-dependent, the use of ATP-competitive inhibitors is possible. Doing so would prevent ATP from binding to the adenylation site of NAE and is the mechanism of action for several FDA-approved small molecule kinase inhibitors, including Crizotinib, an anaplastic lymphoma kinase inhibitor for the treatment of lung cancer (Costa et al., 2015; Wu et al., 2015). In addition, preventing the E1-activating-E2 conjugating enzyme interaction and thus preventing the transfer of NEDD8 is another possible strategy. PYR-41 is an inhibitor that works by targeting the active site cysteine in the E1-conjugating enzyme (Yang et al., 2007). Subsequently, the E1-NEDD8 thioester is unable to form and Cullin activation is prevented. The formation of a NEDD8-AMP mimetic that prevents the subsequent steps of NEDDylation represents the final strategy for NAE inhibitors. An example of this

is the compound MLN4924 (Brownell et al., 2010; Soucy et al., 2009). Interestingly, MLN4924 has been shown to induce autophagy in several human cancer cell lines (Lv et al., 2018; Zhao et al., 2012b). Zhao et. al, demonstrated that treatment with MLN4924 over a 24 hr period resulted in an inhibition of both mTOR activity and mTOR autophosphorylation, and the effect was more pronounced with greater concentrations of MLN4924 (Zhao et al., 2012b). Furthermore, they demonstrated mTOR inactivity was as a result of the accumulation of an mTOR inhibitor DEPTOR. This finding is supported by Lv et.al, who demonstrated that phosphorylated mTOR and phosphorylated AKT levels decreased over time following MLN4924 treatment (Lv et al., 2018). Moreover, the Cul3-KLHL38 complex ubiquitinates BECN1 (a component of the PI3K complex that regulates the formation of autophagosomes in autophagy) and consequently inhibits autophagy (Li et al., 2021). MLN4924 treatment would inactivate Cul3-KLHL38, subsequently inducing autophagy. Inducing autophagy seems like an attractive proposition given the autophagy defects present in C9ALS/FTD patients and the synergistic effect of haploinsufficiency and DPR toxicity. Indeed, the survival of C9orf72 patient-derived iMNs is increased by treatment with the Src/c-Abl inhibitor bosutinib which increases autophagy and neuronal death as a result of DPR toxicity is prevented by autophagy activation (Boivin et al., 2020; Imamura et al., 2017). However, although inducing autophagy could potentially increase motor neuron survival in patients by relieving some of the toxicity induced by DPRs, simply inducing autophagy does not address the issues arising from reduced C9orf72 protein levels such as vesicle trafficking defects. Moreover, as MLN4924 prevents global NEDDylation, all Cullin ligases are affected, leading to the accumulation of their substrates and cytotoxic effects (Sun et al., 2020b; Yu et al., 2020). Therefore, MLN4924 and targeting NEDDylation in general may not represent the most effective strategy for increasing C9orf72 levels. Moreover, Cul3 provides the backbone for all Kelch-like protein binding, so targeting Cul3 is likely to have negative downstream effects.

Instead, targeting the specific Kelch-like protein may represent a more direct strategy. Our data identified for the first time KLHL13 can influence C9orf72 and SMCR8 levels. The identified cellular roles of KLHL13 are limited; it has recently been identified as a driver of tumorigenesis in lung cancer (Xiang et al., 2021). The authors showed altering KLHL13 levels alters cell proliferation in a Cul3-dependent manner, where a reduction in KLHL13 inhibits cell proliferation. Additionally, KLHL13 has been shown to function in a

complex with KLHL9 and Cul3 to mediate the degradation of Insulin Receptor Substrate 1, whereby knockdown of Cul3 or KLHL13 significantly increased the levels of Insulin Receptor Substrate 1 (Frendo-Cumbo et al., 2019). Finally, the Cul3-KLHL9-KLHL13 complex has been shown to ubiquitinate Aurora B, a component of the chromosomal passenger complex, in a Cul3 complex-dependent manner both *in vivo* and *in vitro* (Sumara et al., 2007). The ubiquitinating ability of the KLHL13-containing complex highlights the therapeutic potential of targeting KLHL13 and the pivotal role Kelch-like ligases play in determining substrate specificity. The N-terminus of Cul3 interacts with the 3-box (a conserved domain located between the BTB and BACK domains) of Kelch-like proteins (Canning et al., 2013; Zhuang et al., 2009). Furthermore, the Kelch domain which is C-terminally located is required for substrate recognition (Canning et al., 2013). In terms of therapy, targeting the Kelch-like-substrate interaction may offer a better strategy. This is due to the 3-box motif forming a hydrophobic groove rendering it difficult to access by small molecules, whereas the open pocket formed by the Kelch domain provides adequate space for substrate binding and possible small molecule inhibition (Canning et al., 2013). As our data did not discern whether the effects of knockdown of KLHL13 on C9orf72 levels is as a direct result of loss of KLHL13 or as a consequence of loss of KLHL13 increasing SMCR8 levels, we would first need to establish this before validating targeting Kelch-like as a reliable therapeutic strategy. Nevertheless, knockdown of KLHL13 represents a potential therapeutic strategy for increasing or stabilising C9orf72 levels.

6.4.2. Targeting the deubiquitinating enzyme

The regulation of C9orf72 levels by the deubiquitinating enzyme USP8 was investigated. For both exogenous and endogenous C9orf72, expression of USP8 and the catalytically inactive mutant increased C9orf72 levels demonstrating in this capacity USP8 does not function as a DUB. Therefore, the findings in this thesis demonstrate that targeting USP8 would not represent a viable option and the C9orf72 specific DUB remains to be determined. In any case, targeting DUBs may not signify the best course of action. The therapeutic potential of DUBs have been extensively reviewed, particularly in relation to cancer therapies (D'arcy et al., 2014; Farshi et al., 2015; Harrigan et al., 2018; He et al., 2016; Poondla et al., 2019; Schauer et al., 2020). However, focus is primarily on inhibitors

of DUBs and small molecules to target the active site of DUBs. Activation of possible DUBs will be necessary to impart a potential therapeutic effect on C9orf72. This would involve finding a protein or designing a molecule that can either increase the catalytic turnover of the DUB or increase its substrate affinity. The ease of finding a specific inhibitor over a specific activator showcases targeting Kelch-like proteins is potentially more realistic.

6.4.3. Targeting SMCR8 turnover as a therapeutic strategy for C9ALS/FTD

C9ALS/FTD patients have reduced C9orf72 mRNA levels so given the interaction of C9orf72 and SMCR8 is necessary for the stability of SMCR8, it is logical to assume SMCR8 levels are reduced. Indeed, SMCR8 levels were found to be downregulated in C9ALS/FTD mouse models (with no change in mRNA levels) and patient tissue (Liang et al., 2019). This poses the question whether targeting SMCR8 turnover may be a viable strategy for C9ALS/FTD treatments to stabilise SMCR8 and consequently C9orf72 levels.

As mentioned above, FNIP2-FLCN complex formation prevents FNIP2 from proteasomal degradation, which suggests that SMCR8 stabilisation and subsequently C9orf72 stabilisation may represent a viable therapeutic strategy given the structural similarities of FNIP2-FLCN and C9orf72-SMCR8. We showed that MLN4924 treatment can partially prevent the turnover of SMCR8 (Figure 4.8). To determine whether targeting the turnover of SMCR8 in this manner would potentially be beneficial to C9ALS/FTD patients, siRNA-mediated knockdown of C9orf72 in cells that overexpress SMCR8 followed by CHX/MLN4924 treatment would demonstrate whether preventing SMR8 turnover is able to stabilise C9orf72 levels.

6.4.4. Antisense oligonucleotides as an alternative therapeutic strategy

An alternative therapeutic approach is the use of antisense oligonucleotides (ASOs) drugs to specifically knock down the C9orf72 hexanucleotide expansion. Indeed, intraventricular bolus injection of repeat RNA-targeting ASOs into mice containing the repeat expansion resulted in a reduction in repeat-containing C9orf72 RNA in the cortex

and spinal cord of the mice (Jiang et al., 2016). Importantly, there was no difference in the protein encoding exon 1B-containing C9orf72 RNA level which demonstrates the potential for specifically reducing the expansion but not the protein encoding RNA. Moreover, the accompanying reduction in RNA foci and DPR aggregates lead to an improvement in behaviour and cognitive abilities of these mice.Further evidence of the potential benefit of oligonucleotides in the treatment of ALS/FTD comes from a study that showed in mice stereopure oligonucleotides selectively reduced repeat-containing transcript levels, RNA foci and DPR proteins without disrupting protein expression (Liu et al., 2021). Furthermore, in the same study Liu et, al demonstrated the oligonucleotides protect repeat-containing motor neurons from glutamate-induced toxicity. An IONIS/Biogen collaborative phase I clinical trial for ASOs in adults with C9orf72 ALS has taken place (NCT number NCT03626012) to assess the safety and pharmacokinetics of the drug BIIB078. Given the drug is delivered by repeat injection into the CSF of patients, one potential drawback of these ASOs could arise if the drug is limited to the spinal cord as global therapeutic delivery to the CNS or other tissues may be required given the role of non-neuronal cells in ALS/FTD. To overcome this, the use of adeno-associated viral vectors may be beneficial to target neuronal and non-neuronal cells (Martier et al., 2019).

6.5.   The C9orf72-USP8 interaction

We determined that C9orf72 and USP8 interact via co-immunoprecipitation although C9orf72 is not a substrate for USP8 (Figure 4.2 and Figure 4.3). This suggests that the interaction between C9orf72 and USP8 has a different functional consequence and so exploring this interaction may offer an insight into additional roles of C9orf72. USP8 has been shown to regulate endosomal trafficking and sorting and mitochondrial quality control (Berlin et al., 2010; Durcan et al., 2014; Macdonald et al., 2014; Zhou et al., 2013a). Knockdown of USP8 results in the redistribution of cation-independent mannose-6 phosphate receptor (ci-M6PR) (Macdonald et al., 2014). During lysosome biogenesis, lysosomal proteins are trafficked in mannose-6 phosphate receptor (M6PR) positive vesicles from the trans-Golgi network to early and late endosomes for eventual incorporation into lysosomes. Once the cargo is released, M6PR is recycled back to the trans-Golgi network. Expression of full length USP8, but not a catalytically inactive or truncated version lacking the MIT domain, rescues the distribution of ci-M6PR. This

suggests that both catalytic function and endosomal localisation (provided by the MIT domain) of USP8 is necessary for the transport of ci-M6PR.

The recycling of M6PR from the endosome to the trans-Golgi network has multiple routes. Rab7L1 has been shown to regulate the retrograde trafficking of M6PRs to the trans-Golgi network (Wang et al., 2014). Dysfunction of the trans-Golgi network has been shown to inhibit autophagy and lysosomal degradation pathways (Eskelinen and Saftig, 2009). C9orf72 has been shown to interact with Rab7L1(Aoki et al., 2017). Interestingly, abnormal M6PR localisation was observed in C9ALS/FTD patient-derived fibroblasts. In C9ALS/FTD fibroblasts M6PR was diffusely localised in the cytoplasm compared to around the nucleus in controls. Expression of C9orf72 reversed the defective vesicle trafficking and dysfunctional trans-Golgi network phenotype. Since M6PR mediates trafficking of lysosomal proteins from the Golgi to the lysosome during lysosome biogenesis, dysfunction of the Rab7L1/M6PR pathway may also explain the lysosomal phenotypes observed in C9FTD/ALS. Collectively, this suggests perhaps C9orf72 and USP8 regulate trans-Golgi/endosome trafficking of lysosomes.

Additionally, transport of B subunit of Shiga toxin (STxB) from the plasma membrane to the Golgi was significantly reduced in C9orf72 depleted cells, suggesting endocytosis was inhibited (Farg et al., 2014). Therefore, C9orf72 has been proposed to regulate this endocytic pathway. Levels of the ESCRT-0 (endosomal sorting complexes required for transport) components Hrs (hepatocyte growth factor receptor tyrosine kinase substrate) and STAM (signal transducing adapter molecule) are regulated by USP8 (Ali et al., 2013; Row et al., 2006). Knockdown of USP8 significantly reduced both Hrs and STAM levels. Given Hrs is necessary for retromer-dependent STxB transport, it is possible loss of USP8 affects this pathway, although both retromer-dependent and independent pathways have been shown to result in similar Golgi dysfunction phenotypes (Macdonald et al., 2014). Nonetheless, it would be interesting to explore whether loss of C9orf72 and USP8 act together to affect endosomal trafficking.

6.6.   A role for SUMOylation in C9orf72-SMCR8 complex stability?

Bioinformatic analysis in Chapter 5 identified SIMs and SUMOylation consensus sites in both C9orf72 and SMCR8. We determined that the SIM motif and K90 residue in C9orf72

reduced the stability but not the binding of the C9orf72-SMCR8 complex (Figure 5.2 and Figure 5.4). Separate SUMOylation immunoprecipitation assays for C9orf72 and SMCR8 identified both C9orf72 and SMCR8 interact with unidentified SUMOylated proteins but the results suggested they are not SUMOylated themselves (Figure 5.6). The K428 lysine residue of SMCR8 was identified in a mass spectrometry screen for endogenous SUMO2/3 sites (Hendriks et al., 2018). This contrasts with our results which failed to identify SUMOylated SMCR8. As discussed previously, this could be due to the amount of SUMOylated C9orf72 or SMCR8 being below the detection limit of western blotting. Utilising an in vitro binding assay should overcome this potential issue as it allows investigation of SUMOylation of solely C9orf72 or SMCR8. However, the potential drawback is if C9orf72 or SMCR8 require PTMs prior to SUMOylation, an in vitro approach will be unable to determine this. The K428 SUMO site in SMCR8 is located in its cDENN domain. Recent cryo-EM has revealed that the C9orf72-SMCR8 interaction is mediated by interactions of their respective cDENN domains (Su et al., 2020; Tang et al., 2020). A cryo-EM map identified the interacting residues that contribute to the uDENN – uDENN and cDENN – cDENN interaction in C9orf72-SMCR8 and neither the C9orf72 SIM, C9orf72 K90 or SMCR8 K428 residues were identified (Norpel et al., 2021) suggesting that these residue are not critical for the interaction. This is in line with our results that demonstrate that the C9orf72 SIM and K90 residue did not affect the binding of C9orf72 and SMCR8. Our results did suggest that the C9orf72 SIM and K90 residue affects the stability of the C9orf72-SMCR8 complex although why the SIM and K90 residue decreases stability of the complex has yet to be determined. Speculatively, the binding of SUMOylated C9orf72 and SUMOylated SMCR8 may make the complex more stable but SUMOylation of the proteins may not be a necessity for binding. If this was the case, the C9orf72 SIM could mediate its own SUMOylation by enhancing the interaction between C9orf72 and Ubc9-SUMO. The SUMO site identified in SMCR8 conforms to SUMOylation consensus motif and so presumably occurs in this fashion. This hypothesis may help explain the reduced stability of the C9orf72 SIM and K90 residue. It would be interesting to see whether the stability of SMCR8 K428R-C9orf72 complex differs from the stability of C9orf72-SMCR8 (as we see with C9orf72 SIM and K90R) as this would give an indication as to whether SUMOylation of SMCR8 stabilises the C9orf72-SMCR8 complex. Indeed, the transcriptional regulator protein GTF2IRD1 is SUMOylated and this PTM modulated its interaction with its binding partners, ZMYM5 and the E3 ligase PIASxβ (Widagdo et al., 2012). ZMYM5 binds to GTF2IRD1 near its SUMO site. What's

more, SUMOylation positively modulates GTF2IRD1 ubiquitination; addition of SUMO increases GFT2IRD1 ubiquitination but not the ubiquitination status of its non-SUMO conjugatable mutant. In addition, ZMYM5 preferentially binds to SUMOylated GTF2IRD1.

The identified K428 SUMO site in SMCR8 was only identified under proteasomal inhibition but not heat stress or control conditions (Hendriks et al., 2018). This suggests that SUMOylated SMCR8 is possibly degraded via the proteasome and hints at a possible cross talk between the SUMO and ubiquitin pathways. The SUMOylation of proteins has been shown to act as a signal for proteasomal degradation. RING finger protein 4 (RNF4) is the mammalian orthologue of Rfp1/Rfp2 (Ring finger protein) in yeast. The RING-like domain in Rfp1 and Rfp 2 binds Slx5/Slx8, a RING finger ubiquitin ligase to form a heterodimeric STUbL (SUMO-targeted ubiquitin ligase). Moreover, Rfp contain SIMs that are necessary for SUMO binding. In contrast, RNF4 contains both the SIM and ubiquitin ligase activity necessary for STUbLs (Prudden et al., 2007; Sun et al., 2007). STUbLs mediate the ubiquitination of either SUMO chains of target proteins or the target protein itself (Lallemand-Breitenbach et al., 2008; Prudden et al., 2007; Tatham et al., 2008). RNF4 is recruited to SUMOylated proteins and interacts with SUMO via its N-terminal SIM (Prudden et al., 2007; Sun et al., 2007; Xie et al., 2007). Moreover, RNF4 has been shown to ubiquitinate PML (promyelocytic leukaemia), resulting in its arsenic-induced proteasomal degradation (Lallemand-Breitenbach et al., 2008; Tatham et al., 2008). In the absence of RNF4, PML accumulates in the nucleus and arsenic fails to induce the degradation of PML or SUMOylated PML. This highlights the ability of SUMOylated proteins to acts as signals for ubiquitin proteasome degradation. Taken together, it would be interesting to explore whether SUMOylation of SMCR8 is required for its interaction with C9orf72 or degradation as this may represent a possible avenue to explore for treatment. The interaction of C9orf72 with RNF4 or SMCR8 with RNF4 could be explored via co-immunoprecipitation assays. Intriguingly, when the C9orf72 and SMCR8 protein interactome was investigated by mass spectrometry, SUMO3 was identified in the C9orf72, but not SMCR8 interactome (Goodier et al., 2020) which raises the question of whether C9orf72 is SUMOylated.

6.7. Future directions

Further experimentation will be required to determine the functional consequences of possible C9orf72 or SMCR8 SUMOylation. SUMOylation of proteins is known to regulate many process such as trafficking, protein partner interactions and stability (Chang and Yeh, 2020; Widagdo et al., 2012). Mutation of the C9orf72 SIM and K90 residue appeared to affect the stabilisation of the C9orf72-SMCR8 complex, which suggests that SUMOylation may influence complex stability. Using co-expression assays, the effect of C9orf72 SUMO mutants identified by bioinformatics (K14, K48 and K273) on the stabilisation of the complex can occur by expressing the different C9orf72 SUMO mutants with SMCR8. Similar experiments can be performed with the SMCR8 SUMO mutants which will give an indication as to whether SUMOylation of C9orf72, SMCR8 or neither protein influences complex stability. Proteasomal inhibition, but not heat stress or control conditions identified the K428 SMCR8 SUMO site by mass spectrometry. Therefore, determining whether SUMOylation of SMCR8 on the K428 is a prerequisite for SMCR8 degradation can be established with cycloheximide chase assays utilised in this thesis.

Within our experiments, we determined C9orf72 is not a substrate of USP8 and hypothesise the functional consequences of the interaction may relate to C9orf72 regulating USP8 trafficking. Despite the fact finding an inhibitor of E3 ligases may be clinically more realistic than finding an activator of DUBs, identifying the DUB for either C9orf72 or SMCR8 still represents a viable course of action. Multiple DUBs have been identified in the C9orf72 and SMCR8 protein interactome via mass spectrometry (Goodier et al., 2020; Zhang et al., 2018b) and so in the first instance, the effect of knockdown of the frequently identified DUBs on C9orf72 or SMCR8 levels should be determined. If a specific DUB for C9orf72 or SMCR8 is not identified from this, a high-throughput screen for possible DUBs for C9orf72 can be carried out using a single-guide RNA screening system (Doench et al., 2016; Sanson et al., 2018).

The work in this thesis investigated the degradation pathway for C9orf72 and SMCR8 and determined that C9orf72 is degraded via the ubiquitin proteasome system. Furthermore, KLHL13 was implicated as the potential Kelch-like protein involved in E3 ubiquitination. However, future work will endeavour to determine whether knockdown of KLHL13 increases C9orf72 levels as a direct result of reducing C9orf72 ubiquitination or as an indirect result of increasing SMCR8 levels. This could be achieved by knockdown of both KLHL13 and SMCR8 and determining whether C9orf72 levels are increased.

Knockdown of SMCR8 in known to result in a reduction of C9orf72, possibly as a result of decreased complex stability and subsequent proteasomal degradation. Therefore, an increase in C9orf72 levels would impart confidence that KLHL13 acts directly on C9orf72 and would establish KLHL13 as a *bona fide* target for treatment. Similarly, knockdown of KLHL13 on a C9orf72 deficient background using C9orf72[KO] cells would determine whether KLHL13 acts directly on SMCR8 to increase its levels. Within this thesis, we determined that MLN4924 is able to prevent the turnover of SMCR8. Future work to determine whether this is able to lead to a stabilisation of C9orf72 should be investigated.

As KLHL13 forms a complex with Cul3, determining whether knockdown of Cul3 is also able to increase C9orf72 and SMCR8 levels would provide evidence that the Cul3-KLHL13 complex is able to ubiquitinate C9orf72. However, the translational potential of the finding that knockdown of KLHL13 can increase C9orf72 and SMCR8 levels will need to be assessed. Our current findings were observed in non-neuronal HeLa cells, which do not recapitulate the C9ALS/FTD phenotype. Therefore, although we hypothesise that reducing KLHL13 levels may be beneficial for patients, these findings will need to be confirmed through the use of patient-derived iPSC cell lines. Reducing C9orf72 expression using siRNA recapitulates the p62 pathology seen in C9ALS/FTD patients. Furthermore, reduced autophagy is seen in patient-derived iPSCs and reduced C9orf72 levels exacerbate DPR pathology. Therefore, determining whether increasing C9orf72 or SMCR8 levels through reducing KLHL13 (and possibly Cul3) expression can resolve or reduce the C9ALS/FTD associated pathologies would provide further evidence of the therapeutic potential of targeting KLHL13. This could be done in multiple C9ALS/FTD models - (A) HeLa or HEK293 cells that express DPRs but in which C9orf72 expression is reduced using siRNA, (B) C9ALS/FTD patient-derived iPSCs and (C) cortical neurons transduced with C9orf72-targeting microRNA that express DPRs. Following this, a high throughput drug screen could be utilised to identify any potential inhibitors of KLHL13 as novel drug targets for the treatment of C9ALS/FTD.

7. Bibliography

Abo-Rady, M., Kalmbach, N., Pal, A., Schludi, C., Janosch, A., Richter, T., Freitag, P., Bickle, M., Kahlert, A.K., Petri, S., et al. (2020). Knocking out C9ORF72 Exacerbates Axonal Trafficking Defects Associated with Hexanucleotide Repeat Expansion and Reduces Levels of Heat Shock Proteins. Stem Cell Reports *14*, 390–405.

Abramzon, Y.A., Fratta, P., Traynor, B.J., and Chia, R. (2020). The Overlapping Genetics of Amyotrophic Lateral Sclerosis and Frontotemporal Dementia. Front. Neurosci. *14*, 1–10.

Acs, K., Luijsterburg, M.S., Ackermann, L., Salomons, F.A., Hoppe, T., and Dantuma, N.P. (2011). The AAA-ATPase VCP/p97 promotes 53BP1 recruitment by removing L3MBTL1 from DNA double-strand breaks. Nat. Struct. Mol. Biol. *18*, 1345–1350.

Agar, J., and Durham, H. (2003). Relevance of oxidative injury in the pathogenesis of motor neuron diseases. Amyotroph. Lateral Scler. Other Mot. Neuron Disord. *4*, 232–242.

Aizawa, H., Sawada, J., Hideyama, T., Yamashita, T., Katayama, T., Hasebe, N., Kimura, T., Yahara, O., and Kwak, S. (2010). TDP-43 pathology in sporadic ALS occurs in motor neurons lacking the RNA editing enzyme ADAR2. Acta Neuropathol. *120*, 75–84.

Akizuki, M., Yamashita, H., Uemura, K., Maruyama, H., Kawakami, H., Ito, H., and Takahashi, R. (2013). Optineurin suppression causes neuronal cell death via NF-κB pathway. J. Neurochem. *126*, 699–704.

Al-Chalabi, A., and Hardiman, O. (2013). The epidemiology of ALS: A conspiracy of genes, environment and time. Nat. Rev. Neurol. *9*, 617–628.

Al-Chalabi, A., Jones, A., Troakes, C., King, A., Al-Sarraj, S., and Van Den Berg, L.H. (2012). The genetics and neuropathology of amyotrophic lateral sclerosis. Acta Neuropathol. *124*, 339–352.

Aladesuyi Arogundade, O., Stauffer, J.E., Saberi, S., Diaz-Garcia, S., Malik, S., Basilim, H., Rodriguez, M.J., Ohkubo, T., and Ravits, J. (2019). Antisense RNA foci are associated with nucleoli and TDP-43 mislocalization in C9orf72-ALS/FTD: a quantitative study. Acta Neuropathol. *137*, 527–530.

Alexopoulou, Z., Lang, J., Perrett, R.M., Elschami, M., Hurry, M.E.D., Kim, H.T., Mazaraki, D., Szabo, A., Kessler, B.M., Goldberg, A.L., et al. (2016). Deubiquitinase Usp8 regulates α-synuclein clearance and modifies its toxicity in Lewy body disease. Proc. Natl. Acad. Sci. *9*, 4688–4697.

Ali, N., Zhang, L., Taylor, S., Mironov, A., Urbé, S., and Woodman, P. (2013). Recruitment of UBPY and ESCRT Exchange Drive HD-PTP-Dependent Sorting of EGFR to the MVB. Curr. Biol. *23*, 453–461.

Amick, J., Roczniak-ferguson, A., Ferguson, S.M., and Brill, J. (2016). C9orf72 binds SMCR8 , localizes to lysosomes , and regulates mTORC1 signaling. Mol. Biol. Cell *27*, 3040–3051.

Amick, J., Tharkeshwar, A.K., Amaya, C., and Ferguson, S.M. (2018). WDR41 supports lysosomal response to changes in amino acid availability. Mol. Biol. Cell *29*, 2213–2227.

Amick, J., Tharkeshwar, A.K., Talaia, G., and Ferguson, S.M. (2020). PQLC2 recruits the C9orf72 complex to lysosomes in response to cationic amino acid starvation. J. Cell Biol. *219*.

Anant, J.S., Desnoyers, L., Machius, M., Demeler, B., Hansen, J.C., Westover, K.D., Deisenhofer, J., and Seabra, M.C. (1998). Mechanism of Rab geranylgeranylation: Formation of the catalytic ternary complex. Biochemistry *37*, 12559–12568.

Aoki, Y., Raquel Manzano, Ã., Yi Lee, Ã., Dafinca, R., Aoki, M., L Douglas, A.G., Varela, M.A., Sathyaprakash, C., Scaber, J., Barbagallo, P., et al. (2017). C9orf72 and RAB7L1 regulate vesicle trafficking in amyotrophic lateral sclerosis and frontotemporal dementia. Brain *140*, 887–897.

Arai, T., Hasegawa, M., Akiyama, H., Ikeda, K., Nonaka, T., Mori, H., Mann, D., Tsuchiya, K., Yoshida, M., Hashizume, Y., et al. (2006). TDP-43 is a component of ubiquitin-positive tau-negative inclusions in frontotemporal lobar degeneration and amyotrophic lateral sclerosis. Biochem. Biophys. Res. Commun. *351*, 602–611.

Ash, P.E.A., Bieniek, K.F., Gendron, T.F., Caulfield, T., Lin, W.-L., Dejesus-Hernandez, M., Van Blitterswijk, M.M., Jansen-West, K., Paul Iii, J.W., Rademakers, R., et al. (2013). Unconventional Translation of C9ORF72 GGGGCC Expansion Generates Insoluble Polypeptides Specific to c9FTD/ALS. Neuron *77*, 639–646.

Atanasio, A., Decman, V., White, D., Ramos, M., Ikiz, B., Lee, H., Siao, C., Brydges, S., Larosa, E., Bai, Y., et al. (2016). C9orf72 ablation causes immune dysregulation characterized by leukocyte expansion , autoantibody production , and glomerulonephropathy in mice. Nat. Sci. Reports 1–14.

Baborie, A., Rollinson, S., Infirmary, R.V., Health, M., Hospital, S.R., Baborie, A., Griffiths, T.D., Jaros, E., Perry, R., Mckeith, I.G., et al. (2015). Accumulation of dipeptide repeat proteins predates that of TDP-43 in frontotemporal lobar degeneration associated with hexanucleotide repeat expansions in. Neuropathol. Appl. Neurobiol. *41*, 601–612.

Baker, M., Mackenzie, I.R., Pickering-Brown, S.M., Gass, J., Rademakers, R., Lindholm, C., Snowden, J., Adamson, J., Sadovnick, A.D., Rollinson, S., et al. (2006). Mutations in progranulin cause tau-negative frontotemporal dementia linked to chromosome 17. Nature *442*, 916–919.

Barber, S.C., Mead, R.J., and Shaw, P.J. (2006). Oxidative stress in ALS: A mechanism of neurodegeneration and a therapeutic target. Biochim. Biophys. Acta *1762*, 1051–1067.

Bard, J.A.M., Goodall, E.A., Greene, E.R., Jonsson, E., Dong, K.C., Martin, A., A, E., Greene, E.R., Jonsson, E., Dong, K.C., et al. (2018). Function of the 26S Proteasome. Annu. Rev. Biochem. 1–28.

Barthelme, D., Jauregui, R., and Sauer, R.T. (2015). An ALS disease mutation in Cdc48/p97 impairs 20S proteasome binding and proteolytic communication. Protein Sci. *24*, 1521–1527.

Beers, D.R., Henkel, J.S., Zhao, W., Wang, J., and Appel, S.H. (2008). CD4+ T cells support glial neuroprotection, slow disease progression, and modify glial morphology in an animal model of inherited ALS. Proc. Natl. Acad. Sci. U. S. A. *105*, 15558–15563.

Beers, D.R., Zhao, W., Wang, J., Zhang, X., Wen, S., Neal, D., Thonhoff, J.R., Alsuliman, A.S., Shpall, E.J., Rezvani, K., et al. (2017). Tregs in ALS are Dysfunctional and Predict Progression Rate and Severity. JCI Insight *2*, 1–14.

Beers, D.R., Zhao, W., and Appel, S.H. (2018). The role of regulatory T lymphocytes in amyotrophic lateral sclerosis. JAMA Neurol. *75*, 656–658.

Belle, A., Tanay, A., Bitincka, L., Shamir, R., and O'Shea, E.K. (2006). Quantification of protein half-lives in the budding yeast proteome. Proc. Natl. Acadamey Sci. *103*, 13004–13009.

Belzil, V. V., Bauer, P.O., Prudencio, M., Gendron, T.F., Stetler, C.T., Yan, I.K., Pregent, L., Daughrity, L., Baker, M.C., Rademakers, R., et al. (2013). Reduced C9orf72 gene expression in c9FTD/ALS is caused by histone trimethylation, an epigenetic event detectable in blood. Acta Neuropathol. *126*, 895–905.

Belzil, V. V., Bauer, P.O., Gendron, T.F., Murray, M.E., Dickson, D., and Petrucelli, L. (2014). Characterization of DNA hypermethylation in the cerebellum of c9FTD/ALS patients. Brain Res.

1584, 15–21.

Belzil, V. V, Katzman, R.B., and Petrucelli, L. (2016). ALS and FTD: an epigenetic perspective. Acta Neuropathol. *132*, 487–502.

Bennett, C.L., and La Spada, A.R. (2021). SUMOylated Senataxin functions in genome stability, RNA degradation, and stress granule disassembly, and is linked with inherited ataxia and motor neuron disease. Mol. Genet. Genomic Med. 1–8.

Berlin, I., Higginbotham, K.M., Dise, R.S., Sierra, M.I., and Nash, P.D. (2010). The Deubiquitinating Enzyme USP8 Promotes Trafficking and Degradation of the Chemokine Receptor 4 at the Sorting Endosome. J. Biol. Chem. *285*, 37895–37908.

Bernier-Villamor, V., Sampson, D.A., Matunis, M.J., and Lima, C.D. (2002). Structural basis for E2-mediated SUMO conjugation revealed by a complex between ubiquitin-conjugating enzyme Ubc9 and RanGAP1. Cell *108*, 345–356.

Betteridge, D.J. (2000). What is oxidative stress? Metabolism. *49*, 3–8.

Bilsland, L.G., Sahai, E., Kelly, G., Golding, M., Greensmith, L., and Schiavo, G. (2010). Deficits in axonal transport precede ALS symptoms in vivo. Proc. Natl. Acad. Sci. U. S. A. *107*, 20523–20528.

Blair, I.P., Williams, K.L., Warraich, S.T., Durnall, J.C., Thoeng, A.D., Manavis, J., Blumbergs, P.C., Vucic, S., Kiernan, M.C., and Nicholson, G.A. (2010). FUS mutations in amyotrophic lateral sclerosis: clinical, pathological, neurophysiological and genetic analysis. J. Neurol. Neurosurg. Psychiatry *81*, 639–645.

van Blitterswijk, M., Gendron, T.F., Baker, M.C., DeJesus-Hernandez, M., Finch, N.C.A., Brown, P.H., Daughrity, L.M., Murray, M.E., Heckman, M.G., Jiang, J., et al. (2015). Novel clinical associations with specific C9ORF72 transcripts in patients with repeat expansions in C9ORF72. Acta Neuropathol. *130*, 863–876.

Van Blitterswijk, M., Van Es, M.A., Hennekam, E.A.M., Dooijes, D., Van Rheenen, W., Medic, J., Bourque, P.R., Schelhaas, H.J., Van der Kooi, A.J., De Visser, M., et al. (2012). Evidence for an oligogenic basis of amyotrophic lateral sclerosis. Hum. Mol. Genet. *21*, 3776–3784.

Blokhuis, A.M., Koppers, M., Groen, E.J.N., van den Heuvel, D.M.A., Dini Modigliani, S., Anink, J.J., Fumoto, K., van Diggelen, F., Snelting, A., Sodaar, P., et al. (2016). Comparative interactomics analysis of different ALS-associated proteins identifies converging molecular pathways. Acta Neuropathol. *132*, 175–196.

Blomster, H.A., Imanishi, S.Y., Siimes, J., Kastu, J., Morrice, N.A., Eriksson, J.E., and Sistonen, L. (2010). In vivo identification of sumoylation sites by a signature tag and cysteine-targeted affinity purification. J. Biol. Chem. *285*, 19324–19329.

Boivin, M., Pfister, V., Gaucherot, A., Ruffenach, F., Negroni, L., Sellier, C., and Charlet-Berguerand, N. (2020). Reduced autophagy upon C9ORF72 loss synergizes with dipeptide repeat protein toxicity in G4C2 repeat expansion disorders. EMBO J. *39*, 1–15.

van den Boom, J., Wolf, M., Weimann, L., Schulze, N., Li, F., Kaschani, F., Riemer, A., Zierhut, C., Kaiser, M., Iliakis, G., et al. (2016). VCP/p97 Extracts Sterically Trapped Ku70/80 Rings from DNA in Double-Strand Break Repair. Mol. Cell *64*, 189–198.

Bosch, L. Van Den, Vandenberghe, W., Klaassen, H., Houtte, E. Van, and Robberecht, W. (2000). Ca2+ -permeable AMPA receptors and selective vulnerability of motor neurons. J. Neurol. Sci. *180*, 29–34.

Bosco, D.A., Lemay, N., Ko, H.K., Zhou, H., Burke, C., Kwiatkowski, T.J., Sapp, P., Mckenna-Yasek, D., Brown, R.H., and Hayward, L.J. (2010). Mutant FUS proteins that cause amyotrophic

lateral sclerosis incorporate into stress granules. Hum. Mol. Genet. *19*, 4160–4175.

Boylan, K. (2015). Familial Amyotrophic Lateral Sclerosis. Neurol. Clin. *33*, 807–830.

Braems, E., Swinnen, B., and Van Den Bosch, L. (2020). C9orf72 loss-of-function: a trivial, stand-alone or additive mechanism in C9 ALS/FTD? Acta Neuropathol. *140*, 625–643.

Braten, O., Livneh, I., Ziv, T., Admon, A., Kehat, I., Caspi, L.H., Gonen, H., Bercovich, B., Godzik, A., Jahandideh, S., et al. (2016). Numerous proteins with unique characteristics are degraded by the 26S proteasome following monoubiquitination. Proc. Natl. Acadamey Sci. *113*, 4639–4647.

Brenner, D., Müller, K., Wieland, T., Weydt, P., Böhm, S., Lule, D., Hübers, A., Neuwirth, C., Weber, M., Borck, G., et al. (2016). NEK1 mutations in familial amyotrophic lateral sclerosis. Brain *139*, e28.

Brenner, D., Yilmaz, R., Müller, K., Grehl, T., Petri, S., Meyer, T., Grosskreutz, J., Weydt, P., Ruf, W., Neuwirth, C., et al. (2018). Hot-spot KIF5A mutations cause familial ALS. Brain *141*, 688–697.

Brownell, J.E., Sintchak, M.D., Gavin, J.M., Liao, H., Bruzzese, F.J., Bump, N.J., Soucy, T.A., Milhollen, M.A., Yang, X., Burkhardt, A.L., et al. (2010). Substrate-Assisted Inhibition of Ubiquitin-like Protein-Activating Enzymes: The NEDD8 E1 Inhibitor MLN4924 Forms a NEDD8-AMP Mimetic In Situ. Mol. Cell *37*, 102–111.

Bruijn, L.I., Becher, M.W., Lee, M.K., Anderson, K.L., Jenkins, N.A., Copeland, N.G., Sisodia, S.S., Rothstein, J.D., and Borchelt, D.R. (1997). ALS-Linked SOD1 Mutant G85R Mediates Damage to Astrocytes and Promotes Rapidly Progressive Disease with SOD1-Containing Inclusions. Neuron *18*, 327–338.

Buchan, J.R., Kolaitis, R.M., Taylor, J.P., and Parker, R. (2013). XEukaryotic stress granules are cleared by autophagy and Cdc48/VCP function. Cell *153*, 1461.

Bulatov, E., and Ciulli, A. (2015). Targeting Cullin-RING E3 ubiquitin ligases for drug discovery: Structure, assembly and small-molecule modulation. Biochem. J. *467*, 365–386.

Burberry, A., Suzuki, N., Wang, J., Moccia, R., Mordes, D.A., Stewart, M., Suzuki-uematsu, S., Ghosh, S., Singh, A., Florian, T., et al. (2016). Loss-of-function mutations in the C9ORF72 mouse ortholog cause fatal autoimmune disease. Sci. Transl. Med. *8*, 1–26.

Burrell, J.R., Kiernan, M.C., Vucic, S., and Hodges, J.R. (2011). Motor Neuron dysfunction in frontotemporal dementia. Brain *134*, 2582–2594.

Butti, Z., Pan, Y.E., Giacomotto, J., and Patten, S.A. (2021). Reduced C9orf72 function leads to defective synaptic vesicle release and neuromuscular dysfunction in zebrafish. Commun. Biol. *4*, 792.

Byrne, S., Elamin, M., Bede, P., Shatunov, A., Walsh, C., Corr, B., Heverin, M., Jordan, N., Kenna, K., Lynch, C., et al. (2012). Cognitive and clinical characteristics of patients with amyotrophic lateral sclerosis carrying a C9orf72 repeat expansion: A population-based cohort study. Lancet Neurol. *11*, 232–240.

Cagnin, A., Rossor, M., Sampson, E.L., MacKinnon, T., and Banati, R.B. (2004). In vivo detection of microglial activation in frontotemporal dementia. Ann. Neurol. *56*, 894–897.

Cairns, N.J., Neumann, M., Bigio, E.H., Holm, I.E., Troost, D., Hatanpaa, K.J., Foong, C., White, C.L., Schneider, J.A., Kretzschmar, H.A., et al. (2007). TDP-43 in familial and sporadic frontotemporal lobar degeneration with ubiquitin inclusions. Am. J. Pathol. *171*, 227–240.

Canning, P., Cooper, C.D.O., Krojer, T., Murray, J.W., Pike, A.C.W., Chaikuad, A., Keates, T., Thangaratnarajah, C., Hojzan, V., Marsden, B.D., et al. (2013). Structural basis for Cul3 protein assembly with the BTB-Kelch family of E3 ubiquitin ligases. J. Biol. Chem. *288*, 7803–7814.

Caselli, R.J., Windebank, A.J., Petersen, R.C., Komori, T., Parisi, J.E., Okazaki, H., Kokmen, E., Iverson, R., Dinapoli, R.P., Graff-Radford, N.R., et al. (1993). Rapidly progressive aphasic dementia and motor neuron disease. Ann. Neurol. *33*, 200–207.

Catanese, A., Rajkumar, S., Sommer, D., Freisem, D., Wirth, A., Aly, A., Massa-López, D., Olivieri, A., Torelli, F., Ioannidis, V., et al. (2021). Synaptic disruption and CREB-regulated transcription are restored by K + channel blockers in ALS. EMBO Mol. Med. *13*, 1–16.

Cautain, B., Hill, R., De Pedro, N., and Link, W. (2015). Components and regulation of nuclear transport processes. FEBS J. *282*, 445–462.

Chabot, B., and Shkreta, L. (2016). Defective control of pre-messenger RNA splicing in human disease. J. Cell Biol. *212*, 13–27.

Chai, Q., Webb, S.R., Wang, Z., Dutch, R.E., and Wei, Y. (2016). Study of the degradation of a multidrug transporter using a non-radioactive pulse chase method. Anal. Bioanal. Chem. *408*, 7745–7751.

Chang, H.M., and Yeh, E.T.H. (2020). Sumo: From bench to bedside. Physiol. Rev. *100*, 1599–1619.

Chang, L., and Monteiro, M.J. (2015). Defective proteasome delivery of polyubiquitinated proteins by ubiquilin-2 proteins containing ALS mutations. PLoS One *10*, 1–15.

Chang, C.C., Naik, M.T., Huang, Y.S., Jeng, J.C., Liao, P.H., Kuo, H.Y., Ho, C.C., Hsieh, Y.L., Lin, C.H., Huang, N.J., et al. (2011). Structural and Functional Roles of Daxx SIM Phosphorylation in SUMO Paralog-Selective Binding and Apoptosis Modulation. Mol. Cell *42*, 62–74.

Chen, G., Xu, X., Tong, J., Han, K., Zhang, Z., Tang, J., Li, S., Yang, C., Li, J., Cao, B., et al. (2014a). Ubiquitination of the transcription factor c-MAF is mediated by multiple lysine residues. Int. J. Biochem. Cell Biol. *57*, 157–166.

Chen, J.C., Alvarez, M.J., Talos, F., Dhruv, H., Rieckhof, G.E., Iyer, A., Diefes, K.L., Aldape, K., Berens, M., Shen, M.M., et al. (2014b). Identification of causal genetic drivers of human disease through systems-level analysis of regulatory networks. Cell *159*, 402–414.

Chen, X., Zhang, L., Zheng, S., Zhang, T., Li, M., Zhang, X., Zeng, Z., McCrae, M.A., Zhao, J., Zhuang, H., et al. (2015). Hepatitis B virus X protein stabilizes cyclin D1 and increases cyclin D1 nuclear accumulation through ERK-mediated inactivation of GSK-3β. Cancer Prev. Res. *8*, 455–463.

Chen, X., Liao, S., Makaros, Y., Guo, Q., Zhu, Z., Krizelman, R., Dahan, K., Tu, X., Yao, X., Koren, I., et al. (2021). Molecular basis for arginine C-terminal degron recognition by Cul2FEM1 E3 ligase. Nat. Chem. Biol. *17*, 254–262.

Chen, Y.Z., Bennett, C.L., Huynh, H.M., Blair, I.P., Puls, I., Irobi, J., Dierick, I., Abel, A., Kennerson, M.L., Rabin, B.A., et al. (2004). DNA/RNA helicase gene mutations in a form of juvenile amyotrophic lateral sclerosis (ALS4). Am. J. Hum. Genet. *74*, 1128–1135.

Cheroni, C., Marino, M., Tortarolo, M., Veglianese, P., De Biasi, S., Fontana, E., Zuccarello, L.V., Maynard, C.J., Dantuma, N.P., and Bendotti, C. (2009). Functional alterations of the ubiquitin-proteasome system in motor neurons of a mouse model of familial amyotrophic lateral sclerosis. Hum. Mol. Genet. *18*, 82–96.

Chew, J., Gendron, T.F., Prudencio, M., Sasaguri, H., Zhang, Y.J., Castanedes-Casey, M., Lee, C.W., Jansen-West, K., Kurti, A., Murray, M.E., et al. (2015). C9ORF72 repeat expansions in mice cause TDP-43 pathology, neuronal loss, and behavioral deficits. Science (80-.). *348*, 1151–1154.

Chiò, A., Calvo, A., Moglia, C., Mazzini, L., Mora, G., Mutani, R., Balma, M., Cammarosano, S., Canosa, A., Gallo, S., et al. (2011). Phenotypic heterogeneity of amyotrophic lateral sclerosis: A population based study. J. Neurol. Neurosurg. Psychiatry *82*, 740–746.

Chiu, I.M., Chen, A., Zheng, Y., Kosaras, B., Tsiftsoglou, S.A., Vartanian, T.K., Brown, R.H., and Carroll, M.C. (2008). T lymphocytes potentiate endogenous neuroprotective inflammation in a mouse model of ALS. Proc. Natl. Acad. Sci. U. S. A. *105*, 17913–17918.

Chow, C.Y., Landers, J.E., Bergren, S.K., Sapp, P.C., Grant, A.E., Jones, J.M., Everett, L., Lenk, G.M., McKenna-Yasek, D.M., Weisman, L.S., et al. (2009). Deleterious Variants of FIG4, a Phosphoinositide Phosphatase, in Patients with ALS. Am. J. Hum. Genet. *84*, 85–88.

Cirulli, E.T., Lasseigne, B.N., Petrovski, S., Sapp, P.C., Dion, P.A., Leblond, C.S., Couthouis, J., Lu, Y.F., Wang, Q., Krueger, B.J., et al. (2015). Exome sequencing in amyotrophic lateral sclerosis identifies risk genes and pathways. Science (80-.). *347*, 1436–1441.

Ciura, S., Lattante, S., Le Ber, I., Latouche, M., Tostivint, H., Brice, A., and Kabashi, E. (2013). Loss of function of C9orf72 causes motor deficits in a zebrafish model of amyotrophic lateral sclerosis. Ann. Neurol. *74*, 180–187.

Clausen, L., Stein, A., Grønbæk-Thygesen, M., Nygaard, L., Søltoft, C.L., Nielsen, S. V., Lisby, M., Ravid, T., Lindorff-Larsen, K., and Hartmann-Petersen, R. (2020). Folliculin variants linked to Birt-Hogg-Dubésyndrome are targeted for proteasomal degradation. PLoS Genet. *16*, 1–28.

Conlon, E.G., Lu, L., Sharma, A., Yamazaki, T., Tang, T., Shneider, N.A., and Manley, J.L. (2016). The C9ORF72 GGGGCC expansion forms RNA G-quadruplex inclusions and sequesters hnRNP H to disrupt splicing in ALS brains. Elife *5*, 1–28.

Cooper-Knock, J., Walsh, M.J., Higginbottom, A., Highley, J.R., Dickman, M.J., Edbauer, D., Ince, P.G., Wharton, S.B., Wilson, S.A., Kirby, J., et al. (2014a). Sequestration of multiple RNA recognition motif-containing proteins by C9orf72 repeat expansions. Brain *137*, 2040–2051.

Cooper-Knock, J., Walsh, M.J., Higginbottom, A., Highley, J.R., Dickman, M.J., Edbauer, D., Ince, P.G., Wharton, S.B., Wilson, S.A., Kirby, J., et al. (2014b). Sequestration of multiple RNA recognition motif-containing proteins by C9orf72 repeat expansions. Brain *137*, 2040–2051.

Cooper-Knock, J., Bury, J.J., Heath, P.R., Wyles, M., Higginbottom, A., Gelsthorpe, C., Highley, J.R., Hautbergue, G., Rattray, M., Kirby, J., et al. (2015a). C9ORF72 GGGGCC expanded repeats produce splicing dysregulation which correlates with disease severity in amyotrophic lateral sclerosis. PLoS One *10*, 1–17.

Cooper-Knock, J., Higginbottom, A., Stopford, M.J., Highley, J.R., Ince, P.G., Wharton, S.B., Pickering-Brown, S., Kirby, J., Hautbergue, G.M., and Shaw, P.J. (2015b). Antisense RNA foci in the motor neurons of C9ORF72-ALS patients are associated with TDP-43 proteinopathy. Acta Neuropathol. *130*, 63–75.

Cooper-Knock, J., Moll, T., Ramesh, T., Castelli, L., Beer, A., Robins, H., Fox, I., Niedermoser, I., Van Damme, P., Moisse, M., et al. (2019). Mutations in the Glycosyltransferase Domain of GLT8D1 Are Associated with Familial Amyotrophic Lateral Sclerosis. Cell Rep. *26*, 2298-2306.e5.

Corbo, M., and Hays, A.P. (1992). Peripherin and neurofilament protein coexist in spinal spheroids of motor neuron disease. J. Neuropathol. Exp. Neurol. *51*, 531–537.

Corona, J.C., and Tapia, R. (2004). AMPA receptor activation, but not the accumulation of endogenous extracellular glutamate, induces paralysis and motor neuron death in rat spinal cord in vivo. J. Neurochem. *89*, 988–997.

Costa, D.B., Shaw, A.T., Ou, S.H.I., Solomon, B.J., Riely, G.J., Ahn, M.J., Zhou, C., Martin Shreeve, S., Selaru, P., Polli, A., et al. (2015). Clinical experience with crizotinib in patients with

advanced ALK-rearranged non-small-cell lung cancer and brain metastases. J. Clin. Oncol. *33*, 1881–1888.

Crosby, K., Crown, A.M., Roberts, B.L., Brown, H., Ayers, J.I., and Borchelt, D.R. (2018). Loss of charge mutations in solvent exposed Lys residues of superoxide dismutase 1 do not induce inclusion formation in cultured cell models. PLoS One *13*, 1–18.

Cruts, M., Gijselinck, I., van der Zee, J., Engelborghs, S., Wils, H., Pirici, D., Rademakers, R., Vandenberghe, R., Dermaut, B., Martin, J.-J., et al. (2006). Null mutations in progranulin cause ubiquitin-positive frontotemporal dementia linked to chromosome 17q21. Nature *442*, 920–924.

Custer, K.L., Austin, N.S., Sullivan, J.M., and Bajjalieh, S.M. (2006). Synaptic vesicle protein 2 enhances release probability at quiescent synapses. J. Neurosci. *26*, 1303–1313.

D 'arcy, P., Wang, X., and Linder, S. (2014). Deubiquitinase inhibition as a cancer therapeutic strategy. Pharmacol. Ther. *147*, 32–54.

Dai, R.M., and Li, C.C.H. (2001). Valosin-containing protein is a multi-ubiquitin chain-targeting factor required in ubiquitin-proteasome degradation. Nat. Cell Biol. *3*, 740–744.

Van Damme, P., Robberecht, W., and Van Den Bosch, L. (2017). Modelling amyotrophic lateral sclerosis: Progress and possibilities. DMM Dis. Model. Mech. *10*, 537–549.

Dangoumau, A., Marouillat, S., Burlaud Gaillard, J., Uzbekov, R., Veyrat-Durebex, C., Blasco, H., Arnoult, C., Corcia, P., Andres, C.R., and Vourc'h, P. (2016). Inhibition of pathogenic mutant SOD1 aggregation in cultured motor neuronal cells by prevention of its SUMOylation on lysine 75. Neurodegener. Dis. *16*, 161–171.

Danielsson, F., Wiking, M., Mahdessian, D., Skogs, M., Blal, H.A., Hjelmare, M., Stadler, C., Uhlén, M., and Lundberg, E. (2013). RNA deep sequencing as a tool for selection of cell lines for systematic subcellular localization of all human proteins. J. Proteome Res. *12*, 299–307.

Das, T., Shin, S.C., Song, E.J., and Kim, E.E. (2020). Regulation of deubiquitinating enzymes by post-translational modifications. Int. J. Mol. Sci. *21*, 1–18.

Davidson, Y., Kelley, T., Mackenzie, I.R.A., Pickering-Brown, S., Du Plessis, D., Neary, D., Snowden, J.S., and Mann, D.M.A. (2007). Ubiquitinated pathological lesions in frontotemporal lobar degeneration contain the TAR DNA-binding protein, TDP-43. Acta Neuropathol. *113*, 521–533.

Davis, C., Spaller, B.L., and Matouschek, A. (2021). Mechanisms of substrate recognition by the 26S proteasome. Curr. Opin. Struct. Biol. *67*, 161–169.

Van Deerlin, V.M., Leverenz, J.B., Bekris, L.M., Bird, T.D., Yuan, W., Elman, L.B., Clay, D., McCarty Wood, E., Chen-Plotkin, A.S., Martinez-Lage, M., et al. (2008). TARDBP mutations in amyotrophic lateral sclerosis with TDP-43 neuropathology: a genetic and histopathological analysis. Lancet Neurol. *7*, 409–416.

DeJesus-Hernandez, M., Mackenzie, I.R., Boeve, B.F., Boxer, A.L., Baker, M., Rutherford, N.J., Nicholson, A.M., Finch, N.A., Flynn, H., Adamson, J., et al. (2011). Expanded GGGGCC Hexanucleotide Repeat in Noncoding Region of C9ORF72 Causes Chromosome 9p-Linked FTD and ALS. Neuron *72*, 245–256.

DeJesus-Hernandez, M., Finch, N.C.A., Wang, X., Gendron, T.F., Bieniek, K.F., Heckman, M.G., Vasilevich, A., Murray, M.E., Rousseau, L., Weesner, R., et al. (2017). In-depth clinico-pathological examination of RNA foci in a large cohort of C9ORF72 expansion carriers. Acta Neuropathol. *134*, 255–269.

Deng, H.-X., Chen, W., Hong, S.-T., Boycott, K.M., Gorrie, G.H., Siddique, N., Yang, Y., Fecto, F., Shi, Y., Zhai, H., et al. (2011). Mutations in UBQLN2 cause dominant X-linked juvenile and

adult-onset ALS and ALS/dementia. Nature *477*, 211–215.

Deng, H.X., Zhai, H., Bigio, E.H., Yan, J., Fecto, F., Ajroud, K., Mishra, M., Ajroud-Driss, S., Heller, S., Sufit, R., et al. (2010). FUS-immunoreactive inclusions are a common feature in sporadic and non-SOD1 familial amyotrophic lateral sclerosis. Ann. Neurol. *67*, 739–748.

Deng, J., Yang, M., Chen, Y., Chen, X., Liu, J., Sun, S., Cheng, H., Li, Y., Bigio, E.H., Mesulam, M., et al. (2015). FUS Interacts with HSP60 to Promote Mitochondrial Damage. PLoS Genet. *11*, 1–30.

Desterro, J.M.P., Thomson, J., and Hay, R.T. (1997). Ubch9 conjugates SUMO but not ubiquitin. FEBS Lett. *417*, 297–300.

Desterro, J.M.P., Rodriguez, M.S., Kemp, G.D., and Ronald T, H. (1999). Identification of the enzyme required for activation of the small ubiquitin-like protein SUMO-1. J. Biol. Chem. *274*, 10618–10624.

Dhanoa, B.S., Cogliati, T., Satish, A.G., Bruford, E.A., and Friedman, J.S. (2013). Update on the Kelch-like (KLHL) gene family. Hum. Genomics *7*.

Diaper, D.C., Adachi, Y., Sutcliffe, B., Humphrey, D.M., Elliott, C.J.H., Stepto, A., Ludlow, Z.N., Broeck, L. Vanden, Callaerts, P., Dermaut, B., et al. (2013). Loss and gain of Drosophila TDP-43 impair synaptic efficacy and motor control leading to age-related neurodegeneration by loss-of-function phenotypes. Hum. Mol. Genet. *22*, 1539–1557.

Dice, F. (1990). Peptide sequences that target cytosolic proteins for lysosomal proteolysis, Trends Biochem. Trends Biochem. Sci. *15*, 305–309.

Didonna, A., and Benetti, F. (2016). Post-translational modifications in neurodegeneration. AIMS Biophys. *3*, 27–49.

Diehl, J.A., Cheng, M., Roussel, M.F., and Sherr, C.J. (1995). Glycogen synthase kinase-3 regulates cyclin D1 proteolysis and subcellular localization The activities of cyclin D-dependent kinases serve to integrate extracellular signaling during G 1 phase with the cell-cycle engine that regulates DNA replication and mitosis. Induction of D-type cyclins and their assembly into holoenzyme complexes depend on mitogen stimulation. Kerkhoff Rapp.

Doble, A. (1996). The pharmacology and mechanismriluzole. Neurology *47*, 233–241.

Doench, J.G., Fusi, N., Sullender, M., Hegde, M., Vaimberg, E.W., Donovan, K.F., Smith, I., Tothova, Z., Wilen, C., Orchard, R., et al. (2016). Optimized sgRNA design to maximize activity and minimize off-target effects of CRISPR-Cas9. Nat. Biotechnol. *34*, 184–191.

Dols-Icardo, O., García-Redondo, A., Rojas-García, R., Sánchez-Valle, R., Noguera, A., Gó mez-Tortosa, E., Pastor, P., Hernández, I., Esteban-Pérez, J., Suárez-Calvet, M., et al. (2014). Characterization of the repeat expansion size in C9orf72 in amyotrophic lateral sclerosis and frontotemporal dementia. Hum. Mol. Genet. *23*, 749–754.

Dong, W., Zhang, L., Sun, C., Gao, X., Guan, F., Li, J., Chen, W., Ma, Y., and Zhang, L. (2020). Knock in of a hexanucleotide repeat expansion in the C9orf72 gene induces ALS in rats . Anim. Model. Exp. Med. *3*, 237–244.

Donnelly, C.J., Zhang, P.W., Pham, J.T., Heusler, A.R., Mistry, N.A., Vidensky, S., Daley, E.L., Poth, E.M., Hoover, B., Fines, D.M., et al. (2013). RNA Toxicity from the ALS/FTD C9ORF72 Expansion Is Mitigated by Antisense Intervention. Neuron *80*, 415–428.

Dormann, D., Rodde, R., Edbauer, D., Bentmann, E., Fischer, I., Hruscha, A., Than, M.E., Mackenzie, I.R., Capell, A., Schmid, B., et al. (2010a). ALS-associated fused in sarcoma (FUS) mutations disrupt Transportin-mediated nuclear import. EMBO J. *29*, 2841–2857.

Dormann, D., Rodde, R., Edbauer, D., Bentmann, E., Fischer, I., Hruscha, A., Than, M.E.,

MacKenzie, I.R.A., Capell, A., Schmid, B., et al. (2010b). ALS-associated fused in sarcoma (FUS) mutations disrupt transportin-mediated nuclear import. EMBO J. *29*, 2841–2857.

Duda, D.M., Borg, L.A., Scott, D.C., Hunt, H.W., Hammel, M., and Schulman, B.A. (2008). Structural Insights into NEDD8 Activation of Cullin-RING Ligases: Conformational Control of Conjugation. Cell *134*, 995–1006.

Duncan, C.D.S., and Mata, J. (2011). Widespread cotranslational formation of protein complexes. PLoS Genet. *7*.

Durcan, T.M., Tang, M.Y., Pérusse, J.R., Dashti, E.A., Aguileta, M.A., Mclelland, G.-L., Gros, P., Shaler, T.A., Faubert, D., Coulombe, B., et al. (2014). USP8 regulates mitophagy by removing K6-linked ubiquitin conjugates from parkin. EMBO J. *33*, 2473–2491.

Elden, A.C., Kim, H.J., Hart, M.P., Chen-Plotkin, A.S., Johnson, B.S., Fang, X., Armakola, M., Geser, F., Greene, R., Lu, M.M., et al. (2010). Ataxin-2 intermediate-length polyglutamine expansions are associated with increased risk for ALS. Nature *466*, 1069–1075.

Eletr, Z.M., Wilkinson, K.D., Sommer, T., and Wolf, D.H. (2014). Regulation of proteolysis by human deubiquitinating enzymes. BBA - Mol. Cell Res. *1843*, 114–128.

Elia, L.P., Mason, A.R., Alijagic, A., and Finkbeiner, S. (2019). Genetic regulation of neuronal progranulin reveals a critical role for the autophagy-lysosome pathway. J. Neurosci. *39*, 3332–3344.

Engelhardt, J.I., Tajti, J., and Appel, S.H. (1993). Lymphocytic Infiltrates in the Spinal Cord in Amyotrophic Lateral Sclerosis. Arch. Neurol. *50*, 30–36.

Eskelinen, E.L., and Saftig, P. (2009). Autophagy: A lysosomal degradation pathway with a central role in health and disease. Biochim. Biophys. Acta - Mol. Cell Res. *1793*, 664–673.

Fang, X., Lin, H., Wang, X., Zuo, Q., Qin, J., and Zhang, P. (2015). The NEK1 interactor, C21ORF2, is required for efficient DNA damage repair. Acta Biochim. Biophys. Sin. (Shanghai). *47*, 834–841.

Farg, M.A., Sundaramoorthy, V., Sultana, J.M., Yang, S., Atkinson, R.A.K., Levina, V., Halloran, M.A., Gleeson, P.A., Blair, I.P., Soo, K.Y., et al. (2014). C9ORF72, implicated in amytrophic lateral sclerosis and frontotemporal dementia, regulates endosomal trafficking. Hum. Mol. Genet. *23*, 3579–3595.

Farshi, P., Deshmukh, R.R., Nwankwo, J.O., Arkwright, R.T., Cvek, B., Liu, J., and Dou, Q.P. (2015). Deubiquitinases (DUBs) and DUB inhibitors: A patent review. Expert Opin. Ther. Pat. *25*, 1191–1208.

Fecto, F., Yan, J., Vemula, S.P., Liu, E., Yang, Y., Chen, W., Zheng, J.G., Shi, Y., Siddique, N., Arrat, H., et al. (2011). SQSTM1 mutations in familial and sporadic amyotrophic lateral sclerosis. Arch. Neurol. *68*, 1440–1446.

Fei, E., Jia, N., Yan, M., Ying, Z., Sun, Q., Wang, H., Zhang, T., Ma, X., Ding, H., Yao, X., et al. (2006). SUMO-1 modification increases human SOD1 stability and aggregation. Biochem. Biophys. Res. Commun. *347*, 406–412.

Feiguin, F., Godena, V.K., Romano, G., D'Ambrogio, A., Klima, R., and Baralle, F.E. (2009). Depletion of TDP-43 affects Drosophila motoneurons terminal synapsis and locomotive behavior. FEBS Lett. *583*, 1586–1592.

Felbecker, A., Camu, W., Valdmanis, P.N., Sperfeld, A.D., Waibel, S., Steinbach, P., Rouleau, G.A., Ludolph, A.C., and Andersen, P.M. (2010). Four familial ALS pedigrees discordant for two SOD1 mutations: Are all SOD1 mutations pathogenic? J. Neurol. Neurosurg. Psychiatry *81*, 572–577.

Ferrante, R.J., Browne, S.E., Shinobu, L.A., Bowling, A.C., Baik, M.J., MacGarvey, U., Kowall, N.W., Brown, R.H., and Beal, M.F. (1997). Evidence of increased oxidative damage in both sporadic and familial amyotrophic lateral sclerosis. J. Neurochem. *69*, 2064–2074.

Ferrari, R., Kapogiannis, D., Huey, E.D., and Momeni, P. (2011). FTD and ALS: a tale of two diseases. Curr. Alzheimer Res. *8*, 273–294.

Figlewicz, D. a, Krizus, A., Martinoli, M.G., Meininger, V., Dib, M., Rouleau, G. a, and Julien, J. (1994). Lateral Sclerosis. *3*, 1757–1761.

Filimonenko, M., Stuffers, S., Raiborg, C., Yamamoto, A., Malerød, L., Fisher, E.M.C., Isaacs, A., Brech, A., Stenmark, H., and Simonsen, A. (2007). Functional multivesicular bodies are required for autophagic clearance of protein aggregates associated with neurodegenerative disease. J. Cell Biol. *179*, 485–500.

Flanagan, E.P., Baker, M.C., Perkerson, R.B., Duffy, J.R., Strand, E.A., Whitwell, J.L., MacHulda, M.M., Rademakers, R., and Josephs, K.A. (2015). Dominant frontotemporal dementia mutations in 140 cases of primary progressive aphasia and speech apraxia. Dement. Geriatr. Cogn. Disord. *39*, 281–286.

Fogarty, M.J., Mu, E.W.H., Lavidis, N.A., Noakes, P.G., and Bellingham, M.C. (2017). Motor areas show altered dendritic structure in an amyotrophic lateral sclerosis mouse model. Front. Neurosci. *11*, 1–16.

Fournier, C., Barbier, M., Camuzat, A., Anquetil, V., Lattante, S., Clot, F., Cazeneuve, C., Rinaldi, D., Couratier, P., Deramecourt, V., et al. (2019). Relations between C9orf72 expansion size in blood, age at onset, age at collection and transmission across generations in patients and presymptomatic carriers. Neurobiol. Aging *74*, 234.e1-234.e8.

Frakes, A.E., Ferraiuolo, L., Haidet-Phillips, A.M., Schmelzer, L., Braun, L., Miranda, C.J., Ladner, K.J., Bevan, A.K., Foust, K.D., Godbout, J.P., et al. (2014). Microglia induce motor neuron death via the classical NF-κB pathway in amyotrophic lateral sclerosis. Neuron *81*, 1009–1023.

Frank, B., Haas, J., Heinze, H.J., Stark, E., and Münte, T.F. (1997). Relation of neuropsychological and magnetic resonance findings in amyotrophic lateral sclerosis: Evidence for subgroups. Clin. Neurol. Neurosurg. *99*, 79–86.

Fratta, P., Mizielinska, S., Nicoll, A.J., Zloh, M., Fisher, E.M.C., Parkinson, G., and Isaacs, A.M. (2012). C9orf72 hexanucleotide repeat associated with amyotrophic lateral sclerosis and frontotemporal dementia forms RNA G-quadruplexes. Sci. Rep. *2*, 1–6.

Fratta, P., Poulter, M., Lashley, T., Rohrer, J.D., Polke, J.M., Beck, J., Ryan, N., Hensman, D., Mizielinska, S., Waite, A.J., et al. (2013). Homozygosity for the C9orf72 GGGGCC repeat expansion in frontotemporal dementia. Acta Neuropathol. *126*, 401–409.

Freibaum, B.D., Lu, Y., Lopez-Gonzalez, R., Kim, N.C., Almeida, S., Lee, K.-H., Badders, N., Valentine, M., Miller, B.L., Wong, P.C., et al. (2015). GGGGCC repeat expansion in C9ORF72 compromises nucleocytoplasmic transport. Nature *525*, 549–562.

Freischmidt, A., Wieland, T., Richter, B., Ruf, W., Schaeffer, V., Müller, K., Marroquin, N., Nordin, F., Hübers, A., Weydt, P., et al. (2015). Haploinsufficiency of TBK1 causes familial ALS and fronto-temporal dementia. Nat. Neurosci. *18*, 631–636.

Frendo-Cumbo, S., Jaldin-Fincati, J.R., Coyaud, E., Laurent, E.M.N., Townsend, L.K., Tan, J.M.J., Xavier, R.J., Pillon, N.J., Raught, B., Wright, D.C., et al. (2019). Deficiency of the autophagy gene ATG16L1 induces insulin resistance through KLHL9/KLHL13/CUL3-mediated IRS1 degradation. J. Biol. Chem. *294*, 16172–16185.

Frick, P., Sellier, C., Mackenzie, I.R.A., Cheng, C.Y., Tahraoui-Bories, J., Martinat, C.,

Pasterkamp, R.J., Prudlo, J., Edbauer, D., Oulad-Abdelghani, M., et al. (2018). Novel antibodies reveal presynaptic localization of C9orf72 protein and reduced protein levels in C9orf72 mutation carriers. Acta Neuropathol. Commun. *6*, 72.

Fridovich, I. (1975). Superoxide. Annu. Rev. Biochem. *44*, 147–159.

Fukuda, S., Nishida-Fukuda, H., Nakayama, H., Inoue, H., and Higashiyama, S. (2012). Monoubiquitination of pro-amphiregulin regulates its endocytosis and ectodomain shedding. Biochem. Biophys. Res. Commun. *420*, 315–320.

Furukawa, M., and Xiong, Y. (2005). BTB Protein Keap1 Targets Antioxidant Transcription Factor Nrf2 for Ubiquitination by the Cullin 3-Roc1 Ligase. Mol. Cell. Biol. *25*, 162–171.

Furukawa, M., He, Y.J., Borchers, C., and Xiong, Y. (2003). Targeting of protein ubiquitination by BTB-Cullin 3-Roc1 ubiquitin ligases. Nat. Cell Biol. *5*, 1001–1007.

Gal, J., Zhang, J., Kwinter, D.M., Zhai, J., Jia, H., Jia, J., and Zhu, H. (2011). Nuclear localization sequence of FUS and induction of stress granules by ALS mutants. Neurobiol. Aging *32*, 2323.e27-2323.e40.

Ganley, I.G., Lam, D.H., Wang, J., Ding, X., Chen, S., and Jiang, X. (2009). ULK1 ATG13 FIP200 Complex Mediates mTOR Signaling and Is Essential for Autophagy. J. Biol. Chem. *284*, 12297–12305.

Gareau, J.R., and Lima, C.D. (2010). The SUMO pathway: Emerging mechanisms that shape specificity, conjugation and recognition. Nat. Rev. Mol. Cell Biol. *11*, 861–871.

Genç, B., Jara, J.H., Lagrimas, A.K.B., Pytel, P., Roos, R.P., Mesulam, M.M., Geula, C., Bigio, E.H., and Özdinler, P.H. (2017). Apical dendrite degeneration, a novel cellular pathology for Betz cells in ALS. Sci. Rep. *7*, 1–10.

Gendron, T.F., Bieniek, K.F., Zhang, Y.J., Jansen-West, K., Ash, P.E.A., Caulfield, T., Daughrity, L., Dunmore, J.H., Castanedes-Casey, M., Chew, J., et al. (2013). Antisense transcripts of the expanded C9ORF72 hexanucleotide repeat form nuclear RNA foci and undergo repeat-associated non-ATG translation in c9FTD/ALS. Acta Neuropathol. *126*, 829–844.

Geyer, R., Wee, S., Anderson, S., Yates, J., and Wolf, D.A. (2003). BTB/POZ domain proteins are putative substrate adaptors for cullin 3 ubiquitin ligases. Mol. Cell *12*, 783–790.

Gijselinck, I., Van Langenhove, T., van der Zee, J., Sleegers, K., Philtjens, S., Kleinberger, G., Janssens, J., Bettens, K., Van Cauwenberghe, C., Pereson, S., et al. (2012). A C9orf72 promoter repeat expansion in a Flanders-Belgian cohort with disorders of the frontotemporal lobar degeneration-amyotrophic lateral sclerosis spectrum: A gene identification study. Lancet Neurol. *11*, 54–65.

Gijselinck, I., Van Mossevelde, S., Van Der Zee, J., Sieben, A., Engelborghs, S., De Bleecker, J., Ivanoiu, A., Deryck, O., Edbauer, D., Zhang, M., et al. (2016). The C9orf72 repeat size correlates with onset age of disease, DNA methylation and transcriptional downregulation of the promoter. Mol. Psychiatry *21*, 1112–1124.

Goldberg, A.L. (2003). Protein degradation and protection against misfolded or damaged proteins. Nature *426*, 895–899.

Goldknopf, I.L., Sheta, E.A., Bryson, J., Folsom, B., Wilson, C., Duty, J., Yen, A.A., and Appel, S.H. (2006). Complement C3c and related protein biomarkers in amyotrophic lateral sclerosis and Parkinson's disease. Biochem. Biophys. Res. Commun. *342*, 1034–1039.

Gong, L., and Yeh, E.T.H. (1999). Identification of the activating and conjugating enzymes of the NEDD8 conjugation pathway. J. Biol. Chem. *274*, 12036–12042.

Goodier, J.L., Soares, A.O., Pereira, G.C., Devine, L.R., Sanchez, L., Cole, R.N., and García-

Pérez, J.L. (2020). C9orf72-Associated smcr8 protein binds in the ubiquitin pathway and with proteins linked with neurological disease. Acta Neuropathol. Commun. *8*.

Goto, J., Otaki, Y., Watanabe, T., and Watanabe, M. (2021). The role of hect-type e3 ligase in the development of cardiac disease. Int. J. Mol. Sci. *22*.

Graff-Radford, N.R., and Woodruff, B.K. (2007). Frontotemporal dementia. Semin. Neurol. *27*, 48–57.

Graves, M.C., Fiala, M., Dinglasan, L.A. V., Liu, N.Q., Sayre, J., Chiappelli, F., van Kooten, C., and Vinters, H. V. (2004). Inflammation in amyotrophic lateral sclerosis spinal cord and brain is mediated by activated macrophages, mast cells and t cells. Amyotroph. Lateral Scler. Other Mot. Neuron Disord. *5*, 213–219.

Greenway, M.J., Andersen, P.M., Russ, G., Ennis, S., Cashman, S., Donaghy, C., Patterson, V., Swingler, R., Kieran, D., Prehn, J., et al. (2006). ANG mutations segregate with familial and "sporadic" amyotrophic lateral sclerosis. Nat. Genet. *38*, 411–413.

Gregory, J.M., Livesey, M.R., McDade, K., Selvaraj, B.T., Barton, S.K., Chandran, S., and Smith, C. (2020). Dysregulation of AMPA receptor subunit expression in sporadic ALS post-mortem brain. J. Pathol. *250*, 67–78.

Gros-Louis, F., Larivière, R., Gowing, G., Laurent, S., Camu, W., Bouchard, J.P., Meininger, V., Rouleau, G.A., and Julien, J.P. (2004). A frameshift deletion in peripherin gene associated with amyotrophic lateral sclerosis. J. Biol. Chem. *279*, 45951–45956.

Guadagno, N.A., and Progida, C. (2019). Rab GTPases: Switching to Human Diseases. Cells *8*, 909.

Guo, N., and Peng, Z. (2013). MG132, a proteasome inhibitor, induces apoptosis in tumor cells. Asia. Pac. J. Clin. Oncol. *9*, 6–11.

Gupta-Rossi, N., Six, E., LeBail, O., Logeat, F., Chastagner, P., Olry, A., Israël, A., and Brou, C. (2004). Monoubiquitination and endocytosis direct γ-secretase cleavage of activated Notch receptor. J. Cell Biol. *166*, 73–83.

Hadano, S., Hand, C.K., Osuga, H., Yanagisawa, Y., Otomo, A., Devon, R.S., Miyamoto, N., Showguchi-Miyata, J., Okada, Y., Singaraja, R., et al. (2001). A gene encoding a putative GTPase regulator is mutated in familial amyotrophic lateral sclerosis 2. Nat. Genet. *29*, 166–173.

Haeusler, A.R., Donnelly, C.J., Periz, G., Simko, E.A.J., Shaw, G., Kim, M., Maragakis, N.J., Troncoso, J.C., Pandey, A., Sattler, R., et al. (2014). C9orf72 Nucleotide Repeat Structures Initiate Molecular Cascades of Disease. Nature *507*, 195–200.

Haidet-Phillips, A.M., Hester, M.E., Miranda, C.J., Meyer, K., Braun, L., Frakes, A., Song, S., Likhite, S., Murtha, M.J., Foust, K.D., et al. (2011). Astrocytes from familial and sporadic ALS patients are toxic to motor neurons. Nat. Biotechnol. *29*, 824–828.

Hall, E.D., Oostveen, J.A., and Gurney, M.E. (1998). Relationship of microglial and astrocytic activation to disease onset and progression in a transgenic model of familial ALS. Glia *23*, 249–256.

Hand, C.K., Khoris, J., Salachas, F., Gros-Louis, F., Simões Lopes, A.A., Mayeux-Portas, V., Brown, R.H., Meininger, V., Camu, W., and Rouleau, G.A. (2002). A novel locus for familial amyotrophic lateral sclerosis, on chromosome 18q. Am. J. Hum. Genet. *70*, 251–256.

Hao, M., Chen, X., Zhang, T., Shen, T., Xie, Q., Xing, X., Gu, H., and Lu, F. (2011). Impaired nuclear export of tumor-derived c-terminal truncated cyclin D1 mutant in ESCC cancer. Oncol. Lett. *2*, 1203–1211.

Hara, T., Nakamura, K., Matsui, M., Yamamoto, A., Nakahara, Y., Suzuki-Migishima, R.,

Yokoyama, M., Mishima, K., Saito, I., Okano, H., et al. (2006). Suppression of basal autophagy in neural cells causes neurodegenerative disease in mice. Nature *441*, 885–889.

Hardiman, O., Al-Chalabi, A., Chio, A., Corr, E.M., Logroscino, G., Robberecht, W., Shaw, P.J., Simmons, Z., and Van Den Berg, L.H. (2017). Amyotrophic lateral sclerosis. Nat. Rev. Dis. Prim. *3*.

Harrigan, J.A., Jacq, X., Martin, N.M., and Jackson, S.P. (2018). Deubiquitylating enzymes and drug discovery: Emerging opportunities. Nat. Rev. Drug Discov. *17*, 57–77.

Harteneck, C., Nicholls, D.G., Ward, M.W., and Nicholls, D.G. (2000). Mitochondrial membrane potential and neuronal glutamate excitotoxicity: mortality and millivolts. Trends Neurosci. *23*, 166–174.

Hautbergue, G.M., Castelli, L.M., Ferraiuolo, L., Sanchez-Martinez, A., Cooper-Knock, J., Higginbottom, A., Lin, Y.H., Bauer, C.S., Dodd, J.E., Myszczynska, M.A., et al. (2017). SRSF1-dependent nuclear export inhibition of C9ORF72 repeat transcripts prevents neurodegeneration and associated motor deficits. Nat. Commun. *8*, 1–18.

He, M., Zhou, Z., Shah, A.A., Zou, H., Tao, J., Chen, Q., and Wan, Y. (2016). The emerging role of deubiquitinating enzymes in genomic integrity, diseases, and therapeutics. Cell Biosci. *6*, 1–15.

Hecker, C.-M.M., Rabiller, M., Haglund, K., Bayer, P., and Dikic, I. (2006). Specification of SUMO1- and SUMO2-interacting motifs. J. Biol. Chem. *281*, 16117–16127.

Hendriks, I.A., Lyon, D., Su, D., Skotte, N.H., Daniel, J.A., Jensen, L.J., and Nielsen, M.L. (2018). Site-specific characterization of endogenous SUMOylation across species and organs. Nat. Commun. *9*.

Henkel, J.S., Beers, D.R., Wen, S., Rivera, A.L., Toennis, K.M., Appel, J.E., Zhao, W., Moore, D.H., Powell, S.Z., and Appel, S.H. (2013). Regulatory T-lymphocytes mediate amyotrophic lateral sclerosis progression and survival. EMBO Mol. Med. *5*, 64–79.

Hetz, C., Thielen, P., Matus, S., Nassif, M., Court, F., Kiffin, R., Martinez, G., Cuervo, A.M., Brown, R.H., and Glimcher, L.H. (2009). XBP-1 deficiency in the nervous system protects against amyotrophic lateral sclerosis by increasing autophagy. Genes Dev. *23*, 2294–2306.

Hietakangas, V., Ahlskog, J.K., Jakobsson, A.M., Hellesuo, M., Sahlberg, N.M., Holmberg, C.I., Mikhailov, A., Palvimo, J.J., Pirkkala, L., and Sistonen, L. (2003). Phosphorylation of Serine 303 Is a Prerequisite for the Stress-Inducible SUMO Modification of Heat Shock Factor 1. Mol. Cell. Biol. *23*, 2953–2968.

Hietakangas, V., Anckar, J., Blomster, H.A., Fujimoto, M., Palvimo, J.J., Nakai, A., and Sistonen, L. (2006). PDSM, a motif for phosphorylation-dependent SUMO modification. Proc. Natl. Acad. Sci. U. S. A. *103*, 45–50.

Higelin, J., Catanese, A., Semelink-Sedlacek, L.L., Oeztuerk, S., Lutz, A.K., Bausinger, J., Barbi, G., Speit, G., Andersen, P.M., Ludolph, A.C., et al. (2018). NEK1 loss-of-function mutation induces DNA damage accumulation in ALS patient-derived motoneurons. Stem Cell Res. *30*, 150–162.

Higgins, C.M.J., Jung, C., Ding, H., and Xu, Z. (2002). Mutant Cu, Zn superoxide dismutase that causes motoneuron degeneration is present in mitochondria in the CNS. J. Neurosci. *22*, 1–6.

Higgins, C.M.J., Jung, C., and Xu, Z. (2003). ALS-associated mutant SODIG93A causes mitochondrial vacuolation by expansion of the intermembrane space by involvement of SODI aggregation and peroxisomes. BMC Neurosci. *4*, 1–14.

Hirano, A., Kurland, L.T., and Sayre, G.P. (1967). Familial Amyotrophic Lateral Sclerosis. A

Subgroup Characterized by Posterior and Spinocerebellar Tract Involvement and Hyaline Inclusions in the Anterior Horn Cells. Arch. Neurol. *16*, 232–243.

Hirokawa, N., Niwa, S., and Tanaka, Y. (2010). Molecular motors in neurons: Transport mechanisms and roles in brain function, development, and disease. Neuron *68*, 610–638.

Hjerpe, R., Bett, J.S., Keuss, M.J., Solovyova, A., McWilliams, T.G., Johnson, C., Sahu, I., Varghese, J., Wood, N., Wightman, M., et al. (2016). UBQLN2 Mediates Autophagy-Independent Protein Aggregate Clearance by the Proteasome. Cell *166*, 935–949.

Hodges, J.R., Davies, R., Xuereb, J., Kril, J., and Halliday, G. (2003). Survival in frontotemporal dementia. Neurology *61*, 349–354.

Holtmaat, A., and Caroni, P. (2016). The role of peripheral immune cells in the CNS in steady state and disease. Nat. Neurosci. *19*, 1553–1562.

Hosokawa, N., Sasaki, T., Iemura, S.I., Natsume, T., Hara, T., and Mizushima, N. (2009). Atg101, a novel mammalian autophagy protein interacting with Atg13. Autophagy *5*, 973–979.

Hrycay, E.G., and Bandiera, S.M. (2015). Involvement of Cytochrome P450 in Reactive Oxygen Species Formation and Cancer (Elsevier Inc.).

Huang, D.T., Hunt, H.W., Zhuang, M., Ohi, M.D., Holton, J.M., and Schulman, B.A. (2007). Basis for a ubiquitin-like protein thioester switch toggling E1-E2 affinity. Nature *445*, 394–398.

Huey, E.D., Ferrari, R., Moreno, J.H., Jensen, C., Morris, C.M., Potocnik, F., Kalaria, R.N., Tierney, M., Wassermann, E.M., Hardy, J., et al. (2012). FUS and TDP43 genetic variability in FTD and CBS. Neurobiol. Aging *33*, 1016.e9-1016.e17.

Huisman, M.H.B., De Jong, S.W., Van Doormaal, P.T.C., Weinreich, S.S., Schelhaas, H.J., Van Der Kooi, A.J., De Visser, M., Veldink, J.H., and Van Den Berg, L.H. (2011). Population based epidemiology of amyotrophic lateral sclerosis using capture-recapture methodology. J. Neurol. Neurosurg. Psychiatry *82*, 1165–1170.

Hutton, M., Lendon, C.L., Rizzu, P., Baker, M., Froelich, S., Houlden, H., Pickering-Brown, S., Chakraverty, S., Isaacs, A., Grover, A., et al. (1998). Association of missense and 5'-splice-site mutations in tau with the inherited dementia FTDP-17. Nature *393*, 702–705.

Ikenaka, K., Kawai, K., Katsuno, M., Huang, Z., Jiang, Y.M., Iguchi, Y., Kobayashi, K., Kimata, T., Waza, M., Tanaka, F., et al. (2013). dnc-1/dynactin 1 Knockdown Disrupts Transport of Autophagosomes and Induces Motor Neuron Degeneration. PLoS One *8*.

Imamura, K., Izumi, Y., Watanabe, A., Tsukita, K., Woltjen, K., Yamamoto, T., Hotta, A., Kondo, T., Kitaoka, S., Ohta, A., et al. (2017). The Src/c-Abl pathway is a potential therapeutic target in amyotrophic lateral sclerosis. Sci. Transl. Med. *9*, 1–10.

Jackson, S.P., and Bartek, J. (2009). The DNA-damage response in human biology and disease. Nature *461*, 1071–1078.

Jackson, J.L., Finch, N.C.A., Baker, M.C., Kachergus, J.M., Dejesus-Hernandez, M., Pereira, K., Christopher, E., Prudencio, M., Heckman, M.G., Thompson, E.A., et al. (2020). Elevated methylation levels, reduced expression levels, and frequent contractions in a clinical cohort of C9orf72 expansion carriers. Mol. Neurodegener. *15*, 1–11.

Jacobson, A.D., Zhang, N.-Y., Xu, P., Han, K.-J., Noone, S., Peng, J., and Liu, C.-W. (2009). The Lysine 48 and Lysine 63 Ubiquitin Conjugates Are Processed Differently by the 26 S Proteasome. J. Biol. Chem. *284*, 35485–35494.

Jaiswal, M.K. (2019). Riluzole and edaravone: A tale of two amyotrophic lateral sclerosis drugs. Med. Res. Rev. *39*, 733–748.

Jara, J.H., Villa, S.R., Khan, N.A., Bohn, M.C., and Özdinler, P.H. (2012). AAV2 mediated retrograde transduction of corticospinal motor neurons reveals initial and selective apical dendrite degeneration in ALS. Neurobiol. Dis. *47*, 174–183.

Jean, S., and Kiger, A.A. (2012). Coordination between RAB GTPase functions. Nat. Rev. Mol. Cell Biol. *13*, 463.

Jensen, B.K., Schuldi, M.H., McAvoy, K., Russell, K.A., Boehringer, A., Curran, B.M., Krishnamurthy, K., Wen, X., Westergard, T., Ma, L., et al. (2020). Synaptic dysfunction induced by glycine-alanine dipeptides in C9orf72- ALS / FTD is rescued by SV 2 replenishment . EMBO Mol. Med. *12*, 1–26.

Jiang, J., Zhu, Q., Gendron, T.F., Rigo, F., Cleveland, D.W., Jiang, J., Zhu, Q., Gendron, T.F., Saberi, S., Mcalonis-downes, M., et al. (2016). Gain of Toxicity from ALS / FTD-Linked Repeat Expansions in C9ORF72 Is Alleviated by Antisense Oligonucleotides Targeting GGGGCC-Containing RNAs. Neuron *90*, 535–550.

Jin, P., Duan, R., Qurashi, A., Qin, Y., Tian, D., Rosser, T.C., Liu, H., Feng, Y., and Warren, S.T. (2007). Pur α Binds to rCGG Repeats and Modulates Repeat-Mediated Neurodegeneration in a Drosophila Model of Fragile X Tremor/Ataxia Syndrome. Neuron *55*, 556–564.

Johnson, J.O., Mandrioli, J., Benatar, M., Abramzon, Y., Van Deerlin, V.M., Trojanowski, J.Q., Gibbs, J.R., Brunetti, M., Gronka, S., Wuu, J., et al. (2010). Exome Sequencing Reveals VCP Mutations as a Cause of Familial ALS. Neuron *68*, 857–864.

Johnson, J.O., Pioro, E.P., Boehringer, A., Chia, R., Feit, H., Renton, A.E., Pliner, H.A., Abramzon, Y., Marangi, G., Winborn, B.J., et al. (2014a). Mutations in the Matrin 3 gene cause familial amyotrophic lateral sclerosis. Nat. Neurosci. *17*, 664–666.

Johnson, J.O., Glynn, S.M., Raphael Gibbs, J., Nalls, M.A., Sabatelli, M., Restagno, G., Drory, V.E., Chiò, A., Rogaeva, E., and Traynor, B.J. (2014b). Mutations in the CHCHD10 gene are a common cause of familial amyotrophic lateral sclerosis. Brain *137*, e311.

Johnson, J.O., Pioro, E.P., Boehringer, A., Chia, R., Feit, H., Renton, A.E., Pliner, H.A., Abramzon, Y., Marangi, G., Winborn, B.J., et al. (2014c). Mutations in the Matrin 3 gene cause familial amyotrophic lateral sclerosis. Nat. Neurosci. *17*, 664–666.

Ju, J.S., Fuentealba, R.A., Miller, S.E., Jackson, E., Piwnica-Worms, D., Baloh, R.H., and Weihl, C.C. (2009). Valosin-containing protein (VCP) is required for autophagy and is disrupted in VCP disease. J. Cell Biol. *187*, 875–888.

Jung, C.H., Jun, C.B., Ro, S., Kim, Y., Otto, N.M., Cao, J., Kundu, M., and Kim, D. (2009). ULK-Atg13-FIP200 Complexes Mediate mTOR Signaling to the Autophagy Machinery. Mol. Biol. Cell *20*, 1992–2003.

Jung, J., Nayak, A., Schaeffer, V., Starzetz, T., Kirsch, A.K., Müller, S., Dikic, I., Mittelbronn, M., and Behrends, C. (2017a). Multiplex image-based autophagy RNAi screening identifies SMCR8 as ULK1 kinase activity and gene expression regulator. Elife *6*, 1–32.

Jung, Y., Kim, H.D., Yang, H.W., Kim, H.J., Jang, C.Y., and Kim, J. (2017b). Modulating cellular balance of Rps3 mono-ubiquitination by both Hel2 E3 ligase and Ubp3 deubiquitinase regulates protein quality control. Exp. Mol. Med. *49*, e390-12.

Kabashi, E., Agar, J.N., Taylor, D.M., Minotti, S., and Durham, H.D. (2004). Focal dysfunction of the proteasome: A pathogenic factor in a mouse model of amyotrophic lateral sclerosis. J. Neurochem. *89*, 1325–1335.

Kabashi, E., Valdmanis, P.N., Dion, P., Spiegelman, D., McConkey, B.J., Velde, C. Vande, Bouchard, J.-P., Lacomblez, L., Pochigaeva, K., Salachas, F., et al. (2008). TARDBP mutations in individuals with sporadic and familial amyotrophic lateral sclerosis. Nat. Genet. *40*, 572–574.

Kabashi, E., Agar, J.N., Strong, M.J., and Durham, H.D. (2012). Impaired proteasome function in sporadic amyotrophic lateral sclerosis. Amyotroph. Lateral Scler. *13*, 367–371.

Kabuta, T., Kinugawa, A., Tsuchiya, Y., Kabuta, C., Setsuie, R., Tateno, M., Araki, T., and Wada, K. (2009). Familial amyotrophic lateral sclerosis-linked mutant SOD1 aberrantly interacts with tubulin. Biochem. Biophys. Res. Commun. *387*, 121–126.

Kandlur, A., Satyamoorthy, K., and Gangadharan, G. (2020). Oxidative Stress in Cognitive and Epigenetic Aging: A Retrospective Glance. Front. Mol. Neurosci. *13*, 1–14.

Kaneb, H.M., Folkmann, A.W., Belzil, V. V., Jao, L.E., Leblond, C.S., Girard, S.L., Daoud, H., Noreau, A., Rochefort, D., Hince, P., et al. (2015). Deleterious mutations in the essential mRNA metabolism factor, hGle1, in amyotrophic lateral sclerosis. Hum. Mol. Genet. *24*, 1363–1373.

Kanekura, K., Yagi, T., Cammack, A.J., Mahadevan, J., Kuroda, M., Harms, M.B., Miller, T.M., and Urano, F. (2016). Poly-dipeptides encoded by the C9ORF72 repeats block global protein translation. Hum. Mol. Genet. *25*, 1803–1813.

Kawamata, T., Akiyama, H., Yamada, T., and McGeer, P.L. (1992). Immunologic reactions in amyotrophic lateral sclerosis brain and spinal cord tissue. Am. J. Pathol. *140*, 691–707.

Kawashima, T., Kikuchi, H., Takita, M., Doh-ura, K., Ogomori, K., Oda, M., and Iwaki, T. (1998). Skein-like inclusions in the neostriatum from a case of amyotrophic lateral sclerosis with dementia. Acta Neuropathol. *96*, 541–545.

Kenna, K.P., Van Doormaal, P.T.C., Dekker, A.M., Ticozzi, N., Kenna, B.J., Diekstra, F.P., Van Rheenen, W., Van Eijk, K.R., Jones, A.R., Keagle, P., et al. (2016). NEK1 variants confer susceptibility to amyotrophic lateral sclerosis. Nat. Genet. *48*, 1037–1042.

Kerscher, O., Felberbaum, R., and Hochstrasser, M. (2006). Modification of Proteins by Ubiquitin and Ubiquitin-Like Proteins. Annu. Rev. Cell Dev. Biol. *22*, 159–180.

Khosravi, B., LaClair, K.D., Riemenschneider, H., Zhou, Q., Frottin, F., Mareljic, N., Czuppa, M., Farny, D., Hartmann, H., Michaelsen, M., et al. (2020). Cell-to-cell transmission of C9orf72 poly-(Gly-Ala) triggers key features of ALS / FTD. EMBO J. *39*, 1–19.

Kieran, D., Hafezparast, M., Bohnert, S., Dick, J.R.T., Martin, J., Schiavo, G., Fisher, E.M.C., and Greensmith, L. (2005). A mutation in dynein rescues axonal transport defects and extends the life span of ALS mice. J. Cell Biol. *169*, 561–567.

Kim, H.J., and Taylor, J.P. (2017). Lost in Transportation: Nucleocytoplasmic Transport Defects in ALS and Other Neurodegenerative Diseases. Neuron *96*, 285–297.

Kim, E.T., Kim, K.K., Matunis, M.J., and Ahn, J.H. (2009). Enhanced SUMOylation of proteins containing a SUMO-interacting motif by SUMO-Ubc9 fusion. Biochem. Biophys. Res. Commun. *388*, 41–45.

Kim, H.J., Kim, N.C., Wang, Y., Scarborough, E.A., Diaz, Z., Maclea, K.S., Freibaum, B., Li, S., Kanagaraj, A.P., Carter, R., et al. (2013). Prion-like domain mutations in hnRNPs cause multisystem proteinopathy and ALS. Nature *495*, 467–473.

Kim, J., Kundu, M., Viollet, B., and Guan, K.-L. (2011). AMPK and mTOR regulate autophagy through direct phosphorylation of Ulk1. Nat. Cell Biol. *13*, 132–141.

King, S.M. (2012). Integrated control of axonemal dynein AAA+ motors. J. Struct. Biol. *179*, 222–228.

Kitada, T., Aakawa, S., Hattori, N., Matsumine, H., Yokochi, M., Mizuno, Y., and Shimizu, N. (1998). Mutations in the parkin gene cause autosomal recessive juvenile parkinsonism. Nature *392*, 605–608.

Kjos, I., Vestre, K., Guadagno, N.A., Borg Distefano, M., and Progida, C. (2018). Rab and Arf proteins at the crossroad between membrane transport and cytoskeleton dynamics. Biochim. Biophys. Acta - Mol. Cell Res. *1865*, 1397–1409.

Kolesar, P., Sarangi, P., Altmannova, V., Zhao, X., and Krejci, L. (2012). Dual roles of the SUMO-interacting motif in the regulation of Srs2 sumoylation. Nucleic Acids Res. *40*, 7831–7843.

Komatsu, M., Waguri, S., Chiba, T., Murata, S., Iwata, J.I., Tanida, I., Ueno, T., Koike, M., Uchiyama, Y., Kominami, E., et al. (2006). Loss of autophagy in the central nervous system causes neurodegeneration in mice. Nature *441*, 880–884.

Kong, Q., Chang, L.C., Takahashi, K., Liu, Q., Schulte, D.A., Lai, L., Ibabao, B., Lin, Y., Stouffer, N., Mukhopadhyay, C. Das, et al. (2014). Small-molecule activator of glutamate transporter EAAT2 translation provides neuroprotection. J. Clin. Invest. *124*, 1255–1267.

Koppers, M., Van Blitterswijk, M.M., Vlam, L., Rowicka, P.A., Van Vught, P.W.J., Groen, E.J.N., Spliet, W.G.M., Engelen-Lee, J., Schelhaas, H.J., De Visser, M., et al. (2012). VCP mutations in familial and sporadic amyotrophic lateral sclerosis. Neurobiol. Aging *33*, 837.e7-837.e13.

Koppers, M., Blokhuis, A.M., Westeneng, H.J., Terpstra, M.L., Zundel, C.A.C., Vieira De Sá, R., Schellevis, R.D., Waite, A.J., Blake, D.J., Veldink, J.H., et al. (2015). C9orf72 ablation in mice does not cause motor neuron degeneration or motor deficits. Ann. Neurol. *78*, 426–438.

Koren, I., Timms, R.T., Kula, T., Xu, Q., Li, M.Z., and Elledge, S.J. (2018). The Eukaryotic Proteome Is Shaped by E3 Ubiquitin Ligases Targeting C-Terminal Degrons. Cell *173*, 1622-1635.e14.

Kovanda, A., Zalar, M., Šket, P., Plavec, J., and Rogelj, B. (2015). Anti-sense DNA d(GGCCCC)n expansions in C9ORF72 form i-motifs and protonated hairpins. Sci. Rep. *5*, 3–9.

Kumar, D., Ambasta, R.K., and Kumar, P. (2020). Ubiquitin biology in neurodegenerative disorders: From impairment to therapeutic strategies. Ageing Res. Rev. *61*, 101078.

Kumar, V., Hasan, G.M., and Hassan, M.I. (2017). Unraveling the role of RNA mediated toxicity of C9orf72 repeats in C9-FTD/ALS. Front. Neurosci. *11*.

Kwiatkowski Jr., T.., Bosco, D.A., LeClerc, A.L., Tamrazian, E., Vanderburg, C.R., Russ, C., Davis, A., Gilchrist, J., Kasarskis, E.J., Munsat, T., et al. (2009). Mutations in the FUS/TLS Gene on Chromosome 16 Cause Familial Amyotrophic Lateral Sclerosis. Science (80-.). *323*, 1205–1208.

Kwon, Y.T., and Ciechanover, A. (2017). The Ubiquitin Code in the Ubiquitin-Proteasome System and Autophagy. Trends Biochem. Sci. *42*, 873–886.

Kwon, I., Xiang, S., Kato, M., Wu, L., Theodoropoulos, P., Wang, T., Kim, J., Yun, J., Xie, Y., and McKnight, S.L. (2014). Poly-dipeptides encoded by the C9orf72 repeats bind nucleoli, impede RNA biogenesis, and kill cells. Science (80-.). *345*, 1139–1145.

de la Vega, M., Burrows, J.F., and Johnston, J.A. (2011). Ubiquitination. Small GTPases *2*, 192–201.

Laaksovirta, H., Peuralinna, T., Schymick, J.C., Scholz, S.W., Lai, S.L., Myllykangas, L., Sulkava, R., Jansson, L., Hernandez, D.G., Gibbs, J.R., et al. (2010). Chromosome 9p21 in amyotrophic lateral sclerosis in Finland: A genome-wide association study. Lancet Neurol. *9*, 978–985.

Laflamme, C., McKeever, P.M., Kumar, R., Schwartz, J., Kolahdouzan, M., Chen, C.X.-Q., You, Z., Benalioud, F., Gileadi, O., McBride, H.M., et al. (2019). Mplementation of an antibody characterization procedure and application to the major ALS/FTD disease gene C9ORF72. Elife *8*.

Lagier-Tourenne, C., Polymenidou, M., Hutt, K.R., Vu, A.Q., Baughn, M., Huelga, S.C., Clutario,

K.M., Ling, S.-C., Liang, T.Y., Mazur, C., et al. (2012). Divergent roles of ALS-linked proteins FUS/TLS and TDP-43 intersect in processing long pre-mRNAs. Nat. Neurosci. *15*, 1488–1497.

Lagier-Tourenne, C., Baughn, M., Rigo, F., Sun, S., Liu, P., Li, H.R., Jiang, J., Watt, A.T., Chun, S., Katz, M., et al. (2013). Targeted degradation of sense and antisense C9orf72 RNA foci as therapy for ALS and frontotemporal degeneration. Proc. Natl. Acad. Sci. U. S. A. *110*.

Lall, D., Lorenzini, I., Mota, T.A., Bell, S., Mahan, T.E., Ulrich, J.D., Davtyan, H., Rexach, J.E., Muhammad, A.K.M.G., Shelest, O., et al. (2021). C9orf72 deficiency promotes microglial-mediated synaptic loss in aging and amyloid accumulation. Neuron *109*, 2275-2291.e8.

Lallemand-Breitenbach, V., Jeanne, M., Benhenda, S., Nasr, R., Lei, M., Peres, L., Zhou, J., Raught, B., and de Thé, H. (2008). Arsenic degrades PML or PML-RARα through a SUMO-triggered RNF4/ ubiquitin-mediated pathway. Nat. Cell Biol. *10*, 547–555.

Lamar Seibenhener, M., Ramesh Babu, J., Geetha, T., Wong, H.C., Rama Krishna, N., and Wooten, M.W. (2004). Sequestosome 1/p62 Is a Polyubiquitin Chain Binding Protein Involved in Ubiquitin Proteasome Degradation. Mol. Cell. Biol. *24*, 8055–8068.

Lan, Y., Sullivan, P.M., and Hu, F. (2019). SMCR8 negatively regulates AKT and MTORC1 signaling to modulate lysosome biogenesis and tissue homeostasis. Autophagy *15*, 871–885.

Van Langenhove, T., Van Der Zee, J., Sleegers, K., Engelborghs, S., Vandenberghe, R., Gijselinck, I., Van Den Broeck, M., Mattheijssens, M., Peeters, K., De Deyn, P.P., et al. (2010). Genetic contribution of FUS to frontotemporal lobar degeneration. Neurology *74*, 366–371.

Lattante, S., Ciura, S., Rouleau, G.A., and Kabashi, E. (2015). Defining the genetic connection linking amyotrophic lateral sclerosis (ALS) with frontotemporal dementia (FTD). Trends Genet. *31*, 263–273.

Lazarou, M., Narendra, D.P., Jin, S.M., Tekle, E., Banerjee, S., and Youle, R.J. (2013). PINK1 drives parkin self-association and HECT-like E3 activity upstream of mitochondrial binding. J. Cell Biol. *200*, 163–172.

Lee, B., Yoon, K., Lee, S., Kang, J.M., Kim, J., Shim, S.H., Kim, H.-M., Song, S., Naka, K., Kim, A.K., et al. (2015a). Homozygous Deletions at 3p22, 5p14, 6q15, and 9p21 Result in Aberrant Expression of Tumor Suppressor Genes in Gastric Cancer. Genes. Chromosomes Cancer *54*, 142–155.

Lee, B.H., Lu, Y., Prado, M.A., Shi, Y., Tian, G., Sun, S., Elsasser, S., Gygi, S.P., King, R.W., and Finley, D. (2016). USP14 deubiquitinates proteasome-bound substrates that are ubiquitinated at multiple sites. Nature *532*, 398–401.

Lee, J., Chun, S.K., Son, G.H., and Kim, K. (2015b). Sumoylation of Hes6 regulates protein degradation and Hes1-mediated transcription. Endocrinol. Metab. *30*, 381–388.

Lee, J.A., Liu, L., and Gao, F.B. (2009). Autophagy defects contribute to neurodegeneration induced by dysfunctional ESCRT-III. Autophagy *5*, 1070–1072.

Lee, Y.-B., Baskaran, P., Gomez-Deza, J., Chen, H.-J., Nishimura, A.L., Smith, B.N., Troakes, C., Adachi, Y., Stepto, A., Petrucelli, L., et al. (2017). C9orf72 poly GA RAN-translated protein plays a key role in amyotrophic lateral sclerosis via aggregation and toxicity. Hum. Mol. Genet. *26*, 4765–4777.

Leggett, D.S., Hanna, J., Borodovsky, A., Crosas, B., Schmidt, M., Baker, R.T., Walz, T., Ploegh, H., and Finley, D. (2002). Multiple associated proteins regulate proteasome structure and function. Mol. Cell *10*, 495–507.

Leigh, P.N., Whitwell, H., Garofalo, O., Buller, J., Swash, M., Martin, J.E., Gallo, J.-M., Weller, R.O., and Anderton, B.H. (1991). Ubiquitin-immunoreactive intraneuronal inclusions in

amyotrophic lateral sclerosis. Brain *114*, 775–788.

Levine, J.B., Kong, J., Nadler, M., and Xu, Z. (1999). Astrocytes interact intimately with degenerating motor neurons in mouse amyotrophic lateral sclerosis (ALS). Glia *28*, 215–224.

Levine, T.P., Daniels, R.D., Gatta, A.T., Wong, L.H., and Hayes, M.J. (2013). The product of C9orf72, a gene strongly implicated in neurodegeneration, is structurally related to DENN Rab-GEFs. Bioinformatics *29*, 499–503.

Levivier, E., Goud, B., Souchet, M., Calmels, T.P.G., Mornon, J.P., and Callebaut, I. (2001). uDENN, DENN, and dDENN: Indissociable domains in Rab and MAP kinases signaling pathways. Biochem. Biophys. Res. Commun. *287*, 688–695.

Levy, J.R., Sumner, C.J., Caviston, J.P., Tokito, M.K., Ranganathan, S., Ligon, L.A., Wallace, K.E., LaMonte, B.H., Harmison, G.G., Puls, I., et al. (2006). A motor neuron disease-associated mutation in p150Glued perturbs dynactin function and induces protein aggregation. J. Cell Biol. *172*, 733–745.

Leznicki, P., and Kulathu, Y. (2017). Mechanisms of regulation and diversification of deubiquitylating enzyme function. J. Cell Sci. *130*, 1997–2006.

Li, W.W., Li, J., and Bao, J.K. (2012). Microautophagy: Lesser-known self-eating. Cell. Mol. Life Sci. *69*, 1125–1136.

Li, X., Yang, K. Bin, Chen, W., Mai, J., Wu, X.Q., Sun, T., Wu, R.Y., Jiao, L., Li, D.D., Ji, J., et al. (2021). CUL3 (cullin 3)-mediated ubiquitination and degradation of BECN1 (beclin 1) inhibit autophagy and promote tumor progression. Autophagy *00*, 1–18.

Liang, C., Shao, Q., Zhang, W., Yang, M., Chang, Q., Chen, R., and Chen, J.F. (2019). Smcr8 deficiency disrupts axonal transport-dependent lysosomal function and promotes axonal swellings and gain of toxicity in C9ALS/FTD mouse models. Hum. Mol. Genet. *28*, 3940–3953.

Lillo, P., and Hodges, J.R. (2009). Frontotemporal dementia and motor neurone disease: Overlapping clinic-pathological disorders. J. Clin. Neurosci. *16*, 1131–1135.

Lim, K.H., Joo, J.Y., and Baek, K.H. (2020). The potential roles of deubiquitinating enzymes in brain diseases. Ageing Res. Rev. *61*, 101088.

Lin, J., and Lai, E. (2017). Protein–Protein Interactions: Yeast Two-Hybrid System. Methods Mol. Biol. *1615*, 177–187.

Lin, W.L., and Dickson, D.W. (2008). Ultrastructural localization of TDP-43 in filamentous neuronal inclusions in various neurodegenerative diseases. Acta Neuropathol. *116*, 205–213.

Lin, D.Y., Huang, Y.S., Jeng, J.C., Kuo, H.Y., Chang, C.C., Chao, T.T., Ho, C.C., Chen, Y.C., Lin, T.P., Fang, H.I., et al. (2006). Role of SUMO-Interacting Motif in Daxx SUMO Modification, Subnuclear Localization, and Repression of Sumoylated Transcription Factors. Mol. Cell *24*, 341–354.

Lin, H.C., Yeh, C.W., Chen, Y.F., Lee, T.T., Hsieh, P.Y., Rusnac, D. V., Lin, S.Y., Elledge, S.J., Zheng, N., and Yen, H.C.S. (2018). C-Terminal End-Directed Protein Elimination by CRL2 Ubiquitin Ligases. Mol. Cell *70*, 602-613.e3.

Ling, J.P., Pletnikova, O., Troncoso, J.C., and Wong, P.C. (2015). DP-43 repression of nonconserved cryptic exons is compromised in ALS-FTD. Science (80-.). *2*, 650–655.

Ling, S.C., Polymenidou, M., and Cleveland, D.W. (2013). Converging mechanisms in ALS and FTD: Disrupted RNA and protein homeostasis. Neuron *79*, 416–438.

Lipton, A.M., White, C.L., and Bigio, E.H. (2004). Frontotemporal lobar degeneration with motor neuron disease-type inclusions predominates in 76 cases of frontotemporal degeneration. Acta

Neuropathol. *108*, 379–385.

Liu-Yesucevitz, L., Bassell, G.J., Gitler, A.D., Hart, A.C., Klann, E., Richter, J.D., Warren, S.T., and Wolozin, B. (2011). Local RNA translation at the synapse and in disease. J. Neurosci. *31*, 16086–16093.

Liu-Yesucevitz, L.Q., Lin, A.Y., Ebata, A., Boon, J.Y., Reid, W., Xu, Y.F., Kobrin, K., Murphy, G.J., Petrucelli, L., and Wolozin, B. (2014). ALS-linked mutations enlarge TDP-43-enriched neuronal RNA granules in the dendritic arbor. J. Neurosci. *34*, 4167–4174.

Liu, P., Gan, W., Su, S., Hauenstein, A. V, Fu, T.-M.M., Brasher, B., Schwerdtfeger, C., Liang, A.C., Xu, M., and Wei, W. (2018). K63-linked polyubiquitin chains bind to DNA to facilitate DNA damage repair. Sci. Signal. *11*, 1–12.

Liu, Q., Shu, S., Wang, R.R., Liu, F., Cui, B., Guo, X.N., Lu, C.X., Li, X.G., Liu, M.S., Peng, B., et al. (2016a). Whole-exome sequencing identifies a missense mutation in hnRNPA1 in a family with flail arm ALS. Neurology *87*, 1763–1769.

Liu, Y., Pattamatta, A., Zu, T., Reid, T., Bardhi, O., Borchelt, D.R., Yachnis, A.T., and Ranum, L.P.W. (2016b). C9orf72 BAC Mouse Model with Motor Deficits and Neurodegenerative Features of ALS/FTD. Neuron *90*, 521–534.

Liu, Y., Dodart, J.C., Tran, H., Berkovitch, S., Braun, M., Byrne, M., Durbin, A.F., Hu, X.S., Iwamoto, N., Jang, H.G., et al. (2021). Variant-selective stereopure oligonucleotides protect against pathologies associated with C9orf72-repeat expansion in preclinical models. Nat. Commun. *12*.

Liu, Y.C., Lin, M.C., Chen, H.C., Tam, M.F., and Lin, L.Y. (2011). The role of small ubiquitin-like modifier-interacting motif in the assembly and regulation of metal-responsive transcription factor. J. Biol. Chem. *286*, 42818–42829.

Livak, K.J., and Schmittgen, T.D. (2001). Analysis of relative gene expression data using real-time quantitative PCR and the 2-ΔΔCT method. Methods *25*, 402–408.

Logroscino, G., Traynor, B.J., Hardiman, O., Chió, A., Mitchell, D., Swingler, R.J., Millul, A., Benn, E., and Beghi, E. (2010). Incidence of amyotrophic lateral sclerosis in Europe. J. Neurol. Neurosurg. Psychiatry *81*, 385–390.

Lomen-Hoerth, C., Anderson, T., and Miller, B. (2002). The overlap of amyotrophic lateral sclerosis and frontotemporal dementia. Neurology *59*, 1077–1079.

Lomen-Hoerth, C., Murphy, J., Langmore, S., Kramer, J.H., Olney, R.K., and Miller, B. (2003). Are amyotrophic lateral sclerosis patients cognitively normal? Neurology *60*, 1094–1097.

Lopez-Gonzalez, R., Lu, Y., Gendron, T.F., Miller, B.L., Almeida, S., Gao, F.-B., Karydas, A., Tran, H., Yang, D., and Petrucelli, L. (2016). Poly(GR) in C9ORF72-Related ALS/FTD Compromises Mitochondrial Function and Increases Oxidative Stress and DNA Damage in iPSC-Derived Motor Neurons Correspondence Poly(GR) in C9ORF72-Related ALS/FTD Compromises Mitochondrial Function and Increases Oxidativ. Neuron *92*, 383–391.

Lüningschrör, P., Werner, G., Stroobants, S., Kakuta, S., Dombert, B., Sinske, D., Wanner, R., Lüllmann-Rauch, R., Wefers, B., Wurst, W., et al. (2020). The FTLD Risk Factor TMEM106B Regulates the Transport of Lysosomes at the Axon Initial Segment of Motoneurons. Cell Rep. *30*, 3506-3519.e6.

Lürick, A., Gao, J., Kuhlee, A., Yavavli, E., Langemeyer, L., Perz, A., Raunser, S., and Ungermann, C. (2017). Multivalent Rab interactions determine tether-mediated membrane fusion. Mol. Biol. Cell *28*, 322–332.

Luty, A.A., Kwok, J.B.J., Dobson-Stone, C., Loy, C.T., Coupland, K.G., Karlström, H., Sobow, T.,

Tchorzewska, J., Maruszak, A., Barcikowska, M., et al. (2010). Sigma nonopioid intracellular receptor 1 mutations cause frontotemporal lobar degeneration-motor neuron disease. Ann. Neurol. *68*, 639–649.

Lv, Y., Li, B., Han, K., Xiao, Y., Yu, X., Ma, Y., Jiao, Z., and Gao, J. (2018). The Nedd8-activating enzyme inhibitor MLN4924 suppresses colon cancer cell growth via triggering autophagy. Korean J. Physiol. Pharmacol. *22*, 617–625.

Macdonald, E., Urbé, S., and Clague, M.J. (2014). USP8 controls the trafficking and sorting of lysosomal enzymes. Traffic *15*, 879–888.

Mackenzie, I.R., Arzberger, T., Kremmer, E., Troost, D., Lorenzl, S., Mori, K., Weng, S.M., Haass, C., Kretzschmar, H.A., Edbauer, D., et al. (2013). Dipeptide repeat protein pathology in C9ORF72 mutation cases Clinico-pathological correlations.pdf. Acta Neuropathol. *126*, 859–879.

Mackenzie, I.R.A., Bigio, E.H., Ince, P.G., Geser, F., Neumann, M., Cairns, N.J., Kwong, L.K., Forman, M.S., Ravits, J., Stewart, H., et al. (2007). Pathological TDP-43 distinguishes sporadic amyotrophic lateral sclerosis from amyotrophic lateral sclerosis with SOD1 mutations. Ann. Neurol. *61*, 427–434.

Mackenzie, I.R.A., Frick, P., Grässer, F.A., Gendron, T.F., Petrucelli, · Leonard, Cashman, N.R., Dieter Edbauer, ·, Kremmer, E., Prudlo, J., Troost, · Dirk, et al. (2015). Quantitative analysis and clinico-pathological correlations of different dipeptide repeat protein pathologies in C9ORF72 mutation carriers. Acta Neuropathol. *130*, 845–861.

Madabhushi, R., Pan, L., and Tsai, L.H. (2014). DNA damage and its links to neurodegeneration. Neuron *83*, 266–282.

Maday, S., Wallace, K.E., and Holzbaur, E.L.F. (2012). Autophagosomes initiate distally and mature during transport toward the cell soma in primary neurons. J. Cell Biol. *196*, 407–417.

Magrané, J., Cortez, C., Gan, W., Manfredi, G., and York, N. (2013). Abnormal Mitochondrial Transport and Morphology are Common Pathological Denominators in SOD1 and TDP43 ALS Mouse Models Brain and Mind Research Institute , Weill Medical College of Cornell University , Skirball Institute , Department of Physiology and Neu. *8174*, 1–43.

Mahajan, R., Delphin, C., Guan, T., Gerace, L., and Melchior, F. (1997). A Small Ubiquitin-Related Polypeptide Involved in Targeting RanGAP1 to Nuclear Pore Complex Protein RanBP2. Cell *88*, 97–107.

Mann, D.M., Rollinson, S., Robinson, A., Callister, J.B., Thompson, J.C., Snowden, J.S., Gendron, T., Petrucelli, L., Masuda-Suzukake, M., Hasegawa, M., et al. (2013). Dipeptide repeat proteins are present in the p62 positive inclusions in patients with frontotemporal lobar degeneration and motor neurone disease associated with expansions in C9ORF72. Acta Neuropathol. Commun. *1*, 1–13.

Manner, C.T., Takalo, M., Hiltunen, M., and Haapasalo, A. (2019). C9orf72 Proteins Regulate Autophagy and Undergo Autophagosomal or Proteasomal Degradation in a Cell Type-Dependent Manner. Cells *8*.

Mantovani, S., Garbelli, S., Pasini, A., Alimonti, D., Perotti, C., Melazzini, M., Bendotti, C., and Mora, G. (2009). Immune system alterations in sporadic amyotrophic lateral sclerosis patients suggest an ongoing neuroinflammatory process. J. Neuroimmunol. *210*, 73–79.

Maraschi, A., Gumina, V., Dragotto, J., Colombrita, C., Mompeán, M., Buratti, E., Silani, V., Feligioni, M., and Ratti, A. (2021). SUMOylation Regulates TDP-43 Splicing Activity and Nucleocytoplasmic Distribution. Mol. Neurobiol.

Marat, A.L., Dokainish, H., and McPherson, P.S. (2011). DENN domain proteins: Regulators of Rab GTPases. J. Biol. Chem. *286*, 13791–13800.

Marchetto, M.C.N., Muotri, A.R., Mu, Y., Smith, A.M., Cezar, G.G., and Gage, F.H. (2008). Non-Cell-Autonomous Effect of Human SOD1G37R Astrocytes on Motor Neurons Derived from Human Embryonic Stem Cells. Cell Stem Cell 3, 649–657.

Marino, M., Papa, S., Crippa, V., Nardo, G., Peviani, M., Cheroni, C., Trolese, M.C., Lauranzano, E., Bonetto, V., Poletti, A., et al. (2015). Differences in protein quality control correlate with phenotype variability in 2 mouse models of familial amyotrophic lateral sclerosis. Neurobiol. Aging 36, 492–504.

Martier, R., Liefhebber, J.M., García-Osta, A., Miniarikova, J., Cuadrado-Tejedor, M., Espelosin, M., Ursua, S., Petry, H., van Deventer, S.J., Evers, M.M., et al. (2019). Targeting RNA-Mediated Toxicity in C9orf72 ALS and/or FTD by RNAi-Based Gene Therapy. Mol. Ther. - Nucleic Acids 16, 26–37.

Martinez, F.J., Pratt, G.A., Van Nostrand, E.L., Batra, R., Huelga, S.C., Kapeli, K., Freese, P., Chun, S.J., Ling, K., Gelboin-Burkhart, C., et al. (2016). Protein-RNA Networks Regulated by Normal and ALS-Associated Mutant HNRNPA2B1 in the Nervous System. Neuron 92, 780–795.

Maruyama, H., Morino, H., Ito, H., Izumi, Y., Kato, H., Watanabe, Y., Kinoshita, Y., Kamada, M., Nodera, H., Suzuki, H., et al. (2010). Mutations of optineurin in amyotrophic lateral sclerosis. Nature 465, 223–227.

Matmati, S., Vaurs, M., Escandell, J.M., Maestroni, L., Nakamura, T.M., Ferreira, M.G., Géli, V., and Coulon, S. (2018). The fission yeast Stn1-Ten1 complex limits telomerase activity via its SUMO-interacting motif and promotes telomeres replication. Sci. Adv. 4.

Matsumoto, G., Shimogori, T., Hattori, N., and Nukina, N. (2015). TBK1 controls autophagosomal engulfment of polyubiquitinated mitochondria through p62 / SQSTM1 phosphorylation. Hum. Mol. Genet. 24, 4429–4442.

Matunis, M.J., Wu, J., and Blobel, G. (1998). SUMO-1 modification and its role in targeting the Ran GTPase-activating protein, RanGAP1, to the nuclear pore complex. J. Cell Biol. 140, 499–509.

May, S., Hornburg, D., Schludi, M.H., Arzberger, T., Rentzsch, K., Schwenk, B.M., Grässer, F.A., Mori, K., Kremmer, E., Banzhaf-Strathmann, J., et al. (2014). C9orf72 FTLD/ALS-associated Gly-Ala dipeptide repeat proteins cause neuronal toxicity and Unc119 sequestration. Acta Neuropathol. 128, 485–503.

McCauley, M.E., and Baloh, R.H. (2019). Inflammation in ALS/FTD pathogenesis. Acta Neuropathol. 137, 715–730.

McEachin, Z.T., Parameswaren, J., Raj, N., Bassell, G.J., and Jiang, J. (2020). RNA-mediated toxicity in C9orf72 ALS and FTD. Neurobiol. Dis. 145, 105055.

McGeer, P.L., and McGeer, E.G. (2002). Inflammatory processes in amyotrophic lateral sclerosis. Muscle and Nerve 26, 459–470.

McMillan, C.T., Russ, J., Wood, E.M., Irwin, D.J., Grossman, M., McCluskey, L., Elman, L., Van Deerlin, V., and Lee, E.B. (2015). C9orf72 promoter hypermethylation is neuroprotective: Neuroimaging and neuropathologic evidence. Neurology 84, 1622–1630.

Meerang, M., Ritz, D., Paliwal, S., Garajova, Z., Bosshard, M., Mailand, N., Janscak, P., Hübscher, U., Meyer, H., and Ramadan, K. (2011). The ubiquitin-selective segregase VCP/p97 orchestrates the response to DNA double-strand breaks. Nat. Cell Biol. 13, 1376–1382.

Mejzini, R., Flynn, L.L., Pitout, I.L., Fletcher, S., Wilton, S.D., and Akkari, P.A. (2019). ALS Genetics, Mechanisms, and Therapeutics: Where Are We Now? Front. Neurosci. 13, 1–27.

Mertins, P., Mani, D.R., Ruggles, K. V., Gillette, M.A., Clauser, K.R., Wang, P., Wang, X., Qiao,

J.W., Cao, S., Petralia, F., et al. (2016). Proteogenomics connects somatic mutations to signalling in breast cancer. Nature *534*, 55–62.

Meulmeester, E., Kunze, M., Hsiao, H.H., Urlaub, H., and Melchior, F. (2008). Mechanism and Consequences for Paralog-Specific Sumoylation of Ubiquitin-Specific Protease 25. Mol. Cell *30*, 610–619.

Miller, Z.A., Sturm, V.E., Camsari, G.B., Karydas, A., Yokoyama, J.S., Grinberg, L.T., Boxer, A.L., Rosen, H.J., Rankin, K.P., Tempini, M.L.G., et al. (2016). Increased prevalence of autoimmune disease within C9 and FTD/MND cohorts Completing the picture. Neurol. Neuroimmunol. NeuroInflammation *3*, 1–8.

Minty, A., Dumont, X., Kaghad, M., and Caput, D. (2000). Covalent modification of p73α by SUMO-1: Two-hybrid screening with p73 identifies novel SUMO-1-interacting proteins and a SUMO-1 interaction motif. J. Biol. Chem. *275*, 36316–36323.

Mitra, J., Guerrero, E.N., Hegde, P.M., Liachko, N.F., Wang, H., Vasquez, V., Gao, J., Pandey, A., Paul Taylor, J., Kraemer, B.C., et al. (2019). Motor neuron disease-associated loss of nuclear TDP-43 is linked to DNA double-strand break repair defects. Proc. Natl. Acad. Sci. U. S. A. *116*, 4696–4705.

Mitsumoto, H., Santella, R., Liu, X., Bogdanov, M., Zipprich, J., Wu, H.C., Mahata, J., Kilty, M., Bednarz, K., Bell, D., et al. (2008). Oxidative stress biomarkers in sporadic ALS. Amyotroph. Lateral Scler. *9*, 177–183.

Mitsuyama, Y. (1979). Presenile dementia with motor neuron disease. Arch. Neurol. *36*, 592–593.

Mizielinska, S., Lashley, T., Norona, F.E., Clayton, E.L., Ridler, C.E., Fratta, P., and Isaacs, A.M. (2013). C9orf72 frontotemporal lobar degeneration is characterised by frequent neuronal sense and antisense RNA foci. Acta Neuropathol. *126*, 845–857.

Mizuno-Yamasaki, E., Rivera-Molina, F., and Novick, P. (2012). GTPase networks in membrane traffic. Annu. Rev. Biochem. *81*, 637–659.

Mizuno, Y., Amari, M., Takatama, M., Aizawa, H., Mihara, B., and Okamoto, K. (2006). Transferrin localizes in Bunina bodies in amyotrophic lateral sclerosis. Acta Neuropathol. *112*, 597–603.

Mizusawa, H. (1993). Hyaline and Skein-like Inclusions in Amyotrophic Lateral Sclerosis. Neuropathology *13*, 201–208.

Mizusawa, H., Matsumoto, S., Yen, S.H., Hirano, A., Rojas-Corona, R.R., and Donnenfeld, H. (1989). Focal accumulation of phosphorylated neurofilaments within anterior horn cell in familial amyotrophic lateral sclerosis. Acta Neuropathol. *79*, 37–43.

Moens, T.G., Niccoli, T., Wilson, K.M., Atilano, M.L., Birsa, N., Gittings, L.M., Holbling, B. V., Dyson, M.C., Thoeng, A., Neeves, J., et al. (2019). C9orf72 arginine-rich dipeptide proteins interact with ribosomal proteins in vivo to induce a toxic translational arrest that is rescued by eIF1A. Acta Neuropathol. *137*, 487–500.

Mohideen, F., Capili, A.D., Bilimoria, P.M., Yamada, T., Bonni, A., and Lima, C.D. (2009). A molecular basis for phosphorylation-dependent SUMO conjugation by the E2 UBC9. Nat. Struct. Mol. Biol. *16*, 945–952.

Moller, A., Bauer, C.S., Cohen, R.N., Webster, C.P., and De Vos, K.J. (2017). Amyotrophic lateral sclerosis-associated mutant SOD1 inhibits anterograde axonal transport of mitochondria by reducing Miro1 levels. Hum. Mol. Genet. *26*, 4668–4679.

Moore, K.M., Nicholas, J., Grossman, M., McMillan, C.T., Irwin, D.J., Massimo, L., Van Deerlin,

V.M., Warren, J.D., Fox, N.C., Rossor, M.N., et al. (2020). Age at symptom onset and death and disease duration in genetic frontotemporal dementia: an international retrospective cohort study. Lancet Neurol. *19*, 145–156.

Moreno-Oñate, M., Herrero-Ruiz, A.M., García-Dominguez, M., Cortés-Ledesma, F., and Ruiz, J.F. (2020). RanBP2-Mediated SUMOylation Promotes Human DNA Polymerase Lambda Nuclear Localization and DNA Repair. J. Mol. Biol. *432*, 3965–3979.

Mori, K., Lammich, S., Mackenzie, I.R.A., Forné, I., Zilow, S., Kretzschmar, H., Edbauer, D., Janssens, J., Kleinberger, G., Cruts, M., et al. (2013a). HnRNP A3 binds to GGGGCC repeats and is a constituent of p62-positive/TDP43-negative inclusions in the hippocampus of patients with C9orf72 mutations. Acta Neuropathol. *125*, 413–423.

Mori, K., Arzberger, T., Grässer, F.A., Gijselinck, I., May, S., Rentzsch, K., Weng, S.M., Schludi, M.H., Van Der Zee, J., Cruts, M., et al. (2013b). Bidirectional transcripts of the expanded C9orf72 hexanucleotide repeat are translated into aggregating dipeptide repeat proteins. Acta Neuropathol. *126*, 881–893.

Mori, K., Weng, S., Arzberger, T., May, S., Rentzsch, K., Kremmer, E., Schmid, B., Kretzschmar, H.A., Cruts, M., Broeckhoven, C. Van, et al. (2013c). The C9orf72 GGGGCC Repeat Is Translated into Aggregating Dipeptide-Repeat Proteins in FTLD/ALS. Science (80-.). *339*, 1335–1338.

Morita, M., Al-Chalabi, A., Andersen, P.M., Hosler, B., Sapp, P., Englund, E., Mitchell, J.E., Habgood, J.J., De Belleroche, J., Xi, J., et al. (2006). A locus on chromosome 9p confers susceptibility to ALS and frontotemporal dementia. Neurology *66*, 839–844.

Moumen, A., Virard, I., and Raoul, C. (2011). Accumulation of wildtype and ALS-linked mutated VAPB impairs activity of the proteasome. PLoS One *6*.

Mukhopadhyay, D., and Riezman, H. (2007). Proteasome-Independent Functions of Ubiquitin in Endocytosis and Signaling. Science (80-.). *315*, 201–205.

Müller, M.P., and Goody, R.S. (2018). Molecular control of Rab activity by GEFs, GAPs and GDI. Small GTPases *9*, 5–21.

Münch, C., Meyer, R., Linke, P., Meyer, T., Ludolph, A.C., Haas, J., and Hemmer, B. (2007). The p150 subunit of dynactin (DCTN1) gene in multiple sclerosis. Acta Neurol. Scand. *116*, 231–234.

Murdock, B.J., Zhou, T., Kashlan, S.R., Little, R.J., Goutman, S.A., and Feldman, E.L. (2017). Correlation of peripheral immunity with rapid Amyotrophic lateral sclerosis progression. JAMA Neurol. *74*, 1446–1454.

Nacerddine, K., Lehembre, F., Bhaumik, M., Artus, J., Cohen-Tannoudji, M., Babinet, C., Pandolfi, P.P., and Dejean, A. (2005). The SUMO pathway is essential for nuclear integrity and chromosome segregation in mice. Dev. Cell *9*, 769–779.

Nagai, M., Re, D.B., Nagata, T., Chalazonitis, A., Jessell, T.M., Wichterle, H., and Przedborski, S. (2007). Astrocytes expressing ALS-linked mutated SOD1 release factors selectively toxic to motor neurons. Nat. Neurosci. *10*, 615–622.

Nagy, D., Kato, T., and Kushner, P.D. (1994). Reactive astrocytes are widespread in the cortical gray matter of amyotrophic lateral sclerosis. J. Neurosci. Res. *38*, 336–347.

Nakamura, S., Wate, R., Kaneko, S., Ito, H., Oki, M., Tsuge, A., Nagashima, M., Asayama, S., Fujita, K., Nakamura, M., et al. (2014). An autopsy case of sporadic amyotrophic lateral sclerosis associated with the I113TSOD1 mutation. Neuropathology *34*, 58–63.

Natan, E., Wells, J.N., Teichmann, S.A., and Marsh, J.A. (2017). Regulation, evolution and consequences of cotranslational protein complex assembly. Curr. Opin. Struct. Biol. *42*, 90–97.

Nedelsky, N.B., Todd, P.K., and Taylor, J.P. (2008). Autophagy and the ubiquitin-proteasome system: Collaborators in neuroprotection. Biochim. Biophys. Acta *1782*, 691–699.

Neumann, M., Sampathu, D.M., Kwong, L.K., Truax, A.C., Micsenyi, M.C., Chou, T.T., Bruce, J., Schuck, T., Grossman, M., Clark, C.M., et al. (2006). Ubiquitinated TDP-43 in Frontotemporal Lobar Degeneration and Amyotrophic Lateral Sclerosis. Science (80-.). *314*, 130–133.

Neumann, M., Bentmann, E., Dormann, D., Jawaid, A., Dejesus-Hernandez, M., Ansorge, O., Roeber, S., Kretzschmar, H.A., Munoz, D.G., Kusaka, H., et al. (2011). FET proteins TAF15 and EWS are selective markers that distinguish FTLD with FUS pathology from amyotrophic lateral sclerosis with FUS mutations. Brain *134*, 2595–2609.

Nguyen, H.P., Van Broeckhoven, C., and van der Zee, J. (2018a). ALS Genes in the Genomic Era and their Implications for FTD. Trends Genet. *34*, 404–423.

Nguyen, H.P., Van Mossevelde, S., Dillen, L., De Bleecker, J.L., Moisse, M., Van Damme, P., Van Broeckhoven, C., van der Zee, J., Engelborghs, S., Crols, R., et al. (2018b). NEK1 genetic variability in a Belgian cohort of ALS and ALS-FTD patients. Neurobiol. Aging *61*, 255.e1-255.e7.

Nicolas, A., Kenna, K., Renton, A.E., Ticozzi, N., Faghri, F., Chia, R., Dominov, J.A., Kenna, B.J., Nalls, M.A., Keagle, P., et al. (2018). Genome-wide Analyses Identify KIF5A as a Novel ALS Gene. Neuron *97*, 1268-1283.e6.

Nishimura, A.L., Mitne-Neto, M., Silva, H.C.A., Richieri-Costa, A., Middleton, S., Cascio, D., Kok, F., Oliveira, J.R.M., Gillingwater, T., Webb, J., et al. (2004). A mutation in the vesicle-trafficking protein VAPB causes late-onset spinal muscular atrophy and amyotrophic lateral sclerosis. Am. J. Hum. Genet. *75*, 822–831.

Norpel, J., Cavadini, S., Schenkg, A.D., Graff-Meyer, A., Hessg, D., Seebacher, J., Chao, J.A., and Bhaskar, V. (2021). Structure of the human C9orf72-SMCR8 complex reveals a multivalent protein interaction architecture. PLoS Biol. *19*.

O'Rourke, J.G., Bogdanik, L., Muhammad, A.K.M.G., Gendron, T.F., Kim, K.J., Austin, A., Cady, J., Liu, E.Y., Zarrow, J., Grant, S., et al. (2015). C9orf72 BAC Transgenic Mice Display Typical Pathologic Features of ALS/FTD. Neuron *88*, 892–901.

O 'Rourke, J.G., Bogdanik, L., Yáñez, A., Lall, D., Wolf, A.J., Muhammad, A.K.M.G., Ho, R., Carmona, S., Vit, J.P., Zarrow, J., et al. (2016). C9orf72 is required for proper macrophage and microglial function in mice. Science (80-.). *351*, 1324–1329.

Ohh, M., Kim, W.Y., Moslehi, J.J., Chen, Y., Chau, V., Read, M.A., and Kaelin, W.G. (2002). An intact NEDD8 pathway is required for Cullin-dependent ubiquitylation in mammalian cells. EMBO Rep. *3*, 177–182.

Okamoto, K., Hirai, S., Amari, M., Watanabe, M., and Sakurai, A. (1993). Bunina bodies in amyotrophic lateral sclerosis immunostained with rabbit anti-cystatin C serum. Neurosci. Lett. *162*, 125–128.

Olney, N.T., Spina, S., and Miller, B.L. (2017). Frontotemporal Dementia. Neurol. Clin. *35*, 339–374.

Olney, R.K., Murphy, J., Forshew, D., Garwood, E., Miller, B.L., Langmore, S., Kohn, M.A., and Lomen-Hoerth, C. (2005). The effects of executive and behavioral dysfunction on the course of ALS. Neurology *65*, 1774–1777.

Olszewska, D.A., Lonergan, R., Fallon, E.M., and Lynch, T. (2016). Genetics of Frontotemporal Dementia. Curr. Neurol. Neurosci. Rep. *16*.

Olszewska, D.A., Fallon, E.M., Pastores, G.M., Murphy, K., Blanco, A., Lynch, T., and Murphy, S.M. (2019). Autosomal Dominant Gene Negative Frontotemporal Dementia-Think of SCA17.

Cerebellum *18*, 654–658.

Onesto, E., Colombrita, C., Gumina, V., Borghi, M.O., Dusi, S., Doretti, A., Fagiolari, G., Invernizzi, F., Moggio, M., Tiranti, V., et al. (2016). Gene-specific mitochondria dysfunctions in human TARDBP and C9ORF72 fibroblasts. Acta Neuropathol. Commun. *4*, 47.

Orlacchio, A., Babalini, C., Borreca, A., Patrono, C., Massa, R., Basaran, S., Munhoz, R.P., Rogaeva, E.A., St George-Hyslop, P.H., Bernardi, G., et al. (2010). SPATACSIN mutations cause autosomal recessive juvenile amyotrophic lateral sclerosis. Brain *133*, 591–598.

Pankiv, S., Høyvarde Clausen, T., Lamark, T., Brech, A., Bruun, J.-A., Outzen, H., Øvervatn, A., Bjørkøy, G., and Johansen, T. (2007). p62/SQSTM1 Binds Directly to Atg8/LC3 to Facilitate Degradation of Ubiquitinated Protein Aggregates. J. Biol. Chem. *282*, 24131–24145.

Parkinson, N., Ince, P.G., Smith, M.O., Highley, R., Skibinski, G., Andersen, P.M., Morrison, K.E., Pall, H.S., Hardiman, O., Collinge, J., et al. (2006). ALS phenotypes with mutations in CHMP2B (charged multivesicular body protein 2B). Neurology *67*, 1074–1077.

Pasinelli, P., and Brown, R.H. (2006). Molecular biology of amyotrophic lateral sclerosis: Insights from genetics. Nat. Rev. Neurosci. *7*, 710–723.

Pearson, J.P., Williams, N.M., Majounie, E., Waite, A., Stott, J., Newsway, V., Murray, A., Hernandez, D., Guerreiro, R., Singleton, A.B., et al. (2011). Familial frontotemporal dementia with amyotrophic lateral sclerosis and a shared haplotype on chromosome 9p. J. Neurol. *258*, 647–655.

Pehar, M., Harlan, B.A., Killoy, K.M., and Vargas, M.R. (2018). Role and Therapeutic Potential of Astrocytes in Amyotrophic Lateral Sclerosis. Curr. Pharm. Des. *23*, 5010–5021.

Pelegrini, A.L., Moura, D.J., Brenner, B.L., Ledur, P.F., Maques, G.P., Henriques, J.A.P., Saffi, J., and Lenz, G. (2010). Nek1 silencing slows down DNA repair and blocks DNA damage-induced cell cycle arrest. Mutagenesis *25*, 447–454.

Pelisch, F., Sonneville, R., Pourkarimi, E., Agostinho, A., Blow, J.J., Gartner, A., and Hay, R.T. (2014). Dynamic SUMO modification regulates mitotic chromosome assembly and cell cycle progression in Caenorhabditis elegans. Nat. Commun. *5*, 1–12.

Peng, H., Yang, F., Hu, Q., Sun, J., Peng, C., Zhao, Y., and Huang, C. (2020). The ubiquitin-specific protease USP8 directly deubiquitinates SQSTM1/p62 to suppress its autophagic activity. Autophagy *16*, 698–708.

Perkins, E.M., Burr, K., Banerjee, P., Mehta, A.R., Dando, O., Selvaraj, B.T., Suminaite, D., Nanda, J., Henstridge, C.M., Gillingwater, T.H., et al. (2021). Altered network properties in C9ORF72 repeat expansion cortical neurons are due to synaptic dysfunction. Mol. Neurodegener. *16*, 1–16.

Perry, S., Han, Y., Das, A., and Dickman, D. (2017). Homeostatic plasticity can be induced and expressed to restore synaptic strength at neuromuscular junctions undergoing ALS-related degeneration. Hum. Mol. Genet. *26*, 4153–4167.

Peters, O.M., Toro, G., #1, C., Tran, H., Gendron, T.F., Mckeon, J.E., Metterville, J., Weiss, A., Wightman, N., Salameh, J., et al. (2015). Expression of human C9ORF72 hexanucleotide expansion reproduces RNA foci and dipeptide repeat proteins but not neurodegeneration in BAC transgenic mice. Neuron *88*, 902–909.

Pickart, C.M., and Eddins, M.J. (2004). Ubiquitin: structures, functions, mechanisms. Biochim. Biophys. Acta *1695*, 55–72.

Poondla, N., Chandrasekaran, A.P., Kim, K.S., and Ramakrishna, S. (2019). Deubiquitinating enzymes as cancer biomarkers: New therapeutic opportunities? BMB Rep. *52*, 181–189.

Prudden, J., Pebernard, S., Raffa, G., Slavin, D.A., Jefferson, J., Perry, P., Tainer, J.A., Mcgowan, C.H., and Boddy, M.N. (2007). SUMO-targeted ubiquitin ligases in genome stability. EMBO J. *26*, 1–13.

Qian, K., Huang, H., Peterson, A., Hu, B., Maragakis, N.J., Ming, G. li, Chen, H., and Zhang, S.C. (2017). Sporadic ALS Astrocytes Induce Neuronal Degeneration In Vivo. Stem Cell Reports *8*, 843–855.

Radwan, M., Ang, C.S., Ormsby, A.R., Cox, D., Daly, J.C., Reid, G.E., and Hatters, D.M. (2020). Arginine in C9ORF72 dipolypeptides mediates promiscuous proteome binding and multiple modes of toxicity. Mol. Cell. Proteomics *19*, 640–654.

Ramesh, N., and Pandey, U.B. (2017). Autophagy Dysregulation in ALS: When Protein Aggregates Get Out of Hand. Front. Mol. Neurosci. *10*, 1–18.

Ravikumar, B., Acevedo-Arozena, A., Imarisio, S., Berger, Z., Vacher, C., O'Kane, C.J., Brown, S.D.M., and Rubinsztein, D.C. (2005). Dynein mutations impair autophagic clearance of aggregate-prone proteins. Nat. Genet. *37*, 771–776.

Reaume, A.G., Elliott, J.L., Hoffman, E.K., Kowall, N.W., Ferrante, R.J., Siwek, D.F., Wilcox, H.M., Flood, D.G., Beal, M.F., Brown, R.H., et al. (1996). Motor neurons in Cu/Zn superoxide dismutase-deficient mice develop normally but exhibit enhanced cell death after axonal injury. Nat. Genet. *13*, 43–47.

Reber, S., Stettler, J., Filosa, G., Colombo, M., Jutzi, D., Lenzken, S.C., Schweingruber, C., Bruggmann, R., Bachi, A., Barabino, S.M., et al. (2016). Minor intron splicing is regulated by FUS and affected by ALS -associated FUS mutants . EMBO J. *35*, 1504–1521.

Reddy, K., Zamiri, B., Stanley, S.Y.R., Macgregor, R.B., and Pearson, C.E. (2013). The disease-associated r(GGGGCC)n repeat from the C9orf72 gene forms tract length-dependent uni- and multimolecular RNA G-quadruplex structures. J. Biol. Chem. *288*, 9860–9866.

Reindle, A., Belichenko, I., Bylebyl, G.R., Chen, X.L., Gandhi, N., and Johnson, E.S. (2006). Multiple domains in Siz SUMO ligases contribute to substrate selectivity. J. Cell Sci. *119*, 4749–4757.

Renton, A.E., Duckworth, J., Ding, J., Harmer, D.W., Hernandez, D.G., Johnson, J.O., Mok, K., Ryten, M., Trabzuni, D., Guerreiro, R.J., et al. (2011). A Hexanucleotide Repeat Expansion in C9ORF72 Is the Cause of Chromosome 9p21-Linked ALS-FTD. Neuron *72*, 257–268.

Renton, A.E., Chiò, A., and Traynor, B.J. (2014). State of play in amyotrophic lateral sclerosis genetics. Nat. Neurosci. *17*, 17–23.

Reverter, D., and Lima, C.D. (2005). Insights into E3 ligase activity revealed by a SUMO-RanGAP1-Ubc9-Nup358 complex. Nature *435*, 687–692.

Reyes-Turcu, F.E., Ventii, K.H., and Wilkinson, K.D. (2009). Regulation and cellular roles of ubiquitin-specific deubiquitinating enzymes. Annu. Rev. Biochem. *78*, 363–397.

Van Rheenen, W., Shatunov, A., Dekker, A.M., McLaughlin, R.L., Diekstra, F.P., Pulit, S.L., Van Der Spek, R.A.A., Võsa, U., De Jong, S., Robinson, M.R., et al. (2016). Genome-wide association analyses identify new risk variants and the genetic architecture of amyotrophic lateral sclerosis. Nat. Genet. *48*, 1043–1048.

Richter, B., Sliter, D.A., Herhaus, L., Stolz, A., Wang, C., and Beli, P. (2016). Phosphorylation of OPTN by TBK1 enhances its binding to Ub chains and promotes selective autophagy of damaged mitochondria. Proc. Natl. Acadamey Sci. *113*, 4039–4044.

Ringholz, G.M., Appel, S.H., Bradshaw, M., Cooke, N.A., Mosnik, D.M., and Schulz, P.E. (2005). Prevalence and patterns of cognitive impairment in sporadic ALS. Neurology *65*, 586–590.

Riva, N., Agosta, F., Lunetta, C., Filippi, M., and Quattrini, A. (2016). Recent advances in amyotrophic lateral sclerosis. J. Neurol. *263*, 1241–1254.

Rizzu, P., Blauwendraat, C., Heetveld, S., Lynes, E.M., Castillo-Lizardo, M., Dhingra, A., Pyz, E., Hobert, M., Synofzik, M., Simón-Sánchez, J., et al. (2016). C9orf72 is differentially expressed in the central nervous system and myeloid cells and consistently reduced in C9orf72, MAPT and GRN mutation carriers. Acta Neuropathol. Commun. *4*, 37.

Robinson, J.L., Geser, F., Stieber, A., Umoh, M., Kwong, L.K., Van Deerlin, V.M., Lee, V.M.Y., and Trojanowski, J.Q. (2013). TDP-43 skeins show properties of amyloid in a subset of ALS cases. Acta Neuropathol. *125*, 121–131.

Rodriguez, M.S., Desterro, J.M.P., Lain, S., Lane, D.P., and Hay, R.T. (2000). Multiple C-Terminal Lysine Residues Target p53 for Ubiquitin-Proteasome-Mediated Degradation. Mol. Cell. Biol. *20*, 8458–8467.

Rohrer, J.D., Guerreiro, R., Vandrovcova, J., Uphill, J., Reiman, D., Beck, J., Isaacs, A.M., Authier, A., Ferrari, R., Fox, N.C., et al. (2009). The heritability and genetics of frontotemporal lobar degeneration. Neurology *73*, 1451–1456.

Rosen, D.R., Siddique, T., Patterson, D., Figlewicz, D.A., Sapp, P., Hentati, A., Donaldson, D., Goto, J., O'Regan, J.P., and Deng, H.X. (1993a). Mutations in Cu/Zn superoxide dismutase gene are associated with familial amyotrophic lateral sclerosis. Nature *362*, 59–62.

Rosen, D.R., Siddique, T., Patterson, D., Figlewicz, D.A., Sapp, P., Hentati, A., Donaldson, D., Goto, J., O'Regan, J.P., Deng, H.-X., et al. (1993b). Mutations in Cu/Zn superoxide dismutase gene are associated with familial amyotrophic lateral sclerosis. Nature *362*, 59–62.

Rosenblum, L.T., and Trotti, D. (2017). EAAT2 and the molecular signature of amyotrophic lateral sclerosis. Adv. Neurobiol. *16*, 117–136.

Rothstein, J., Dykes-Hoberg, M., Pardo, C., Bristol, L., Jin, L., Kuncl, R., Kanai, Y., Hediger, M., Wang, Y., Schielke, J., et al. (1996). Knockout of Glutamate Transporters Reveals a Major Role for Astroglial Transport in Excitotoxicity and Clearance of Glutamate. Neuron *16*, 675–686.

Rothstein, J.D., Tsai, G., Kuncl, R.W., Clawson, L., Cornblath, D.R., Drachman, D.B., Pestronk, A., Stauch, B.L., and Coyle, J.T. (1990). Abnormal excitatory amino acid metabolism in amyotrophic lateral sclerosis. Ann. Neurol. *28*, 18–25.

Rott, R., Szargel, R., Shani, V., Hamza, H., Savyon, M., Elghani, F.A., Bandopadhyay, R., and Engelender, S. (2017). SUMOylation and ubiquitination reciprocally regulate α-synuclein degradation and pathological aggregation. Proc. Natl. Acad. Sci. U. S. A. *114*, 13176–13181.

Row, P.E., Prior, I.A., McCullough, J., Clague, M.J., and Urbé, S. (2006). The ubiquitin isopeptidase UBPY regulates endosomal ubiquitin dynamics and is essential for receptor down-regulation. J. Biol. Chem. *281*, 12618–12624.

Row, P.E., Liu, H., Hayes, S., Welchman, R., Charalabous, P., Hofmann, K., Clague, M.J., Sanderson, C.M., and Urbé, S. (2007). The MIT domain of UBPY constitutes a CHMP binding and endosomal localization signal required for efficient epidermal growth factor receptor degradation. J. Biol. Chem. *282*, 30929–30937.

Rubinsztein, D.C., Shpilka, T., and Elazar, Z. (2012). Mechanisms of autophagosome biogenesis. Curr. Biol. *22*, R29–R34.

Russ, J., Liu, E.Y., Wu, K., Neal, D., Suh, E.R., Irwin, D.J., McMillan, C.T., Harms, M.B., Cairns, N.J., Wood, E.M., et al. (2015). Hypermethylation of repeat expanded C9orf72 is a clinical and molecular disease modifier. Acta Neuropathol. *129*, 39–52.

Saberi, S., Stauffer, J.E., Jiang, J., Garcia, S.D., Amy, E., Schulte, D., Ohkubo, T., Schloffman,

C.L., Maldonado, M., Baughn, M., et al. (2018). Sense-encoded poly-GR dipeptide repeat proteins correlate to neurodegeneration and uniquely co-localize with TDP-43 in dendrites of repeat-expanded C9orf72 amyotrophic lateral sclerosis. Acta Neuropathol. *135*, 459–474.

Sahadevan, S., Hembach, K.M., Tantardini, E., Pérez-Berlanga, M., Hruska-Plochan, M., Megat, S., Weber, J., Schwarz, P., Dupuis, L., Robinson, M.D., et al. (2021). Synaptic FUS accumulation triggers early misregulation of synaptic RNAs in a mouse model of ALS. Nat. Commun. *12*.

Sakai, S., Watanabe, S., Komine, O., Sobue, A., and Yamanaka, K. (2021). Novel reporters of mitochondria-associated membranes (MAM), MAMtrackers, demonstrate MAM disruption as a common pathological feature in amyotrophic lateral sclerosis. FASEB J. *35*.

Sako, W., Ito, H., Yoshida, M., Koizumi, H., Kamada, M., Fujita, K., Hashizume, Y., Izumi, Y., and Kaji, R. (2012). Nuclear factor k B expression in patients with sporadic amyotrophic lateral sclerosis and hereditary amyotrophic lateral sclerosis with optineurin mutations. Clin. Neuropathol. *31*, 418–423.

Salam, S., Tacconelli, S., Smith, B.N., Mitchell, J.C., Glennon, E., Nikolaou, N., Houart, C., and Vance, C. (2021). Identification of a novel interaction of FUS and syntaphilin may explain synaptic and mitochondrial abnormalities caused by ALS mutations. Sci. Rep. *11*, 13613.

Sambataro, F., Pennuto, M., and Tosolini, A.P. (2017). Post-translational Modifications and Protein Quality Control in Motor Neuron and Polyglutamine Diseases. Front. Mol. Neurosci. *10*, 1–13.

Sampson, D.A., Wang, M., and Matunis, M.J. (2001). The Small Ubiquitin-like Modifier-1 (SUMO-1) Consensus Sequence Mediates Ubc9 Binding and is Essential for SUMO-1 Modification. J. Biol. Chem. *276*, 21664–21669.

Sancak, Y., Peterson, T.R., Shaul, Y.D., Lindquist, R.A., Thoreen, C.C., Bar-Peled, L., and Sabatini, D.M. (2008). The rag GTPases bind raptor and mediate amino acid signaling to mTORC1. Science (80-.). *320*, 1496–1501.

Sancak, Y., Bar-Peled, L., Zoncu, R., Markhard, A.L., Nada, S., and Sabatini, D.M. (2010). Ragulator-rag complex targets mTORC1 to the lysosomal surface and is necessary for its activation by amino acids. Cell *141*, 290–303.

Sanson, K.R., Hanna, R.E., Hegde, M., Donovan, K.F., Strand, C., Sullender, M.E., Vaimberg, E.W., Goodale, A., Root, D.E., Piccioni, F., et al. (2018). Optimized libraries for CRISPR-Cas9 genetic screens with multiple modalities. Nat. Commun. *9*, 1–15.

Sapp, P.C., Hosler, B.A., McKenna-Yasek, D., Chin, W., Gann, A., Genise, H., Gorenstein, J., Huang, M., Sailer, W., Scheffler, M., et al. (2003). Identification of two novel loci for dominantly inherited familial amyotrophic lateral sclerosis. Am. J. Hum. Genet. *73*, 397–403.

Sardiello, M., Palmieri, M., Ronza, A. di, Medina, D.L., Valenza, M., Gennarino, V.A., Malta, C. Di, Donaudy, F., Embrione, V., Polishchuk, R.S., et al. (2009). A Gene Network Regulating Lysosomal Biogenesis and Function. Science (80-.). *325*, 473–477.

Scekic-Zahirovic, J., Sanjuan-Ruiz, I., Kan, V., Megat, S., De Rossi, P., Dieterlé, S., Cassel, R., Jamet, M., Kessler, P., Wiesner, D., et al. (2021). Cytoplasmic FUS triggers early behavioral alterations linked to cortical neuronal hyperactivity and inhibitory synaptic defects. Nat. Commun. *12*.

Schauer, N.J., Magin, R.S., Liu, X., Doherty, L.M., and Buhrlage, S.J. (2020). Advances in Discovering Deubiquitinating Enzyme (DUB) Inhibitors. J. Med. Chem. *63*, 2731–2750.

Schiffer, D., Cordera, S., Cavalla, P., and Migheli, A. (1996). Reactive astrogliosis of the spinal cord in amyotrophic lateral sclerosis. J. Neurol. Sci. *139*, 27–33.

Schludi, M.H., May, S., Grässer, F.A., Rentzsch, K., Kremmer, E., Küpper, C., and Klopstock, T. (2015). Distribution of dipeptide repeat proteins in cellular models and C9orf72 mutation cases suggests link to transcriptional silencing. Acta Neuropathol. *130*, 537–555.

Schröder, B., Wrocklage, C., Pan, C., Jäger, R., Kösters, B., Schäfer, H., Elsässer, H.P., Mann, M., and Hasilik, A. (2007). Integral and associated lysosomal membrane proteins. Traffic *8*, 1676–1686.

Schwenk, B.M., Lang, C.M., Hogl, S., Tahirovic, S., Orozco, D., Rentzsch, K., Lichtenthaler, S.F., Hoogenraad, C.C., Capell, A., Haass, C., et al. (2014). The FTLD risk factor TMEM106B and MAP6 control dendritic trafficking of lysosomes. EMBO J. *33*, 450–467.

Sellier, C., Campanari, M., Julie Corbier, C., Gaucherot, A., Kolb-Cheynel, I., Oulad-Abdelghani, M., Ruffenach, F., Page, A., Ciura, S., Kabashi, E., et al. (2016). Loss of C9orf72 impairs autophagy and synergizes with polyQ Ataxin-2 to induce motor neuron dysfunction and cell death. EMBO J. *35*, 1276–1297.

Settembre, C., Malta, C. Di, Polito, V.A., Arencibia, M.G., Vetrini, F., Erdin, S., Erdin, S.U., Huynh, T., Medina, D., Colella, P., et al. (2011). TFEB Links Autophagy to Lysosomal Biogenesis. Science (80-.). *332*, 1429–1433.

Shao, Q., Yang, M., Liang, C., Ma, L., Zhang, W., Jiang, Z., Luo, J., Lee, J.K., Liang, C., and Chen, J.F. (2019a). C9orf72 and smcr8 mutant mice reveal MTORC1 activation due to impaired lysosomal degradation and exocytosis. Autophagy *16*, 1635–1650.

Shao, Q., Liang, C., Chang, Q., Zhang, W., Yang, M., and Chen, J.F. (2019b). C9orf72 deficiency promotes motor deficits of a C9ALS/FTD mouse model in a dose-dependent manner. Acta Neuropathol. Commun. *7*, 32.

Sharma, A., Lyashchenko, A.K., Lu, L., Nasrabady, S.E., Elmaleh, M., Mendelsohn, M., Nemes, A., Tapia, J.C., Mentis, G.Z., and Shneider, N.A. (2015). ALS-associated mutant FUS induces selective motor neuron degeneration through toxic gain of function. Nat. Commun. *7*, 1–14.

Sharma, K., D'Souza, R.C.J., Tyanova, S., Schaab, C., Wiśniewski, J.R., Cox, J., and Mann, M. (2014). Ultradeep Human Phosphoproteome Reveals a Distinct Regulatory Nature of Tyr and Ser/Thr-Based Signaling. Cell Rep. *8*, 1583–1594.

Shatunov, A., Mok, K., Newhouse, S., Weale, M.E., Smith, B., Vance, C., Johnson, L., Veldink, J.H., van Es, M.A., van den Berg, L.H., et al. (2010). Chromosome 9p21 in sporadic amyotrophic lateral sclerosis in the UK and seven other countries: A genome-wide association study. Lancet Neurol. *9*, 986–994.

Shaw, P.J., Ince, P.G., Falkous, G., and Mantle, D. (1995a). Oxidative damage to protein in sporadic motor neuron disease spinal cord. Ann. Neurol. *38*, 691–695.

Shaw, P.J., Forrest, V., Ince, P.G., Richardson, J.P., and Wastell, H.J. (1995b). CSF and plasma amino acid levels in motor neuron disease: Elevation of CSF glutamate in a subset of patients. Neurodegeneration *4*, 209–216.

Sheean, R.K., McKay, F.C., Cretney, E., Bye, C.R., Perera, N.D., Tomas, D., Weston, R.A., Scheller, K.J., Djouma, E., Menon, P., et al. (2018). Association of regulatory T-Cell Expansion with progression of amyotrophic lateral sclerosis a study of humans and a transgenic mouse model. JAMA Neurol. *75*, 681–689.

Shen, K., Rogala, K.B., Chou, H.T., Huang, R.K., Yu, Z., and Sabatini, D.M. (2019). Cryo-EM Structure of the Human FLCN-FNIP2-Rag-Ragulator Complex. Cell *179*, 1319-1329.e8.

Shi, X., Xiang, S., Cao, J., Zhu, H., Yang, B., He, Q., and Ying, M. (2019). Kelch-like proteins: Physiological functions and relationships with diseases. Pharmacol. Res. *148*, 104404.

Shi, Y., Lin, S., Staats, K.A., Li, Y., Chang, W.-H., Hung, S.-T., Hendricks, E., Linares, G.R., Wang, Y., Son, E.Y., et al. (2018). Haploinsuffiency leads to neurodegeneration in C9ALS/FTD human induced neurons. Nat. Med. *24*, 313–325.

Shibata, N., Nagai, R., Uchida, K., Horiuchi, S., Yamada, S., Hirano, A., Kawaguchi, M., Yamamoto, T., Sasaki, S., and Kobayashi, M. (2001). Morphological evidence for lipid peroxidation and protein glycoxidation in spinal cords from sporadic amyotrophic lateral sclerosis patients. Brain Res. *917*, 97–104.

Singh, A.N., Oehler, J., Torrecilla, I., Kilgas, S., Li, S., Vaz, B., Guérillon, C., Fielden, J., Hernandez-Carralero, E., Cabrera, E., et al. (2019). The p97–Ataxin 3 complex regulates homeostasis of the DNA damage response E3 ubiquitin ligase RNF 8 . EMBO J. *38*, 1–25.

Sivasathiaseelan, H., Marshall, C.R., Agustus, J.L., Benhamou, E., Bond, R.L., Van Leeuwen, J.E.P., Hardy, C.J.D., Rohrer, J.D., and Warren, J.D. (2019). Frontotemporal Dementia: A Clinical Review. Semin. Neurol. *39*, 251–263.

Smit, J.J., Monteferrario, D., Noordermeer, S.M., Van Dijk, W.J., Van Der Reijden, B.A., and Sixma, T.K. (2012). The E3 ligase HOIP specifies linear ubiquitin chain assembly through its RING-IBR-RING domain and the unique LDD extension. EMBO J. *31*, 3833–3844.

Smith, B.N., Ticozzi, N., Fallini, C., Gkazi, A.S., Topp, S., Kenna, K.P., Scotter, E.L., Kost, J., Keagle, P., Miller, J.W., et al. (2014). Exome-wide rare variant analysis identifies TUBA4A mutations associated with familial ALS. Neuron *84*, 324–331.

Smith, B.N., Topp, S.D., Fallini, C., Shibata, H., Chen, H.J., Troakes, C., King, A., Ticozzi, N., Kenna, K.P., Soragia-Gkazi, A., et al. (2017). Mutations in the vesicular trafficking protein Annexin A11 are associated with amyotrophic lateral sclerosis Bradley N. Smith. Sci. Transl. Med. *9*, 1–16.

Smith, E.F., Shaw, P.J., and De Vos, K.J. (2019). The role of mitochondria in amyotrophic lateral sclerosis. Neurosci. Lett. *710*, 132933.

Smith, G.A., Fearnley, G.W., Abdul-Zani, I., Wheatcroft, S.B., Tomlinson, D.C., Harrison, M.A., and Ponnambalam, S. (2016). VEGFR2 Trafficking, Signaling and Proteolysis is Regulated by the Ubiquitin Isopeptidase USP8. Traffic *17*, 53–65.

Song, J., Durrin, L.K., Wilkinson, T.A., Krontiris, T.G., and Chen, Y. (2004). Identification of a SUMO-binding motif that recognizes SUMO-modified proteins. Proc. Natl. Acad. Sci. U. S. A. *101*, 14373–14378.

Soucy, T.A., Smith, P.G., Milhollen, M.A., Berger, A.J., Gavin, J.M., Adhikari, S., Brownell, J.E., Burke, K.E., Cardin, D.P., Critchley, S., et al. (2009). An inhibitor of NEDD8-activating enzyme as a new approach to treat cancer. Nature *458*, 732–736.

Sreedharan, J., Blair, I.P., Tripathi, V.B., Hu, X., Vance, C., Rogelj, B., Ackerley, S., Durnall, J.C., Williams, K.L., Buratti, E., et al. (2008). TDP-43 Mutations in Familial and Sporadic Amyotrophic Lateral Sclerosis. Science (80-.). *319*, 1668–1672.

Stagi, M., Klein, Z.A., Gould, T.J., Bewersdorf, J., and Strittmatter, S.M. (2014). Lysosome size, motility and stress response regulated by fronto-temporal dementia modifier TMEM106B. Mol. Cell. Neurosci. *61*, 226–240.

Starr, A., and Sattler, R. (2018). Synaptic dysfunction and altered excitability in C9ORF72 ALS/FTD. Brain Res. *1693*, 98–108.

Stehmeier, P., and Muller, S. (2009). Phospho-Regulated SUMO Interaction Modules Connect the SUMO System to CK2 Signaling. Mol. Cell *33*, 400–409.

Stenmark, H. (2009). Rab GTPases as coordinators of vesicle traffic. Nat. Rev. Mol. Cell Biol.

10, 513–525.

Stephenson, D.T., Stephenson, D.T., and Wright, S. (1991). Reactive astrogliosis is widespread in the subcortical white matter of amyotrophic lateral sclerosis brain. J. Neuropathol. Exp. Neurol. *50*, 263–277.

Stevanin, G., Santorelli, F.M., Azzedine, H., Coutinho, P., Chomilier, J., Denora, P.S., Martin, E., Ouvrard-Hernandez, A.M., Tessa, A., Bouslam, N., et al. (2007). Mutations in SPG11, encoding spatacsin, are a major cause of spastic paraplegia with thin corpus callosum. Nat. Genet. *39*, 366–372.

Stoica, R., De Vos, K.J., Paillusson, S., Mueller, S., Sancho, R.M., Lau, K.F., Vizcay-Barrena, G., Lin, W.L., Xu, Y.F., Lewis, J., et al. (2014). ER-mitochondria associations are regulated by the VAPB-PTPIP51 interaction and are disrupted by ALS/FTD-associated TDP-43. Nat. Commun. *5.*

Stoica, R., Paillusson, S., Gomez-Suaga, P., Mitchell, J.C., Lau, D.H., Gray, E.H., Sancho, R.M., Vizcay-Barrena, G., De Vos, K.J., Shaw, C.E., et al. (2016). ALS / FTD -associated FUS activates GSK -3β to disrupt the VAPB – PTPIP 51 interaction and ER –mitochondria associations . EMBO Rep. *17*, 1326–1342.

Su, M.Y., Fromm, S.A., Zoncu, R., and Hurley, J.H. (2020). Structure of the C9orf72 ARF GAP complex that is haploinsufficient in ALS and FTD. Nature *585*, 251–255.

Su, Y.-T., Gao, C., Liu, Y., Guo, S., Wang, A., Wang, B., Erdjument-Bromage, H., Miyagi, M., Tempst, P., and Kao, H.-Y. (2013). Monoubiquitination of Filamin B Regulates Vascular Endothelial Growth Factor-Mediated Trafficking of Histone Deacetylase 7. Mol. Cell. Biol. *33*, 1546–1560.

Sudria-Lopez, E., Koppers, M., De Wit, M., Van Der Meer, C., Westeneng, H., Zundel, C.A.C., Sameh, ·, Youssef, A., Harkema, L., De Bruin, A., et al. (2016). Full ablation of C9orf72 in mice causes immune system-related pathology and neoplastic events but no motor neuron defects. Acta Neuropathol *132*, 145–147.

Sullivan, P.M., Zhou, X., Robins, A.M., Paushter, D.H., Kim, D., Smolka, M.B., and Hu, F. (2016). The ALS/FTLD associated protein C9orf72 associates with SMCR8 and WDR41 to regulate the autophagy-lysosome pathway. Acta Neuropathol. Commun. *4*, 51.

Sumara, I., Quadroni, M., Frei, C., Olma, M.H., Sumara, G., Ricci, R., and Peter, M. (2007). A Cul3-Based E3 Ligase Removes Aurora B from Mitotic Chromosomes, Regulating Mitotic Progression and Completion of Cytokinesis in Human Cells. Dev. Cell *12*, 887–900.

Sun, L., and Chen, Z.J. (2004). The novel functions of ubiquitination in signaling. Curr. Opin. Cell Biol. *16*, 119–126.

Sun, H., Leverson, J.D., and Hunter, T. (2007). Conserved function of RNF4 family proteins in eukaryotes: Targeting a ubiquitin ligase to SUMOylated proteins. EMBO J. *26*, 4102–4112.

Sun, Y., Miller Jenkins, L.M., Su, Y.P., Nitiss, K., Nitiss, J.L., and Pommier, Y. (2020a). A conserved SUMO pathway repairs topoisomerase DNA-protein croos-links by engaging ubiquitin-mediated proteasomal degradation. Sci. Adv. *6*, 1–17.

Sun, Y., Wei, W., and Jin, J. (2020b). Cullin-RING Ligases and Protein Neddylation.

Swinnen, B., Bento-Abreu, A., Gendron, T.F., Boeynaems, S., Bogaert, E., Nuyts, R., Timmers, M., Scheveneels, W., Hersmus, N., Wang, J., et al. (2018). A zebrafish model for C9orf72 ALS reveals RNA toxicity as a pathogenic mechanism. Acta Neuropathol. *135*, 1–17.

Takahashi, Y., Fukuda, Y., Yoshimura, J., Toyoda, A., Kurppa, K., Moritoyo, H., Belzil, V. V., Dion, P.A., Higasa, K., Doi, K., et al. (2013). Erbb4 mutations that disrupt the neuregulin-erbb4

pathway cause amyotrophic lateral sclerosis type 19. Am. J. Hum. Genet. *93*, 900–905.

Talaia, G., Amick, J., and Ferguson, S.M. (2021). Receptor-like role for PQLC2 amino acid transporter in the lysosomal sensing of cationic amino acids. Proc. Natl. Acad. Sci. U. S. A. *118*, 1–8.

Tan, C.F., Eguchi, H., Tagawa, A., Onodera, O., Iwasaki, T., Tsujino, A., Nishizawa, M., Kakita, A., and Takahashi, H. (2007). TDP-43 immunoreactivity in neuronal inclusions in familial amyotrophic lateral sclerosis with or without SOD1 gene mutation. Acta Neuropathol. *113*, 535–542.

Tan, J.M.M., Wong, E.S.P., Kirkpatrick, D.S., Pletnikova, O., Ko, H.S., Tay, S.-P., Ho, M.W.L., Troncoso, J., Gygi, S.P., Lee, M.K., et al. (2008). Lysine 63-linked ubiquitination promotes the formation and autophagic clearance of protein inclusions associated with neurodegenerative diseases. Hum. Mol. Genet. *17*, 431–439.

Tan, R.H., Yang, Y., Kim, W.S., Dobson-Stone, C., Kwok, J.B., Kiernan, M.C., and Halliday, G.M. (2017). Distinct TDP-43 inclusion morphologies in frontotemporal lobar degeneration with and without amyotrophic lateral sclerosis. Acta Neuropathol. Commun. *5*, 76.

Tanaka, Y., Suzuki, G., Matsuwaki, T., Hosokawa, M., Serrano, G., Beach, T.G., Yamanouchi, K., Hasegawa, M., and Nishihara, M. (2017). Progranulin regulates lysosomal function and biogenesis through acidification of lysosomes. Hum. Mol. Genet. *26*, 969–988.

Tang, D., Sheng, J., Xu, L., Zhan, X., Liu, J., Jiang, H., Shu, X., Liu, X., Zhang, T., Jiang, L., et al. (2020). Cryo-EM structure of C9ORF72–SMCR8–WDR41 reveals the role as a GAP for Rab8a and Rab11a. Proc. Natl. Acad. Sci. U. S. A. *117*, 9876–9883.

Tanida, I., Ueno, T., and Kominami, E. (2008). LC3 and Autophagy. Methods Mol. Biol. *445*, 77–88.

Tatham, M.H., Geoffroy, M.C., Shen, L., Plechanovova, A., Hattersley, N., Jaffray, E.G., Palvimo, J.J., and Hay, R.T. (2008). RNF4 is a poly-SUMO-specific E3 ubiquitin ligase required for arsenic-induced PML degradation. Nat. Cell Biol. *10*, 538–546.

Teyssou, E., Chartier, L., Amador, M.D.M., Lam, R., Lautrette, G., Nicol, M., Machat, S., Da Barroca, S., Moigneu, C., Mairey, M., et al. (2017). Novel UBQLN2 mutations linked to amyotrophic lateral sclerosis and atypical hereditary spastic paraplegia phenotype through defective HSP70-mediated proteolysis. Neurobiol. Aging *58*, 239.e11-239.e20.

Therrien, M., Rouleau, G.A., Dion, P.A., and Parker, J.A. (2013). Deletion of C9ORF72 results in motor neuron degeneration and stress sensitivity in C. elegans. PLoS One *8*, 1–10.

Thul, P.J., Åkesson, L., Wiking, M., Mahdessian, D., Geladaki, A., Ait Blal, H., Alm, T., Asplund, A., Björk, L., Breckels, L.M., et al. (2017). A subcellular map of the human proteome. Science (80-.). *356*, eaal3321.

Tiloca, C., Ratti, A., Pensato, V., Castucci, A., Sorarù, G., Del Bo, R., Corrado, L., Cereda, C., D'Ascenzo, C., Comi, G.P., et al. (2012). Mutational analysis of VCP gene in familial amyotrophic lateral sclerosis. Neurobiol. Aging *33*, 630.e1-630.e2.

Todi, S. V., Scaglione, K.M., Blount, J.R., Basrur, V., Conlon, K.P., Pastore, A., Elenitoba-Johnson, K., and Paulson, H.L. (2010). Activity and cellular functions of the deubiquitinating enzyme and polyglutamine disease protein ataxin-3 are regulated by ubiquitination at lysine 117. J. Biol. Chem. *285*, 39303–39313.

Troilo, A., Alexander, I., Muehl, S., Jaramillo, D., Knobeloch, K.P., and Krek, W. (2014). HIF1α deubiquitination by USP8 is essential for ciliogenesis in normoxia. EMBO Rep. *15*, 77–85.

Trojanowski, J.Q., Kelsten, M.L., and Lee, V.M.Y. (1989). Phosphate-dependent and

independent neurofilament protein epitopes are expressed throughout the cell cycle in human medulloblastoma (D283 MED) cells. Am. J. Pathol. *135*, 747–758.

Tsun, Z.Y., Bar-Peled, L., Chantranupong, L., Zoncu, R., Wang, T., Kim, C., Spooner, E., and Sabatini, D.M. (2013). The folliculin tumor suppressor is a GAP for the RagC/D GTPases that signal amino acid levels to mTORC1. Mol. Cell *52*, 495–505.

Ugolino, J., Ji, Y.J., Conchina, K., Chu, J., Nirujogi, R.S., Pandey, A., Brady, N.R., Hamacher-brady, A., and Wang, J. (2016). Loss of C9orf72 Enhances Autophagic Activity via Deregulated mTOR and TFEB Signaling. PLoS Genet. *12*, 1–26.

Ullmann, R., Chien, C.D., Avantaggiati, M.L., and Muller, S. (2012). An Acetylation Switch Regulates SUMO-Dependent Protein Interaction Networks. Mol. Cell *46*, 759–770.

Urushitani, M., Kurisu, J., Tsukita, K., and Takahashi, R. (2002). Proteasomal inhibition by misfolded mutant superoxide dismutase 1 induces selective motor neuron death in familial amyotrophic lateral sclerosis. J. Neurochem. *83*, 1030–1042.

Urushitani, M., Kurisu, J., Tateno, M., Hatakeyama, S., Nakayama, K.I., Kato, S., and Takahashi, R. (2004). CHIP promotes proteasomal degradation of familial ALS-linked mutant SOD1 by ubiquitinating Hsp/Hsc70. J. Neurochem. *90*, 231–244.

Uversky, V.N. (2017). The roles of intrinsic disorder-based liquid-liquid phase transitions in the "Dr. Jekyll–Mr. Hyde" behavior of proteins involved in amyotrophic lateral sclerosis and frontotemporal lobar degeneration. Autophagy *13*, 2115–2162.

Vance, C., Al-Chalabi, A., Ruddy, D., Smith, B.N., Hu, X., Sreedharan, J., Siddique, T., Schelhaas, H.J., Kusters, B., Troost, D., et al. (2006). Familial amyotrophic lateral sclerosis with frontotemporal dementia is linked to a locus on chromosome 9p13.2-21.3. Brain *129*, 868–876.

Vance, C., Rogelj, B., Hortobágyi, T., De Vos, K.J., Nishimura, A.L., Sreedharan, J., Hu, X., Smith, B., Ruddy, D., Wright, P., et al. (2009). Mutations in FUS, an RNA processing protein, cause familial amyotrophic lateral sclerosis type 6. Science (80-.). *323*, 1208–1211.

Vance, C., Scotter, E.L., Nishimura, A.L., Troakes, C., Mitchell, J.C., Kathe, C., Urwin, H., Manser, C., Miller, C.C., Hortobágyi, T., et al. (2013). ALS mutant FUS disrupts nuclear localization and sequesters wild-type FUS within cytoplasmic stress granules. Hum. Mol. Genet. *22*, 2676–2688.

Vargas, M.R., and Johnson, J.A. (2010). Astrogliosis in Amyotrophic Lateral Sclerosis: Role and Therapeutic Potential of Astrocytes. Neurotherapeutics *7*, 471–481.

Vatsavayai, S.C., Yoon, S.J., Gardner, R.C., Gendron, T.F., Vargas, J.N.S., Trujillo, A., Pribadi, M., Phillips, J.J., Gaus, S.E., Hixson, J.D., et al. (2016). Timing and significance of pathological features in C9orf72 expansion-associated frontotemporal dementia. Brain *139*, 3202–3216.

Veldink, J.H. (2017). ALS genetic epidemiology 'How simplex is the genetic epidemiology of ALS?' J. Neurol. Neurosurg. Psychiatry *88*, 537.

Verbeeck, C., Deng, Q., Dejesus-Hernandez, M., Taylor, G., Ceballos-Diaz, C., Kocerha, J., Golde, T., Das, P., Rademakers, R., Dickson, D.W., et al. (2012). Expression of Fused in sarcoma mutations in mice recapitulates the neuropathology of FUS proteinopathies and provides insight into disease pathogenesis. Mol. Neurodegener. *7*, 1–13.

Viodé, A., Fournier, C., Camuzat, A., Fenaille, F., Latouche, M., Elahi, F., Le Ber, I., Junot, C., Lamari, F., Anquetil, V., et al. (2018). New antibody-free mass spectrometry-based quantification reveals that C9ORF72 long protein isoform is reduced in the frontal cortex of hexanucleotide-repeat expansion carriers. Front. Neurosci. *12*, 1–11.

Voges, D., Zwickl, P., and Baumeister, W. (1999). THE 26S PROTEASOME: A MOLECULAR

MACHINE DESIGNED FOR CONTROLLED PROTEOLYSIS. Annu. Rev. Biochem. *68*, 1015–1068.

De Vos, K.J., and Hafezparast, M. (2017). Neurobiology of axonal transport defects in motor neuron diseases: Opportunities for translational research? Neurobiol. Dis. *105*, 283–299.

De Vos, K.J., Chapman, A.L., Tennant, M.E., Manser, C., Tudor, E.L., Lau, K.F., Brownlees, J., Ackerley, S., Shaw, P.J., Mcloughlin, D.M., et al. (2007). Familial amyotrophic lateral sclerosis-linked SOD1 mutants perturb fast axonal transport to reduce axonal mitochondria content. Hum. Mol. Genet. *16*, 2720–2728.

Waite, A.J., Bäumer, D., East, S., Neal, J., Morris, H.R., Ansorge, O., and Blake, D.J. (2014). Reduced C9orf72 protein levels in frontal cortex of amyotrophic lateral sclerosis and frontotemporal degeneration brain with the C9ORF72 hexanucleotide repeat expansion. Neurobiol. Aging *35*, 1779.e5-1779.e13.

Walden, H., Podgorski, M.S., Huang, D.T., Miller, D.W., Howard, R.J., Minor, D.L., Holton, J.M., and Schulman, B.A. (2003). The Structure of the APPBP1-UBA3-NEDD8-ATP Complex Reveals the Basis for Selective Ubiquitin-like Protein Activation by an E1. Mol. Cell *12*, 1427–1437.

Walker, C., and El-Khamisy, S.F. (2018). Perturbed autophagy and DNA repair converge to promote neurodegeneration in amyotrophic lateral sclerosis and dementia. Brain *141*, 1247–1262.

Waltersa, T.S., McIntosha, D.J., Ingram, S.M., Tillery, L., Motley, E.D., Arinze, I.J., and Misra, S. (2021). SUMO-modification of human Nrf2 at K110 and K533 regulates its nucleocytoplasmic localization, stability and transcriptional activity. Cell. Physiol. Biochem. *55*, 141–159.

Wang, D., Ma, L., Wang, B., Liu, J., and Wei, W. (2017a). E3 ubiquitin ligases in cancer and implications for therapies. Cancer Metastasis Rev. *36*, 683–702.

Wang, G., Yang, H., Yan, S., Wang, C.E., Liu, X., Zhao, B., Ouyang, Z., Yin, P., Liu, Z., Zhao, Y., et al. (2015). Cytoplasmic mislocalization of RNA splicing factors and aberrant neuronal gene splicing in TDP-43 transgenic pig brain. Mol. Neurodegener. *10*, 1–20.

Wang, J., Zhang, J., Lee, Y.M., Ng, S., Shi, Y., Hua, Z.C., Lin, Q., and Shen, H.M. (2017b). Nonradioactive quantification of autophagic protein degradation with L-azidohomoalanine labeling. Nat. Protoc. *12*, 279–288.

Wang, L., He, G., Zhang, P., Wang, X., Jiang, M., and Yu, L. (2011). Interplay between MDM2, MDMX, Pirh2 and COP1: The negative regulators of p53. Mol. Biol. Rep. *38*, 229–236.

Wang, S., Ma, Z., Xu, X., Wang, Z., and Sun, L. (2014). A Role of Rab29 in the Integrity of the Trans-Golgi Network and Retrograde Trafficking of Mannose-6-Phosphate Receptor. PLoS One *9*, 96242.

Wang, W., Wang, L., Lu, J., Siedlak, S.L., Fujioka, H., Liang, J., Jiang, S., Ma, X., Jiang, Z., Da Rocha, E.L., et al. (2016). The inhibition of TDP-43 mitochondrial localization blocks its neuronal toxicity. Nat. Med. *22*, 869–878.

Wang, W.Y., Pan, L., Su, S.C., Quinn, E.J., Sasaki, M., Jimenez, J.C., MacKenzie, I.R.A., Huang, E.J., and Tsai, L.H. (2013). Interaction of FUS and HDAC1 regulates DNA damage response and repair in neurons. Nat. Neurosci. *16*, 1383–1391.

Webster, C.P., Smith, E.F., Bauer, C.S., Moller, A., Hautbergue, G.M., Ferraiuolo, L., Myszczynska, M.A., Higginbottom, A., Walsh, M.J., Whitworth, A.J., et al. (2016). The C9orf72 protein interacts with Rab1a and the ULK1 complex to regulate initiation of autophagy. EMBO J. *35*, 1656–1676.

Wenzel, D.M., Lissounov, A., Brzovic, P.S., and Klevit, R.E. (2011). UBCH7 reactivity profile

reveals parkin and HHARI to be RING/HECT hybrids. Nature *474*, 105–108.

Weydt, P., Yuen, E.C., Ransom, B.R., and Möller, T. (2004). Increased cytotoxic potential of microglia from ALS-transgenic mice. Glia *48*, 179–182.

White, M.R., Mitrea, D.M., Zhang, P., Stanley, C.B., Cassidy, D.E., Nourse, A., Phillips, A.H., Tolbert, M., Taylor, J.P., and Kriwacki, R.W. (2019). C9orf72 Poly(PR) Dipeptide Repeats Disturb Biomolecular Phase Separation and Disrupt Nucleolar Function. Mol. Cell *74*, 713-728.e6.

Widagdo, J., Taylor, K.M., Gunning, P.W., Hardeman, E.C., and Palmer, S.J. (2012). SUMOylation of GTF2IRD1 Regulates Protein Partner Interactions and Ubiquitin-Mediated Degradation. PLoS One *7*, 1–10.

Widago, J., Taylor, K.M., Gunning, P.W., Hardeman, E.C., and Palmer, S.J. (2012). Sumoylation of GTF2IRD1 regulates protein partner interaction and ubiquitin-mediated degradation. PLoS One *7*, 1–10.

Wijesekera, L.C., Mathers, S., Talman, P., Galtrey, C., Parkinson, M.H., Ganesalingam, J., Willey, E., Ampong, M.A., Ellis, C.M., Shaw, C.E., et al. (2009). Natural history and clinical features of the flail arm and flail leg ALS variants. Neurology *72*, 1087–1094.

Wild, P., Farhan, H., McEwan, D.G., Wagner, S., Rogov, V. V., Brady, N.R., Richter, B., Korac, J., Waidmann, O., Choudhary, C., et al. (2011). Phosphorylation of the Autophagy Receptor Optineurin Restricts Salmonella Growt. Science (80-.). *333*, 228–233.

Williams, K.L., Topp, S., Yang, S., Smith, B., Fifita, J.A., Warraich, S.T., Zhang, K.Y., Farrawell, N., Vance, C., Hu, X., et al. (2016). Ccnf mutations in amyotrophic lateral sclerosis and frontotemporal dementia. Nat. Commun. *48*, 829–834.

Williamson, T.L., Bruijn, L.I., Zhu, Q., Anderson, K.L., Anderson, S.D., Julien, J.P., and Cleveland, D.W. (1998). Absence of neurofilaments reduces the selective vulnerability of motor neurons and slows disease caused by a familial amyotrophic lateral sclerosis-linked superoxide dismutase 1 mutant. Proc. Natl. Acad. Sci. U. S. A. *95*, 9631–9636.

Wójcik, C., Yano, M., and DeMartino, G.N. (2004). RNA interference of valosin-containing protein (VCP/p97) reveals multiple cellular roles linked to ubiquitin/proteasome-dependent proteolysis. J. Cell Sci. *117*, 281–292.

Wong, P.C., Pardo, C.A., Borchelt, D.R., Lee, M.K., Copeland, N.G., Jenkins, N.A., Sisodia, S.S., Cleveland, D.W., and Price, D.L. (1995). An adverse property of a familial ALS-linked SOD1 mutation causes motor neuron disease characterized by vacuolar degeneration of mitochondria. Neuron *14*, 1105–1116.

Woollacott, I.O.C.C., and Rohrer, J.D. (2016). The clinical spectrum of sporadic and familial forms of frontotemporal dementia. J. Neurochem. *138*, 6–31.

Woolley, J.D., Khan, B.K., Murthy, N.K., Miller, B.L., and Rankin, K.P. (2011). The Diagnostic Challenge of Psychiatric Symptoms in Neurodegenerative Disease. J. Clin. Psychiatry *72*, 126–133.

Wu, C.H., Fallini, C., Ticozzi, N., Keagle, P.J., Sapp, P.C., Piotrowska, K., Lowe, P., Koppers, M., McKenna-Yasek, D., Baron, D.M., et al. (2012). Mutations in the profilin 1 gene cause familial amyotrophic lateral sclerosis. Nature *488*, 499–503.

Wu, J.T., Lin, H.C., Hu, Y.C., and Chien, C.T. (2005). Neddylation and deneddylation regulate Cul1 and Cul3 protein accumulation. Nat. Cell Biol. *7*, 1014–1020.

Wu, P., Nielsen, T.E., and Clausen, M.H. (2015). FDA-approved small-molecule kinase inhibitors. Trends Pharmacol. Sci. *36*, 422–439.

Wu, X., Yen, L., Irwin, L., Sweeney, C., Carraway, K.L., and Carraway Iii, K.L. (2004).

Stabilization of the E3 Ubiquitin Ligase Nrdp1 by the Deubiquitinating Enzyme USP8. Mol. Cell. Biol. *24*, 7748–7757.

Wu, X., Lei, C., Xia, T., Zhong, X., Yang, Q., and Shu, H.B. (2019). Regulation of TRIF-mediated innate immune response by K27-linked polyubiquitination and deubiquitination. Nat. Commun. *10*.

Xi, Z., Zinman, L., Moreno, D., Schymick, J., Liang, Y., Sato, C., Zheng, Y., Ghani, M., Dib, S., Keith, J., et al. (2013). Hypermethylation of the CpG island near the G4C2 repeat in ALS with a C9orf72 expansion. Am. J. Hum. Genet. *92*, 981–989.

Xi, Z., Zhang, M., Bruni, A.C., Maletta, R.G., Colao, R., Fratta, P., Polke, J.M., Sweeney, M.G., Mudanohwo, E., Nacmias, B., et al. (2015). The C9orf72 repeat expansion itself is methylated in ALS and FTLD patients. Acta Neuropathol. *129*, 715–727.

Xia, C.H., Roberts, E.A., Her, L.S., Liu, X., Williams, D.S., Cleveland, D.W., and Goldstein, L.S.B. (2003). Abnormal neurofilament transport caused by targeted disruption of neuronal kinesin heavy chain KIF5A. J. Cell Biol. *161*, 55–66.

Xiang, S., Shi, X., Chen, P., Chen, Y., Bing, S., Jin, X., Cao, J., Wang, J., Yang, B., Shao, X., et al. (2021). Targeting Cul3-scaffold E3 ligase complex via KLHL substrate adaptors for cancer therapy. Pharmacol. Res. *169*, 105616.

Xiao, Q., Zhao, W., Beers, D.R., Yen, A.A., Xie, W., Henkel, J.S., and Appel, S.H. (2007). Mutant SOD1G93A microglia are more neurotoxic relative to wild-type microglia. J. Neurochem. *102*, 2008–2019.

Xiao, S., MacNair, L., McGoldrick, P., McKeever, P.M., McLean, J.R., Zhang, M., Keith, J., Zinman, L., Rogaeva, E., and Robertson, J. (2015). Isoform-specific antibodies reveal distinct subcellular localizations of C9orf72 in amyotrophic lateral sclerosis. Ann. Neurol. *78*, 568–583.

Xiao, S., McKeever, P.M., Lau, A., and Robertson, J. (2019). Synaptic localization of C9orf72 regulates post-synaptic glutamate receptor 1 levels. Acta Neuropathol. Commun. *7*, 1–13.

Xiao, Y., Zou, Q., Xie, X., Liu, T., Li, H.S., Jie, Z., Jin, J., Hu, H., Manyam, G., Zhang, L., et al. (2017). The kinase TBK1 functions in dendritic cells to regulate T cell homeostasis, autoimmunity, and antitumor immunity. J. Exp. Med. *214*, 1493–1507.

Xie, Y., Kerscher, O., Kroetz, M.B., Mcconchie, H.F., Sung, P., and Hochstrasser, M. (2007). The Yeast Hex3Slx8 Heterodimer Is a Ubiquitin Ligase Stimulated by Substrate Sumoylation. J. Biol. Chem. *282*, 34176–34184.

Xu, D., Shan, B., Lee, B.-H., Zhu, K., Zhang, T., Sun, H., Liu, M., Shi, L., Liang, W., Qian, L., et al. (2015). Phosphorylation and activation of ubiquitin-specific protease-14 by Akt regulates the ubiquitin-proteasome system. Elife *4*, 1–16.

Xu, D., Shan, B., Sun, H., Xiao, J., Zhu, K., Xie, X., Li, X., Liang, W., Lu, X., Qian, L., et al. (2016). USP14 regulates autophagy by suppressing K63 ubiquitination of Beclin. Genes Dev. *30*, 1718–1730.

Xu, Z., Poidevin, M., Li, X., Li, Y., Shu, L., Nelson, D.L., Li, H., Hales, C.M., Gearing, M., Wingo, T.S., et al. (2013). Expanded GGGGCC repeat RNA associated with amyotrophic lateral sclerosis and frontotemporal dementia causes neurodegeneration. Proc. Natl. Acad. Sci. U. S. A. *110*, 7778–7783.

Yamamoto, A., Tagawa, Y., Yoshimori, T., Moriyama, Y., Masaki, R., and Tashiro, Y. (1998). Bafilomycin A1 Prevents Maturation of Autophagic Vacuoles by Inhibiting Fusion between Autophagosomes and Lysosomes in Rat Hepatoma Cell Line, H-4-II-E Cells. Cell Struct. Funct. *23*, 33–42.

Yanagitani, K., Juszkiewicz, S., and Hegde, R.S. (2017). UBE2O is a quality control factor for orphans of multiprotein complexes. Science (80-.). *357*, 472–475.

Yang, C., Wang, H., Qiao, T., Yang, B., Aliaga, L., Qiu, L., Tan, W., Salameh, J., McKenna-Yasek, D.M., Smith, T., et al. (2014). Partial loss of TDP-43 function causes phenotypes of amyotrophic lateral sclerosis. Proc. Natl. Acad. Sci. U. S. A. *111*, 1121–1129.

Yang, M., Chen, L., Swaminathan, K., Herrlinger, S., Lai, F., Shiekhattar, R., and Chen, J.F. (2016). A C9ORF72/SMCR8-containing complex regulates ULK1 and plays a dual role in autophagy. Sci. Adv. *2*, 1–17.

Yang, S.H., Galanis, A., Witty, J., and Sharrocks, A.D. (2006). An extended consensus motif enhances the specificity of substrate modification by SUMO. EMBO J. *25*, 5083–5093.

Yang, Y., Kitagaki, J., Dai, R.M., Yien, C.T., Lorick, K.L., Ludwig, R.L., Pierre, S.A., Jensen, J.P., Davydov, I. V., Oberoi, P., et al. (2007). Inhibitors of ubiquitin-activating enzyme (E1), a new class of potential cancer therapeutics. Cancer Res. *67*, 9472–9481.

Yasuda, K., Clatterbuck-Soper, S.F., Jackrel, M.E., Shorter, J., and Mili, S. (2017). FUS inclusions disrupt RNA localization by sequestering kinesin-1 and inhibiting microtubule detyrosination. J. Cell Biol. *216*, 1015–1034.

Yeh, T.-H.H., Liu, H.-F.F., Li, Y.-W.W., Lu, C.-S.S., Shih, H.-Y.Y., Chiu, C.-C.C., Lin, S.-J.J., Huang, Y.-C.C., and Cheng, Y.-C.C. (2018). C9orf72 is essential for neurodevelopment and motility mediated by Cyclin G1. Exp. Neurol. *304*, 114–124.

Yu, Q., Jiang, Y., and Sun, Y. (2020). Anticancer drug discovery by targeting cullin neddylation. Acta Pharm. Sin. B *10*, 746–765.

Yu, Y., Chi, B., Xia, W., Gangopadhyay, J., Yamazaki, T., Winkelbauer-Hurt, M.E., Yin, S., Eliasse, Y., Adams, E., Shaw, C.E., et al. (2015). U1 snRNP is mislocalized in ALS patient fibroblasts bearing NLS mutations in FUS and is required for motor neuron outgrowth in zebrafish. Nucleic Acids Res. *43*, 3208–3218.

Yuan, N., Song, L., Zhang, S., Lin, W., Cao, Y., Xu, F., Fang, Y., Wang, Z., Zhang, H., Li, X., et al. (2015). Bafilomycin A1 targets both autophagy and apoptosis pathways in pediatric B-cell acute lymphoblastic leukemia. Haematologica *100*, 345–356.

Yunus, A.A., and Lima, C.D. (2009). Structure of the Siz/PIAS SUMO E3 Ligase Siz1 and Determinants Required for SUMO Modification of PCNA. Mol. Cell *35*, 669–682.

Yuseff, M.I., Farfan, P., Bu, G., and Marzolo, M.P. (2007). A cytoplasmic PPPSP motif determines megalin's phosphorylation and regulates receptor's recycling and surface expression. Traffic *8*, 1215–1230.

Zhang, J., Wang, J., Ng, S., Lin, Q., and Shen, H.-M. (2014a). Development of a novel method for quantification of autophagic protein degradation by AHA labeling. Autophagy *10*, 901–912.

Zhang, K., Donnelly, C.J., Haeusler, A.R., Grima, J.C., Machamer, J.B., Steinwald, P., Daley, E.L., Miller, S.J., Cunningham, K.M., Vidensky, S., et al. (2015). The C9orf72 repeat expansion disrupts nucleocytoplasmic transport. Nature *525*, 56–61.

Zhang, K., Daigle, J.G., Cunningham, K.M., Coyne, A.N., Ruan, K., Grima, J.C., Bowen, K.E., Wadhwa, H., Yang, P., Rigo, F., et al. (2018a). Stress Granule Assembly Disrupts Nucleocytoplasmic Transport. Cell *173*, 958-971.e17.

Zhang, K., Liu, Q., Shen, D., Tai, H., Liu, S., Wang, Z., Shi, J., Fu, H., Wu, S., Ding, Q., et al. (2019). Mutation analysis of KIF5A in Chinese amyotrophic lateral sclerosis patients. Neurobiol. Aging *73*, 229.e1-229.e4.

Zhang, K.Y., Yang, S., Warraich, S.T., and Blair, I.P. (2014b). Ubiquilin 2: A component of the

ubiquitin-proteasome system with an emerging role in neurodegeneration. Int. J. Biochem. Cell Biol. *50*, 123–126.

Zhang, R., Gascon, R., Miller, R.G., Gelinas, D.F., Mass, J., Hadlock, K., Jin, X., Reis, J., Narvaez, A., and McGrath, M.S. (2005). Evidence for systemic immune system alterations in sporadic amyotrophic lateral sclerosis (sALS). J. Neuroimmunol. *159*, 215–224.

Zhang, R., Hadlock, K.G., Do, H., Yu, S., Honrada, R., Champion, S., Forshew, D., Madison, C., Katz, J., Miller, R.G., et al. (2011). Gene expression profiling in peripheral blood mononuclear cells from patients with sporadic amyotrophic lateral sclerosis (sALS). J. Neuroimmunol. *230*, 114–123.

Zhang, Y., Jansen-West, K., Xu, Y., Gendron, T.F., Bieniek, K.F., Lin, W., Sasaguri, H., Caulfield, T., Hubbard, J., Daughrity, L., et al. (2014c). Aggregation-prone c9FTD/ALS poly (GA) RAN-translated proteins cause neurotoxicity by inducing ER stress. Acta Neuropathol. *128*, 505–524.

Zhang, Y., Burberry, A., Wang, J.Y., Sandoe, J., Ghosh, S., Udeshi, N.D., Svinkina, T., Mordes, D.A., Mok, J., Charlton, M., et al. (2018b). The C9orf72-interacting protein Smcr8 is a negative regulator of autoimmunity and lysosomal exocytosis. Genes Dev. *32*, 929–943.

Zhang, Y.J., Gendron, T.F., Grima, J.C., Sasaguri, H., Jansen-West, K., Xu, Y.F., Katzman, R.B., Gass, J., Murray, M.E., Shinohara, M., et al. (2016). C9ORF72 poly(GA) aggregates sequester and impair HR23 and nucleocytoplasmic transport proteins. Nat. Neurosci. *19*, 668–677.

Zhao, Q., Xie, Y., Zheng, Y., Jiang, S., Liu, W., Mu, W., Liu, Z., Zhao, Y., Xue, Y., and Ren, J. (2014). GPS-SUMO: A tool for the prediction of sumoylation sites and SUMO-interaction motifs. Nucleic Acids Res. *42*, 1–6.

Zhao, Q., Ma, Y., Li, Z., Zhang, K., Zheng, M., and Zhang, S. (2020). The Function of SUMOylation and Its Role in the Development of Cancer Cells under Stress Conditions: A Systematic Review. Stem Cells Int. *2020*.

Zhao, S., Ru, W., Chen, X., Liao, S., Zhu, Z., Zhang, J., and Xu, C. (2021). Structural insights into SMCR8 C-degron recognition by FEM1B. Biochem. Biophys. Res. Commun. *557*, 236–239.

Zhao, W., Xie, W., Le, W., Beers, D.R., He, Y., Henkel, J.S., Simpson, E.P., Yen, A.A., Xiao, Q., and Appel, S.H. (2004). Activated microglia initiate motor neuron injury by a nitric oxide and glutamate-mediated mechanism. J. Neuropathol. Exp. Neurol. *63*, 964–977.

Zhao, W., Beers, D.R., Henkel, J.S., Zhang, W., Urushitani, M., Julien, J.P., and Appel, S.H. (2010). Extracellular mutant SOD1 induces microglial-mediated motoneuron injury. Glia *58*, 231–243.

Zhao, W., Beers, D.R., Liao, B., Henkel, J.S., and Appel, S.H. (2012a). Regulatory T lymphocytes from ALS mice suppress microglia and effector T lymphocytes through different cytokine-mediated mechanisms. Neurobiol. Dis. *48*, 418–428.

Zhao, Y., Xiong, X., Jia, L., and Sun, Y. (2012b). Targeting Cullin-RING ligases by MLN4924 induces autophagy via modulating the HIF1-REDD1-TSC1-mTORC1-DEPTOR axis. Cell Death Dis. *3*, 1–13.

Zheng, Q., Huang, T., Zhang, L., Zhou, Y., Luo, H., Xu, H., and Wang, X. (2016). Dysregulation of ubiquitin-proteasome system in neurodegenerative diseases. Front. Aging Neurosci. *8*, 1–10.

Zheng, Y., Jayappa, K.D., Ao, Z., Qiu, X., Su, R.C., and Yao, X. (2019). Noncovalent SUMO-interaction motifs in HIV integrase play important roles in SUMOylation, cofactor binding, and virus replication. Virol. J. *16*, 1–14.

Zhou, P. (2004). Determining protein half-lives. Methods Mol. Biol. *284*, 67–77.

Zhou, R., Tomkovicz, V.R., Butler, P.L., Ochoa, L.A., Peterson, Z.J., and Snyder, P.M. (2013a).

Ubiquitin-specific peptidase 8 (USP8) regulates endosomal trafficking of the epithelial Na+ channel. J. Biol. Chem. *288*, 5389–5397.

Zhou, Y.F., Liao, S.S., Luo, Y.Y., Tang, J.G., Wang, J.L., Lei, L.F., Chi, J.W., Du, J., Jiang, H., Xia, K., et al. (2013b). SUMO-1 Modification on K166 of PolyQ-Expanded aTaxin-3 Strengthens Its Stability and Increases Its Cytotoxicity. PLoS One *8*, 1–9.

Zhu, J., Zhu, S., Guzzo, C.M., Ellis, N.A., Ki, S.S., Cheol, Y.C., and Matunis, M.J. (2008). Small ubiquitin-related modifier (SUMO) binding determines substrate recognition and paralog-selective SUMO modification. J. Biol. Chem. *283*, 29405–29415.

Zhu, Q., Jiang, J., Gendron, T.F., McAlonis-Downes, M., Jiang, L., Taylor, A., Diaz Garcia, S., Ghosh Dastidar, S., Rodriguez, M.J., King, P., et al. (2020). Reduced C9ORF72 function exacerbates gain of toxicity from ALS/FTD-causing repeat expansion in C9orf72. Nat. Neurosci. *23*, 615–624.

Zhuang, M., Calabrese, M.F., Liu, J., Waddell, M.B., Nourse, A., Hammel, M., Miller, D.J., Walden, H., Duda, D.M., Seyedin, S.N., et al. (2009). Structures of SPOP-Substrate Complexes: Insights into Molecular Architectures of BTB-Cul3 Ubiquitin Ligases. Mol. Cell *36*, 39–50.

Zondler, L., Müller, K., Khalaji, S., Bliederhäuser, C., Ruf, W.P., Grozdanov, V., Thiemann, M., Fundel-Clemes, K., Freischmidt, A., Holzmann, K., et al. (2016). Peripheral monocytes are functionally altered and invade the CNS in ALS patients. Acta Neuropathol. *132*, 391–411.

Zu, T., Liu, Y., Bañez-Coronel, M., Reid, T., Pletnikova, O., Lewis, J., Miller, T.M., Harms, M.B., Falchook, A.E., Subramony, S.H., et al. (2013). RAN proteins and RNA foci from antisense transcripts in C9ORF72 ALS and frontotemporal dementia. Proc. Natl. Acad. Sci. U. S. A. *110*.